DEVELOPING EFFECTIVE PARAMETERS FOR SIMULATION OF SELF-PIERCE RIVET INSERTION

The University Of Sheffield.

By:

Zuzana Kotercova

Faculty of Civil and Structural Engineering

University of Sheffield

A thesis submitted in partial fulfilment of the requirements for the degree

of Doctor of Philosophy

Submission Date: May 2020

DECLARATION

I, the author, confirm that the Thesis is my own work. I am aware of the University's Guidance on the Use of Unfair Means (www.sheffield.ac.uk/ssid/unfair-means). This work has not been previously been presented for an award at this, or any other, university.

This work includes nothing, which is the outcome of work done in collaboration except where specifically indicated in the text. It has not been previously submitted, in part or whole, to any university of institution for any degree, diploma, or other qualification. All sources of information have been acknowledged by references.

Signed:_____

Zuzana Kotercova

Date: 14th November 2019

ABSTRACT

The car manufacturing industry is going through a time of significant change under pressure to provide stronger crash safe structures while at the same time making car bodies lighter to enable electric drive. This is forcing car designers to choose very high strength materials and to use a mixture of steel for strength and aluminium for lightness. The result is a large number of riveted joint stack configurations on one car body each requiring different riveting parameters. The amount of physical testing required to find solutions has now become much bigger than the testing time available on the vehicle design programs. To solve this car manufacturers are keen to switch from physical lab testing to simulated joint testing.

There is also pressure on rivet suppliers to rapidly develop new rivets designs for making the new joint stack combinations which are increasingly evolving into higher and higher strength materials. Simulation of rivet designs is needed to accelerate rivet development projects and to conduct process window testing to check the proposed new designs can cope with production variables.

This project first created a validated base model for simulating rivet insertion and then applied this model to a number of research tasks.

Through testing a large number of variety of rivet types, this work developed a set of friction parameters that have proven to work reliably for two different coatings, a standard SPR plating as well as low friction lubricant. The project also focused on accurately replicating the mid-clamping method used by AC setters with promising results. The developed base model been succesfully used to simulate several completely new SPR products that have not been simulated to date such as tubular rivets for standard and narrow flange and solid (swage) riveting.

It has also been utilized in studies focusing on creating a process window for materials to account for manufacturing variables. And finally, the model was used in a study supporting rivet design by bringing together the worst possible combination of lowest rivet manufacturing tolerances in order to predict the worst case scenario in rivet production. The results of this study were particularly accurate and allowed for mitigation of the worst combination of tolerances by informing subsequent rivet geometry amendments.

Following completion of this project, the simulation can be seen as particularly useful tool in design of new products by predicting trends and mapping out process windows for manufacturing variables of both geometries and materials and can potentially replace a large part of physical testing.

ACKNOWLEDGEMENTS

I would like to thank Atlas Copco IAS UK Ltd and EPSRC for sponsoring this PhD project via a EPSRC Case Award. I would also like to extend my thanks to the people that gave me technical guidance, including the academic supervisor Prof Luca Susmel, the industrial supervisor Dr Paul Briskham, and the team of riveting engineers in the applications lab and the R&D lab at the Atlas Copco site in Deeside who allowed me to conduct simulations on the live company projects, enabling me to ensure the PhD work was focussed on the latest new and novel aspects of benefit SPR technology.

Word Template for Thesis Architecture & Design 2014

CONTENTS

1 INTRODUCTION & OBJECTIVES 1

1.1 Trend towards aluminium and mixed metal car bodies 1

1.2 PhD Objectives 4

1.2.1 Objective 1 – Selection and Evaluation of the simulation software. 4

1.2.2 Objective 2 – Development of the base model 4

1.2.3 Objective 3 – Application of base model 5

1.2.4 Objective 4 – Utilization of validated simulation models 7

1.3 Overview of the thesis structure 8

2 REVIEW OF SELF PIERCE RIVETING (SPR) 10

2.1 Self-Pierce Riveting - Introduction 10

2.2 Evolution of SPR from 1970 to present day 14

2.3 Rivet types 19

2.3.1 Rivet length 19

2.3.2 Rivet Types and Head Styles 20

2.3.3 Rivet diameter 21

2.3.4 Rivet hardness 21

2.3.5 Rivet hole style 23

2.4 Die types 23

2.5 Rivet Insertion Equipment types 24

2.5.1 Simulation of different rivet insertion equipment 24

2.5.2 Rivet insertion equipment used in this study for the physical lab tests 25

2.5.3 RivLite Portable Battery Tool 25

2.5.4 Hydraulic double acting and pre-clamping tools 25

2.5.5 Servo tools 26

2.6 Advantages and disadvantages of SPR 27

2.6.1 Versatility 27

2.6.2 Joint Strength and Fatigue Durability 28

2.6.3 Costs 30

2.6.4 Access 30

2.6.5 High force 31

2.6.6 Process limitations 31

2.6.7 Permanency of the joint 31
2.6.8 Use of consumable (i.e. rivet) 32
2.6.9 Appearance 32
2.6.10 Not suitable for brittle materials 32
2.6.11 Each joint needs individual configuration 32

2.7 Physical joint assessment 33
2.7.1 Visual inspection of a joint 33
2.7.2 Cross sectioning 34
2.7.3 Force displacement curves 38
2.7.4 Tensile Strength 39

2.8 Types of testing in SPR 41
2.8.1 Feasibility testing 41
2.8.2 Further assessments 41

2.9 Current use of SPR 42

2.10 SPR innovations 42
2.10.1 Laser assisted SPR (LSPR) 43
2.10.2 Friction SPR (F-SPR) 44
2.10.3 Hydro-formed SPR (HF-SPR) 45
2.10.4 Adjustable die option 45
2.10.5 Kerb Konus Solid SPR (S-SPR) 45

3 REVIEW OF FINITE ELEMENT ANALYSIS (FEA) 47

3.1 What is Finite Element Analysis - Introduction 47

3.2 Brief history of Finite Element Analysis 48

3.3 Finite Element Analysis stages 48
3.3.1 Stage 1 – Pre-processing 48
3.3.2 Stage 2 – Solution 49
3.3.3 Stage 3 – Post-processing 49

3.4 Types of FEA 50
3.4.1 Static analysis 50
3.4.2 Dynamic analysis 51
3.4.3 Quasi static analysis 51
3.4.4 Implicit analysis 52
3.4.5 Explicit analysis 52

Word Template Style Guide © Monash 2014

3.5 Specific methods used by Simufact software **53**

4 REVIEW OF FEA IN CONTEXT OF SPR **58**

4.1 Parameters to consider in FE analysis of SPR **58**
4.1.1 Simulation process parameters 59
4.1.2 Process description 79
4.1.3 Material characterization 86
4.1.4 Rivets', dies', sheets' and tools' geometries 117
4.1.5 Friction, lubrication and coatings 119

4.2 FEA of SPR to date – Current state of the art **130**
4.2.1 Software types 134
4.2.2 Different types of materials in simulation 135
4.2.3 Optimisation of rivet and die geometries 136
4.2.4 Areas for future development 137

5 RESEARCH METHODS **138**

5.1 Physical SPR tests **138**

5.2 FE analysis **140**

5.3 Validation of simulation by experimental tests **142**

6 EXPERIMENTAL STAGE **143**

6.1 Simulation assessment and accuracy tolerances **144**
6.1.1 Simulation assessment – Joint measurements 144
6.1.2 Simulation assessment – Joint visual attributes 146
6.1.3 Simulation assessment – Agreeability scorecard 147

6.2 Software selection **151**
6.2.1 Evaluation of the software 152

6.3 Simulation process description **156**
6.3.1 Friction 156
6.3.2 Clamping 184
6.3.3 Press selection 191
6.3.4 Mesh 202
6.3.5 Damage mechanics 209
6.3.6 Temperature effects 213

6.3.7 Materials characterisation 224
6.3.8 Influence of geometries 243

6.4 Summary 253

7 PRACTICAL APPLICATIONS 257

7.1 Simulation of process window for sheet and rivet properties for BG rivet joining UHSS. 257

7.2 Simulation to aid design of fully tubular rivet for narrow flange joining 264
7.2.1 Test 1 – Narrowing down tolerance band 265
7.2.2 Test 2 – Coupled effect of rivet hardness and tip geometry 267
7.2.3 Test 3 – Process capability 271
7.2.4 Test 4 – Coupled effect of improved tip geometry and flare angle 274

7.3 Simulation of Solid SPR riveting joining process (Swage riveting) 275
7.3.1 Development of the swage simulation model 277
7.3.2 Validation of the swage model 281

7.4 Summary 286

8 DISCUSSION 289

8.1 Introduction 289

8.2 Selection and evaluation of out of the box version of the selected software (Objective 1A and 1B) 289

8.3 Development of the base simulation model (Objective 2) 290
8.3.1 Development of friction parameters (Objective 2A) 290
8.3.2 Effect of different joint clamping methods (Objective 2B) 292

8.4 Simulation of fully tubular rivets (Objective 3A) 294

8.5 Mixed material riveting of UHSS to aluminium and Process window for sheet and rivet properties (Objective 3B & 4A) 295

8.6 Simulation to aid design optimisation of new 4mm shank diameter T-rivets in combination with new narrow flange equipment (Objective 3C & 4B) 296

8.7 Swage solid SPR riveting joining process (Objective 3D) 298

9 CONCLUSIONS 299

Word Template Sofie Andersson & Morgan 2014

9.1 Conclusions **299**

9.2 Recommendations for Future Work **305**

10 REFERENCES **307**

List of Tables

Table 1, Rivet length availability table (Atlas Copco Rivet Brochure 2019) 20
Table 2, Table showing the standard hardness levels available for rivets. 22
Table 3, Specification for how to measure a cross section (Atlas Copco SPR spec 2019) 35
Table 4, Further power models for extrapolation of flow curves 104
Table 5, Rivet Hardness Levels 114
Table 6, Types of rivet coating available from Atlas Copco (AC SPR coatings overview 2019) 127
Table 7, Results of study comparing different lubricants in a ring compression test and their effects on μ and m. 129
Table 8, Test results – Three different levels of friction 155
Table 9, Testing matrix – Hardness tests 158
Table 10, Comparison of experimental and simulation results for RC575 159
Table 11, Comparison of experimental and simulation results for AC600T4 159
Table 12, Comparison of experimental and simulation results for AC300T61 159
Table 13, Visual demonstration of the experimental vs. simulation results. 159
Table 14, Comparison of experimental and simulation results for RC5754 at load 5kgf 160
Table 15, Comparison of experimental and simulation results for RC5754 at load 10kgf 160
Table 16, Comparison of experimental and simulation results for RC5754 at load 20kgf 160
Table 17, Testing matrix – Previous friction research 163
Table 18, Results – Previous friction research 164
Table 19, Testing matrix – Assessing effect of friction levels, joint 1 and 1 167
Table 20, Test results – Assessing effect of friction levels, joint 1 168
Table 21, Test results – Assessing effect of friction levels, joint 2 171
Table 22, Testing matrix – Friction design of experiment 175
Table 23, Test results – Verification joint 180
Table 24, Test results – verification joint 194
Table 25, Results - physical test of differing forces. 195
Table 26, Result - simulation of differing forces 196
Table 27, Test results for verification joint with 0.1mm HH 196
Table 28, Test results – verification joint 199
Table 29, Results –Speed of insertion 200
Table 30, Test results 201
Table 31, Results – Mesh sensitivity study for hardness testing 204
Table 32, Summary of element sizes checked by mesh comparison and shape deviation checks. 206
Table 33, Test matrix – Mesh sensitivity study for sheet mesh 207
Table 34, Physical joint test results 208
Table 35, Test results – Mesh sensitivity study for sheet mesh 208
Table 36, Testing matrix – Damage mechanics 211
Table 37, Test results – Damage mechanics 211
Table 38, Test results – Verification joint 214

TABLE 39, TEST RESULTS - VERIFICATION JOINT 219
TABLE 40, TEST RESULTS – VERIFICATION JOINT 222
TABLE 41, TEST RESULTS – MATERIAL DEFINITIONS USING RESULTS FROM DIFFERENT MECHANICAL TESTS 227
TABLE 42, TEST RESULTS – MATERIAL DEFINITIONS USING RESULTS FROM DIFFERENT EXTRAPOLATION METHODS 232
TABLE 43, TESTING MATRIX - MATERIAL DEFINITIONS USING VARYING STRAIN RATES 235
TABLE 44, TEST RESULT – VERIFICATION JOINT 236
TABLE 45, TEST RESULTS - MATERIAL DEFINITIONS USING VARYING STRAIN RATES 236
TABLE 46, TEST RESULTS - MATERIAL DEFINITIONS USING VARYING STRAIN RATES 237
TABLE 47, TEST RESULTS - MATERIAL DEFINITIONS USING MULTIPLE FLOW CURVES 239
TABLE 48, YIELD STRESS AND UTS OF AC600T4 ALLOY 241
TABLE 49, TEST RESULT – VERIFICATION JOINT 241
TABLE 50, RESULTS – TESTING DIFFERENT LEVELS OF HARDNESS OR AGED AC600T4 ALLOY 242
TABLE 51, POSSIBLE PRODUCTION VARIATIONS AREAS OF THE RIVET AND THEIR LIMITING TOLERANCES 244
TABLE 52, TESTING MATRIX – RIVET GEOMETRY VARIATION 245
TABLE 53, TEST RESULT – VERIFICATION JOINT 245
TABLE 54, TEST RESULT – RIVET GEOMETRY VARIATION 246
TABLE 55, RESULTS - JOINT 1 249
TABLE 56, RESULTS – JOINT 2 250
TABLE 57, SNAPSHOT OF VARIATION BETWEEN SHEET THICKNESS 251
TABLE 58, FRICTION MODEL 253
TABLE 59, GENERAL VALUES FOR MINIMUM THICKNESS CRITERIA 255
TABLE 60, HARDNESS LEVELS OF AC RIVETS 259
TABLE 61, TESTING MATRIX – SUBSTRATE MATERIAL ADJUSTED TO REFLECT MANUFACTURING VARIABLES 260
TABLE 62, RESULTS – VERIFICATION JOINT 261
TABLE 63, RESULTS – SUBSTRATE MATERIAL ADJUSTED TO REFLECT MANUFACTURING VARIABLES 262
TABLE 64, TESTING MATRIX – NARROW FLANGE T RIVETS 265
TABLE 65, TEST RESULTS – NARROWING OF THE TOLERANCE BANDS 266
TABLE 66, TESTING MATRIX - COUPLED EFFECT OF RIVET HARDNESS AND TIP GEOMETRY 268
TABLE 67, TEST RESULTS - COUPLED EFFECT OF RIVET HARDNESS AND TIP GEOMETRY 269
TABLE 68, COMPARISON OF PHYSICAL AND SIMULATION RESULTS USING SCORECARD. 271
TABLE 69, RESULTS – VERIFICATION JOINT 271
TABLE 70, TESTING MATRIX - PROCESS CAPABILITY 272
TABLE 71, TEST RESULTS - PROCESS CAPABILITY 272
TABLE 72, TESTING MATRIX - COUPLED EFFECT OF IMPROVED TIP GEOMETRY AND FLARE ANGLE 274
TABLE 73, TEST RESULTS - COUPLED EFFECT OF IMPROVED TIP GEOMETRY AND FLARE ANGLE 274
TABLE 74, RESULTS – JOINT 1 283
TABLE 75, RESULTS – JOINT 2 284
TABLE 76, RESULTS – COMPARISON OF FORCES FROM PHYSICAL AND SIMULATION TESTS 286

List of Figures

Figure 1, Current and planned future grades of Ultra High Strength Aluminium (UHSAL). (Source Whitacre-2019) 1

Figure 2, Strength v ductility chart for conventional steel grades versus Advanced High Strength Steel (AHSS) grades (WorldAutoSteel, 2017) 2

Figure 3, Image of 2018 JLR Electric I-Pace (Source EuroCarBody 2018) 3

Figure 4, Cadillac CT6 car body showing rivbonding of sheet/cast/extruded aluminium with sheet steel. (Source Visnic 2019) 3

Figure 5 Image of 2017 Audi A7 (Source: JoiningInCarBodyEngineering 2017) 3

Figure 6, Nomenclature of the industry terms assigned to different parts of the rivet and die 10

Figure 7 Schematic of SPR process drawn by the author 10

Figure 8, Example of a cross section of SPR joint showing the rivet does not pierce through the bottom sheet (SPR ES, 2018). 11

Figure 9, Marginal SPR joint with low bottom sheet thickness 'Tmin' on left leg (SPR ES, 2018) 11

Figure 10, Image of cross sectioned joints with measurements (SPR ES, 2018) 12

Figure 11, Initial design of solid SPR invented in 1970s for producing aluminium ladders. 14

Figure 12, Initial Semi-tubular SPR design with square rivet tips 14

Figure 13, Profiled shape of the rivet tips introduce in the 1990s to create the C-rivet. (Atlas Copco Rivet Brochure 2019) 15

Figure 14, the first rivet design with a thin web and profiled tip geometry was called the C-rivet (Briskham, 2016). 15

Figure 15, Cross section of C-rivet left & K-rivet right, showing the greater web & leg thickness on K-rivets. 16

Figure 16, Fully tubular rivet for thick stack aluminium joints, known as the T-rivet 16

Figure 17, Semi-tubular versus fully tubular rivet in 3.0mm+3.0mm+3.0mm AA6111 17

Figure 18, Successful riveting of very thin 0.75mm to 0.75mm aluminium for a car door using sharp tip A-rivet. 17

Figure 19, 3T aluminium joint 0.9mm Ac600 + 0.9mm Ac170 + 1.2mm RC5754, C-rivet fail (right) versus A-rivet pass (left) 18

Figure 20, Picture of the latest rivet design called the BG-rivet, developed for joining UHSS to aluminium 18

Figure 21, Riveting parameters involved in making a good SPR joint (SPR ES, 2016, with support from the author) 19

Figure 22, Diagram showing the standard Figure 23rivet types and head styles. (Atlas Copco Rivet Brochure 2019) 21

Figure 24, Cross section image showing 3mm, 5mm and 5.5mm shank dimater rivets 21

Figure 25, Rivet Production Process (Clarke, 2007) 21

Word Template by Dr Andrew R Morgan 2014

FIGURE 26, ILLUSTRATION OF EFFECT OF RIVET HARDNESS LEVEL ON RIVET INSERTION - SAME JOINT WITH H1 RIVET (LEFT) AND H2 RIVET (RIGHT) 23
FIGURE 27, IMAGES OF C-RIVET, T-RIVET, AND PG-RIVET 23
FIGURE 28, FROM LEFT TO RIGHT,3D DWG OF DG, DP AND DZ TYPE DIES. 24
FIGURE 29, FROM LEFT TO RIGHT 2D CROSS SECTION DWG OF DG, DP AND DZ TYPE DIES. 24
FIGURE 30, RIVLITE PORTABLE BATTERY TOOL 25
FIGURE 31, PICTURE OF STAND MOUNTED AND HANGER MOUNTED HYDRAULIC TOOLS 26
FIGURE 32, STANDARD ROBOT MOUNTED HENROB SERVO TOOL FOR BLOW FEED RIVET SUPPLY 27
FIGURE 33, COMPARISON OF STATIC STRENGTH OF SELF-PIERCE RIVETED JOINTS WITH JOINTS MADE USING OTHER METHODS 28
FIGURE 34, COMPARISON OF FATIGUE PROPERTIES OF SELF-PIERCE RIVETED JOINTS WITH JOINTS MADE USING OTHER METHODS (BLOWS, 2014) 29
FIGURE 35, CROSS SECTIONED RIVETS SHOWING HOW SPR JOINTS LOSE STIFFNESS AFTER SEVERE CYCLIC LOADING (BLOWS 2014) 29
FIGURE 36, ACCESS STUDIES TO CHECK C-FRAME DESIGN NEEDED FOR SELF-PIERCE RIVETING (ATLAS COPCO RIVETING GUIDELINES 2019) 31
FIGURE 37, RIVET INSERTION DIRECTION, LEFT THICK BOTTOM SHEET, RIGHT THIN BOTTOM SHEET 31
FIGURE 38, VARIABLES INFLUENCING SPR PROCESS (ATLAS COPCO RIVETING GUIDELINES 2019) 33
FIGURE 39, (LEFT) RIVET HEAD HEIGHT GAUGE WITH 18MM NOSE AND FLAT TIP, (RIGHT) USER GUIDE DIAGRAM. (AC SPR SPEC 2019) 33
FIGURE 40, EXAMPLE OF BUTTON CRACKING IN AN ALUMINIUM CASTING BEING SOLVED BY HEAT TREATING THE CASTING. (BRISKHAM 2019) 34
FIGURE 41, CROSS SECTIONED JOINT WITH MEASUREMENTS RECORDED ON THE IMAGE IN THE STANDARD MANNER. (AC SPR SPEC 2019) 34
FIGURE 42, RECOMMENDED SPECIFICATION FOR PASS/FAIL CROSS SECTION MEASUREMENT VALUES A (ATLAS COPCO SPR SPEC 2019) 35
FIGURE 43, HEAD HEIGHT MEASUREMENT EXAMPLES, FROM LEFT TO RIGHT, HEAD HIGH, HEAD FLUSH, HEAD BURIED 36
FIGURE 44, LEFT TO RIGHT, EXAMPLE OF DIFFERENT AMOUNTS OF INTERLOCK – GOOD, OUT OF SPEC, AND NON-EXISTENT 36
FIGURE 45, DIAGRAM SHOWING HOW INTERLOCK IS MEASURE ON DIFFERENT JOINT STACKS (ATLAS COPCO SPR SPEC 2019) 37
FIGURE 46, EXAMPLE OF A GOOD TMIN AND FAILURE TMIN 37
FIGURE 47, DIAGRAM SHOWING HOW TMIN IS MEASURED (ATLAS COPCO SPR SPEC 2019) 37
FIGURE 48, (LEFT) BUCKLED RIVET, (CENTRE) COLLAPSED RIVET, (RIGHT) RIVET TOO LONG. 38
FIGURE 49, (LEFT) ASYMMETRIC RIVET LEGS, (CENTRE) CRACKS IN RIVET, (RIGHT) MISALIGNED DIE 38
FIGURE 50, FORCE-DISPLACEMENT CURVE (TWI, 2016) 39
FIGURE 51, TENSILE TEST JOINT CONFIGURATIONS FOR SPR JOINTS. (ATLAS COPCO SPR SPEC 2019) 39
FIGURE 52, EXAMPLE OF A GRAPH FROM TENSILE TEST OF A LAP SHEAR JOINT, AND DIAGRAM OF GRIPS HOLDING THE TEST SAMPLE (PR ES, 2018). 40
FIGURE 53, FAILURE MODES OF SPR JOINT. (ATLASCOPCO SPR SPEC 2019) 40

FIGURE 54, CRACKS IN THE BUTTON LEADING TO THE BUTTON FALLING OFF EXPOSING THE RIVET TIPS. (JÄCKEL 2016) 43
FIGURE 55, DIFFERENCE IN BUTTON CRACKS WITHOUT USE OF LASER AND WITH USE OF LASER (DURANDET, 2008) 44
FIGURE 56, SCHEMATIC DIAGRAM SHOWING THE PROCESS OF FRICTION STIR SPR 44
FIGURE 57, SCHEMATIC DIAGRAM OF HYDRO FORMING SPR PROCESS (HAQUE, 2017). 45
FIGURE 58, EXAMPLES OF KERB KONUS SOLID SELF-PIERCE RIVETING (JÄCKEL ET AL, 2014). 45
FIGURE 59, POST PROCESSING TASKS (DIXIT ET AL, 2013) 50
FIGURE 60, 2D MODEL OF BAR IN TENSION 53
FIGURE 61, SIMULATION USING IMPLICIT AND EXPLICIT ANALYSIS. (A) IN THREE STEPS, (B) IN TWENTY STEPS (YAW, 2009). 53
FIGURE 62, LAGRANGIAN METHOD (LEFT), EULERIAN METHOD (RIGHT) (BELYTSCHKO 2000). 55
FIGURE 63, EXAMPLE OF MODEL SIMPLIFICATION FROM 3D TO 2D AXISYMMETRIC (MSC.MARC, 2013). 59
FIGURE 64, EXAMPLE OF MODEL SIMPLIFICATION FROM 3D MODEL TO 2D PLANE STRAIN MODEL (MSC.MARC, 2013). 59
FIGURE 65, AXISYMMETRIC VIEW OF AN SPR JOINT COMPLETED IN SIMULATION 60
FIGURE 66, COMPLETED SIMULATION OF 2D AXISYMMETRIC MODEL VIEWED AS 3D 60
FIGURE 67, SIMPLIFIED VIEW OF ELEMENTS (MSC.MARC, 2013). 60
FIGURE 68, TYPES OF ELEMENTS (BENHAM, 1996) 61
FIGURE 69, COURSE AND FINE MESH ILLUSTRATION (MSC.MARC, 2013) 61
FIGURE 70, TWO DIFFERENT TYPES OF MESHING DIRECTIONS. 62
FIGURE 71, REFINEMENT OF MESH (MSC.MARC, 2013). 63
FIGURE 72, SCHEMATIC OF LEVELS OF MESH REFINEMENT (MSC.MARC, 2013). 63
FIGURE 73, ILLUSTRATION OF NODE (LEFT) AND SEGMENT (RIGHT) 66
FIGURE 74, EXAMPLE OF HEAT SPECIFIC HEAT CAPACITY AND THERMAL CONDUCTIVITY IN RIVET MATERIALS (HARDNESS LEVEL 2) (SIMUFACT, 2015) 70
FIGURE 75, EXAMPLE OF HEAT SPECIFIC HEAT CAPACITY AND THERMAL CONDUCTIVITY IN SOFT ALUMINIUM SHEET MATERIALS (AA-5182) (SIMUFACT, 2015) 70
FIGURE 76, EXAMPLE OF HEAT SPECIFIC HEAT CAPACITY AND THERMAL CONDUCTIVITY IN MILD STEEL SHEET MATERIALS (DP600) (SIMUFACT, 2015) 71
FIGURE 77, EXAMPLE OF FLOW CURVES OBTAINED AT MULTIPLE TEMPERATURES. 72
FIGURE 78, CRITERIA USED IN LEMAITRE DAMAGE MODEL (SIMUFACT, 2015) 76
FIGURE 79, MINIMUM THICKNESS CRITERIA MESH SEPARATION, SPECIFYING THE SMALLEST THICKNESS THE MATERIAL CAN REACH 78
FIGURE 80, MIMINUM THICKNESS CRITERIA SET TO 0.10MM (LEFT) SETTING NOT ACTIVATED (RIGHT) 78
FIGURE 81, (LEFT) SPR INSERTION EQUIPMENT, (RIGHT) SIMPLIFIED MODEL OF INSERTION EQUIPMENT 80
FIGURE 82, SCHEMATIC ILLUSTRATION OF THE HYDRAULIC PRESS 81
FIGURE 83, SCHEMATIC ILLUSTRATION OF THE HAMMER PRESS 81
FIGURE 84, SCHEMATIC ILLUSTRATION OF THE SCREW PRESS 81
FIGURE 85, SCHEMATIC ILLUSTRATION OF THE CRANK PRESS 82
FIGURE 86, SCHEMATIC ILLUSTRATION OF THE ORBITAL FORGING PRESS 82

FIGURE 87, SCHEMATIC ILLUSTRATION OF THE SCOTCH YOKE DRIVE PRESS 83
FIGURE 88, CLAMP MECHANISM ON SERVO SETTER 83
FIGURE 89, MODEL OF BLANKHOLDER/NOSE 84
FIGURE 90, POINT AT WHICH THE CLAMP COMES ON AND THE NOSE IS PRESSED DOWN WITH 8KN. 85
FIGURE 91, DIE SPRING REPLICATING THE CLAMP MECHANISM 86
FIGURE 92, RELEASED SPRING (LEFT) AND COMPRESSED SPRING (RIGHT) (SIMUFACT, 2015) 86
FIGURE 93, EXAMPLE OF MATERIAL PROPERTY DATA AVAILABLE FROM MATERIAL SUPPLIER NOVELIS. 88
FIGURE 94, DEFORMATION OF TENSILE TEST SAMPLE (ALTAN, 2011) 89
FIGURE 95, ENGINEERING STRESS AND STRAIN CURVE AND (B) TRUE STRESS AND STRAIN CURVE 90
FIGURE 96, EXAMPLE OF STRESS AND STRAIN CURVES (ASTM STANDARD 370) 91
FIGURE 97, ILLUSTRATION OF DETERMINING YIELD POINT 92
FIGURE 98, EXAMPLE OF A FLOW CURVE IN THE SOFTWARE 92
FIGURE 99, EXAMPLE OF EXTRAPOLATED FLOW CURVE 93
FIGURE 100, TYPES OF SPECIMENS FOR TENSILE TESTS FLAT OR TUBULAR 94
FIGURE 101, TENSILE TEST MACHINE 95
FIGURE 102, TENSILE TESTING STRESS V STRAIN CURVE FOR AA6111-T4 WITH ENGINEERING STRAIN ON X AND ENGINEERING STRESS ON Y 95
FIGURE 103, SCHEMATIC OF COMPRESSION TEST (ALVES, 2011). 96
FIGURE 104, COMPARISON OF TENSILE AGAINST COMPRESSION TEST RESULTS (NPTEL, 2016) 96
FIGURE 105, TYPICAL RESULT OF STACK COMPRESSION TEST (ALVES, 2011) 97
FIGURE 106, SAMPLE USED FOR STACK COMPRESSION TEST BY ALVES (2011) 97
FIGURE 107, BULGING BEHAVIOUR IN STACK COMPRESSION TEST WITH GLUED STACKS. (HOCHHOLDINGER, 2009) 98
FIGURE 108, FLOW CURVES CREATED BY COMPRESSION TESTING WITH AND WITHOUT ACCOUNTING FOR FRICTION. (HOCHHOLDINGER, 2009) 98
FIGURE 109, EXAMPLE OF INHOMOGENOUS FLOW IN STACK COMPRESSION TEST (ALVES, 2011) 99
FIGURE 110, HYDRAULIC BULGE TESTING SET UP (JUNHE ET AL, 2013) 99
FIGURE 111, TENSILE TESTING STRAINS REACHING 0.2 (LEFT), HYDRAULIC BULGE TESTING UP TO STRAIN VAKUE OF 0.6 (RIGHT) (NOVELIS, 2017) 100
FIGURE 112, COMBINATION OF TENSILE AND BULGE TEST FOR PRODUCING FLOW CURVES (FALLAHIAREZOODAR 2015) 101
FIGURE 113, SAMPLE SET UP OF IN-PLANE TORSION TEST 101
FIGURE 114, COMBINATION OF TWO OF THE HARDENING LAWS (ZHU ET AL, 2018) 104
FIGURE 115, EXAMPLE OF USING SWIFT AND MODIFIED VOCE SEPARATELY (ELLER, 2015) 105
FIGURE 116, COMPARISON OF HOCKETT AND SHERBY FLATTER FLOW CURVES WITH HIGHER EXTRAPOLATIONS SUCH AS LUDWIK AND VOCE. 105
FIGURE 117, FLOW CURVES FOR THE SAME RIVET MATERIAL, A - SINGLE FLOW CURVE (TOP) AND B - FLOWCURVES THAT A COMBINATION OF FIVE DIFFERENT TEMPERATURE AND FOUR DIFFERENT STRAIN RATES (BOTTOM) (SIMUFACT SOFTWARE, 2015) 107
FIGURE 118, INCREASED FORMABILITY SHOWN AT HIGHER TEMPERATURES. (PELLERGRINI ET AL 2011) 108

FIGURE 119, SET-UP OF GLEEBLE MACHINE LEFT. RIGHT – BORON INCREASED FORMABILITY WITH INCREASED TEMPERATURE. 108
FIGURE 120, SET- UP OF A SPLIT HOPKINSON PRESSURE BAR 109
FIGURE 121, COMPARISON OF STATIC AND DYNAMIC STRESS STRAIN CURVES FOR DC04 MATERIAL. (VERLEYSEN, 2011) 109
FIGURE 122, A) INDENTER SHAPE B) INDENTER TIP C) INDENT IN THE SAMPLE 111
FIGURE 123, NAMING CONVENTION FOR HARDNESS TEST RESULTS 112
FIGURE 124, THE FIRST HARDENING CURVE (POLMEAR, 2004) 115
FIGURE 125, OFFSET YIELD POINT SCALE FACTOR - $R_{P0.2}$ 116
FIGURE 126, HARDENING SCALE FACTOR - R_M 117
FIGURE 127, COMPLETE C FRAME ON THE LEFT, SIMPLIFIED VERSIONS MIDDLE AND RIGHT. 118
FIGURE 128, ASPERITIES ON SURFACES OF MATERIALS 120
FIGURE 129, ASPERITIES IN CONTACT 120
FIGURE 130, FACTORS AFFECTING THE FRICTION IN METAL FORMING (KARDES, 2012). 121
FIGURE 131, COULOMB FRICTION MODEL SCHEMATIC PRESENTATION 122
FIGURE 132, SHEAR FRICTION MODEL SCHEMATIC PRESENTATION 123
FIGURE 133, SCHEMATIC DEMONSTRATION OF COMBINED FRICTION MODEL 124
FIGURE 134, FOUR TYPES OF FRICTION STATE (SIMUFACT, 2015) 124
FIGURE 135, RING COMPRESSION TEST BEFORE & AFTER COMPRESSION, WITH LOW FRICTION & HIGH FRICTION. 128
FIGURE 136, CYLINDER SAMPLE FOR RING COMPRESSION TEST 128
FIGURE 137, TEST RIG FOR TRANSLATIONAL SLIDING 129
FIGURE 138, SAMPLE RIVET MEASURED USING TRANSLATIONAL SLIDING TEST 129
FIGURE 139, EXAMPLES OF SIMULATION PRESENTATION – EFFECTIVE PLASTIC STRAIN (TOP LEFT), EQUIVALENT STRESS (TOP RIGHT) AND GEOMETRY (BOTTOM) 141
FIGURE 140, SIMULATION VALIDATION CHART 142
FIGURE 141, EXAMPLE OF A 2D AXISYMMETRIC RESULT FOR A HALF CROSS SECTION 145
FIGURE 142, EXAMPLE OF SAME SIMULATION USING SOFTER (LEFT) AND HARDER (RIGHT) MATERIAL IN THE SAME JOINT. 146
FIGURE 143, EXAMPLE OF SAME SIMULATION USING DIFFERENT FRICTION SETTINGS, LOW (LEFT) AND HIGH (RIGHT) IN THE SAME JOINT. 146
FIGURE 144, EXAMPLE OF SAME JOINT USING DIFFERENT CLAMPING METHODS, PRECLAMP (LEFT) AND MID-CLAMP (RIGHT) IN CAUSING INTERNAL GAPS IN THE SAME JOINT. 146
FIGURE 145, INDIVIDUAL EXAMPLES OF TYPICAL RIVET AND SHEET BEHAVIOUR. VARIOUS EXAMPLES OF TYPICAL RIVET AND MATERIALS BEHAVIOUR E.G. BUCKLING (A), INTERNAL GAPS (B), FLOW PATTERN DEFORMATION FEATURE UNDER THE RIVET LEG (C), EXCESSIVE FLARING (D) ANDFLOW MATERIAL FORMING IN THE CORNER OF THE SHEET AND BUTTON (E). 147
FIGURE 146, COMPARISON OF MEASUREMENTS OF SIMULATION AND PHYSICAL TEST RESULTS. 148
FIGURE 147, EXAMPLE OF COMPARISON OF SIMULATION AND PHYSICAL RESULTS 148
FIGURE 148, EXAMPLE OF A SCORECARD 149
FIGURE 149, COMPLETED AGREEABILITY SCORECARD EXAMPLE – SAME PHYSICAL JOINT REPLICATED WITH TWO DIFFERENT MATERIALS SHOWING TWO DIFFERENT LEVELS OF AGREEMENT. 149

FIGURE 150, EXAMPLE OF A SPECIFIC FEATURE MISSING COMPLETELY IN A SIMULATION 150
FIGURE 151, EXAMPLES OF BORE FILLED IN LESS IN A SIMULATION THEN IN THE PHYSICAL TEST. 150
FIGURE 152, EXAMPLES OF A SIMULATION WITH OUT OF THE BOX SOFTWARE MODEL WITH GOOD AGREEMENT ... 153
FIGURE 153, EXAMPLE OF A SIMULATION WITH 'OUT OF THE BOX' SOFTWARE MODEL SHOWING POOR AGREEMENT 153
FIGURE 154, JOINTS USING DEFAULT CLAMP METHOD (LEFT) AND NO CLAMP (RIGHT) 154
FIGURE 155, PRELIMINARY TESTS OF FRICTION $\mu = 0.01$ (A), $\mu = 0.2$ (B) AND 155
FIGURE 156, SIMPLIFIED FRICTION TEST – RIVET INSERTED INTO A BLOCK OF ALUMINIUM WITH FRICTION $\mu = 0.01$ (LEFT) AND $\mu = 1.0$ (RIGHT) 156
FIGURE 157, TEST MACHINE SET UP 157
FIGURE 158, SIMULATION MODEL SET UP 157
FIGURE 159, EXPERIMENTAL TEST SAMPLE AND SIMULATION SAMPLE 158
FIGURE 160, VERIFICATION JOINT 1 162
FIGURE 161, VERIFICATION JOINT 2 162
FIGURE 162, VERIFICATION JOINT 1 164
FIGURE 163, VISUAL ATTRIBUTES OF JOINT – PREVIOUS FRICTION RESEARCH 165
FIGURE 164, COMPARISON OF CROSS SECTION WITH SIMULATION WITH LOW FRICTION BASED IN LITERATURE 165
FIGURE 165, RESULTS – ASSESSING EFFECT OF FRICTION LEVELS, JOINT 1. JOINTS ON AFTER THEY HAVE PIERCED THE SECOND SHEET AND ARE ABOUT TO START FLARING FURTHER 169
FIGURE 166, ASSESSING EFFECT OF FRICTION LEVELS, JOINT 1- EFFECTS OF APPLYING LOW TO HIGH FRICTION (LEFT TO RIGHT) 170
FIGURE 167, FRICTION LEVELS COMPARISON, JOINT 1. CONTRASTING LOWEST FRICTION LEVEL (LEFT) μ=0.01 AND HIGHEST FRICTION LEVEL (RIGHT) μ=0.5 170
FIGURE 168, ASSESSING EFFECT OF FRICTION LEVELS, JOINT 2. SIMULATION OF TRIVET WITH 3 SHEETS OF ALUMINIUM 171
FIGURE 169, SAME JOINT WITH EXCESSIVE AMOUNT OF LUBRICANT ON THE LEFT AND WITH STANDARD TRIVET COATING ON THE RIGHT. 173
FIGURE 170, FRICTION PARTNERS IN 2T AND 3T STACKS 174
FIGURE 171, RESULTS – PROPOSED FRICTION SETTINGS FOR 2T STACK 175
FIGURE 172, RESULTS – PROPOSED FRICTION SETTINGS FOR T STACK 176
FIGURE 173, COMPARISON OF BUILT-IN SPR MODEL FRICTION AND NEW FRICTION SETTINGS IN TEST JOINT 1 177
FIGURE 174, COMPARISON OF BUILT-IN SPT MODEL DEFAULT FRICTION AND NEW FRICTION SETTINGS IN TEST JOINT 11 178
FIGURE 175, COMPARISON OF NEW FRICTION SETTINGS WITH SETTING WITH TOO HIGH A FRICTION IN TEST JOINT 5. 178
FIGURE 176, BG RIVET SIMULATED WITH LOW (A) AND HIGH (B) FRICTION SETTINGS IN TEST JOINT 10 179
FIGURE 177, COMPARISON OF LOW AND HIGH FRICTION COATINGS 181
FIGURE 178, COMPARISON OF COATING LEVELS UNDER ULTRAVIOLET LIGHT BEFORE AND AFTER INSERTION 182
FIGURE 179, RIVET REMOVED FROM JOINT TO SHOW WEAR OF THE COATING 183
FIGURE 180, SIMULATION CORRESPONDING WITH PHYSICAL TEST IN TO CONFIRM THE EXTENT OF STRESS IN THIS AREA AND PROBABILITY OF SHEET COATING BEING WORN OFF 183

FIGURE 181, FORCE-DISPLACEMENT FOR CLAMP 185
FIGURE 182, THE RED LINE ILLUSTRATES THE APPROXIMATE POINT WHEN THE NOSE STARTS PUSHING ON THE SHEETS WITH 8KN FORCE 185
FIGURE 183, INTERMEDIATE CLAMP MODEL SET UP - USE OF 'RELEASED' SPRING (LEFT), EXAPLE GRAPH CONTROLLING MOVEMENT FOR A NOSE WITH INTERMEDIATE CLAMP WITH RIVET FULLY INSERTED AT 5.0MM. 186
FIGURE 184, EXAMPLE OF PRE-CLAMP AND INTERMEDIATE CLAMP FORCE DISPLACEMENT CURVES. 186
FIGURE 185, JOINT 1 VISUAL RESULTS 188
FIGURE 186, JOINT 2 VISUAL RESULTS 188
FIGURE 187, JOINT 3 VISUAL RESULTS 189
FIGURE 188, JOINT 3 WITH PRE-CLAMP (LEFT) AND INTERMEDIATE CLAMP (RIGHT) CAPTURED AT 4.4MM INTO THE STROKE. 189
FIGURE 189, EXAMPLES OF JOINTS COMPLETED WITH PRE-CLAMP ON THE LEFT AND INTERMEDIATE CLAMP ON THE RIGHT. 190
FIGURE 190, EXAMPLE OF A SMALL DIE USED WITH INTERMEDIATE CLAMP 190
FIGURE 191, EXAMPLE OF RIVET INSERTED WITH HIGH ENERGY (LEFT) AND LOW ENERGY (RIGHT). 193
FIGURE 192, PHYSICAL TEST OF DIFFERING FORCES 195
FIGURE 193, FORCE-DISPLACEMENT CURVE FOR JOINT WITH 0.10MM HEAD HEIGHT 197
FIGURE 194, FORCE-DISPLACEMENT CURVE FOR JOINT WITH 0.00MM HEAD HEIGHT 197
FIGURE 195, COMPARISON OF PHYSICAL AND SIMULATION CROSS SECTION RESULTS 198
FIGURE 196, AXISYMMETRIC VIEW OF JOINTS TESTED AT DIFFERENT VELOCITIES WITH SINGLE FLOW CURVE COMPARED TO A PHYSICAL RESULT. 200
FIGURE 197, SINGLE FLOW (LEFT) CURVE VS MULTIPLE FLOW CURVES (RIGHT) 201
FIGURE 198, AXISYMMETRIC VIEW OF JOINTS TESTED AT DIFFERENT VELOCITIES WITH MULTIPLE FLOW CURVE COMPARED TO A PHYSICAL RESULT. 201
FIGURE 199, LOCATION OF THE MESH AREA USED FOR SENSITIVITY STUDY FOR HARDNESS TESTS. 203
FIGURE 200, VISUAL RESULTS OF MESH SENSITIVITY STUDY ON COUPONS FOR HARDNESS TESTING 203
FIGURE 201, OUTLINES OF MESH AT DIFFERENT SIZES 205
FIGURE 202, DEVIATION FROM THE SHAPE 205
FIGURE 203, COARSENING OF THE INTERNAL PART OF RIVET MESH, NO COARSENING (LEFT), LEVEL 1 (MIDDLE) AND LEVEL 2 (RIGHT) 206
FIGURE 204, AXISYMMETRIC VIEW OF MESH WITH REFINEMENT WINDOWS 207
FIGURE 205, INTERNAL STEP IN GEOMETRY OF THE RIVET 209
FIGURE 206, MODELLING OF THE INTERNAL STEP IN THE RIVET GEOMETRY 209
FIGURE 207, EXAMPLE OF COMPLETION OF SHEET PIERCING 210
FIGURE 208, MESH INSTABILITY EXAMPLE 212
FIGURE 209, COMPARISON OF MINIMUM THICKNESS SET AT 0.5MM (LEFT) AND 0.015MM (RIGHT) 212
FIGURE 210, ZOOMED IN VIEW OF COMPARISON OF MINIMUM THICKNESS OF MATERIAL VS PHYSICAL TEST 213
FIGURE 211, EXAMPLE OF LOWER DUCTILITY DISPLAYED BY DP600. 213
FIGURE 212, HIGHEST TEMPERATURE SHOWN IN THE JOINT IS SHOWING AT 179° IN THE HOTSPOTS 215
FIGURE 213, THERMAL STRIPS 216

FIGURE 214, EXAMPLES OF WHERE THERMAL STRIPS MIGHT BE PLACED. 216
FIGURE 215, ILLUSTRATION OF THE NON-CONTACT HANDHELD THERMOMETER 217
FIGURE 216, THERMOCOUPLE 217
FIGURE 217, SCHEMATIC VIEW OF PLACEMENT OF THERMOCOUPLE 218
FIGURE 218, THERMOCOUPLE EMBEDDED IN THE SHEET 218
FIGURE 219, TEMPERATURES CAPTURED IN SIMULATION 219
FIGURE 220, TEST RESULTS – TEMPERATURE COMPARISON OF EXPERIMENTAL AND SIMULATION TESTS 220
FIGURE 221, FLOW CURVES CAPTURED AT VARIOUS TEMPERATURES (SIMÕES ET AL, 2018) 221
FIGURE 222, SCHEMATIC VIEW OF THE SAMPLE (LEFT) AND A COMPLETED PHYSICAL SAMPLE (RIGHT) 222
FIGURE 223, TEMPERATURES CAPTURED IN SIMULATION 223
FIGURE 224, TEST RESULTS – TEMPERATURE COMPARISON OF EXPERIMENTAL AND SIMULATION TESTS 223
FIGURE 225, JOINT WITH THE SAME MATERIAL, LEFT – POORLY DEFINED FLOW CURVE, RIGHT – GOOD QUALITY FLOW CURVE. 224
FIGURE 226, FLOW CURVES GENERATED AS PART OF THE FLOW CURVE STANDARDISATION OF FLOW CURVES PROJECT (JÄCKEL, M. ET AL, 2018) 225
FIGURE 227, JOINT 1 - IN-PLANE TORSION TEST VISUAL RESULTS ON THE LEFT, HYDRAULIC BULGE TEST RESULTS ON THE RIGHT. 228
FIGURE 228, JOINT 2 - IN-PLANE TORSION TEST VISUAL RESULTS ON THE LEFT, HYDRAULIC BULGE TEST RESULTS ON THE RIGHT. 228
FIGURE 229, JOINT 3 - IN-PLANE TORSION TEST VISUAL RESULTS ON THE LEFT, HYDRAULIC BULGE TEST RESULTS ON THE RIGHT. 228
FIGURE 230, JOINT 4 - IN-PLANE TORSION TEST VISUAL RESULTS ON THE LEFT, HYDRAULIC BULGE TEST RESULTS ON THE RIGHT. 228
FIGURE 231, JOINT 5 - IN-PLANE TORSION TEST VISUAL RESULTS ON THE LEFT, HYDRAULIC BULGE TEST RESULTS ON THE RIGHT. 228
FIGURE 232, EXTRAPOLATION OF IN-PLANE TORSION TEST USING SWIFT, HOCKETT-SHERY AND VOCE MODELS .. 230
FIGURE 233, EXAMPLE OF VISUAL RESULT – COMPARISON OF HOCKETT-SHERBY (LEFT) AND SWIFT (RIGHT) HARDENING LAWS 233
FIGURE 234, AA6111 MATERIAL – MULTIPLE FLOW CURVE 234
FIGURE 235, AXISYMMETRIC VIEW OF RESULTS WITH VARYING STRAIN RATES. 236
FIGURE 236, AXISYMMETRIC VIEW OF RESULTS WITH VARYING TEMPERATURES 237
FIGURE 237, VARYING STRAIN RATES AT 25°C 238
FIGURE 238, VARYING TEMPERATURES AT 0.015 1/S 238
FIGURE 239, COMPARISON OF MULTIPLE VS SINGLE FLOW CURVES – TEST C1 (TOP LEFT) AND HIGHEST AND LOWEST STRAIN RATES AND TEMPERATURE VALUES – TEST C2 (TOP RIGHT) AND SINGLE FLOW CURVE - TEST C3 (BOTTOM) 239
FIGURE 240, AC600T4 FLOW CURVES PROVIDED BY THE MATERIAL SUPPLIER (NOVELIS, 2016) 241
FIGURE 241, AXISYMMETRIC VIEW OF JOINTS WITH 1, 3 AND 6 MONTHS OLD AC600T4 ALLOY 242
FIGURE 242, COMPARISON OF JOINT WITH 1 MONTH OLD (TOP LEFT), 3 MONTHS (TOP RIGHT) AND 6 MONTHS (BOTTOM) OLD AC600T4 242
FIGURE 243, ILLUSTRATION OF THE RIVET PRODUCTION VARIATION 244

Figure 244, Axisymmetric view of results of Test A10 - Rivet tip radius 247
Figure 245, Joint 1 - Close up of results 250
Figure 246, Joint 1 - Close up of results 250
Figure 247, Inconsistencies within rivet 252
Figure 248, Standard 16mm dia Nose CAD model was replaced with a 18mm Nose diameter 253
Figure 249, Clamp model 254
Figure 250, Example of rivet and sheet mesh 255
Figure 251, Differences caused by small changes in rivet tip geometry (reference/ standard rivet tip = 0.15mm, blunt tip = 0.22, sharp tip = 0.08mm) 256
Figure 252, Axisymmetric view of all tested joints 262
Figure 253, Example joint on the left – 1.5mm Fortiform (1050 MPa) + 1.5mm 5182. Example joint 2 on the right – 1.4mm Fortiform (hardness 1050MPa) + 3.0mm RC5754. 263
Figure 254, Illustartion of differences between standard and narrow flange, left, and new smaller nose, on the right 264
Figure 255, Comparison of the proposed new smaller tubular rivets with a standard size tubular rivet 265
Figure 256, Axisymmetric view of results of initial geometry study with +/= 0.07mm tolerance band 266
Figure 257, Axisymmetric view of results of initial geometry study with +/= 0.07mm tolerance band 267
Figure 258, Head width and flare angle parameters highlighted in dashed red line. 267
Figure 259, Axisymmetric view of joints completed in order to evaluate the coupled effect of hardness of tip sharpness 269
Figure 260, Graph capturing instability in measurements of interlock (top left), Tmin (top right) and HH (bottom) with changing rivet hardness and tip geometry 270
Figure 261, Axisymmetric view of joints with longest, sharpest and softest rivets and three different levels of flare angle – 82.5°, 84.5° and 80.5°. Results left to right – F 7, F8 and F9. 273
Figure 262, Axisymmetric view of joints with shortest, bluntest and hardest rivets and three different levels of flare angle – 82.5°, 84.5° and 80.5° Results left to right – F4, F5 and F6. 273
Figure 263, Axisymmetric view of joints with shortest, bluntest and hardest rivets and three different levels of flare angle – 82.5°, 84.5° and 80.5°. Results left to right - G1, G2 and G3. 274
Figure 264, Example of a slug not being displaced int othe bore of the rivet 276
Figure 265, Shallow die to causes the rivet to collapse 276
Figure 266, Deeper die creates a better joint but causes cracking on the button 276
Figure 267, Example of swaged rivets 277
Figure 268, Solid SPR – schematic of stage 1 rivet insertion process 278
Figure 269, Solid SPR – schematic of stage 2 rivet insertion process 278
Figure 270, Stage 1 – hollow die (left), stage 2 – raised die (right) 279

FIGURE 271, ILLUSTRATION OF JIGS USED FOR SWAGE 279
FIGURE 272, PROPERTIES TRANSFERRED FROM 1ST STAGE OF SOLID RIVETING (SWAGE) 280
FIGURE 273, DISHING OF THE STOP SHEET IN ABSENCE OF FIXTURES AND SUPPORT OF A DIE 280
FIGURE 274, DEMONSTRATION OF THE FIXTURES ADDED TO THE PROCESS 281
FIGURE 275, CORRECT EXAMPLES OF HH IN SWAGE RIVETING 281
FIGURE 276, FLOW CURVE USED FOR THIS TEST IS USIBOR 1500 282
FIGURE 277, FORCE-DISPLACEMENT CURVES FOR SWAGE JOINT 1 – PHYSICAL TESTING 283
FIGURE 278, FORCE-DISPLACEMENT CURVES FOR SWAGE JOINT 1 – SIMULATION 283
FIGURE 279, FORCE-DISPLACEMENT CURVES FOR SWAGE JOINT 2 – SIMULATION 284
FIGURE 280, FORCE-DISPLACEMENT CURVES FOR SWAGE JOINT 2 – SIMULATION 285
FIGURE 281, EXAMPLE OF GOOD AGREEMENT BETWEEN MID STAGE OF SWAGE 285
FIGURE 282, SHARPEST, LONGEST AND SOFTEST RIVET RESULTING FROM PRODUCTION VARIABILITY 287
FIGURE 283 287
FIGURE 284, COMPARISON OF PHYSICAL CROSS SECTION WITH SIMULATION USING WITH FRICTION LEVELS FROM LITERATURE (LEFT) AND NEWLY ESTABLISHED FRICTION SETTINGS (RIGHT) 291
FIGURE 285, EXAMPLE OF EXCESSIVE FRICTION SET TO FIND LIMITING PARAMETERS 291
FIGURE 286, JOINT COMPLETED WITH EXCESSIVE AMOUNT OF COATING VS STANDARD COATING 291
FIGURE 287, JOINT COMPLETED WITH STANDARD COATING VS NO COATING 292
FIGURE 288, FORCE-DISPLACEMENT CURVES EXTRACTED FROM SERVO SETTER (LEFT) AND NEW SIMULATION INTERMEDIATE CLAMP METHOD (RIGHT) 293
FIGURE 289, A JOINT WITH PRECLAMP (LEFT) AND INTERMEDIATE CLAMP (RIGHT) CAPTURED CC4.4NM INTO THE STROKE. 293
FIGURE 290, A JOINT WITH PRECLAMP (LEFT) AND INTERMEDIATE CLAMP (RIGHT) 293
FIGURE 291, EXAMPLE OF TRIVET SIMULATIONS 294
FIGURE 292, AN EXAMPLE OF DIFFERENCE IN DRAWING 295
FIGURE 293, NOMINAL AND WORTS CASE SCENARIO UHSS STEEL JOINT 296
FIGURE 294, OPTIMISATION OF DIES BY ABE ET AL (2009) 297
FIGURE 295, RESULTS OF RIVET OPTIMISATION STUDY ON NARROW FLANGE T RIVET 297
FIGURE 296, EXAMPLE OF AGREEMENET OF SIMULATION AND PHYSICAL TEST OF FIRST STAG OF SWAGE JOINING . 298
FIGURE 297, EXAMPLE OF AGREEMENT OF FORCE-DISPLACEMENT CURVES CORRESPONDING TO THE IMAGE ABOVE. 298
FIGURE 298, EXAMPLE OF A CORRECT NARROW FLANGE JOINT SIMULATION. 302

List of Abbreviations and Acronyms

SPR	Self-pierce riveting
Tmin	Minimum distance in bottom sheet
HH	Head height
HHDTI	Head height measured by DTI device
HHM	Head height measured on a photograph
FE	Finite element
FEA	Finite element analysis
FEM	Finite elements methods
HSS	High Strength Steels
UHSS	Ultra High Strength Steels
UHSAL	Ultra High Strength Aluminium
PHS	Press Hardened Steels
GUI	Graphic use interface
SSPR	Solid self-pierce riveting
USP	Unique selling point
UHR	Underhead radius
UTS	Ultimate tensile strength
AC6111	6xxx series aluminium alloy in temper T4 (anti corrodal)
AC600	6xxx series aluminium alloy in temper T4 (anti corrodal)
AC300	6xxx series aluminium alloy in temper T61 (anti corrodal)
RC5754	5xxx series aluminium alloy with recycled content
DP600	Dual phase steel with 600 MPa hardness
DP900	Dual phase steel with 900 MPa hardness
$R_{p0.2}$	Yield point
R_m	Ultimate tensile strength
DC04	Mild steel grade

Word Template by Styles and Wrapper 2014

1 INTRODUCTION & OBJECTIVES

1.1 Trend towards aluminium and mixed metal car bodies

The assembly of car bodies used to be mainly achieved by spot welding of mild steel, but in recent years the demand for lighter, more fuel efficient vehicles and electric vehicles, combined with the conflicting consumer demand for stronger structures to achieve 5 star crash protection has led to a shift away from 350MPa mild steels and towards using lighter and stronger material combination. These are mainly combinations of 200 to 350MPa 6XXX series aluminium, 300 to 450MPa 7XXX series aluminium, 600 to 1000MPa High Strength Steels (HSS), and 1200 to 1500MPa Ultra High Strength Steels (UHSS) (Briskham, 2016).

The major steel and aluminium producers are competing to get their materials onto new car body platforms by striving to produce stronger Ultra High Strength (UHS) grades of material to enable thinner components to be designed to provide attractive weight savings (Whitacre, 2019). The bar chart in Figure 1 shows an example of a recent publication by Novelis, the leading automotive aluminium sheet producer, comparing its current and planned future grades of 6XXX and 7XXX series Ultra High Strength Aluminium (UHSAL) against the latest grades of Ultra High Strength Steels (UHSS), also known as Advanced High Strength Steels (AHSS) which offer the advantage of high strength but also have lowered ductility as shown in Figure 2 . The AHSS & UHSS materials are pressed in a hot condition to enable good formability and then water quenched while still on the forming press to achieve high hardness values, for this reason they are often called Press Hardened Steels (PHS) (WorldAutoSteel, 2017, Tech Spec 2018).

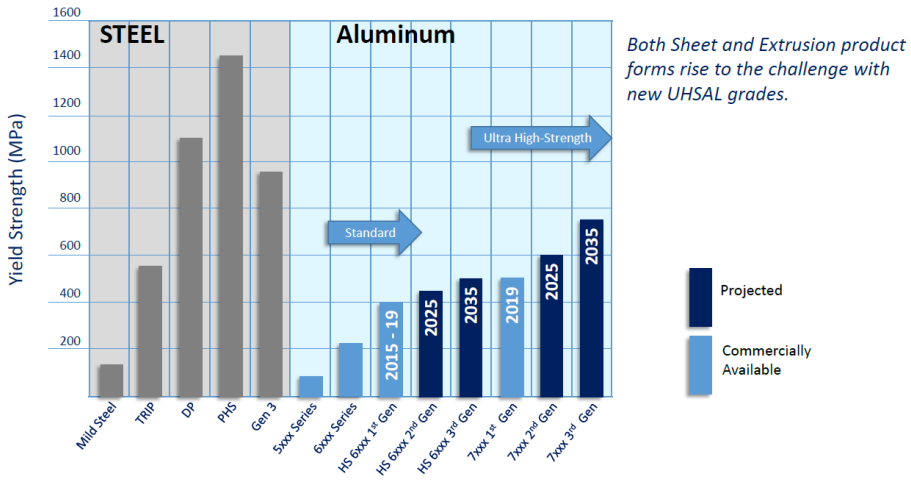

Figure 1, Current and planned future grades of Ultra High Strength Aluminium (UHSAL). (Source Whitacre-2019)

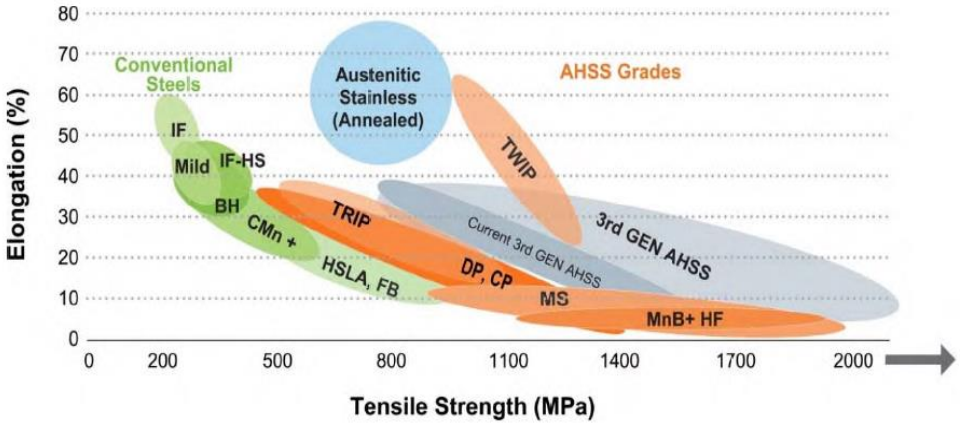

Figure 2, Strength v ductility chart for conventional steel grades versus Advanced High Strength Steel (AHSS) grades (WorldAutoSteel, 2017)

The majority of car makers are now designing car bodies which combine press formed HSS and UHSS with press formed 6XXX aluminium sheet and aluminium die castings. The use of aluminium die castings is helping to simplify the designs by replacing multi-part fabrications. The use of aluminium extrusions has tended to be very little in the past, but is currently rapidly increasing due to extruded profiles being very well suited for making battery case structures to mount underneath the passenger compartment on Battery Electric Vehicles (BEVs) (Tech Spec, 2018).

The standard and most frequently used joining methods, such as spot welding, are not suitable for joining steel to aluminium (Casalino et al, 2008) due to the different melting temperatures and metallurgy of these materials (Abe et al, 2006). Carmakers need reliable mixed material joining methods and the ability to design cars assembled by these joining methods in the virtual world. Self-pierce riveting combined with structural adhesive, known as hybrid joining or rivbonding, has become the primary way to assembly mixed material car bodies and aluminium intensive car bodies. Car makers are currently using around 150m of structural adhesive bead on every car body to create very stiff structures and for the aluminium or steel to aluminium joints the adhesive is usually combined with self-pierce riveting. The current global consumption of self-piercing rivets on car bodies is over 10 billion rivets per year and this is forecast to grow to 20 billion over the next 10 years to support the growing use of mixed material and aluminium on battery powered electric cars (Briskham, 2016).

A recent example of a battery powered electric car where rivbonding was extensively used is the 2018 JLR IPace, shown in Figure 3; this low volume electric car body is a combination of aluminium castings, aluminium sheet and aluminium extrusions, the body is assembled using 2633 rivets combined with 184m of adhesive bead.

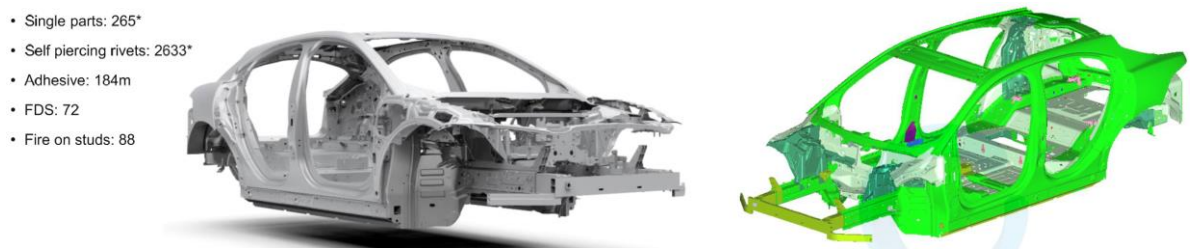

Figure 3, Image of 2018 JLR Electric I-Pace (Source EuroCarBody 2018)

The Cadillac CT6 car body is a good example of the joining of sheet, cast, and extruded aluminium with sheet steel, all joined using Self-pierce riveting combined with structural adhesive, this is one of today's most impressive production examples of a significantly mixed material assembly. The riveted joints attaching the cast shocktower to the sheet metal on the CT6 is shown in Figure 4.

Figure 4, Cadillac CT6 car body showing rivbonding of sheet/cast/extruded aluminium with sheet steel. (Source Visnic 2019)

Due to the high cost of aluminium and its lower strength, the latest high volume cars bodies are tending to use Press Hardened Steel (PHS) to create strong pillars and ring shapes in the crash cage and then clad the crash cage with thin aluminium panels and closures to save weight. A good example of this design trend is the 2017 Audi A7, shown in Figure 5, which employs UHSS to create a strong crash cage (shown in purple) and press formed aluminium (shown in green) for weight reduction (Briskham, 2016, ,Tech Spec, 2019).

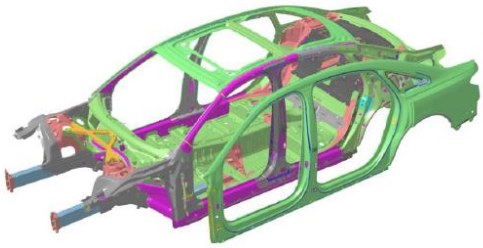

Figure 5 Image of 2017 Audi A7 (Source: JoiningInCarBodyEngineering 2017)

1.2 PhD Objectives

1.2.1 Objective 1 – Selection and Evaluation of the simulation software.

This objective has two stages:

1.2.1.1 Objective 1A: Selection of the software

Before any research work starts, a careful consideration needs to be given to a selection of the FE software to be used. This will be addressed by research into the progress of FE analysis and what software types were used.

1.2.1.2 Objective 1B: Evaluation of the software

This research objective proposes two actions:

Evaluation of accuracy of the 'out of the box' version of software's Simulation template

- The evaluation will be carried out by comparing the results produced by out of the box simulation version of the software without any changes with physical test in order to establish its current capability.
- This activity will be carried out through via two types of activities:
    - Simulation
    - Physical tests

Identification of influencing parameters in 'the out of the box' version of software's Simulation template

- An investigation of parameters that influence the results and extent of this influence is to be conducted as part of this process via sensitivity studies on friction, clamping, temperature.

1.2.2 Objective 2 – Development of the base model

The focus of this objective is to improve the parameters of the out of the box identified as in need of improvement in objective 1 and to develop an optimized and reliable simulation base model that can be used across all simulations of SPR. In order achieve this, a number of simulation sensitivity studies will be conducted and their effect will be analysed and compared with physical testing (Chapter 6 – Experimental stage).

Two parameters that have been identified (amongst others) in objective 1B as not being suitable for AC SPR methods and having most significant effect on the accuracy of the result will be the main focus of this objective and are explained below.

1.2.2.1 Objective 2A: Develop friction parameters for different rivet coatings.

Although friction in SPR has been researched extensively for purposes of simulation, the friction settings found through these studies are usually tightly configured to a small number of very similar joint stacks and assume all rivets coatings and therefore fail to simulate the effect of different rivet coatings. The research task proposed is to investigate the friction settings and values in the simulation model to determine appropriate settings for standard and low friction rivet coatings.

1.2.2.2 Objective 2B: Investigate the effect of different joint stack clamping methods using simulation

When inserting a rivet, the sheet stack can be clamped in different ways, such as a pre-clamp before rivet insertion, an instant clamp at the start of rivet insertion, or an intermediate clamp during rivet insertion. The choice of clamping method is known to influence the riveting result for some types of joint stack. Little or no work has been carried out and published on this topic. The research task proposed is to determine the effect of the clamping by comparing pre-clamp with intermediate clamp methods and then reflect this process in the base simulation model to enable correct simulation of this part of the process.

1.2.3 Objective 3 – Application of base model

This research objective aims to apply to the optimized simulation base model developed as part of the objective 2 to real case scenarios. The initial purpose of practical application is to validate the optimized base model by comparing the simulation results to the physical results and to inform the author whether any further changes need to be made to the optimized model. Once this interactive process has led to a fully optimized simulation model providing accurate and reliable results, the simulation model can be then utilized in further studies. This involves simulation of new rivet types and processes in the field of SPR as well as supporting R&D with design of new rivets via sensitivity studies aimed at determining tolerances and robustness of new products in production.

These sub-objectives are described below in greater detail:

1.2.3.1 Objective 3A: Apply SPR simulation to fully tubular rivets

Until recently all SPR rivets were semi-tubular, Atlas Copco recently launched a new type of SPR rivet which is fully tubular and has a new low friction coating. Simulation studies have not yet been conducted and published on this new type of rivet and major customers like Ford & JLR want to be able to simulate joining with this rivet. The research task proposed is to apply the base model developed in objective 1 to this new type of rivet and determine the parameters required to perform accurate simulations.

1.2.3.2 Objective 3B: Apply SPR simulation to mixed material riveting of UHSS to aluminium

SPR was developed for aluminium to aluminium joining but is currently being adapted for joining very high strength hot stamp steels to aluminium which is one its biggest challenges. Joining these materials requires the development of new rivet designs. Little or no previous SPR simulation work has been conducted on riveting UHSS to aluminium in the field so far. The research task proposed is to apply the base model developed in objective 1 to simulate the new rivet designs being developed for this new joint stack requirement to determine the parameters required to perform accurate simulations and support the development and testing of the new rivet designs.

1.2.3.3 Objective 3C: Apply SPR simulation to the new development of joining narrow flanges

Car companies are seeking to reduce the size of the pillars in cars to improve driver visibility and reduce weight. To do this they are requesting SPR be adapted to work on narrow flanges, this requires the development of a new smaller nose and die for the equipment and new smaller rivet sizes. The research task proposed is to modify the base model developed in objective 1 to employ the new smaller nose and die diameter, and to test this with new smaller development rivet designs.

1.2.3.4 Objective 3D: Apply SPR simulation to the new swage solid SPR riveting joining process

As mentioned also in objective 3B, a challenge for joining industry is the ever improving materials which are increasing in hardness in order to reduce weight. Whilst there is already rivet for UHSS materials on top sheet, the UHSS bottom sheet remains a challenge requesting SPR joining solutions for joints with UHSS on the bottom sheet which are not possible with conventional SPR due to a ductile bottom sheet being required. A new solid type of SPR riveting is being developed for making this type of joint. The research task proposed is to develop and validate a simulation model for this new type of riveting.

1.2.4 Objective 4 – Utilization of validated simulation models

Following the application of the simulation model to a variety of new products with various changes to the model to account for these, and their successful validation with physical tests in laboratory conditions, it is possible to try to see how can these simulation models further benefit to the industry. An area that cannot be examined in laboratory conditions is a manufacturing variability i.e. the fact that small changes to the production of rivet or sheets (batch to batch variablility) can ultimately result in a different outcome for the joint and simulation could be used to map out these differences and potentially improve this. As part of this exercise, the base models for tubular narrow flange rivet (T4 rivet) and higher column strength rivet (BG rivet) were utilized to conduct entire studies that would evaluate a process window for these products.

1.2.4.1 Objective 4A: Process window simulation for tolerance range of sheet material and rivet properties

A significant weakness of the current physical lab testing approach is that the lab can only test the material and rivets supplied, they cannot test the range of material and rivet properties that could be supplied to a production line. One of the most obvious uses for SPR simulation is to expand on the capabilities of physical testing by simulating upper and lower tolerances to check if the proposed rivet and die solution has a suitable process window to be robust in a production environment. The research task proposed is to apply the base model developed in objective 1 with upper and lower values for sheet and rivet material properties to investigate the effect on joint quality to check process window.

1.2.4.2 Objective 4B: Explore using SPR Simulation to aid the design and optimisation of new rivets

Testing small changes in the rivet design on a range of joint stacks by physical lab work is time consuming and expensive as each design has to be machined, heat treated, coated, inserted, cross sectioned and measured. The result is that rivets developed by physical testing alone are not highly optimised due to it only being possible to evaluate a small number of design changes. The research task proposed is to apply the base model developed in objective 1 to evaluate making a series of changes to a rivet geometry to investigate optimisation of the design and also the production tolerances required on the rivet geometry to ensure consistently good joining results in production.

1.3 Overview of the thesis structure

Chapter number	Chapter name	Brief description
1	Introduction and Objectives	The purpose of this section is to outline the challenging demands of automotive industry on joining and explain the rationale and objectives of this work.
2	Review of Self-pierce riveting (SPR)	A detailed introduction to SPR method. The chapter further covers various aspects of this method such as advantages and disadvantages, its current use and innovations in field of SPR.
3	Review of Finite element Analysis (FEA)	An introduction to FEA which outlines types, stages of FEA and covers specific methods used by Simufact software.
4	Review of FEA in context of SPR	This chapter aims to explain various aspects that are specific to setting up a process of SPR simulation FEA such as insertion methods, clamping of the rivet throughput the process, friction etc. This chapter further details the latest status of simulation of SPR.
5	Research methods	A brief outline of the research methods used throughout this thesis for both physical and simulation tests.
6	Experimental stage	This chapter focuses on establish a working simulation model through exploration of SPR simulation process parameters and their effects on the process via a number of sensitivity studies. This includes process parameters such as materials definitions, damage criteria, meshing, clamping etc.
7	Practical applications	The aim of this chapter is a practical application of the simulation model developed in chapter 6 to real case scenarios to obtain feedback and test its viability.

Chapter number	Chapter name	Brief description
8	Discussion	This chapter discusses the findings of the literature review and the experimental simulation studies in relation to the objectives set for this research project.
9	Conclusions	This chapter aims to bring the research together by determining whether the objectives of the PhD thesis were met.

2 REVIEW OF SELF PIERCE RIVETING (SPR)

The two main elements of SPR are the self-piercing rivet and the die, an example of the most commonly used rivet and die designs are shown in Figure 6 below. The standard industry terms assigned to the different features on the rivet and die design are explained in the image below.

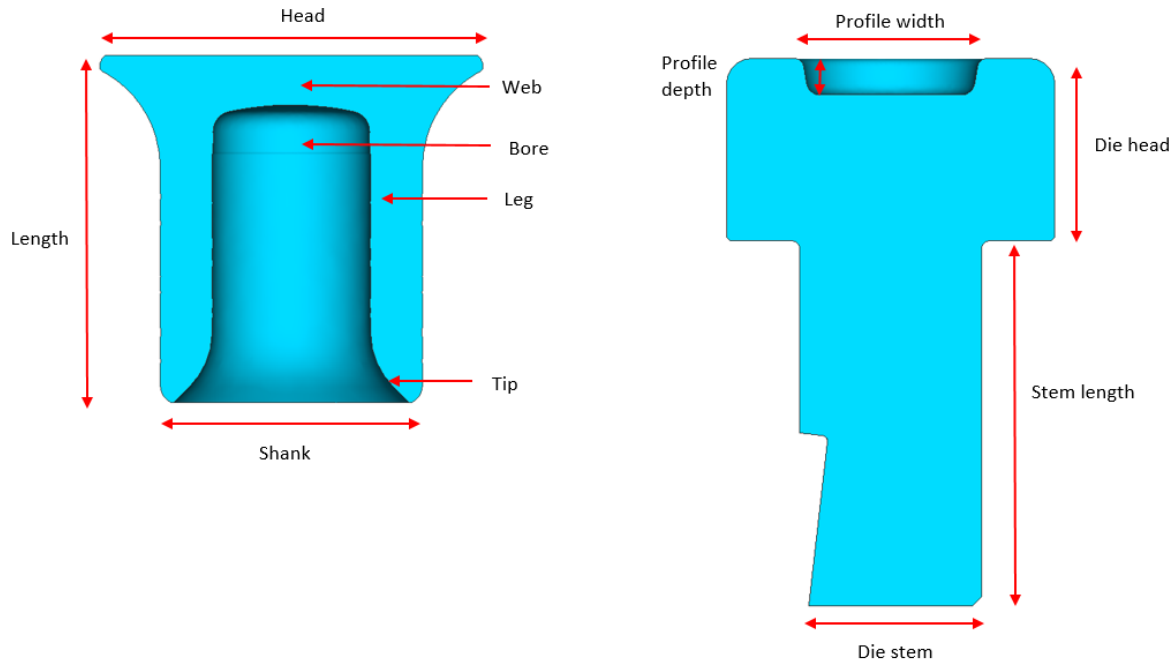

Figure 6, Nomenclature of the industry terms assigned to different parts of the rivet and die

2.1 Self-Pierce Riveting - Introduction

The self-pierce riveting is a cold forming joining method where a tubular rivet is inserted into a stack of sheets by a punch positioned centrally over a die. The rivet pierces the top sheet and the displaced material flows into a die, the pressure on the rivet skirt created by the progressive filling of the die causes the rivet to flare into the bottom sheet to create a mechanical interlock.

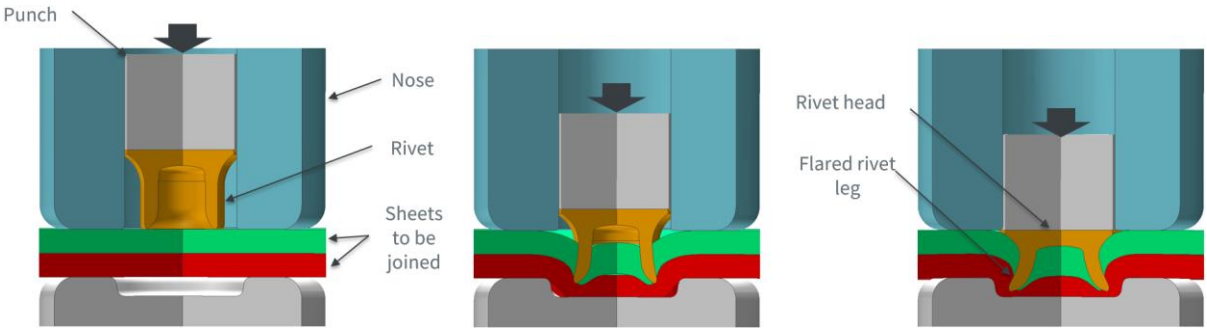

Figure 7 Schematic of SPR process drawn by the author

If rivet and die are selected in accordance with the material properties, the rivet does not pierce through the bottom sheet, this is the main advantage of the SPR process because it enables car makers to rivet from the dry inside the car to the wet area outside the car without breaking through to the wet side. This avoids exposing the fastener to the corrosive wet environment on the underside of the car (Casalino 2008).

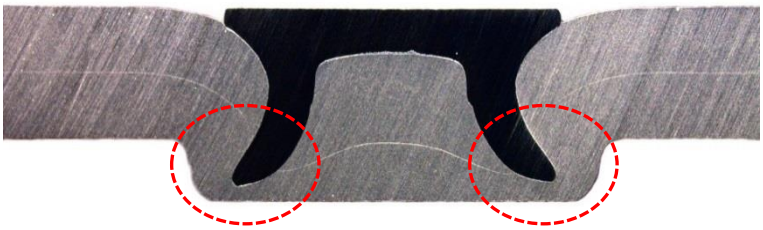

Figure 8, Example of a cross section of SPR joint showing the rivet does not pierce through the bottom sheet (SPR ES, 2018).

Whilst there are useful advantages to using SPR over aluminium spot welding, such as much greater fatigue life (Briskham, 2016), there are also some drawbacks to the process. One of the main issues car producers experience difficulties with is the number of process variables (He et al, 2007) affecting the mechanical behaviour of a joint. The process variables require extensive physical testing, firstly to confirm joining feasibility, and then to create groups of joint stacks to assign a number of different joint stacks to one robot tool running two rivet types and one die. (Carandente at al, 2016);The main aim of the physical testing being to find robust joining solutions with large process windows avoiding marginal combinations that risk causing consistency issues in production. An example of a production issue that car makers seek to avoid is the rivet breaking through the bottom sheet, as this condition exposes the rivet tips to the wet side of the car body and in severe cases can result in the formed button separating from the bottom sheet and falling off leaving the whole of the rivet bore exposed to the wet side of the vehicle.

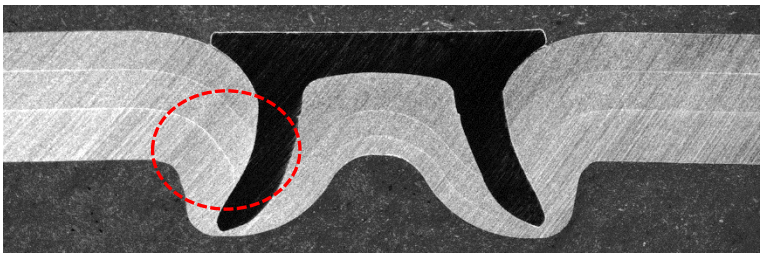

Figure 9, Marginal SPR joint with low bottom sheet thickness ‘Tmin’ on left leg (SPR ES, 2018)

Extensive physical lab testing requires a lot of staff labour and consumes a lot of sample material. There are a number of steps involved in the process such as obtaining representative materials to test, cutting these materials into test coupons, conducting riveting tests, cross sectioning the joints,

photographing measuring the joints, then analysing the results to determine which parameters are most suitable for use on the production line.

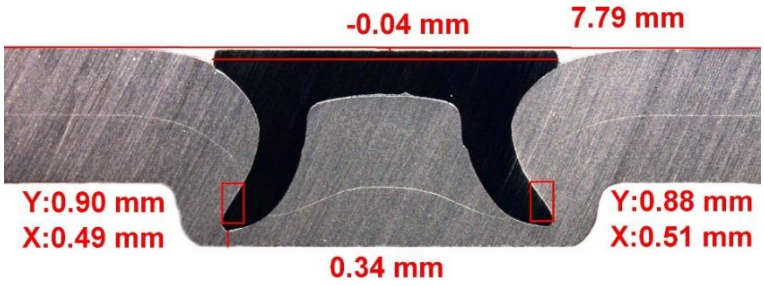

Figure 10, Image of cross sectioned joints with measurements (SPR ES, 2018)

Most rivet insertion equipment (called rivet setters) are limited to riveting joints using one die and two rivets. This means that even after a satisfactory rivet & die solution has been achieved for a specific joint in the initial feasibility testing, the need to group joint stacks onto the same tool to minimise the amount of equipment required means a lot more testing is required to find one solution that works for a number of different joint stacks. The number of stacks assigned to one setter can be as high as eleven, and these will usually include a range of stack thicknesses, this makes it a difficult task to find a rivet length and die depth that is optimal for every stack, which means some of the stacks need to be made using non-optimal rivet types; this reduces the process window available to cope with process variables. Simulation has great potential to conduct optimisation routines to help with finding the most optimum joint groups to provide the best available process window.

A good example of the cost and challenge of conducting this work using only physical testing was a recent three year lab testing project conducted for the Jaguar-XE and F-Pace production line. The project task was to select the rivets and die grouping to produce 250 different joint stacks with the minimum number of robot cells. This study required 40,000 physical rivet insertion tests, consuming 100,000 coupons of material and 5,000 hours of staff time.

The total cost of conducting this physical testing study was over 1 million pounds (Henrob 2016) Following this very expensive study a clear mandate was set to develop the ability to simulate the rivet insertion to reduce the amount of physical lab testing required and the time required to design the riveting cell layout.

The project mentioned above was an all aluminium car body structure, the rapid introduction by car makers of mixed material steel/aluminium car bodies means there are now increased challenges involved in conducting joint feasibility and grouping studies. A number of new designs of rivet need to be developed over the next few years to keep up with the changing material types and combinations being used by car body designers. The process of designing new rivets has historically been done by

physically making and testing every design iteration, this is a very slow and expensive approach, which does not allow the new designs to be fully optimised to a) cover a wide range of joint stacks, or b) cope with a wide range of material properties.

The use of simulation has massive potential to aid the development of new rivet designs by enabling more optimisation of the designs to be conducted, and enabling the evaluation of a wider range of joint stack combinations. Perhaps the biggest benefit of using simulation is that physical testing can only test the material condition that is supplied for testing, it is not usually possible to get materials in an upper and lower ductility condition; simulation enables these upper and lower material conditions to be tested, this will give a much higher confidence level in the ability of the chosen solution to cope with the variations of a real production line.

From the above explanation it is clear that investing in the development of rivet insertion simulation is very justified with a strong business case. This research project has potential to help the Atlas Copco SPR business in two key areas: 1) The initial joining feasibility testing followed by the joint stack grouping studies conducted during the layout planning of car assembly lines, 2) The design and optimisation of new rivet and die designs for joining new material combinations.

To remain a leading SPR company Atlas Copco a key part of the companies R&D strategy is to develop simulation solutions for these two market requirements. To implement this strategy Atlas Copco contacted Sheffield University to organise a case award PhD project and set these industry needs were as the main objectives of the PhD project.

2.2 Evolution of SPR from 1970 to present day

Self-pierce riveting was invented in Australia in 1970's for making aluminium ladders. The original concept used a solid rivet which was driven through two aluminium sheets onto a fluted die, which split the rivet into three parts and folded these outwards to form a mechanical interlock. (Briskham, 2016).

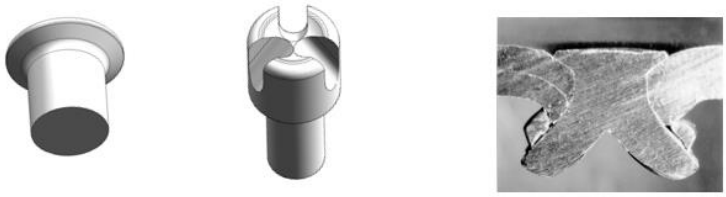

Figure 11, Initial design of solid SPR invented in 1970s for producing aluminium ladders.

In the 1980's a semi-tubular rivet design was developed to enable the rivet to flare inside the bottom sheet so that it could remain contained within the bottom sheet and not break through. The initial semi-tubular design had a square tip geometry and required the use of a die with a raised central pip to create the pressure needed on the rivet skirt to flare the rivet to create a mechanical interlock. (Briskham, 2016). This early rivet design was mainly used for assembling steel framed buildings.

Figure 12, Initial Semi-tubular SPR design with square rivet tips

In the 1990s Audi developed the first riveted and bonded aluminium intensive car, called the A8, for this project the rivet design needed to be improved; the semi tubular rivet was changed to have a thin 1mm web and given a shaped rivet tip geometry (Litherland, 2016). The profiled tapered shape of the rivet tips enabled the rivet to self-flare inside the bottom sheet when the die became full and the pressure on the tips increased.

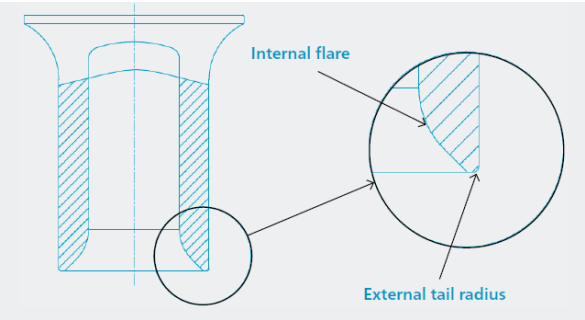

Figure 13, Profiled shape of the rivet tips introduce in the 1990s to create the C-rivet. (Atlas Copco Rivet Brochure 2019)

The self-flaring ability enabled flat bottom dies to be introduced as dies with a raised central pip were no longer needed. (Briskham, 2016). The new semi tubular rivets developed for the Audi A8 project were called C-rivets and this rivet design is still widely used today.

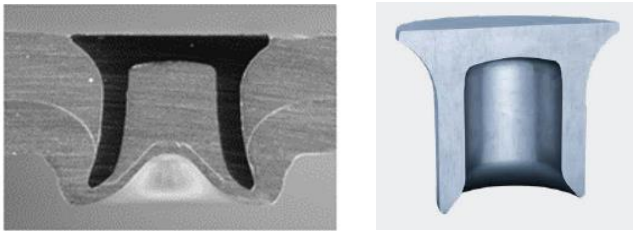

Figure 14, the first rivet design with a thin web and profiled tip geometry was called the C-rivet (Briskham, 2016).

The C-rivet was given a thin wall thickness to encourage the rivet to flare inside thinner joint stacks. In the early cars SPR joining was restricted to two thickness (2T) joints, this avoided the need to join three layers together using longer rivets.

To extend the riveting capability to thicker joint stacks a rivet design with a slightly thicker wall thickness was developed, this stronger rivet was called the K-rivet. The main difference between a C-rivet and a K-rivet is that the wall thickness is slight thicker on the K-rivet.

C-rivets are used for joints requiring rivet lengths from 3mm to 6.5mm, K-rivets are used for joints requiring rivet lengths between 7mm to 11mm. (Briskham, 2016). These two rivet designs are excellent for a wide range of aluminium to aluminium joints and have been the most commonly used rivet types for the last twenty years. (Litherland, 2016)

C-rivets have a thin 1mm web, this enables them to make 3 thickness (3T) joints. In contrast the longer K-rivets have a thicker web and this makes them unsuitable for making 3T joints. The reason K-rivets have a thicker web is simply that all lengths of K-rivet are forged with the same bore depth as the 6.5mm long C-rivets, so as the K-rivets length increases the web thickness also increases, (Briskham, 2016).

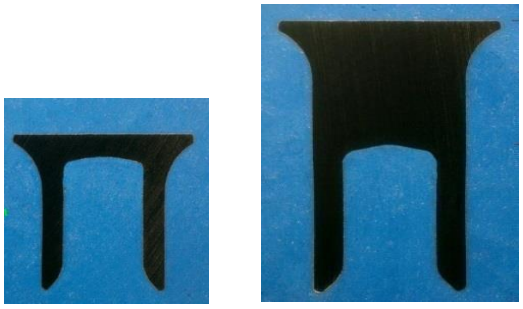

Figure 15, Cross section of C-rivet left & K-rivet right, showing the greater web & leg thickness on K-rivets.

The early aluminium car structures were made using a very ductile and easy to rivet AA5754 alloy, which enabled deep dies to be used. In 2003 car makers started to test stronger lower ductility 6XXX alloys, such as AA6111 and AA6451, by 2008 they were ready to use these stronger alloys to make car bodies. This created a challenge for the riveting as K-rivets were not capable of making thick stack joints in 6XXX alloys.

In 2012 Ford and JLR requested a new rivet be developed for riveting three layer joints of 3mm thick 6XXX materials, because this joint stack was required to enable the planned design for both the new F150 truck and XE car body structures. (Briskham, 2016). The problem Ford and JLR were facing was that 6XXX alloys have limited ductility and cannot be riveted with the deep die that is needed by the K-rivet due to its thick rivet web. A new rivet design with a much smaller web thickness was needed to enable a shallow die to be used with long rivets. The new rivet design had to have the same external dimensions as the C-rivet and K-rivet to enable it to be used in the same standard rivet feeding and setting equipment. The solution found was to completely remove the rivet web on the K-rivet and create a fully tubular version of the rivet called the T-rivet. The T-rivet was launched in 2014, the first production vehicles made using the T-rivet were the Ford F150 & F250, Jaguar XE & F-Pace.

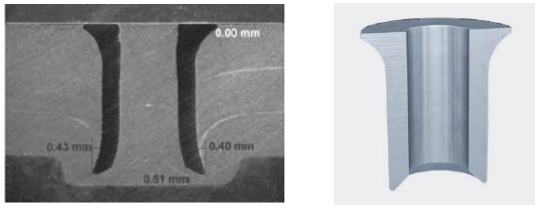

Figure 16, Fully tubular rivet for thick stack aluminium joints, known as the T-rivet

The extra bore volume created inside the rivet by removing the rivet web enabled a lot more aluminium to be displaced upwards inside the rivet meaning the shallow dies required with low ductility 6XXX alloys could be used. (Briskham, 2016). Figure 17, shows the huge improvement in joint quality gained using a T-rivet with no web compared to a K-rivet with a thick web for joining a joint with three layers of 3mm aluminium. This image shows very clearly why Ford and JLR could not use the K-rivet and requested a new rivet solution to be developed.

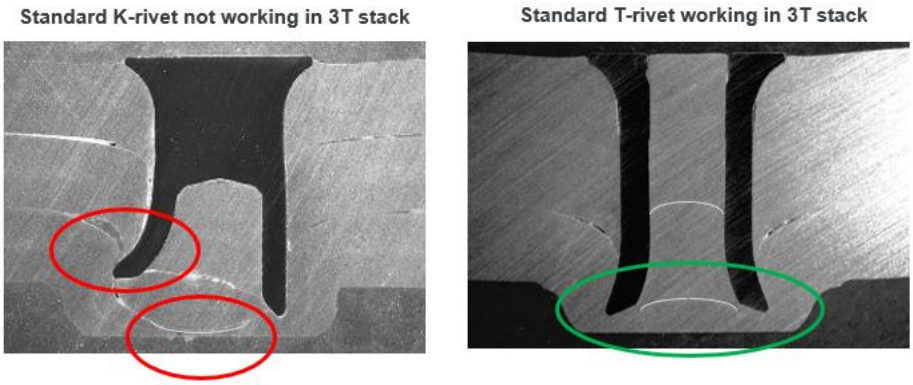

Figure 17, Semi-tubular versus fully tubular rivet in 3.0mm+3.0mm+3.0mm AA6111

The original C-rivet was made in a 5mm diameter shank version for structural joining on car bodies, and in a 3mm diameter shank version for non-structural joining on closures such as doors and bonnets. The 3mm diameter shank C-rivet is able to rivet stacks with a minimum 1mm bottom sheet thickness and for a number of years this was enough to meet the demands of the car industry. However, car makers are now under pressure to use even thinner materials to reduce vehicle weight.

In 2017 Ford asked for help to make a joint 0.8mm to 0.8mm thick for a new light weight door designed to be used on the new Ford Explorer. When very thin bottom sheets are used the standard C-rivets do not flare enough and can break through the bottom sheet. If the rivet almost breaks through in a lab test this is classed as a fail because in production the process variable could cause a marginal joint to switch to a fail condition.

The simple solution found was to make a new version of the C-rivet with a much sharper rivet tip. The sharper tip caused the rivet to flare more rapidly preventing the rivet tips from breaking through the thin bottom sheet. The new modified design of C-rivet was called the A-rivet and was first used in vehicle production to make the aluminium doors for the new Ford explorer launched in 2019.

Figure 18, Successful riveting of very thin 0.75mm to 0.75mm aluminium for a car door using sharp tip A-rivet.

The same solution was used to create a 5mm shank diameter version of the A-rivet for making structural joints on car bodies where joints with thin bottom sheets were required. Figure 19 shows a failure result in bottom sheet thickness using a C-rivet, versus a much better bottom sheet thickness result for an A-rivet. The new 5mm A-rivet will first be used in 2020 in Japan on a new model of Nissan where thin sheets needed to be joined to enable a lightweight construction.

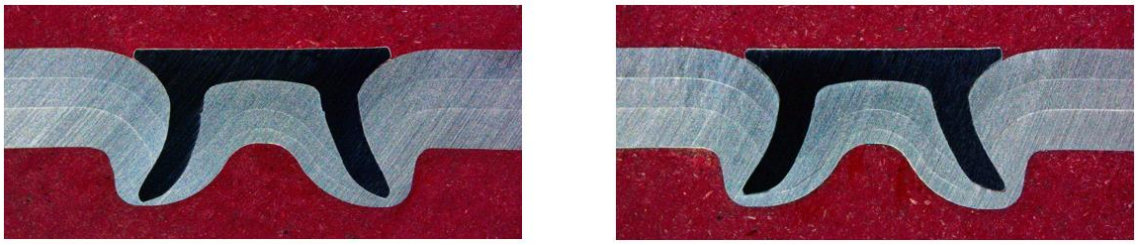

Figure 19, 3T aluminium joint 0.9mm Ac600 + 0.9mm Ac170 + 1.2mm RC5754, C-rivet fail (right) versus A-rivet pass (left)

SPR was developed for joining aluminium but most of the latest car models are using a mix of ultra-high strength steel and aluminium. The new generation of car bodies are using Press Hardened Steel (PHS) to produce a strong safety cage with thin steel sheet for maximum passenger protection while achieving some light weighting compared to using thicker conventional steels. The high strength steel crash structure is being combined with aluminium to gain some weight reductions on other parts of the car body, this combination is enabling these cars to be fitted electric drive systems.

This trend is being followed by all of the car companies, in the last three years several car companies have contacted Atlas Copco to request riveting solutions for joining Ultra-High Strength Steel (UHSS) to aluminium to enable these new generation of mixed material car bodies to be made.

To meet this new market demand a new rivet called the BG-rivet has recently been developed, the new rivet has a thick shank to provide the column strength needed to pierce through UHSS and has a shaped rivet tip to enable flaring into the aluminium bottom sheet. The BG-rivet has been predominantly designed for a PHS material called Usibor which is a UHSS specifically made for automotive applications by Arcilor Mittal.

Due to its high mechanical strength, UHSS allows 30% to 50% weight saving as opposed to other cold rolled grades (Matweb.com, 2019), which is why this material is being used in many new car models. Figure 20, shows an example of a UHSS to aluminium joint made using the new BG-rivet. The first production vehicle to be made with the new BG rivet with be the Jaguar electric MLA platform launching in 2020, and an electric car made in China by a new car company called Ai-Ways also launching in 2020.

Figure 20, Picture of the latest rivet design called the BG-rivet, developed for joining UHSS to aluminium

The car makers are planning to use even stronger and thinner materials on the future generations of car bodies and there is a clear requirement for Atlas Copco to invest in R&D work during the next five years to develop new rivet designs for joining these materials. Simulation of the rivet insertion will play a big role in this rivet development work and also in the testing of different joint stacks to choose and the rivet and die solutions for each group of joint stacks.

2.3 Rivet types

The riveting parameters involved in making an SPR joint are listed in Figure 21 below.

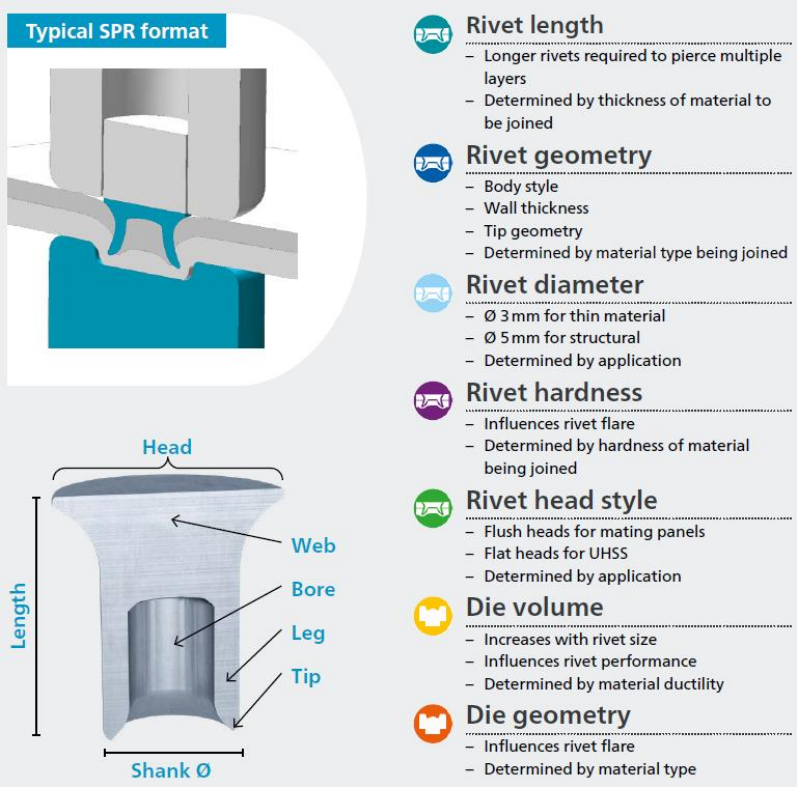

Figure 21, Riveting parameters involved in making a good SPR joint (SPR ES, 2016, with support from the author)

2.3.1 Rivet length

Rivets produced by Atlas Copco have a length range from 3.25mm to 19mm. Originally the rivets were only made at 1mm length intervals. When the materials being joined by the customers changed from easy to rivet 5XXX alloys to less ductile 6XXX alloys, 0.5mm length intervals were added. Recently the introduction of very thin material such as 0.8mm aluminium has required the introduction of 0.25mm increments for the short rivets used for joining closures. The table shows the available lengths of the rivet which generally cover the requirements of the stacks.

The 'XX' code specifies the nominal rivet length, L. See tables below:

xxxxxxAxxx/xxxx
xxxxxxCxxx/xxxx

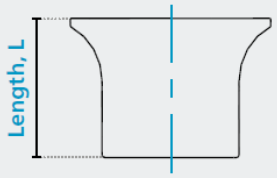

xxxxxxMxxx/xxxx
xxxxxxLxxx/xxxx

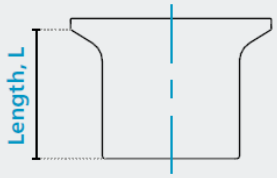

xxxxxxPxxx/xxxx
xxxxxxFxxx/xxxx

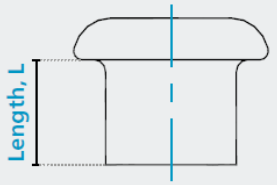

XX code	Length, L (mm)	XX code	Length, L (mm)
0F	3.25	09	9.0
0N	3.5	0C	9.5
0J	3.75	10	10.0
04	4.0	1C	10.5
0P	4.25	11	11.0
0E	4.5	1K	11.5
0B	4.75	12	12.0
05	5.0	1D	12.5
0G	5.5	13	13.0
06	6.0	1E	13.5
0D	6.5	14	14.0
07	7.0	15	15.0
0M	7.5	16	16.0
08	8.0	18	18.0
0A	8.5	19	19.0

Table 1, Rivet length availability table (Atlas Copco Rivet Brochure 2019)

2.3.2 Rivet Types and Head Styles

The most widely used automotive rivets have already been introduced in the overview of how SPR developed. Figure 22 below shows the range of standard rivet types.

Most automotive joints are made using countersink head rivets to achieve a flush surface to enable other parts to be added later without the rivet heads getting in the way. Figure 22 below shows the range of standard rivet head styles.

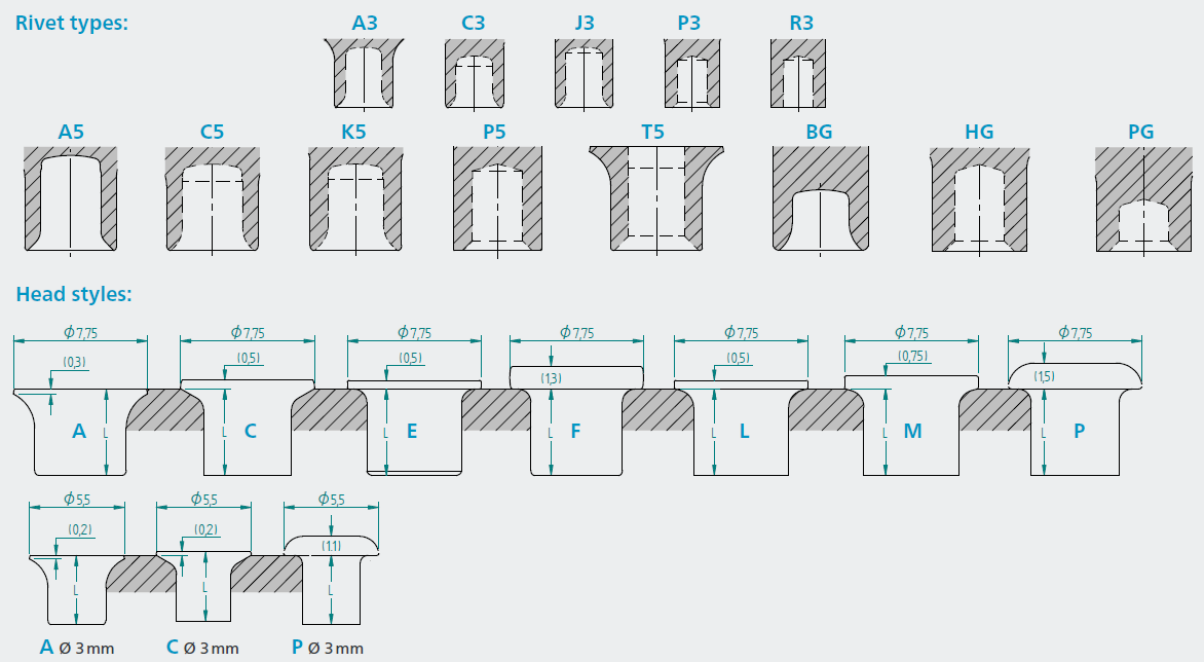

Figure 22, Diagram showing the standard Figure 23rivet types and head styles. (Atlas Copco Rivet Brochure 2019)

2.3.3 Rivet diameter

- 3.0mm shank diameter rivet, these are used for thin materials for non-structural joining.
- 5.0mm shank diameter rivet, these are used for structural joining of aluminium or mild steel.
- 5.5mm shank diameter rivet, these are used for structural joining of high strength steel.

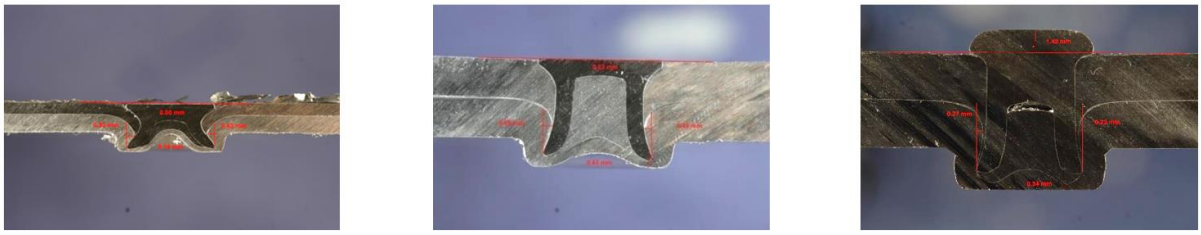

Figure 24, Cross section image showing 3mm, 5mm and 5.5mm shank dimater rivets

2.3.4 Rivet hardness

Rivets are made by a forging and extrusion process using cold forming boron steel wire and they go through four main process stages as shown below:

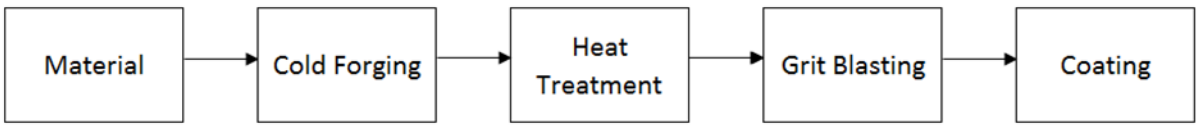

Figure 25, Rivet Production Process (Clarke, 2007)

It is the heat treatment stage that determines the hardness of rivets, the rivets are all hardened at the same 900^{o}C temperature and oil quenched to achieve a fully martensitic structure, then tempered at different temperatures to achieve different hardness levels, these are shown in Table 2 below.

Due to new aluminium alloys being employed by car makers, extra hardness levels have been introduced for the softer rivets. From Table 2 below, it can be seen that between levels 2 to 6 there is a small overlap in Hv range in each of the neighbouring hardness levels. Previously, between hardness levels 1 to 2, there was no overlap which resulted in the rivet design process window having a gap to remove this gap, two new hardness levels, G and H, were introduced.

Heat treatment level	Hardness range (Hv 10kgf)
0	As forged
1	255-305
G	290-350
H	330-390
2	380-440
3	420-480
4	450-510
5	480-540
6	530-580
7	550-600

Table 2, Table showing the standard hardness levels available for rivets.

Hardness of the rivet can have a great effect on the quality of the joint depending on the material used as substrates. The below pictures illustrate this by showing the same joint with an Aluminium top sheet and two subsequent layers of mild steel. The first joint is using rivet level H1 whilst the next one is using level H2. The H1 rivet, due to being softer is not able to pierce the steel and is forced to flare out excessively in the aluminium layer. Using the harder H2 rivet sees an improvement in the joint and the rivet manages to pierce through the steel layer and flare out to a reasonable extent.

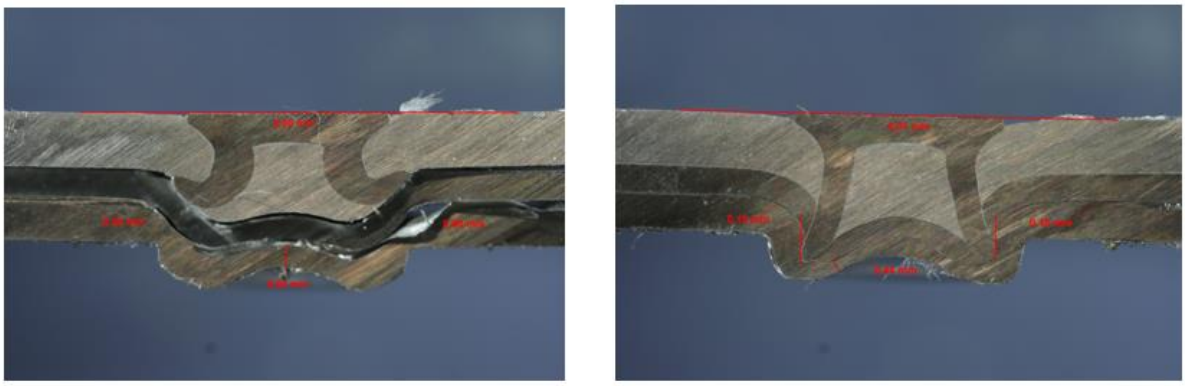

Figure 26, Illustration of effect of rivet hardness level on rivet insertion - same joint with H1 rivet (left) and H2 rivet (right)

2.3.5 Rivet hole style

- C-rivet and K-rivet: the rivet has a flared hole with a thin web, also referred to as semi-tubular.
- T-rivet: the rivet has a flared hole with web removed, also referred to as fully tubular.
- PG-rivet and BG-rivet: this rivet has a flared hole with a thick web, also referred to as semi-tubular.

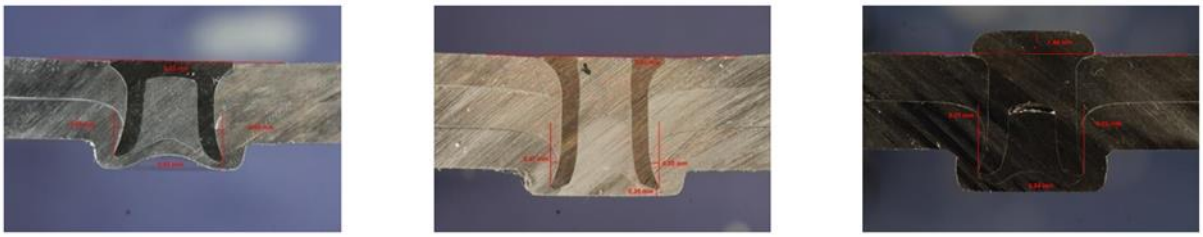

Figure 27, Images of C-rivet, T-rivet, and PG-rivet

2.4 Die types

Die geometry is not as intricate as the rivet geometry, but the shape and volume of the die cavity are equally important in producing a good quality joint. There are many different die types, many of them have been designed for very specific joint stack applications. 90% of joints are made using just three die types, these are DG, DP and DZ.

- 'DG' profile style – Flat bottomed die profile, normally used with Ø3mm, Ø5mm and Ø5.5mm rivets and preferred profile due to low wear and good damage tolerance.
- 'DP' profile style – Radiused die profile with small central pip, normally used with Ø3mm and Ø5mm rivets.
- 'DZ' profile style – Radiused die profile with large central pip, normally used with Ø3mm and Ø5mm rivets and useful when joining thin sheets.

Figure 28, From left to right,3D dwg of DG, DP and DZ type dies.

Different length rivets and different rivet web thicknesses require different die cavity volumes, the die cavity is adjusted in small incremental steps by adjusting the die depth from 1.mm to 2.4mm deep 0.2mm increments and adjusting the die diameter from 6.0mm to 11mm in 0.5mm increments.

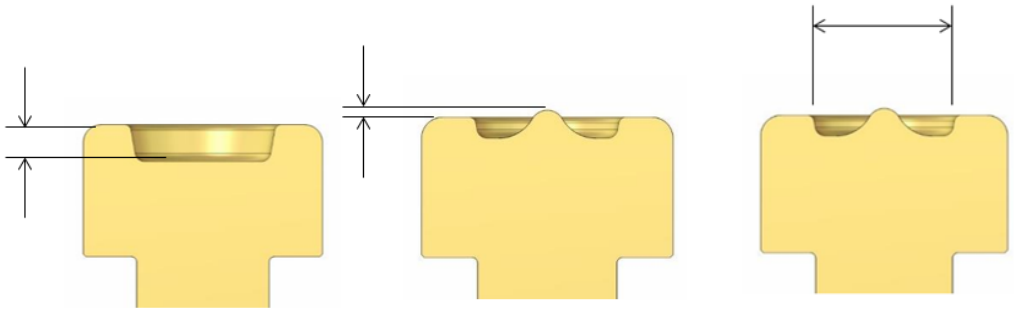

Figure 29, From left to right 2D cross section dwg of DG, DP and DZ type dies.

2.5 Rivet Insertion Equipment types

2.5.1 Simulation of different rivet insertion equipment

The development of rivet insertion simulation opens up the potential for a useful work stream to simulate the difference in riveting results made with different types of rivet insertion tools. For example, the difference between tools which apply a preclamp to the joint stack before inserting the rivet, versus tools which apply a late clamp to the joint stack after the rivet has been inserted. Or for a further example, the difference between tools which achieve different rivet insertion speeds or different maximum insertion forces. (TechSpec 2019)

This PhD project focusses on developing an accurate simulation method for the high speed servo tool because this is by far the most commonly used tool. There is scope to expand this study to investigate the effect of other equipment setups. For example, it would be very useful to be able to accurately simulate the effect of making the same joint stack with different riveting equipment arrangements, such as, the effect of different clamping loads or the effect of different nose and die diameters.

2.5.2 Rivet insertion equipment used in this study for the physical lab tests

The self-piercing rivets used in this thesis were inserted by either using a servo setter where the velocity of the servo riveting tool is the main adjustment control, or by a hydraulic setter where changing the oil pressure is the main adjustment control. There are several different types of equipment that can insert the rivet, these are briefly described below.

2.5.3 RivLite Portable Battery Tool

RivLite tools are primarily used for car crash repair purposes in garages and for low volume car production. The rivlite tool has a proper preclamp function and delivers a rivet insertion force of 50KN, this is an impressive capability for a small portable battery powered tool.

From a riveting capability perspective, the most significant difference compared to the industrial tools used on car assembly lines is that the rivet is inserted much more slowly; the piercing and flow of high strength materials tends to be better when the rivet is inserted at high speed. The second difference is the C-frame deflection tends to be a lot more due to the smaller size of C-frame. (TechSpec 2019)

Figure 30, Rivlite Portable Battery Tool

2.5.4 Hydraulic double acting and pre-clamping tools

Hydraulic double acting tools have an external electrically driven hydraulic powerpack, connected by two hoses to the riveting tool. The setting force exerted by the tool is controlled by adjusting the hydraulic oil pressure, up to a maximum of 210bar with a standard C frame or 250bar with a heavy duty C frame. The hydraulic pressure is adjusted until the correct rivet setting depth is achieved. The rivet setting depth can be limited by installing a shim inside the riveting tool to act as a mechanical stop. Using a shim is common practice for general industry tools that always insert the same rivet into the same stack and require no flexibility.

Hydraulic tools are mainly used for general industry applications where they are mounted on a fixed stand or a hanger tool. Automotive companies do not like to use hydraulic tools due to the difficulty

of feeding hydraulic fluid through pipes onto a robot tool that needs to move into many different positions, and due to the risk of hydraulic oil leakage in the event of pipe damage. (TechSpec 2019).

Figure 31, Picture of stand mounted and hanger mounted hydraulic tools

2.5.5 Servo tools

The Henrob servo electric tool works by adding kinetic energy to a rotating flywheel and then releasing this energy into a linear travel roller screw to create very rapid rivet insertion speeds. The main benefit of this approach is higher insertion speeds compared to a direct drive servo setter and a longer gearbox life due to disconnecting the drive from the insertion punch to avoid stressing the gearbox.

The energy exerted onto the rivet is adjusted by changing the steady state velocity reached by the tool in the flight across space stage before the rivet is inserted. To provide some fine control over the rivet insertion depth the servo motor continues to add some extra energy during the rivet insertion process, this extra energy is torque limited to minimise stress on the equipment. (TechSpec 2019)

This method of rivet insertion gives a high initial speed to pierce the top sheet and then a slower speed for the last stage of flaring the rivet inside the bottom sheet, this approach is believed to be the ideal way to insert a rivet, especially for joints with high strength steel on the top sheet and aluminium on the bottom sheet. (TechSpec 2019)

The Henrob servo tools are capable of achieving insertion forces upto 120kN, but for production applications the tools are limited to 80kN to enable a 10 million cycle tool usage before a major service. Figure 32 below shows a standard Henrob servo tool, in this image the flywheel on top of the setter is clearly visible (TechSpec 2019).

Figure 32, Standard robot mounted Henrob servo tool for blow feed rivet supply

The competitor servo riveting systems use direct drive rivet insertion, the main disadvantage of this approach is slower rivet insertion speeds, the main advantage is the ability to monitor both force and position during the rivet insertion and use these readings to instruct the tool to stop at a max force value or a set position depending on which limit setting is reached first. (TechSpec 2019) Thousands of both types of servo rivet setter are in service at car plants and both approaches have been proven to work well with excellent reliability and very little downtime. Car plants usually have a minimum requirement of 99.8% operating availability for the riveting equipment during each shift

2.6 Advantages and disadvantages of SPR

As with any technology, SPR has some advantages but also some disadvantages in comparison with other methods of sheet material joining. The advantages of using SPR are as follows:

2.6.1 Versatility

As opposed to some other joining methods, SPR allows a number of dissimilar (Barnes, 2000) and unweldable materials such as steel and aluminium, plastic and aluminium, epoxy and aluminium, to be joined (Henrob, 2005). It can also be used with coated and painted materials (e.g. heavily zinc-coated and organic coated sheet material) as well as adhesive (paste or film form) and in some case can join plastics to metal (Gerritsen, 2016).

Compared to conventional solid rivets or blind rivets SPRs create their own hole so there is no need for a predrilled hole (Barnes, 2000) This saves time and manpower thus lowering costs in comparison to other types of riveting and increasing productivity. During car body assembly it is considered

difficult to align pre-made holes in overlapping sheets to insert a rivet, for this reason the use of fasteners that require premade holes is generally avoided on high volume car production. Blind rivets are usually only used on low volume car production lines where mainly manual assembly is used.

Of growing importance is the environmental impact benefits compared to resistance spot welding where toxic fumes are emitted due to vapourising the adhesive between the sheets where they are welded, and where a large amount of electricity is required to generate the resistance heating required to melt highly conductive aluminium sheets. (TechSpec 2019)

Some of the commonly quoted benefits of SPR are listed per below: (Henrob, 2005)

- No sparks, fumes or heat produced during the rivet insertion
- No fume extraction is required, giving an equipment cost and power usage benefit
- No cooling water required, giving an equipment cost and power usage benefit
- No swarf produced during insertion, simplifying cleaning prior to e-coating
- Low noise emission (<80dB), spot welding is louder
- Rivet insertion does not require any heat as it is compatible with adhesives
- Low energy cost per rivet insertion, £0.000085 energy cost per rivet. (TechSpec 2019)
- No waste material is produced (Barnes et al, 2000)

2.6.2 Joint Strength and Fatigue Durability

Using SPR creates joints with better static strength than for example that of spotwelding and better fatigue properties (Barnes et al, 2000, Henrob, 2005) as demonstrated by Figure 33 and Figure 34.

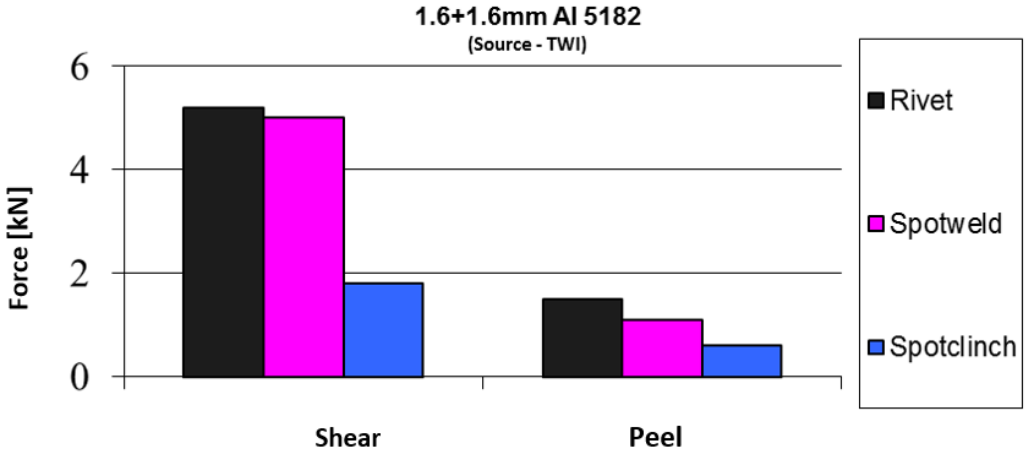

Figure 33, Comparison of static strength of self-pierce riveted joints with joints made using other methods.

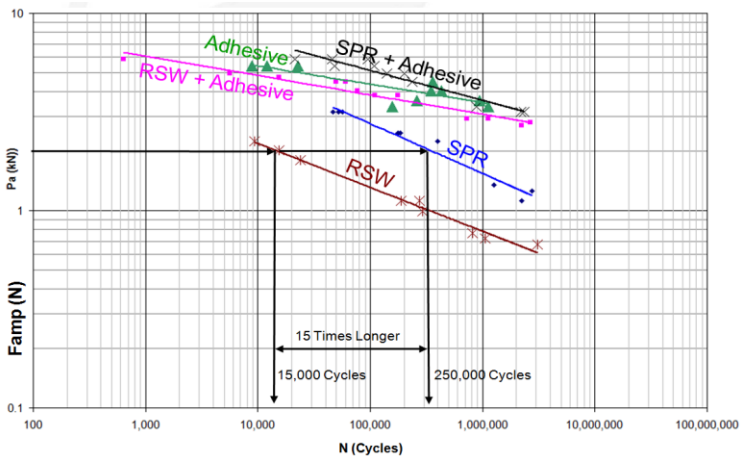

Figure 34, Comparison of fatigue properties of self-pierce riveted joints with joints made using other methods (Blows, 2014)

SPR joints perform very well under cyclic fatigue loading, testing of whole car bodies on four poster test rigs has shown that when a rivet loses its stiffness due to the hole in the aluminium around the rivet growing in size, the load path switches to another rivet, meaning that many rivets have to be fatigue damaged before a significant affect is achieved on the whole body structure.

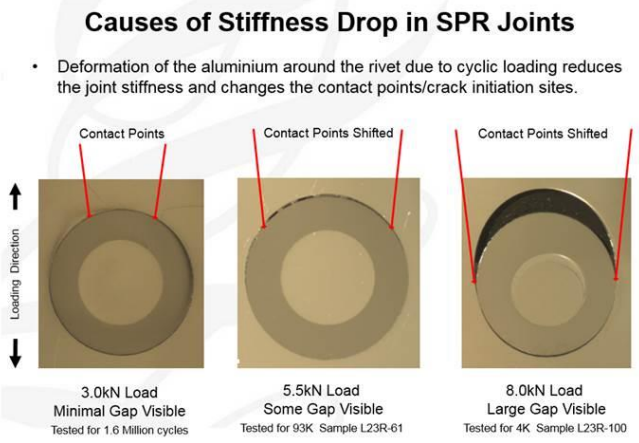

Figure 35, Cross sectioned rivets showing how SPR joints lose stiffness after severe cyclic loading (Blows 2014)

SPR rivets create a water-tight seal which makes them resistant to corrosion due to rivet not piercing the bottom sheet (Vorobyov, 2013). Due to rivet insertion being a cold forming process there are no changes in material properties (on microstructural level) and there is little or no damage to pre-coated materials (Henrob, 2005, Gerritsen, 2016).

The quality of SPR joints can be checked visually to a certain extent e.g. the button is symmetrical, of the correct diameter and shape and with no cracks. The tip of the rivet should not pierce the bottom sheet and the head of the rivet should be close as possible to the top sheet with no gaps under the rivet head (Gerritsen, 2016).

2.6.3 Costs

The cost of rivets has fallen significantly over the last 20 years due to the increased production volumes enabling increased efficiency and utilisation of production plant; the cost of a rivet in 2006 was around 4 to 5 pence, the cost of a rivet in 2019 is around 1 to 2 pence. This makes SPR far more cost competitive per joint against RSW which requires a lot of electrical power (Briskham, 2019). The cost of SPR equipment has also fallen and is now comparable to the cost of the adaptive RSW equipment used for aluminium or UHSS joining (Briskham, 2019). The lower costs are a result of number of combined aspects such as easiness of automation (Barnes, 2000), low energy consumption, fast cycle times, no requirements for pre-drilled holes (Barnes, 2000), water cooling, or extraction systems (Carle and Blount, 1999) all saving time, manpower and additional costs.

In addition, the installation of SPR systems is relatively simple and less costly than for example equipment for welding (Barnes, 2000) as services like water cooling, high ampage electricity, and fume extraction are not required (Henrob, 2005, Vorobyov et al, 2013, Gerritsen, 2016).

There are a few disadvantages to the SPR process which are outlined below.

2.6.4 Access

Access is required to both sides of the joints and an overlap flange large enough an 18mm nose and die are required. (Gerritsen, 2016) C-frame access studies are an important part of planning a SPR production cell to ensure there are no clashes as demonstrated in Figure 36, (Vorobyov 2013). Modern 3D CAD systems make it simple to conduct access studies by importing different setter models into a CAD model of a car body and moving them around to check for clashes.

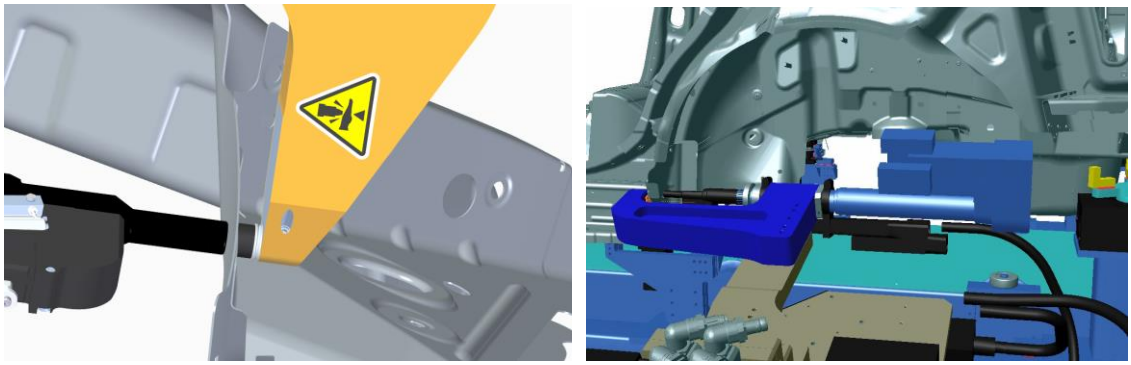

Figure 36, Access studies to check C-frame design needed for self-pierce riveting (Atlas Copco Riveting Guidelines 2019)

2.6.5 High force

Relatively high force is required for this forming process (He 1, 2016) which means that a heavy C-frame is needed to align the nose and the die which might limit the capability of the tool (Gerritsen, 2016).

2.6.6 Process limitations

There are some limitations in terms of the riveting direction, the main requirement is that stacks must have a thick enough sheets at the bottom so that there is enough space for the rivet to flare and to produce strong interlock. (Briskham, 2016, Vorobyov, 2013) as demonstrated in Figure 37.

Figure 37, Rivet insertion direction, left thick bottom sheet, right thin bottom sheet

2.6.7 Permanency of the joint

There is no easy option of removing the joint once the rivet has been set, as the material local to the rivet has been deformed and cold worked, (Gerritsen, 2016). If rivets need to be removed they can be pushed out (extracted) using a handheld rivlite tool with a cone shaped plunger and a hollow die to push on the rivet tail and push the rivet out 'head first' into the hole in the die; removing rivets using this tool is a fast and simple process. Replacement rivets are usually positioned next to where rivets were removed and not in the same location, to avoid the risk of lower performance to work hardening.

2.6.8 Use of consumable (i.e. rivet)

The rivets are the primary costs of this joining technique (Gerritsen, 2016) and it means continued dependency on rivet suppliers. SPR supplies rely on high volume rivet sales to generate most of their operating profits, there is usually a very low profit margin on the equipment, (Briskham, 2016).

2.6.9 Appearance

The presence of a raised button on the die side of the joint is undesirable for some applications. The rivets are usually only used in locations where they will be hidden by trim and will not be visible to the customer using the car. Some car designs require a small number of visible joints, such as joining a car roof panel to a side panel, for these joints laser welding is usually used and the weld surface may be ground and polished before painting. (Gerritsen, 2016).

2.6.10 Not suitable for brittle materials

During the rivet insertion process a large scale plastic deformation occurs and the sheet materials need to have enough ductility to cope with this without cracking. SPR requires a ductile bottom sheet to flow into a die and allow the rivet to flare inside the sheet. The top sheet only needs to be pierced and does not need to be so ductile, but needs to be tough enough to resist cracking.

2.6.11 Each joint needs individual configuration

A key strength of SPR is that it is a repeatable and consistent joining process, however, each joint stack needs the correct configuration of rivet and die. Choosing the rivet type, length, diameter, hardness level, and coating, and combining this with the correct die profile requires good process knowledge and can require a lot of physical lab testing; this work will be significantly aided by the development of simulation.

Current tooling restrictions mean that only one die and maximum of two rivets can be used on one rivet setter. In scenarios where several joints are requested on one setter, the testing needs to take this into a consideration and find one die and two rivets that are able to join all the stacks. This challenge is becoming simpler on the latest equipment models which can feed four different rivet types and have die changers. Combining four rivet feeds and a die changer makes the SPR setter far more flexible and means one cell can be used to make a number of different car body assemblies. Car makers are starting to use the same lines to make different car models; in order to be able to adjust the production volumes for each model based on customer order levels. The development of four rivet feeds and die changers has been conducted to respond to this new demand for very flexible

production cells, (Briskham, 2019). Figure 38 shows the variables influencing the quality of a self-pierce riveted joint.

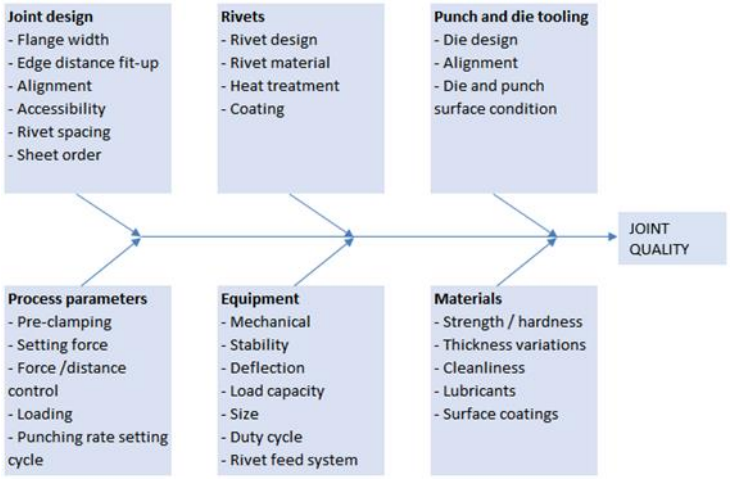

Figure 38, Variables influencing SPR process (Atlas Copco Riveting Guidelines 2019)

2.7 Physical joint assessment

With so many variables affecting the quality of a joint it is essential to have the means of assessing whether a joint is good quality and whether it will hold the sheets together with the strength required. There are several methods through which a joint can be assessed.

2.7.1 Visual inspection of a joint

By visually checking the joint after riveting, the following aspects can be assessed:

Head height measurement with a hand held depth measuring device (DTI fitted with 18mm nose and flat tip). A high rivet head is a clear sign of not enough force or too longer a rivet being used.

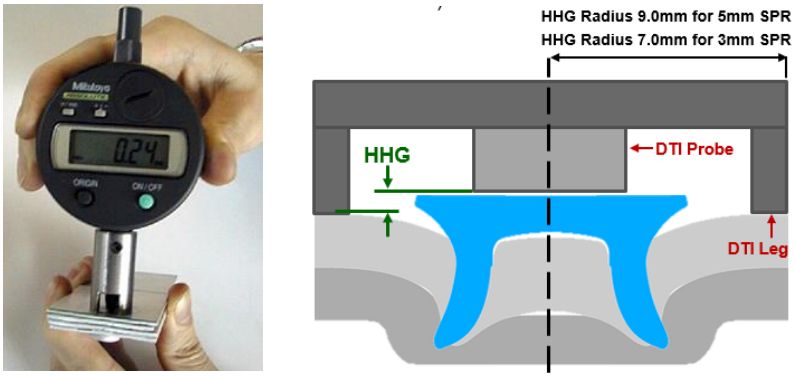

Figure 39, (left) Rivet Head Height Gauge with 18mm nose and flat tip, (right) User guide diagram. (AC SPR spec 2019)

Gaps under the rivet head increase the corrosion risk and it is good practice to select riveting parameters that ensure the head is fully down. This can be checked by the naked eye or by testing

with a thin sheet of paper to try to get the paper under the head, if the paper can be pushed under the head, the rivet head is not down and the rivet should be inserted deeper.

Cracks visible on the button – most customers do not accept deep tears or cracks in the button, surface tears are allowed by some customers as long as they do not reach the rivet tip.

Button cracking is rare when riveting ductile aluminium, but is a major joint quality topic when riveting low ductility aluminium die castings or 6XXX alloys in T6 condition. The best way to avoid button cracking is to use very shallow dies or to heat treat the part to increase the ductility. Figure 40 below shows the difference between a good button and a button with cracking, these two buttons were from the same casting riveted before and after conducting a heat treatment.

Figure 40, Example of button cracking in an aluminium casting being solved by heat treating the casting. (Briskham 2019)

2.7.2 Cross sectioning

External inspection of the joint can check a few things but does not check a number of parameters that can only be seen by opening up the joint. Cross sectioning shown in Figure 41 is frequently used in the industry to check SPR joint quality (Gerritsen, 2016). It is also used to compare simulated results with physical test results. The process of cross sectioning involves cutting the sample across the centre, followed by photographing and measuring the pictures. The joint is then assessed based on the criteria of three main measurements of head height, interlock and Tmin, which are usually specified by a customer with the guidance of the rivet manufacturer.

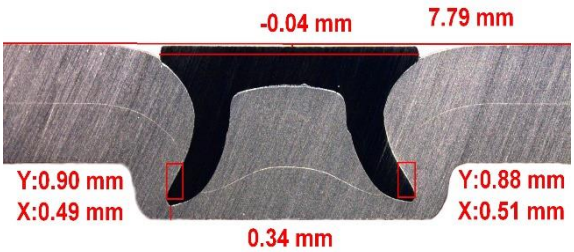

Figure 41, Cross sectioned joint with measurements recorded on the image in the standard manner. (AC SPR spec 2019)

2.7.2.1 Measuring cross sectioned joints

Explanations and specifications for the three main measurements are explained below. The range of values used for assessing joint quality were developed over many years by the most experienced riveting engineers at Henrob. Most customers use this criteria, some use their own pass/fail values.

Key	
HHM	Head Height Macro
Head Ø	Rivet Head Diameter
L dY	Left sided lockdepth in Y direction
L intX	Left sided interlock in X direction
R dY	Right sided lockdepth in Y direction
R intX	Right sided interlock in X direction
Tmin	Minimum bottom sheet thickness

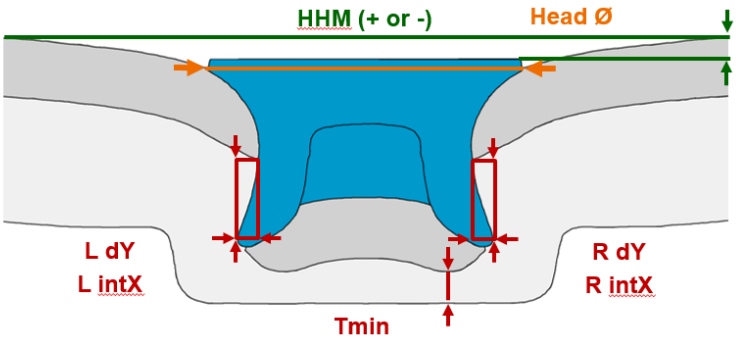

Table 3, Specification for how to measure a cross section (Atlas Copco SPR spec 2019)

Acceptance Criteria	HH Process Window Test (Nominal = Flush)		Nominal Shank Ø	
			Ø5 Rivet	Ø3 Rivet
Tmin	Upper	+0.2mm	≥0.15mm	≥0.15mm
	Nominal	0.0mm	≥0.15mm	≥0.15mm
	Lower	-0.2mm(1)	No break-through(3)	
Average intX (LintX+RintX)/2	Upper	+0.2mm	≥0.1mm(2)	≥0.1mm(2)
	Nominal	0.0mm	≥0.2mm(2)	≥0.1mm(2)
	Lower	-0.2mm(1)	≥0.2mm(2)	≥0.1mm(2)
Interlock X (LintX or RintX)	-		≥0.1mm	≥0.1mm
lockdepth Y (LdY or RdY)	-		≥0.3mm	≥0.2mm

1) If -0.2mm cannot be reached at maximum setting force specified in manual by equipment supplier, use value achieved at maximum setting force
2) If Avg intX cannot be achieved, conduct Coach Peel tensile tests to confirm joint achieves minimum peel strength required for the application
3) If break-through occurs, corrosion testing or further preventative measures should be considered, especially in wet areas

Figure 42, Recommended specification for pass/fail cross section measurement values a (Atlas Copco SPR spec 2019)

2.7.2.2 Head height

This is a distance by which the top of the rivet is sticking up above the top sheet or is buried below the surface of the top sheet. The ideal value for head height for Henrob rivets is to have a flush head i.e. 0.00mm and the recommended value range for production operation is to stay between -0.2mm and +0.2mm. The images below show examples of different head height levels on two different joints.

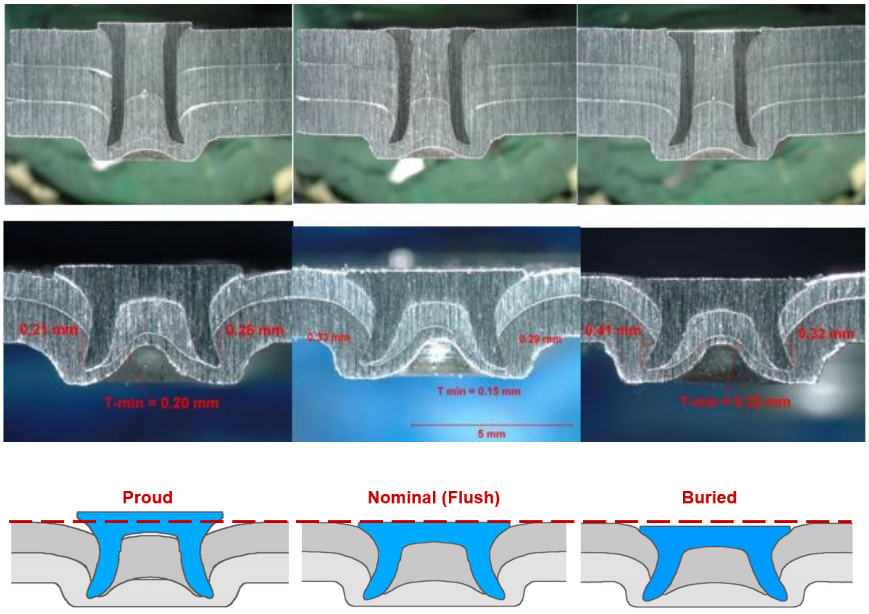

Figure 43, Head height measurement examples, from left to right, head high, head flush, head buried

2.7.2.3 Interlock

This is the distance by which the rivet leg is inserted (flared) into the bottom sheet. The minimum recommended value for interlock is 0.4mm for 5mm rivets and / or when riveting together aluminium sheets and 0.2mm for 3mm rivets and / or when riveting together steel sheets.

If interlock is less than 0.40mm in aluminium or less than 0.2mm in steel, the joint is considered to be a fail. Occasionally, the rivet does not manage to fully pierce the top or middle sheet which stays wrapped around the leg this is called 'Wrap-around interlock'. This is potentially sign of blunt tip or unsuitable choice of rivet, but is acceptable in some specific instances. Figure 44 & Figure 45, below shows examples of different amounts of interlock and how interlock is measured.

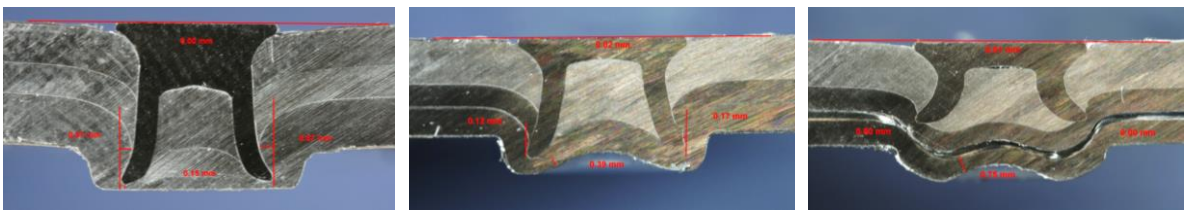

Figure 44, Left to right, example of different amounts of interlock – good, out of spec, and non-existent

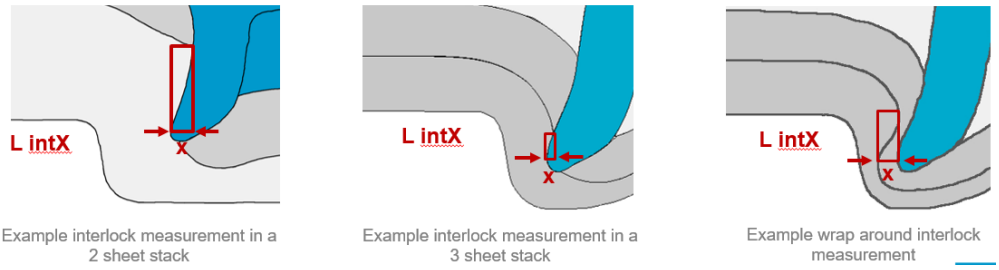

Figure 45, Diagram showing how interlock is measure on different joint stacks (Atlas Copco SPR spec 2019)

2.7.2.4 Tmin

This is the thickness of the thinnest section of bottom sheet after the rivet has been inserted. The minimum recommended value for Tmin is 0.2mm, some automotive manufactures accept a lower value as minimum spec.

Failure mode for Tmin is a breakthrough or a value below the spec as this might lead to breakthrough due to vibrations and fatigue of the joint later down the line which might give rise to corrosion in the joint. The images below show examples of good and bad Tmin as well as a breakthrough.

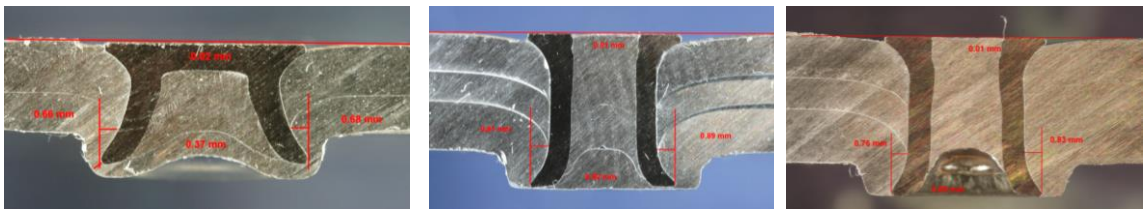

Figure 46, Example of a good Tmin and failure Tmin

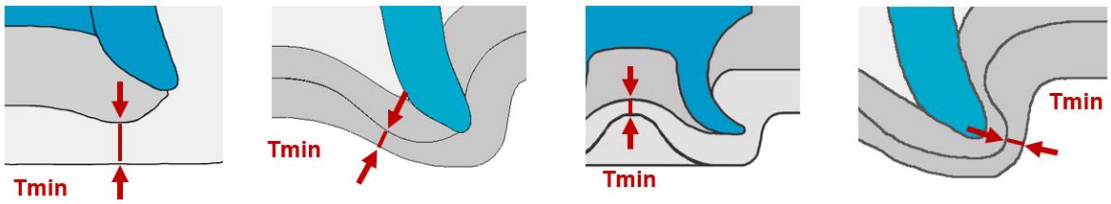

Figure 47, Diagram showing how Tmin is measured (Atlas Copco SPR spec 2019)

On some joints it is difficult to achieve good measurement values on all areas and a compromise is made where Tmin is sacrified for interlock by pushing the rivet deeper to create a stronger interlock.

2.7.2.5 Other joint assessment criteria

Joints quality also depends on other criteria, such as

- Cracked rivet leg – sign of rivet over stressed, see Figure 49
- Asymmetric rivet legs – sign of unsuitable rivet/die selection, see Figure 49

- Gaps under the rivet head – sign of not enough force used
- Cracks on the button - sign of die depth too deep for a brittle bottom sheet material
- Buckled or collapsed rivet – sign of unsuitable rivet or a non-feasible joint, see Figure 48
- Rivet too long, see Figure 48
- Unfilled bore in a T-rivet joint – sign of stiff material or unsuitable rivet selection.
- Lack of flaring – unsuitable die selection.
- Asymmetrical button – sign of misaligned die, see Figure 49

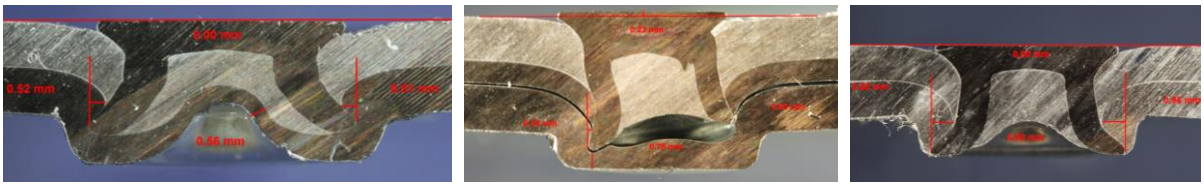

Figure 48, (left) Buckled rivet, (centre) Collapsed rivet, (right) Rivet too long.

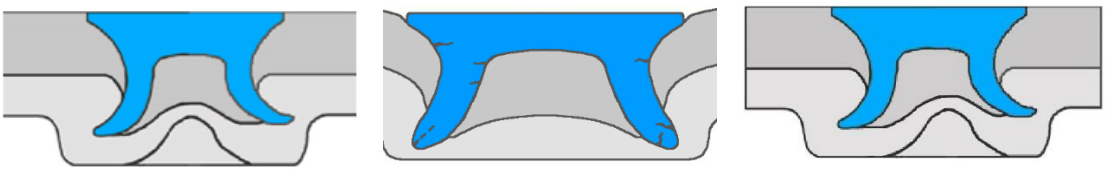

Figure 49, (Left) Asymmetric rivet legs, (centre) Cracks in rivet, (right) Misaligned die

It is recommended that for statistical reasons minimum of five samples are made for each type of joint being compared. A number of statistical values are calculated for each of the measurements, such as average, maximum and minimum values, coefficient of variation, standard deviation, + and – 3SD. For a large test study this data is presented in a line graph or a Bell curve distribution graph.

It is common for the measurements for all of the joint stacks on a car body to be combined on a single table and for a traffic light system to be used to colour the joints as pass, marginal, or fail.

2.7.3 Force displacement curves

The process of rivet insertion can also be plotted as a force-displacement curve as illustrated below. Data for this curve is obtained by correlating the force with which the rivet is inserted with the punch displacement or time of stroke. The curve usually has a very characteristic shape and is used as a method of quality control checking on the rivet setting equipment which looks for a deviation from the typical shape as a deviation indicates faults in the process (Gerritsen, 2016). The literature review has revealed that this curve has been used for comparison between the numerical and experimental results in almost every study available.

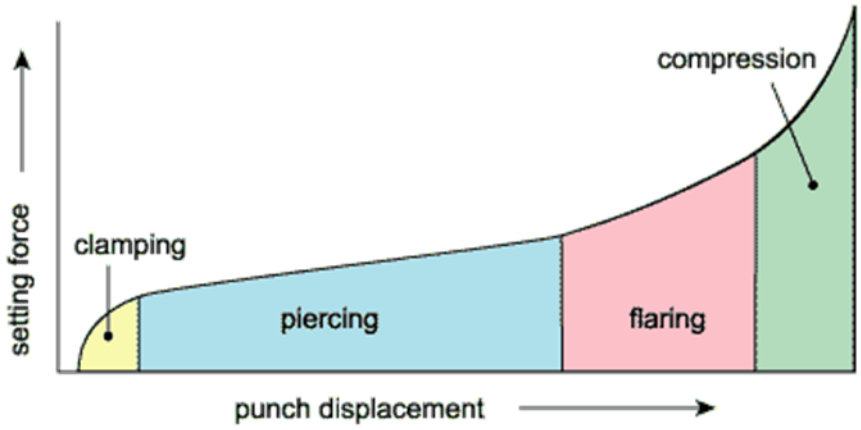

Figure 50, Force-displacement curve (TWI, 2016)

2.7.4 Tensile Strength

This test is used to assess the strength of a joint by pulling apart on an Instron tensile test machine. It is predominantly used only when the interlock value does not meet the SPR spec to check if a below spec joint can be used on a car body. There are three main types of strength tests for shear and peel modes of loading. The joints are riveted together in a different manner for each as shown below.

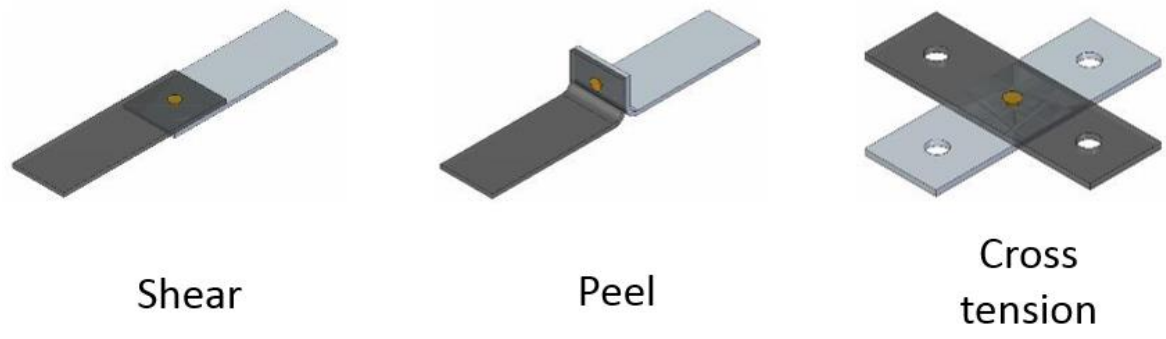

Figure 51, Tensile test joint configurations for SPR joints. (Atlas Copco SPR spec 2019)

For simplicity all three joint types are made using the same 120x38mm coupons. The joints are held in wedge grips or test fixtures and pulled apart until the sample breaks. The resulting graph below shows a typical example of a force v displacement output curve and max strength measurement.

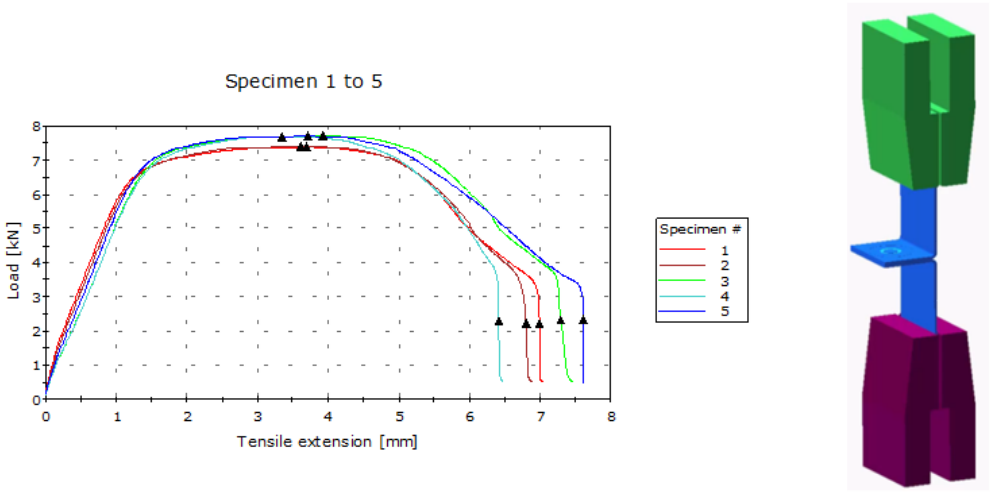

Figure 52, Example of a graph from tensile test of a lap shear joint, and diagram of grips holding the test sample (PR ES, 2018).

There are several modes of joint failure occurring in a strength test, as shown in the images below.

Typical Failures Modes	Description	Example image
Tail pull-out	Joint has failed due to the rivet tail pulling through the bottom layer(s) via a loss of interlock. A mechanical interlock is still maintained between the rivet head and the upper sheet(s)	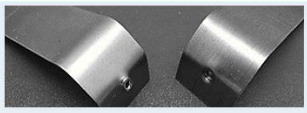
Head pull-out	Joint has failed due to the rivet head pulling through the top layer(s) via a loss of interlock. A mechanical interlock is still maintained between the rivet tail and the bottom sheet(s)	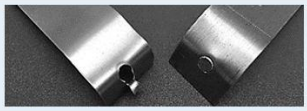
Simultaneous pull-out	Joint has failed due to a combination of rivet tail pull-out and head pull-out as described above, mechanical interlock in both sheets is wholly compromised	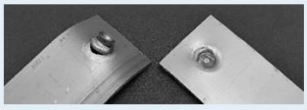
Rivet fracture	Joint has failed due to a reduction of the rivet's structural integrity, such as a fracture, resulting in workpiece separation.	

Typical Failures Modes	Description	Example image
Top sheet tear	Joint has failed due to a separation of the workpieces via a ductile fracture. A mechanical interlock is still maintained between the rivet tail and the bottom sheet(s)	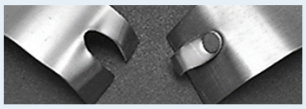
Bottom sheet tear	Joint has failed due to a separation of the workpieces via a ductile fracture. A mechanical interlock is still maintained between the rivet head and the top sheet(s)	
Top sheet fracture	Joint has failed due to a separation of the workpieces via a brittle fracture. A mechanical interlock is still maintained between the rivet tail and the bottom sheet(s)	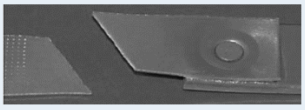
Bottom sheet fracture	Joint has failed due to a separation of the workpieces via a brittle fracture. A mechanical interlock is still maintained between the rivet head and the top sheet(s)	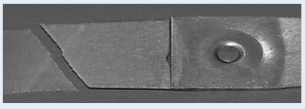

Figure 53, Failure modes of SPR joint. (AtlasCopco SPR Spec 2019)

The strength of the joint is then evaluated and a decision is made whether to move the joint to a different setter or leave it in its current location.

2.8 Types of testing in SPR

One of the disadvantages of SPR, as mentioned previously, is the fact that all joints need to be individually configured. This means that a correct rivet and die type need to be selected based on the characteristics of the materials to be joined. There are some rough guidelines on what works and what does not, for example, if one or more sheets in the joint is steel a harder rivet might need to be selected. Overall thickness of the sheets is also an important factor and general rule is to select a rivet that is 2mm longer than the total thickness of all sheets to be joined.

Alongside of the rivet selection, shape, depth, and width of the die needs to be considered. For example, if the material on the die side (bottom sheet) is a brittle material, then a shallow and wide die should be used to prevent cracking of the material.

2.8.1 Feasibility testing

These tests are usually either a single or a 5 off sample tests to estimate how the material responds to a rivet and die selected based on the tacit knowledge. The selection might need to be adjusted if a cross section shows some shortcomings such as insufficient Tmin or interlock. Or for example a softer rivet or shorter rivet might be selected next to encourage flaring or improve Tmin respectively. However, there is an additional complication to these feasibility tests which leads to more tests.

2.8.2 Further assessments

As mentioned above, there are joints that may not comply with the AC specification, the suggested measurements generally provide a good balance of a strong joint and realistic joint.

If a rivet is selected as part of the rationalisation process meaning that it might not the perfect configuration for a given joint (for example too long to accommodate other joints on the setter) it occasionally happens that the rivet is not set to its full length to preserve the Tmin. This could create a problem if the joint is situated in an area where corrosion is likely to occur. This condition was recently observed on a new electric car made by a competitors' riveting equipment, where a number of rivets in potential wet areas had proud heads with underhead gaps.

In case of Tmin, the failure mode is usually a breakthrough or possibility of a breakthrough due to Tmin values around 0.10mm and less. The same corrosion concerns apply here, as if the rivet tip breaks

through the tip is exposed and could corrode in a wet environment if the paint coating added after rivet insertion is damaged.

In case of both, a decision needs to be made if the location of the joint will be likely to see moisture. If not, the rivet is usually allowed to remain in its location, if yes, a change to fastener planning needs to be made e.g. different rivet or rivet coating needs to be selected.

If the interlock does not comply with the engineering specification, the concern shifts from corrosion to the strength of the joint. In this case, a subsequent testing of the strength of the joint takes place and the strength of the joint is then evaluated and a decision is made whether to move the joint to a different setter to use a different rivet/die combination to make a stronger joint or leave the joint in its current location and accept the reduced interlock.

2.9 Current use of SPR

Following Audi's pioneering research into SPR in collaboration with Henrob in the 1990s, other automobile producers followed suit and in 2004 Jaguar-Landrover's XJ used over 3000 rivets in their vehicle body made of Aluminium 5XXX with Aluminium 6XXX skin panels (Davies, 2012) and has been continuing this trend with all their subsequent vehicles. Volvo used the SPR method to join high strength steel on their FH12 truck (He et al., 2008, Litherland, 2016).

Other automobile producers who now employ this joining method to various degrees include Daimler, Ford, Toyota, Nissan, London Taxi, BMW, Hyundai, and Aston Martin, especially in aluminium intensive vehicle designs (Henrob, 2016, Briskham, 2016) The typical use of self-pierce riveting is in car bodies, closures (i.e. bonnets, hoods, trunk lids, boot lids, doors, window regulators etc. (Henrob, 2016), sub-assemblies and truck cabs (Briskham, 2016). Tier one suppliers also use SPR in sunroof manufacturing (Henrob 1, 2016). SPR is also widely used across transportation industry and includes buses and coaches, boats and seating on aeroplanes, caravans and trailers (Henrob 1, 2016). Other uses of SPR include industries such as air-conditioning (Henrob 2, 2016), road signs manufacturing (Henrob 3, 2016) and manufacturing of water tanks and grain silos (Henrob 4, 2016). The predomninant use of SPR, however, remains with automotive industry and this is currently expanding from Europe into Chinese and Japanese markets too.

2.10 SPR innovations

There is demand from car manufacturers to continuously improve the technology and come up with new and improved designs (Lai and Brun, 2007). Due to this demand there is already a vast body of

research on SPR. The rivet manufactures (e.g. Henrob, Tucker, Bolhoff) as well as various institutions for materials joining such as TWI (2016) have produced publications about SPR. Fu 2001, started exploration into the effects of geometry as well as process parameters such as rivet length, diameter, hardness, die shape etc. on the joints. This was followed by similar experimental research by Abe et al, (2006), Sun and Khaleel (2007) and Sun et al (2007) which concentrated on three areas of the self-pierce riveting, i) effect of various process parameters and geometry on the joint, ii) mechanical testing to define static and dynamic strength using a number of different types of loading (e.g. shear, tensile) and iii) determining relationships between the SPR process parameters and mechanical behaviour of joints.

Pickin (2007) conducted research aimed at joining lightweight sandwich sheets to aluminium using SPR in order to see how sensitive these materials are when joined with aluminium. Mutsumura (2007) also used SPR to join dissimilar materials, in particular and aluminium alloy roof with a steel car body.

Fratini and Rusi (2009) explored use of SPR with hybrid joints of aluminium and composites. Johnson et al worked on online monitoring methods of the mechanical interlock without destructive testing (2010). Also in 2010, Han et al focused attention on comparing the resistance spot welded and SPR joints. More recently, Wood et al (2011) focused on exploring the reliability of SPR joints at typical automotive crash speeds using U-shaped tensile test pieces.

In addition there are other technologies being combined with SPR to improve the joining ability of SPR, these will be briefly described in the following paragraphs.

2.10.1 Laser assisted SPR (LSPR)

One of the disadvantages of SPR is that all sheets to be jointed require a sufficient ductility to form around the rivet and inside the die. However, some materials do not have this level of ductility and riveting these as bottom sheets would result in cracking in the bottom sheet (Liu et al, 2012). If the cracks are too severe the entire bottom part of the joint can essentially fall off – as shown in the below image.

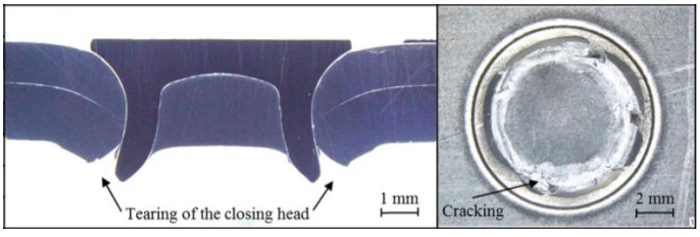

Figure 54, Cracks in the button leading to the button falling off exposing the rivet tips. (Jäckel 2016)

This was the case with a joint required to have AZ31 magnesium sheets on the bottom of the joint which was attempted by Durandet et al (2010) as well as a joint with 7075 T6 series aluminium which is known for low ductility, as researched Jäckel (2016). To invent a solution, the joint stack was pre-heated by a laser beam before the rivet insertion. This produced a joint without cracks and revealed that the ductility was increased to an optimum at temperature between 180°C and 210°C. However, this also resulted in increased costs by adding heating equipment (Jäckel et al, 2014), increased cycle time (up to 5s) and it potentially can cause liquid metal embrittlement failure of the rivet due to melting the zinc alloy rivet coating. (Durandet et al, 2010, Wang, 2011).

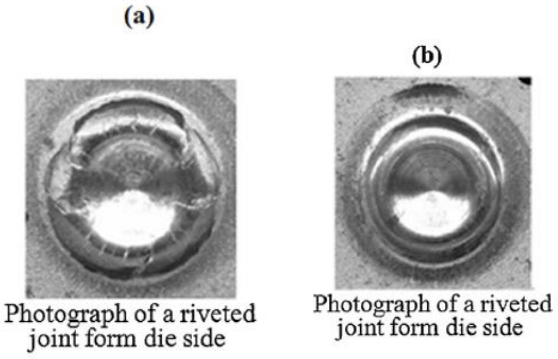

Figure 55, Difference in button cracks without use of laser and with use of laser (Durandet, 2008)

2.10.2 Friction SPR (F-SPR)

Due to the increased use of low ductility 7xxx series aluminium along another method combining SPR with friction stir spot joining has been researched. In this method, a rivet with a slotted drive head is inserted into the sheets whilst also being rotated. The high speed rotation combined with downward force creates frictional heat which heats the substrate material and increases its ductility helping the rivet to penetrate and flare more easily. The heat generated in the top sheet passes through to the bottom sheet helping to also raise the ductility of the bottom sheet. (Wei et al, 2015, Ma et al, 2015)

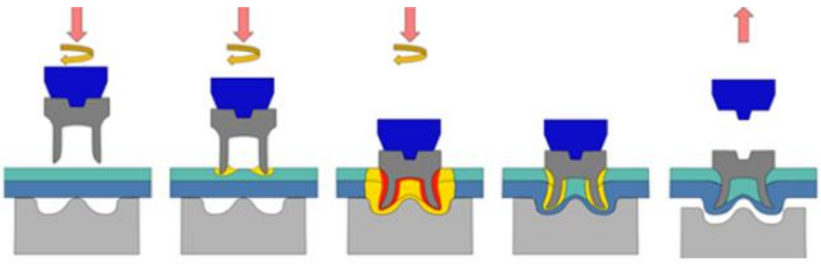

Figure 56, Schematic diagram showing the process of friction stir SPR

2.10.3 Hydro-formed SPR (HF-SPR)

As with the previous method, this method has been researched with materials with low ductility in mind. In this process, a die is replaced by highly pressured fluid which is used the shape bottom sheet. The fluid provides constant support while the button is formed reducing the occurrence of cracks (Neugebauer, 2005).

Figure 57, Schematic diagram of hydro forming SPR process (Haque, 2017).

2.10.4 Adjustable die option

Another variant of the above method is to use a flexible die instead of high pressure fluid, as researched by Drossel (2014) when working on a joint with a hard and brittle cast aluminium as bottom sheet. This also provided constant support while the button was formed, reducing cracking.

2.10.5 Kerb Konus Solid SPR (S-SPR)

Another method that has recently been developed is solid self-pierce riveting using rivets with grooved shanks. In this method, a hollow die is used to punch out a disc and allow it to fall away, a raised ring around the die is then used to push aluminium against the rivet shank to fill the grooves ion the rivet shank and hold the rivet in place. (Jäckel et al, 2014). The main weakness of this approach is that the joint strength is dictated by the strength of the aluminium pushed into the grooves on the rivet shank.

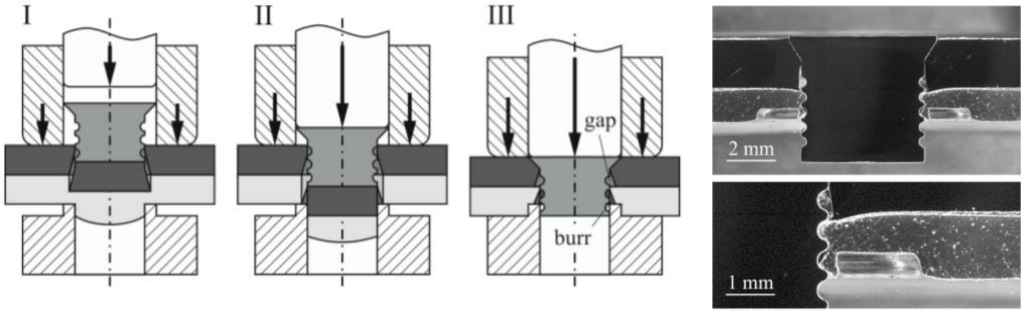

Figure 58, Examples of Kerb Konus solid self-pierce riveting (Jäckel et al, 2014).

Conducting research investigations of this type using physical testing is lengthy and costly, and it is difficult to cover a thorough design of experiment on each of the aspects of the process. (Miller, 2016).

Furthermore, apart from the few aspects of the process which can be properly monitored such as punch force and displacement, a lot of the process aspects cannot be monitored in real life and can only be studied once the test is completed (Gruijicic et al 2014). For example it is not possible to stop a rivet insertion part way through to examine the cross section when the rivet is being inserted at very high speed, as the speed must be slowed down to stop at a part way through position.

FEA simulation of rivet insertion has significant potential to support rivet development studies and reduce the amount of physical testing required as well as expanding the range of conditions that can be investigated.

3 REVIEW OF FINITE ELEMENT ANALYSIS (FEA)

The field of finite element analysis has improved immensely in recent years and is frequently employed to aid engineering processes. However, insertion of self-pierce rivets is a rather complex process including a number of stages such as forming, piercing and large scale plastic deformation. Coupled with the fact that the behaviour of joints is influenced by a large number of variables, successful simulation of an SPR joint is a complex and demanding task.

The rest of this chapter is a review of Finite Element Analysis (FEA) in general to provide a platform for the next chapter which is a focused review of FEA work conducted on SPR insertion.

3.1 What is Finite Element Analysis - Introduction

In short, the finite element analysis (FEA) is a numerical method for solving problems of engineering and mathematical physics. It is generally used for problems with complex geometries and where the accuracy of results is required to be much higher than that of an analytical solution (Hutton, 2004). The fundamental concept behind the finite element analysis has been explained very simply by Zienkiewics , the author of what is considered to be the first textbook on FEA (1967) who proposes that our minds cannot grasp behaviour of our complex surroundings in one operation and therefore we divide them into parts, or elements, behaviour of which can be comprehended more easily. These are assembled into a model, behaviour of which can then be studied more readily. This process of dividing systems into elements is called discretization and models created this way can be called discrete problem. (Zienkiewics, 1967).

There are situations where this subdivision continues infinitely and the problem can be defined only by using the mathematical fiction of an infinitesimal. This can be referred to as continuum. Having established this, Zienkiewics (1967) proposes that finite element method can be seen as a "general discretization of continuum problems posed by mathematically defined statements". This process will enable approximation to the solution of continuum problems. In his book, he further suggests that approximation to the continuum occurs as per below:

- "The continuum is divided into a finite number of parts (elements), the behaviour of which is specified by a finite number of parameters, and
- The solution of the complete system as an assembly of its elements follows precisely the same rules as those applicable to standard discrete problems."

3.2 Brief history of Finite Element Analysis

The first interest in the subject can be traced as far back as 17th and 18th century when atomic structure of matter was explored which led to discovery of crystallinity. By the end of 18th century, scientists laid the foundations for mathematical and physical descriptions of material properties and materials processing (Schmitz et al, 2016). Since then the theory of plasticity has been developed and explored by many different scientists (Schmitz et al, 2016) with Ritz establishing a method for solving mechanics in deformable solids in 1909. This theory involved a minimization of energy functional and system of equations (Ritz, 1909). This system had a restriction in that the minimized functions do not satisfy the boundary conditions.

This has been solved by Courant in 1943 by adding special linear functions defined over triangular regions. This was followed by a development by Clough, resembling that of Ritz and Courant, and this work for the first time introduced finite element (Clough, 1960). Further development of FEM was facilitated by invention and continuous improvement of computers which allowed high volume of mathematical calculations needed for FEM (Smitchz, 2016). Further contribution was made to this field by scientists such as Zienkewics (1967), Turner (1956), Hrennikov (1941) etc. in 1960 and followed by introduction of Nastran software in 1965 by John Davidson (Smitchz, 2016).

This led to establishment of FEM as a tool in manufacturing (Smitchz, 2016) and structural and solid mechanics (Barkanov, 2001) since 1980 and with many software packages available at present day it is now widely used in order to solve problems in various other engineering areas such as heat transfer, fluid dynamics (Barkanov, 2001), electromagnetic fields, soil mechanics, acoustics and biomechanics (Tura, 2016). Some of the most used ones are Ansys, MSC.Nastran, LS-Dyna, MSC.Marc, Abaqus, Lisa, Simufact (Barkanov, 2001).

3.3 Finite Element Analysis stages

The FEA process can generally be divided into three main stages which are all carried out by an FEA software. Each of these stages is described in the following section.

3.3.1 Stage 1 – Pre-processing

This stage could also be described as discretizing the continuum (Nikishkov, 2004). In the first step of this stage, a geometric domain of the problem needs to be determined which means converting an engineering problem into a model that can be solved by FEA (Hutton, 2004).

This is followed by division of the model parts into system of many smaller bodies or units. These are called finite elements and are interconnected at points (or nodes) common to two or more elements or boundary lines or surfaces (Hutton, 2004).

This step also includes establishing the types of elements to be used as well as establishing their geometrical properties (i.e. length) and material properties since the elements represent the physical properties of the domain for example mass, stiffness etc. (Simufact, 2013, MSC.Marc, 2013).

Next stage is the definition of the element connectivities i.e. meshing followed by definition of the loads as well as physical constraints i.e. boundary conditions. (Hutton, 2004) which for example includes prescribed force, displacement etc. (Qi, 2006). All of these steps apart from the first one (converting the engineering problem into a model) is done by a part of the FEA software called mesher. The first step is usually completed by CAD or similar engineering software.

3.3.2 Stage 2 – Solution

During this stage, the FEA software computes the unknown values of the primary field variable takes place (Hutton, 2004). In order to achieve this, the interpolation functions are determined. These are used to interpolate the field variables over the element and often are polynomials. Degree of polynomials is determined by the number of nodes allocated to the element. This stage also aims to find the global equation system by assembling all element equations and formulation of an equation matrix which connects the nodal values of the unknown functions to other parameters (Nikishkov, 2004) and this is solved by direct and iterative methods.

Once the solving of the global equation system takes place which results in the resulting nodal values of the function are available (Nikishkov, 2004) additional parameters such as stresses, strains, reaction forces, heat flow etc. can be calculated by back substitution (Hutton, 2004).

3.3.3 Stage 3 – Post-processing

In this stage the postprocessor software is employed and processes the results by for example sorting, plotting and visualising the new shape of the object, animating the model and producing colour-coded charts detailing various parameters of the model (Hutton 2004, Qi, 2006).

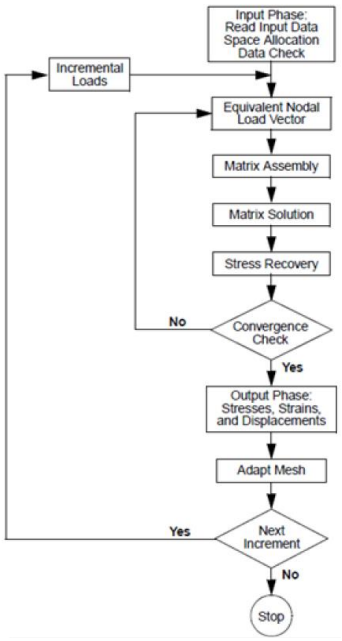

Figure 59, Post processing tasks (Dixit et al, 2013)

3.4 Types of FEA

Based on the level of stress exerted on the workpiece, FE analysis can be classed as static, dynamic or quasi static. These are considered separately below.

3.4.1 Static analysis

A simulation is classed as static when yield strength of the material remains greater than stress generated by external loading.

$$\sigma \leq \sigma_{yield} \qquad \text{Eq. (1)}$$

This means that the workpiece is remaining in the elastic range of the stress-strain curve and does not undergo a plastic deformation.

Any change in shape is usually neglected in the next step as it is assumed that the workpiece undergoes elastic recovery.

The external loading can further be considered time independent and acceleration in this case equals zero which means the sum of external forces are also zero and mass can therefore be neglected (Mashayekhi, 2016, Harish, 2019).

$$\sum F = m * a = m * 0 = 0 \quad \text{Eq. (2)}$$

Static analysis is often used to solve structural problems (Mashayekhi, 2016).

3.4.2 Dynamic analysis

Dynamic analysis on the other hand involves those simulations in which the generated stresses from external loads are higher than yield strength of the material.

$$\sigma > \sigma_{yield} \quad \text{Eq. (3)}$$

This means that due to the external stress the workpiece entering the plastic range of the stress strain curve is undergoing a plastic deformation which is no longer linear. The loads and changes of shape are no longer neglected and instead are considered as a continuous variable and the calculations in each step reflect this. The external loading is time dependent and the acceleration is not zero which means that inertia effects should be considered as prescribed by equation

$$\sum F = m * a \quad \text{Eq. (4)}$$

This type of analysis can be used to resolve high impact problems (Mashayekhi, 2016, Harish, 2019).

3.4.3 Quasi static analysis

The last category, a quasi-static analysis, is placed between the above two, where the external loading is time dependent but inertia effects are so small that they can be neglected and the system can be solved as a static problem.

$$\sum F \sim 0 \quad \text{Eq. (5)}$$

This type of analysis can be used in cases such as metal forming, where non-linear problem up has been broken down to a set of linear equations at very small increments using for example Newton-Raphson method (Mashayekhi, 2016, Harish, 2019).

Whilst the differences between the analyses' types listed above are based on physics, there is also another classification of FEM analysis based on the how the solver is calculating the results - explicit and implicit (Mashayekhi, 2016, Harish, 2019).

3.4.4 Implicit analysis

Both explicit and implicit analyses start in the same way, with expectation of non-linearities, the load is not applied all at once, but rather split into smaller parts called steps or time steps and applied progressively. The steps are further split into sub steps that are referred to as increments and this is where the differences between the two come to the fore (Crisfield, 1991, Yaw 2009).

In both types, after each increment stiffness matrix is updated, however, the implicit analysis attempts to balance the externally applied forces with the internal reaction forces at the end of each increment. However, it is not easy to reach a complete equilibrium and to make this more possible, tolerances are set determining a value acceptably close to equilibrium that the balancing of the forces should aim to reach

In order to do this, Newton Raphson iterations are used. This, in very simplistic terms means that the software takes a guess at reaching the equilibrium. If it is within the specified tolerances, the increment can be completed and the solver moves onto the next one. If it exceeds the tolerance, the software carries out an iteration of the calculations starting with a smaller value in order to reach the equilibrium. The process is repeated until the tolerances are achieved and this can also be referred to as converged solution (Crisfield, 1991, Yaw 2009).

The results are regarded as unconditionally stable as large timesteps are possible and this method provides a great degree of accuracy. Disadvantage can be that this is resource heavy process, which, when short process time or complex processes are required, is not suitable.

3.4.5 Explicit analysis

In the explicit analysis on the other hand, there is no requirement to achieve the equilibrium between forces and so there are no tolerances set and consequently there are iterations and no convergence check. Due to lack of equilibrium enforcement, the provided solution may not be as accurate as the one achieved by implicit solver in the same amount of steps. This is because small variations in results are magnified with each step without the tolerances, causing the result to continuously deviate from physical results. The accuracy of results can be improved but a large number of very small steps must be used which may lead to the process be only conditionally stable (Crisfield, 1991, Yaw 2009, Dixit 2013).

An example of the differences can be demonstrated by looking at results of displacement calculations in a simple 2D model of a bar in tension (Yaw, 2009).

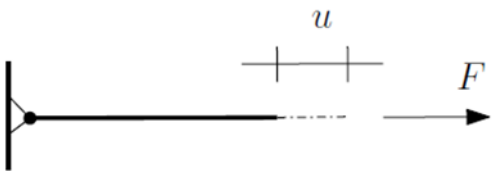

Figure 60, 2D model of bar in tension

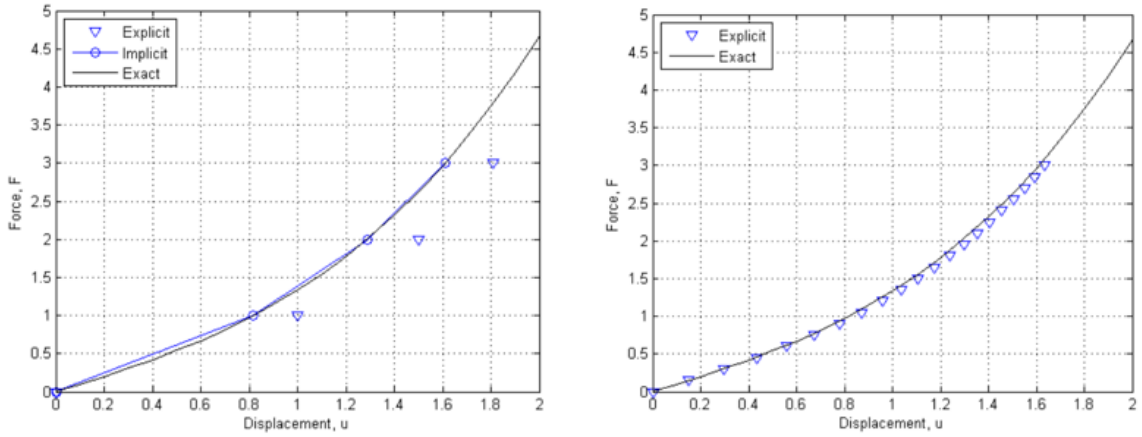

a b

Figure 61, Simulation using implicit and explicit analysis. (a) in three steps, (b) in twenty steps (Yaw, 2009).

In Figure 61 (a) a simulation has been completed using both implicit and explicit analysis in three steps. When compared against the exact solution a visible deviation can be seen from the measured results whilst this has been improved in Figure 61 (b) where the same explicit analysis has been carried out but using twenty steps which means they are much smaller.

In term of decisions as to which solver to use, both explicit and implicit can do all three type of FE analyses – static, quasi static and dynamic, however, there are factors that may influence suitability of each for a specific purpose. For example, the implicit analysis might give better results however, it is on the expense of time and hence is used more often in static problems where the calculations may not be as extensive (Yaw, 2009).

3.5 Specific methods used by Simufact software

Since the software was selected before the PhD started, it is appropriate to focus on the specific software and look at the type of methods it employs.

The selected software, as mentioned earlier, is Simufact forming and as a solver, it uses an improved version of MSC.Marc software from MSC Software company (Dixit et al, 2013, Simufact, 2011).

This solver uses both implicit and explicit analysis in its two available technologies, implicit for Finite element solver and explicit for Finite volume solver. The finite volume solver tends to be used for flash forgings such as crankshaft hot forging whilst the finite element solver can be used for majority of all other cases (Dixit et al, 2013, Simufact, 2011) and is used forming and SPR. The focus of this work, therefore will be on Finite element implicit analysis.

Material forming is usually governed by non-linearities and hence non-linear equations. The MSC.Marc solver includes equations that cover the following (Dixit, 2013, Simufact, 2011):

Material non-linearities – includes various dependencies of material descriptions on for example temperature, deformation rate, porosity and whether the material is subjected to elastic deformation only or elasto-plastic deformation.

Geometric non-linearities – includes for example large deformation, present in most of the metal forming problems.

Non-linear boundary conditions – includes contact of workpiece and die, friction behaviour etc.

To solve these types of non-linear equations an incremental approach is needed by the solver. As explained in the section on implicit FEA, Newton-Raphson iterations are used by Marc solver to solve the non-linear equations which means that calculations are repeated until the solution is within the criteria set by the solver i.e. and only then it is considered to be converged (Yaw, 2009, Dixit, 2013, Simufact, 2011). There are two methods to check if the increment meets criteria:

Residual checking – with this method, as explained earlier in the section in implicit analysis, the solver checks the residual which in this instances is the difference between the externally applied forces and internal reaction forces. If the forces are in equilibrium and the difference between the two is within pre-specified criteria i.e. control tolerance, the solution for that specific increment has converged and the calculations can move onto the next increment (Yaw, 2009, Dixit, 2013, Simufact, 2011).

Displacement checking – this is the alternative to the residual checking in implicit analysis and the criteria is considered to be met when the maximum displacement of the last iteration is smaller than the displacement change of the increment (Dixit, 2013, Simufact, 2011). MSC.Marc solver uses this method for its calculations.

In terms of the mesh approach, the MSC.Marc solver uses the updated Langrangian method (Dixit, 2013, Simufact, 2011). The simplest way to explain this method might be to demonstrate the difference between this method and its counterpart that is used as an alternative, the Eulerian approach.

Langrangian method – with this method the materials, which essentially refer to all meshed parts of simulation (in this case the rivet and sheets) are moving with the mesh which deforms at the same time with the material. The quadrature of the elements coincide with the points of the material throughout the simulation and the boundary nodes remain on the boundaries of the materials (Belytschko et al, 2000).

Eulerian method – with this method, the same materials pass through the mesh which however is fixed in space and so does not deform with materials (Belytschko 2000).

The below image provides a simple illustration of the two methods.

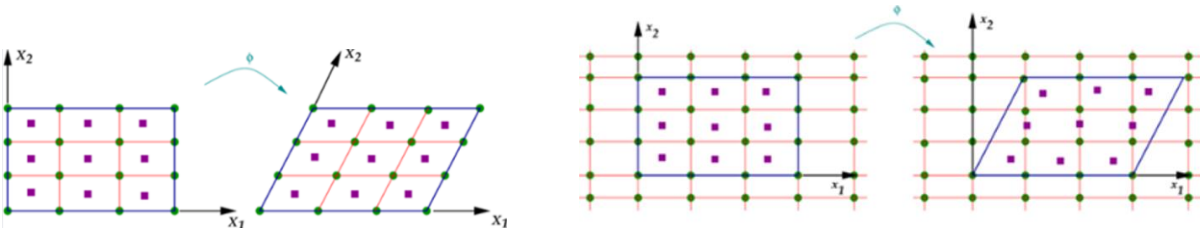

Figure 62, Lagrangian method (left), Eulerian method (right) (Belytschko 2000).

In terms of the solution stage, the solver used in this software, MSC.Marc, is based on the displacement method. This method relates the force displacements to the stiffness of the system. For example, the basic force displacement for a linear static problem is (Dixit et al, 2013, Simufact, 2011)

$$Ku = f \quad \text{Eq. (6)}$$

K – stiffness matrix

u – nodal displacement

f – force vector

In 2D case, the governing equation would be:

$$\begin{matrix} K11 & K12 & u1 \\ K21 & K22 & u2 \end{matrix} = \begin{matrix} f1 \\ f2 \end{matrix} \quad \text{Eq. (7)}$$

Calculation of displacement leads to further calculation of the strain can in individual elements can based on the element displacement:

$$\varepsilon_{el} = \beta u_{el} \quad \text{Eq. (8)}$$

The stresses in the element are obtained from the stress – strain relations:

$$\sigma_{el} = L\mathcal{E}_{el} \quad \text{Eq. (9)}$$

ε_{el} – strain in element

σ_{el} - stress in element

u_{el} – displacement vector associated with the element nodal points

β – strain-displacement relation

L – stress-strain relation

The equations for other procedures within the solving process also use stiffness method and therefore similar to the above. For example, a governing equation for thermo-mechanical calculation will be as follows:

$$K(T)u = f \quad \text{Eq. (10)}$$

$$C(T)T + k(T)T = Q + Q^I$$

C – heat capacity matrix

K- thermal conductivity matrix

Q – thermal load vector (flux)

T – time derivative of the temperature

Q^1 - internal heat generated due to inelastic deformation

In both equations, the stiffness matrix K, heat-capacity matrix C, and thermal-conductivity matrix k are all dependent on temperature.

The finite element system is comprised of local element systems. So for example, the global stiffness matrix K can be expressed in terms of element stiffness matrix K_{el}^{i}

$$K = \sum_{i-l}^{n} K_i^{el} \quad \text{Eq. (11)}$$

n is the number of elements in the system. Then element stiffness matrix can be then expressed as

$$\int_{vel} \beta T\, L\beta dV_{el} \quad \text{Eq. (12)}$$

V_{el}- Volume of element

It should be highlighted that all the equations and calculations are handled entirely by the software and the user selects parameters via graphic user interface (GUI).

4 REVIEW OF FEA IN CONTEXT OF SPR

4.1 Parameters to consider in FE analysis of SPR

The ever increasing capabilities of the CAE and specifically FEA softwares and codes is becoming an essential part of manufacturing (Altan, Tekayya, 2012), however, to use these methods effectively, some understanding of the main variables involved in simulation of the given process is essential. According to Altan and Tekayya (2012), the following areas are of metal forming are to be considered in context of simulation:

- Material behaviour – material characterization
- Friction, lubrication and coatings
- Process description –e.g. boundary conditions, type of press, speed of insertion, clamping, C-frame deflection.
- Rivets', dies', sheets' and tools' geometries

In addition, in FEA process itself there are several factors that are considered important to the simulation process. Correct set up of these will influence the simulation and its accuracy

- Simulation process parameters:
- Process type selection - 2D or 3D
- Mesh
- Selection of contact and time step type
- Process type selection - mechanical or thermo-mechanical model
- Mechanics of damage

The above factors will be introduced in depth in the next few sections in order to lay foundations for the experimental part of this project.

4.1.1 Simulation process parameters

4.1.1.1 Process type

A general procedure to accelerate simulation is to reduce dimensions of model i.e. from 3D to 2D where possible. Therefore, the software allows the user to select whether the numerical analysis should be in:

- 3D
- 2D axisymmetric models
- 2D planar

An example of such simplification can be a process of a ring compression (Figure 63). By selecting the 2D-axisymmetric model, the Figure 63a can be simplified to Figure 63b.

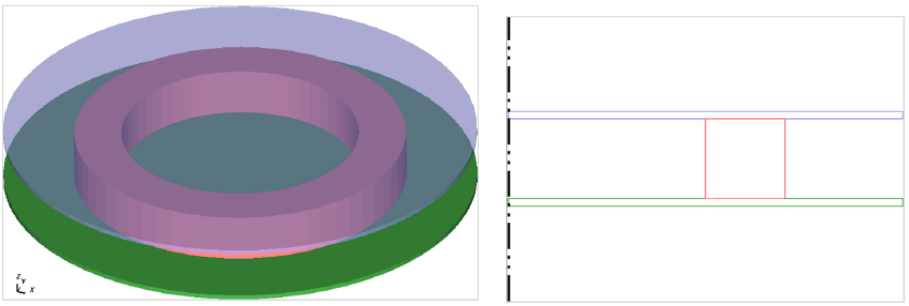

a b

Figure 63, Example of model simplification from 3D to 2D axisymmetric (MSC.Marc, 2013).

If the model geometry and forming conditions are homogeneous in one of the three dimensions and the length of that dimension is much longer than the other two dimensions, the simulation type 2D plane strain can be selected as shown in Figure 64.

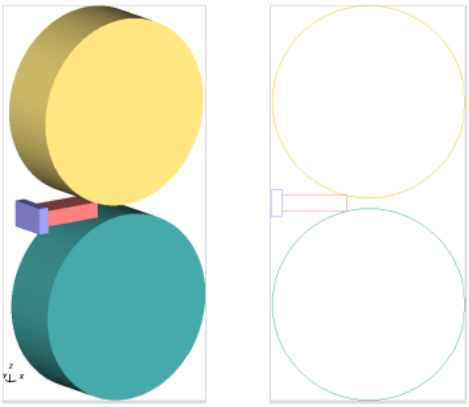

a b

Figure 64, Example of model simplification from 3D model to 2D plane strain model (MSC.Marc, 2013).

Due to rotationally symmetric nature of SPR, a 2D axisymmetric model has been determined the most suitable (example in Figure 65) and has been therefore used in all simulations throughout this work.

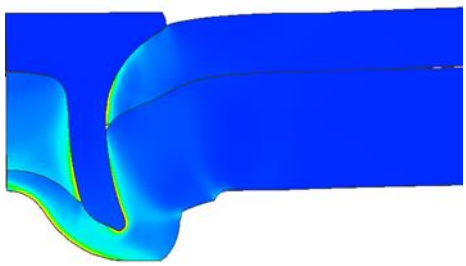

Figure 65, Axisymmetric view of an SPR joint completed in simulation

For presentation of the results, the software can revolve 2D axisymmetric model to be presented as the full 3D model – as shown in the image below.

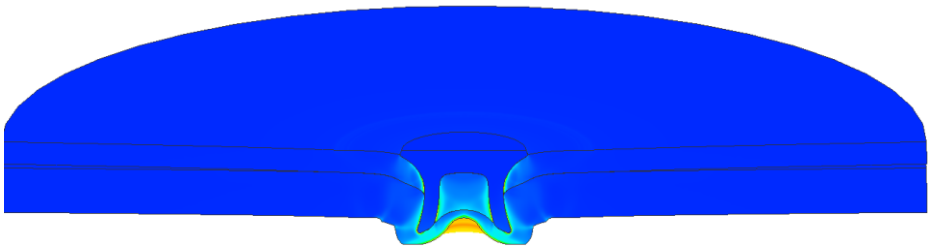

Figure 66, Completed simulation of 2D axisymmetric model viewed as 3D

Most of the results in this work are presented in the 2D axisymmetric mode for ease of comparison with a physical cross section for purposes of model validation.

4.1.1.2 Meshing

4.1.1.2.1 Initial mesh creation

Another parameter of setting the simulation process up is creating mesh or discretizing. As mentioned previously in the introduction of the FEA section, discretizing is one of the processes that takes place during the pre-processing stage of the simulation. This means that a body is split into smaller parts, the behaviour of which can be more readily calculated and predicted. These small parts are called elements and they are connected by nodes to create a mesh. A simplified view of this is offered in Fig. 33.

Figure 67, Simplified view of elements (MSC.Marc, 2013).

4.1.1.2.2 Types of elements

There are different types of elements which can be generally divided into categories based on number of dimensions they are taking into consideration (Benham et al, 1996):

Element type	Dimension	Visual representation	Used for modelling of
Spring	1D		Simple spring
Line	1D		Rod, bar, beam
Triangle	2D		Membrane, thin plate, sheet. Modelling plane strain and plane stress situations and 2D axisymmetric scenarios e.g. rivet insertion.
Quadrilateral	2D		Membrane, thin plate, sheet. Modelling plane strain and plane stress situations and 2D axisymmetric scenarios e.g. rivet insertion.
Tetrahedron	3D		Membrane, thin plate, sheet. Modelling plane strain and plane stress situations and 2D axisymmetric scenarios e.g. rivet insertion.
Hexahedron	3D		Thick plates, bricks. Modelling 3D scenarios e.g. tensile tests.

Figure 68, Types of elements (Benham, 1996)

In general, the more elements the analysed body is subdivided into i.e. the smaller the elements, the greater the accuracy of simulation results. However, a very high number of elements can also lead to a very long computational time (Benham, 1996, Hutton, 2004).

There are a few general rules that are suggested to follow when attempting to mesh components of the simulation model.

- The mesh should have at least three elements (better still five elements) over the workpiece thickness to cover bending stresses.
- The mesh should be fine enough to describe the geometry accurately.
- The mesh should be fine enough to cover gradients as accurate as possible (MSC.Marc, 2013).

To demonstrate the difference between a coarse and a finer mesh see Fig. 34. In the first picture the visibly coarser mesh does not describe the geometry as accurately as the smaller elements in the second picture.

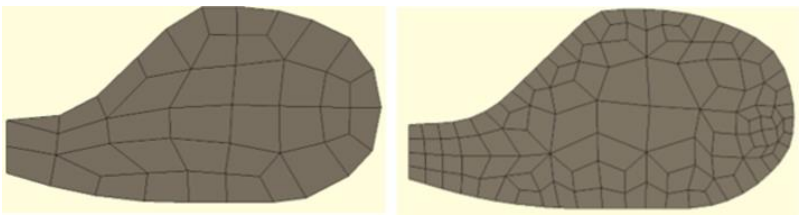

Figure 69, Course and fine mesh illustration (MSC.Marc, 2013).

It is recommended to conduct a sensitivity study to arrive at an ideal element size for any simulation. This involves running multiple simulations of the same process with different element sizes and comparing the results until there is no notable difference between the accuracy and resemblance with the experimental test. The ideal element size is one that follows the suggested rules as per above and is a good compromise between results accuracy and reasonable computation time.

One other important aspect of meshing is also the direction of meshing. There are two directions, the mesher can start building the mesh from the middle of a component outwards (Figure 70a) or the other way round, starting from the edges and moving towards the middle of the component (Figure 70b).

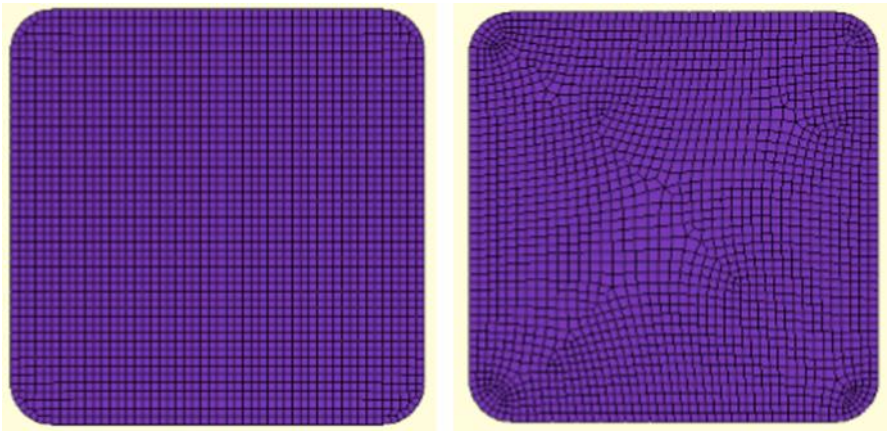

a b

Figure 70, Two different types of meshing directions.

a) Mesh being built from middle outwards, b) Mesh being built from edges towards the middle (MSC.Marc, 2013)

Both instances have advantages and disadvantages but essentially the area in which the mesher starts building the mesh first is going to have solid good quality elements whilst the parts in which the mesh is created last might be elements that are not as solid. It is recommended to use the meshing direction from outside towards the middle and hence good quality mesh on the outside for components that are likely to experience damage as this usually starts from the outside (MSC.Marc, 2013).

4.1.1.2.3 Refinement windows

This compromise can be helped by selecting areas of the model where changes e.g. deformations are expected and / or where the components have particularly complicated geometries and refining the mesh in this area only as shown in Figure 71.

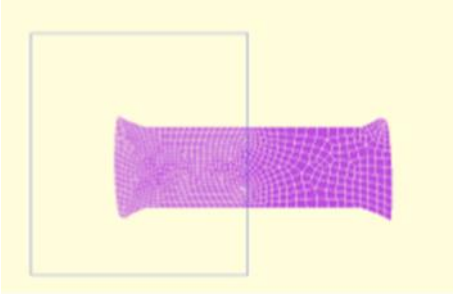

Figure 71, Refinement of mesh (MSC.Marc, 2013).

This can also go in the opposite direction, and areas where no deformation is expected, as this is not an area that will affect the simulation very much, the elements can be coarsened to save computational time.

The refinement is usually done in levels whereby each level mean an element is split four ways, one at a time. The best way to demonstrate this is schematically on a quadrilateral element as per below:

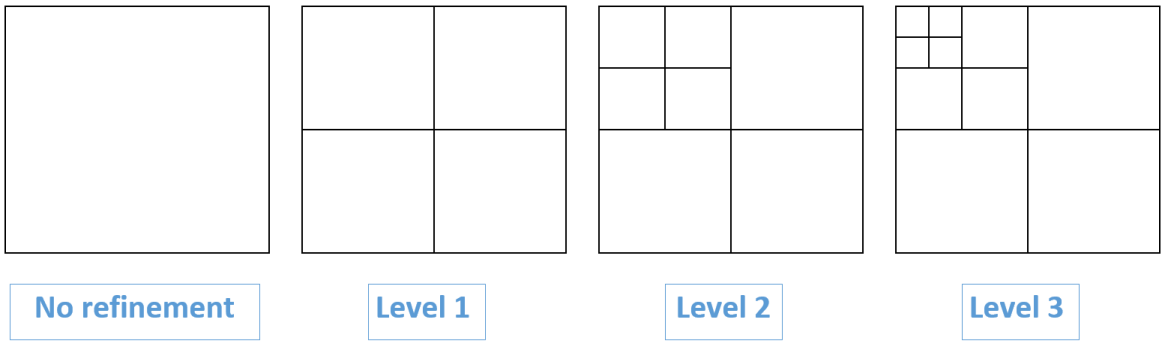

Figure 72, Schematic of levels of mesh refinement (MSC.Marc, 2013).

Refinement windows can be applied anywhere in the model and can be either fixed in space (for example placed in a location where a complex change is anticipated later on in the simulation and the deformed mesh moves into it) or can be attached to a geometry and move with the mesh at the same time (MSC.Marc, 2013).

4.1.1.2.4 Remesh

In simulations of forming processes it is a frequent occurrence that the initial mesh becomes distorted due to the large displacements and does not meet the requirements of mesh quality anymore. In this case, a remeshing is performed and the simulation continues using the new mesh from that point. The remeshing parameters can be the same as the initial mesh or a completely different type of mesh can be selected.

4.1.1.2.5 Types of remesh

Criteria based - remeshing is triggered by one or multiple criteria that are defined at the start of simulation.

- Forced – this option allows the solver to perform a remeshing to prevent a failure of the simulation (e.g. due to huge element distortion).
- None – disables any remeshing during the simulation in the entire process, i.e. remeshing is disabled in all existing remeshing objects of the process.

The point at which remeshing is trigerred is when it exceeds remeshing criteria. These are as follows:

- Immediate – an immediate remeshing is performed before the simulation starts.
- Increment frequency – a remeshing is triggered after the pre-specified number of increments.
- Tool penetration – a remeshing is triggered if the tool penetration is larger than a pre-specified value.
- Angle deviation – remeshing is performed when the angle deviation of one element is larger than a pre-specified value.
- Element distortion – a remeshing is performed when a pre-specified element distortion level is exceeded.
- Strain change – a remeshing is performed when a strain change that is larger than the pre-specified value occurs
- Minimum thickness – a remeshing follows when the workpiece element is thinner than the pre-specified value. This option is compulsory for the 2D mesh splitting functions including SPR. This option also includes a further setting on removal of small parts which is usually specified as a percentage. If this criteria is exceeded, the part is removed from the process (usually used when very small parts cause issues with stress calculations).

4.1.1.3 Cut distance

During the rivet insertion process, splitting of the sheet occurs which can cause the elements size to decrease in process. If these become too small, they can cause issues with meshing further into the simulation and therefore it is recommended to remove these from the process. The software offers an option to specify what size element should be removed from the process. This is calculated as a percentage of the workpiece area.

4.1.1.4 Time step

A related concept to mesh, also used in simulation is called time step. Time step can be defined as a division of the process of simulation into a number of small steps / increments during which the software calculates small part of stresses, strains and displacements in each individual elements, which are always the starting point for the next time step (MSC.Marc, 2013, Simufact, 2015).

There are two different types of the time stepping control, automatic and manual. In the automatic option, the time step is selected by the solver based on the previous selection of process for the simulation (e.g. mechanical joining > self-piercing). In the manual option, there are two further options, one of which includes the user setting a number of steps themselves. This option is predominantly used for the simulation of stationary processes such as upsetting. The second one is adaptive time stepping, with this method the step size can be adapted by solver during the course of simulation. Depending on the selected criterion and the current state of process, the step size could be increased if the given threshold is not reached and be decreased if the threshold is exceeded in the increment (MSC.Marc, 2013).

It can be specified to be calculated based on displacement, force or stress. Generally, however, an adaptive time step is used which means that the software determines the size of time step by itself based on the level of difficulties it comes across at each individual increment. If for example, the calculations are fairly simple such as when for instance the punch is coming down towards the rivet, the timestep can be quite large and the software determines the next step be of equal size (MSC.Marc, 2013, Simufact, 2015).

However, the next step might be more difficult as the punch hits the rivet which in turn starts piercing the top sheet. In this case, the software retraces its steps and reduces the size of the time step. What generally applies is that the finer the mesh and /or the more complicated geometry and/ or prescribed movements of the workpiece and dies, the smaller the time step and the longer the calculation time as the solver part of the software is doing a number of adjustments and iterations (MSC.Marc, 2013, Simufact, 2015).

- Distortion: the step size is controlled based on the element distortion during simulation. You can either select Automatic or input a value manually. The input value here is an estimate number of steps. The actual number of steps in simulation could be more or less than the defined value, as it is adapted by solver based on the element distortion. This method is best used with dynamic processes such as die forging.

- Increment strain change: the step size is controlled based on the max allowed strain change of each increment. This value represents the percentage strain change so it must be between 0 and 1. Default value is 0.05.
- Temperature change: the step size is controlled based on the max allowed temperature change of each increment. This is defined by the input value here. It is only available for heating, cooling and heat treatment process.
- Displacement change: the step size is controlled based on the max allowed displacement of each increment. This is defined by the input value here. This is especially useful for a process with alternating velocities. Auto step for table: the step size is adapted to all table points in table press. It is only available for processes containing a table press. For more details please read the info sheet for table press. (MSC.Marc, 2013, Simufact, 2015).

4.1.1.5 Contact

In FE modelling, contact means defining how the bodies within the simulation model contact each other is another important aspect of the simulation and there are two options currently available in the software:

- Node-to-segment
- Segment-to-segment

Node is a location on an element (Simufact, 2015) as shown in figure Figure 73a whilst segment refers to a portion of a deformable body that is used in in simulations i.e. rivet segment as shown in Figure 73.

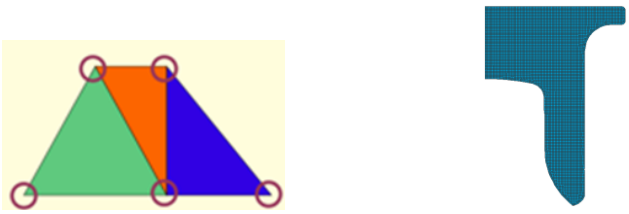

Figure 73, Illustration of node (left) and segment (right)

Node-to-segment contact

Node-to-segment contact is the default contact method for a wide range of applications. The contact is checked between nodes of one body to segments of the other body.

The contacts are applied by direct constraint conditions based on the current contact state assumptions. Contact accuracy is achieved in an iterative manner. Thus extra convergence criteria for

separation and friction are applied, which control whether the iteration process is completed or not (Simufact, 2015).

Node-to-segment contact is the preferred contact type for:

- All forming processes, that consist of one single workpiece
- Coupled die stress analysis
- Separation problems with high demands on accuracy (sheet forming, part ejection, backstroke)

Node-to-segment contact reaches its limits in applications where deformable-body–to-deformable-body (e.g. rivet to sheets, sheet to sheet) contact occurs, especially in cases where high contact pressure is applied. This can lead to penetration and performance problems within the simulation process (Simufact, 2015)

The behaviour can be improved by following the rules below:

- Define single sided contact from the body with lower stiffness to the body with higher stiffness
- Define single sided contact from the body with smaller element size to the body with bigger element size

Even after the above measures are put in place, the following limitations remain for node-to-segment contact:

- Contact depends on direction of contact definition
- Contact depends on element sizes of the contact bodies
- Contact depends on stiffness of the materials

4.1.1.5.1 Segment-to-segment contact

Segment-to-segment contact is a newly developed contact algorithm that overcomes the limitations of the node-to-segment contact. Contact is checked between segments of one body to segments of the other contact body. It can be described as an unconstrained optimization problem with the objective to minimize the penetration by adding terms to the stiffness matrix. (Simufact, 2015)

Segment-to-segment contact can be used in two modes:

Simple mode

The contact is described by adding a penalty stiffness term to the contact body boundary nodes being in contact. This is done with a penalty factor that describes the force being applied to eliminate a certain amount of penetration.

$$F_n = k_n g_n \quad \text{Eq. (13)}$$

F_n – Force in normal direction

k_n – Penalty factor in normal direction

g_n – Penetration in normal direction

If force in normal direction equals zero, then penetration in normal direction is also zero.

The found solution is the equilibrium of forces and displacements based on both, the material and contact stiffness (Simufact, 2015).

$$F_t = k_t g_t \quad \text{Eq. (14)}$$

F_t – Force in tangential direction

k_t – Penalty factor in tangential direction

g_t – Penetration in tangential direction

Same rule applies here too, if force in tangential direction equals zero, then penetration in tangential direction is also zero.

Augmentation mode

The augmentation mode adds another term to the stiffness matrix in order to enforce the penetration to be smaller than a certain threshold value. This threshold is called “penetration distance“.

Segment-to-segment contact is the preferred contact type for deformable-body-to-deformable-body contact. The benefits are:

- No direction dependencies
- No element size dependencies
- Better stress continuity at contact interfaces

There are also limitations to this model and this is mainly that it is less accurate for separation problems (Simufact, 2015).

For SPR, it is suggested that the segment-to-segment contact method as multiple rigid and deformable bodies are in contact (TechSpec1, 2019). Carandente (2018) suggested using the same method in his work on numerical analysis of aluminium alloy joints using the same software.

4.1.1.6 Temperature

Part of the setting up the simulation model is a requirement for the user is required to decide whether this should be a thermo-mechanical or mechanical only calculation. If mechanical process is selected, no temperature is calculated. If on the other hand a thermo-mechanical simulation is selected, the software uses a number of parameters to calculate the temperature, which are essential to running a simulation, if thermos mechanical model is chosen. These are thermal conductivity, specific head capacity and dissipation factor and will be explained in the following section.

4.1.1.6.1 Thermal conductivity

The heat can spread through object in three different ways; conduction, convection and radiation. The conduction is the most frequent type in solids, whilst convection mostly occurs in fluids and gases and via radiation the heat can spread through anything that does not form a barrier against it (Caltech, 2018). Conduction happens when heat transfers between a warmer and cooler object until the temperature is levelled in both. As an object is heated, its molecules gain heat and start moving faster and when they come into contact with cooler and slower moving molecules, they pass some of the energy to these. This process is repeated until the heat has spread throughout the whole object. Thermal conductivity, therefore is a measure of a solid object's ability to conduct heat.

All metals are conductors of heat although they vary in their abilities. For example metal silver, copper, gold, aluminium and bras are the top five metals with highest thermal conductivity, whilst steel and bronze have the lowest thermal conductivity. Thermal conductivity is a transport property and depends on the physical structure of the matter (Elmelin, 2019). By Fourier's law can be correlated to the heat flux across a surface (q") and the momentary temperature gradient ():

$$\sigma k = - \frac{q''}{\Delta T} \qquad \text{Eq. (15)}$$

ΔT - Momentary temperature gradient

q" - Heat flux across a surface

Typical units are W/(m K) or J/(m s K) (Simufact, 2015).

4.1.1.6.2 Specific heat capacity

The specific heat capacity (c) is the amount of energy (q) needed to raise the temperature of 1 kg of mass (m) by 1 °K. The value must be defined with respect to the temperature. A simple approach is given by (Simufact, 2015, Helmenstine, 2019):

$$c = \frac{\Delta q}{m \Delta T} \qquad \text{Eq. (16)}$$

Below are some examples of the above mentioned material properties in different materials.

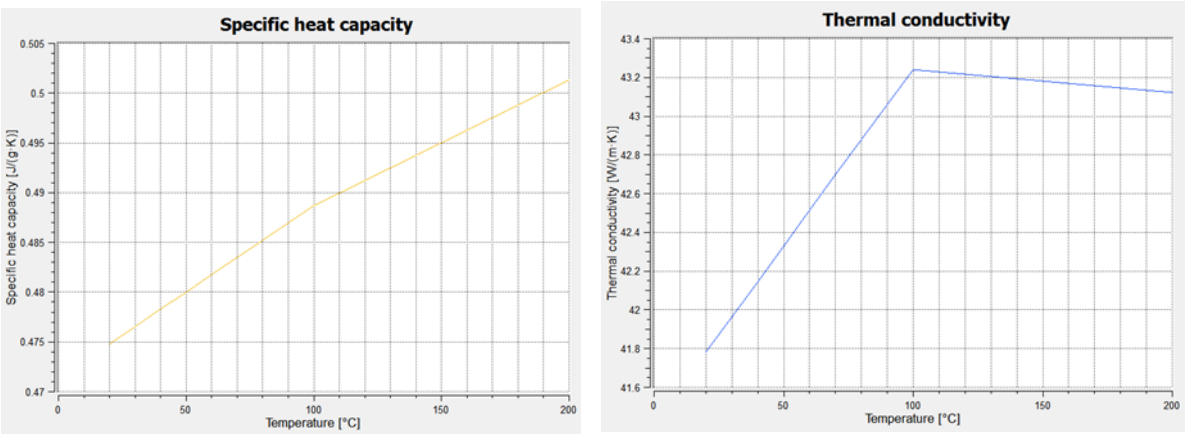

Figure 74, Example of heat Specific heat capacity and thermal conductivity in rivet materials (Hardness level 2) (Simufact, 2015)

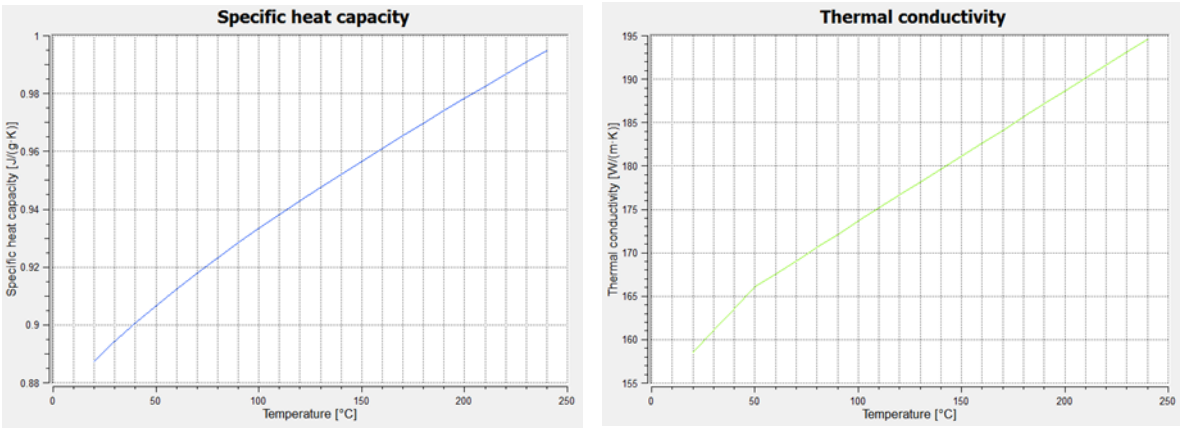

Figure 75, Example of heat specific heat capacity and thermal conductivity in soft aluminium sheet materials (AA-5182) (Simufact, 2015)

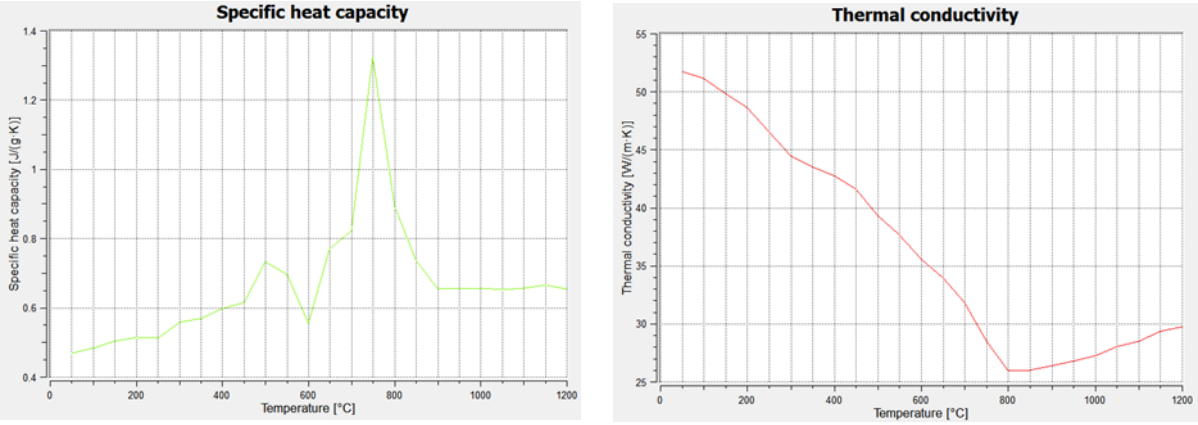

Figure 76, Example of heat specific heat capacity and thermal conductivity in mild steel sheet materials (DP600) (Simufact, 2015)

4.1.1.6.3 Dissipation factor

Dissipation factor is the last property that is needed for simulation to be able to calculate the temperatures. This is a conversion factor between the plastic energy dissipated and the heat generated. This is a dimensionless quantity that is constant in the entire model (Simufact, 2015).

4.1.1.6.4 Latent heat

There are several parameters that can be input under this category but all are non-essential values that can be added for better accuracy, however, the simulation can run without them.

- Solidus temperature – The temperature at which the material is completely solid
- Melting temperature – The lowest temperature at which the material is completely liquid. The melting temperature must be greater than the solidus temperature.
- Evaporation temperature – The temperature at which a liquid is in the gaseous state.
- Latent heat for melting – The amount of energy needed to make a solid sample liquid.
- Latent heat for evaporation - The heat needed to convert a certain amount of a liquid into a gaseous state.
- Ac1 temperature – The temperature at which the austenite formation begins.
- Ac3 temperature – The temperature at which the transformation of the ferrite into austenite ends (Simufact, 2015).

4.1.1.7 Flow curves

In addition to the above factors within the thermal properties, the flow curves provide an additional element of accuracy if obtained at multiple temperatures such as shown below.

The software carries out a coupled analysis which is referred to as thermo-mechanical calculation. This means that the analysis is divided into a thermal calculation and a stress (or mechanical) calculation and these follow each other alternately with each increment of simulation process (the result of the thermal calculation is fed into to stress one and so on).

In the thermal calculation, a heat transfer analysis is completed that takes into account thermal conductivity, specific heat capacity, mass density and latent heat if used. The resulting temperature field is then used for the mechanical calculation in order to adjust all mechanical properties to the right temperature. This is where the flow curve, if data for multiple temperatures is provided, becomes useful by interpolating between the temperature and finding the right temperature according to the strain the material is submitted to. In addition to this dissipation and friction, conversion factors are then used and the heat that comes from mechanical work is added to the next thermal calculation (TechSpec1, 2019). Caradente (2016) has advised in his paper that thermo-mechanical model with flow curves obtained at different temperatures has been beneficial to numerical modelling of 5xxx series of aluminium alloys.

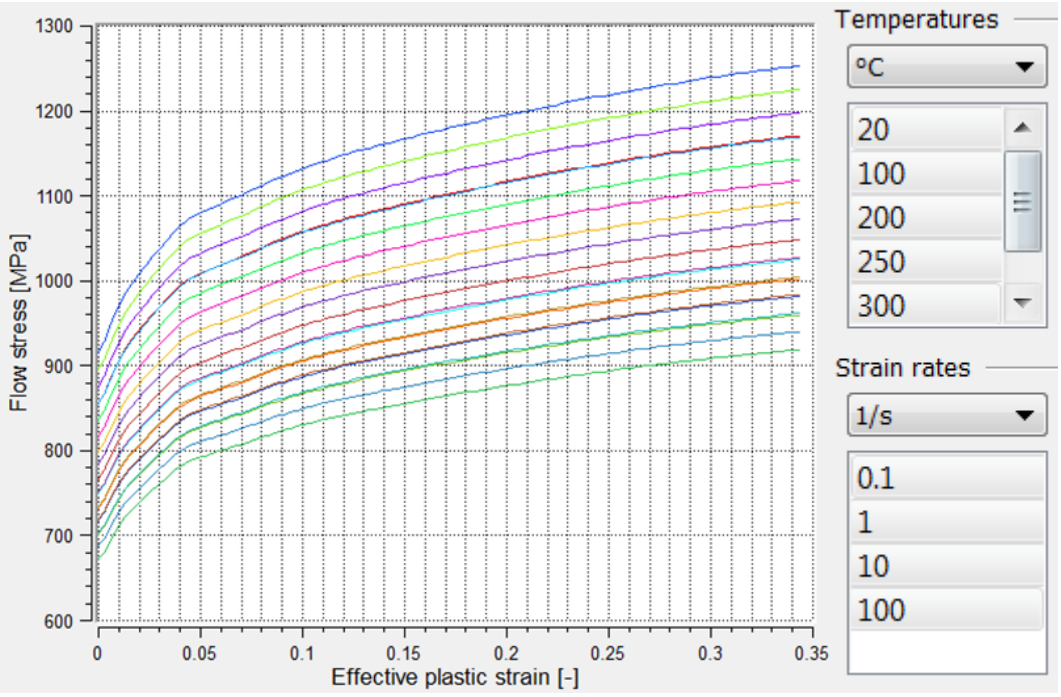

Figure 77, Example of flow curves obtained at multiple temperatures.

If a mechanical only calculations are chosen, then temperature is not calculated. This option is usually recommended in processes where temperature remains constant throughout the process or where flow curves for all materials are only available at one temperature.

4.1.1.8 Mechanics of damage

Apart from just forming, another process that takes place during the SPR insertion is damage by rivet piercing the sheets which subsequently split into two. To be able to describe this process, either a damage criteria or damage models are needed. The below section will describe options of characterizing damage that are available in the software.

There are a number of damage models used in simulations and four most used one will be will be elaborated on in this report.

- Lemaitre damage model
- Oyane damage model
- Cockroft-Latham damage model
- Johnson-Cook damage model

These models can be divided into two groups, micro mechanical and macro mechanical models:

Micro mechanical models

- Aim is to describe crack initiation and propagation of the ductile fracture
- Concerned with void formation, void growth and material de-cohesion
- Detailed description, mathematically complex, complex material parameters
- Lemaitre & Oyane

Macro mechanical models

- Aim is to investigate the causes of critical material states – stresses and strains
- Concerned with stresses and strains parameters, temporal evolution, strain related
- Easy models, no parameters, not universal
- Cockroft-Latham & Johnson Cook

4.1.1.9 Lemaitre damage model

The Lemaitre damage model describes the ductile fracture due to large plastic deformations likely caused in forming processes. The model requires material parameters which have to be calibrated in the simulation. The damage prediction is very accurate if well calibrated parameters are used. It combines the realistic description of the ductile fracture with a relatively simple recording of the material parameters (Simufact, 2015).

For this, the body is divided into very small volume elements. If a void is initiated and grows inside a volume element, it reduces its surface base. Now the element has to transfer the same load to a

smaller area, i.e. the acting stress increases with increasing damage. (In reality, the stress "avoids" the remaining "areas" , but here the effect of damage itself is simulated). The absolute (ductile) damage D is the measure for the enforcement of a volume element with voids. When D = 0 there is no damage, in the case of D = 1 the entire base surface is destroyed.

In cold forming processes with common steels D reaches a value between 0.1 and 0.3. At higher temperatures, as is the case in ductile materials, this value may increase (e.g. D = 0.90 for copper in the hot area).

In the post processing the absolute damage shows the cumulative damage. The incremental formula for the absolute damage is as follows (Simufact, 2015):

$$dD = \frac{f(\eta)\sigma^2}{2\,ES\,(1-D)^2}\,d\epsilon^p \qquad \text{Eq. (17)}$$

D - Absolute damage

$F_{(n)}$ - Function of triaxiality

σ – Von Mises stress

E – Young's modulus

S – Damage resistance

Triaxiality of materials means that if material properties are obtained in the most frequently used material test i.e. tensile test, this is in uniaxial direction only. However, in the later stages of the tensile test, referred to as necking, the material is deformed in three directions which can decrease the total stress and this needs to be accounted for.

Triaxiality is defined as the ratio of hydrostatic pressure, or mean stress and von Mises equivalent stress (Ashby, 1996).

$$\eta = \frac{\sigma_m}{\sigma_v} \qquad \text{Eq. (18)}$$

η - Triaxiality

σ_m – Hydrostatic / mean normal stress

σ_v – Von Mises stress

Hydrostatic/ mean normal stress can be calculated as follows:

$$\sigma_m = \frac{\sigma_1 + \sigma_2 + \sigma_3}{3} \quad \text{Eq. (19)}$$

$\sigma_1, \sigma_2, \sigma_3$ - Principal stress in all three directions

Von Mises stress can be calculated as follows:

$$\sigma_v = \frac{1}{\sqrt{2}} \sqrt{(\sigma_1 - \sigma_2)^2 + (\sigma_2 - \sigma_3)^2 (\sigma_3 - \sigma_1)^2} \quad \text{Eq. (20)}$$

Function of triaxiality can be calculated as follows:

$$f(\eta) = \frac{2}{3}(1+\nu) + 3(1-2\nu)\eta^2 \quad \text{Eq. (21)}$$

ν – Poisson ratio

While the material defects are more statistical and difficult to describe, a critical value for stresses / stress states can be defined easily.

Critical damage Dc is a reference value which indicates the vulnerability of a forming zone for the occurrence of cracks, i.e. susceptibility to cracking.

$$D_c = D_{1C} \frac{Q_U^2}{\sigma_v \sqrt{f(\eta))^2}} (1-D)^2 \quad \text{Eq. (22)}$$

D_c - Critical damage

D - Absolute damage

$F_{(n)}$ - Function of triaxiality

$$f(\eta) = \frac{2}{3}(1+\nu) + 3(1-2\nu)\eta^2\,\nu \quad \text{Eq. (23)}$$

σ_v - Von Mises stress

D_{1c} - critical damage in a uniaxial tension test

η – Triaxiality

With the decrease of the critical damage the probability of cracking increases (Simufact, 2015). Crack sensitivity can be determined by comparing the absolute damage D in the material and the crack

sensitivity of the forming zone D_c. When both values approach, a macroscopic crack occurs. This comparison is captured by relative damage D_{rel}. In Simufact forming this is displayed as Relative Lemaitre Damage. The higher the value tends towards $D_{rel} = 1$, the more likely is the crack occurrence (Simufact, 2015).

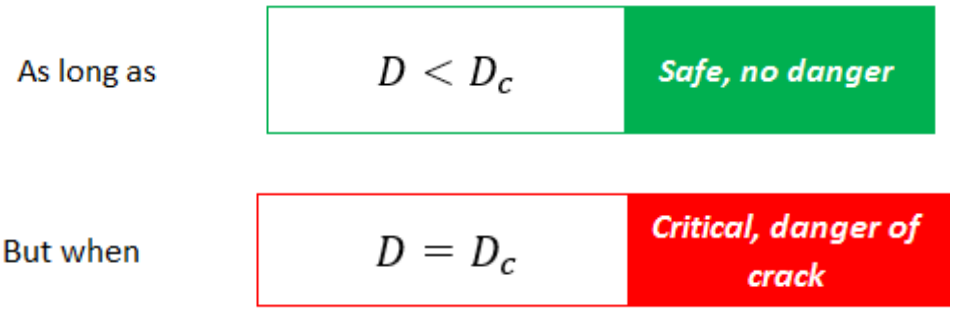

Figure 78, Criteria used in Lemaitre damage model (Simufact, 2015)

4.1.1.10 Oyane damage model

The damage model according to Oyane is based on the model conception of the ductile fracture. Like all micro mechanical models, this model is also engaged with void formation, void growth, void association and the resulting material de-cohesion. The damage calculation is based on the cavity growth, for which the change in density of the material is used. The density changes are summed up until fracture where they reach a critical value (MSC.Marc, 2013, Packo, 2011).

$$\int \left(\frac{\sigma_m}{\sigma} + B\right) \dot{\varepsilon}\, dt \geq C \qquad \text{Eq. (24)}$$

C – element removal threshold

σ_{max} – maximum tensile stress

σ – flow stress

$\dot{\varepsilon}$ – strain rate

B – material constant

4.1.1.11 Cockroft-Latham damage model

The Cockroft-Latham damage model is a macro mechanical damage model. This model is a standard model in bulk forming industries and does not require any material parameters. It can be used to compare different forming processes (MSC.Marc, 2013, Packo, 2011). Out of the four models, this is

the only one that does not require input of parameters obtained in external measurements and uses only values generated in process of simulation.

$$\int \frac{\sigma_{max}}{\sigma} \dot{\varepsilon} \, dt \geq C \qquad \text{Eq. (25)}$$

C – element removal threshold

σ_{max} – maximum tensile stress

σ – flow stress

$\dot{\varepsilon}$ - strain rate

4.1.1.12 Johnson-Cook damage model

The Johnson-Cook damage model is a macro mechanical model. The damage is described by comparing the actual effective plastic strain to the crack critical plastic strain, hence stresses are not used to determine the damage. Three dimensionless material constants and a damage threshold value are used in the model.

$$D = \sum \frac{\Delta \varepsilon^{pl}}{\varepsilon^{f}} \qquad \text{Eq. (26)}$$

The damage D is a value between 0 and 1, whereas 1 is maximum damage. The crack critical plastic strain can be determined using the following formula:

$$\varepsilon^{f} = (D_1 + D_2 \, exp(\eta^*)) \qquad \text{Eq. (27)}$$

η* - triaxiality of the actual stress state

D1 - D3 - Material parameters

Material parameters can be determined in tensile tests. At least three tensile tests with three different triaxiality states at crack zone have to be done.

All of the above models can be used in 2D as well as 3D simulations although they are more used in 3D tensile, shear and cross tension tests where they can pinpoint potential areas of cracks. The 2D option generally used for SPR does not have the cappability to model cracking in rivets or sheet and therefore the damage models are not required. The damage that occurs in a simpler 2D axisymmetric simulation of insertion is instead modelled using a minimum thickness criteria. This is a similar method to the one employed in other FE software types such as Deform.

4.1.1.13 Minimum thickness criteria mesh separation

As mentioned previously, most of the models apart from Cockroft-Latham require additional data to function which is not always easy to obtain, and therefore another method to estimate when damage in form of cracking should happen to the sheet is Minimum thickness criteria mesh separation. This model involves pre-specifying the smallest thickness the material can reach following during deformation before sheet completely splitting to simulate the fracture and simulation removing any split elements below certain criteria to prevent any issues with remeshing. This can be applicable in SPR where the top (and middle) sheets need to be fractured by the rivet leg as demonstrated in the image below.

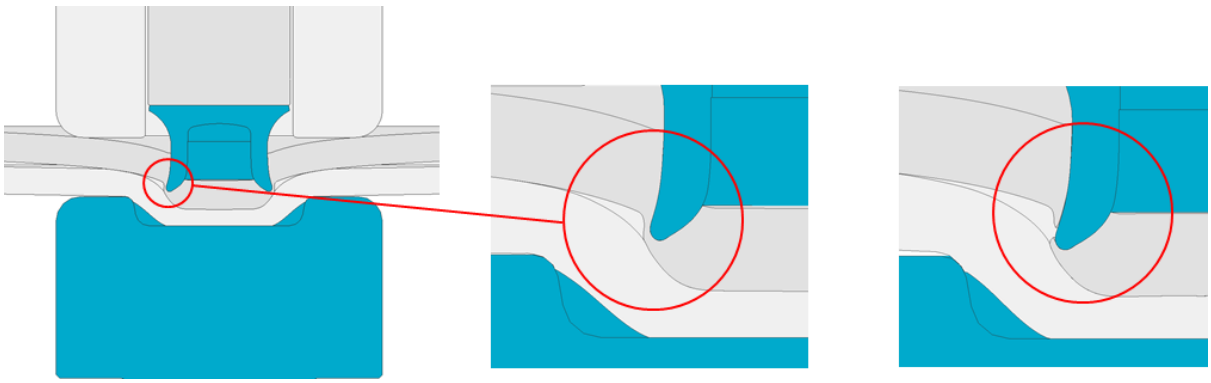

Figure 79, Minimum thickness criteria mesh separation, specifying the smallest thickness the material can reach

If this criteria is not set, the splitting is disallowed and eventually the simulation will reach very high load pressing on the sheets but not being allowed to deform. This can lead to unrealistic stresses calculation and eventually early termination of the simulation.

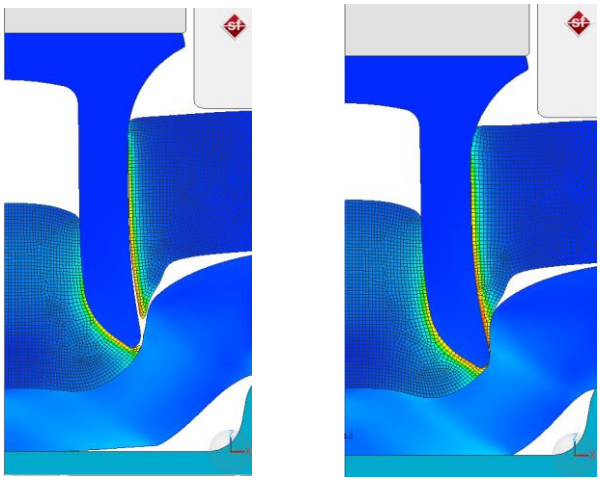

Figure 80, Miminum thickness criteria set to 0.10mm (left) setting not activated (right)

The rule of the thumb advised by Simufact staff is to use thickness no less than 1/3 of the element size as this can lead to instabilities in the mesh and consequently simulations may not run their full course.

4.1.1.14 Assessment of damage simulation based on literature

Khezri (2000) used a damage model, Cockroft and Latham, in order to model the damage created by the rivet. This model is further described in section 4.1.1.17 and is available in the Simufact software.

Atzeni et al (2009) opted for Gurson-Tvergaard damage model which describes the piercing of the sheet material as a ductile failure phenomenon. This would be a useful model for SPR as the process is based on presumption that ductile materials are used, however, this model is currently not available in the software.

A combined approach was employed by Bouchard et al (2008) who used Lemaitre-coupled damage model to describe the damage using effective stress along with erosion technique which removes elements to simulate the fracture. Lemaitre damaged model has been further explained in chapter 4.1.1.15. This approach yielded accurate results for simpler stacks, however less so for complex stacks, where results were less accurate.

Kato et al (2007) and Casalino et al (2008) and Carandente (2016) all selected to use minimum thickness fracture criteria to delete an element that has reached a pre-specified minimum thickness after which it is deemed fractured and leads to total fracture of the sheet. Casalino (2008) documented success with this method with both visual match of the joint as well force-displacement curves. He further identified that finer mesh was conducive to preserving the volume of material caused by removal of element after its fracture.

4.1.2 Process description

4.1.2.1 Model set-up and boundary conditions

The simulation model is usually a simplification of reality with some of the elements removed in order to make sure that the computational time is not excessive. In SPR, the essential components of the model are considered to be the punch, nose or blank holder, rivet, die and stacks of sheets to be joined. As can be seen from Figure 81 the C-frame and the setter (a) can be removed from the model and replaced by simpler models of nose and punch.

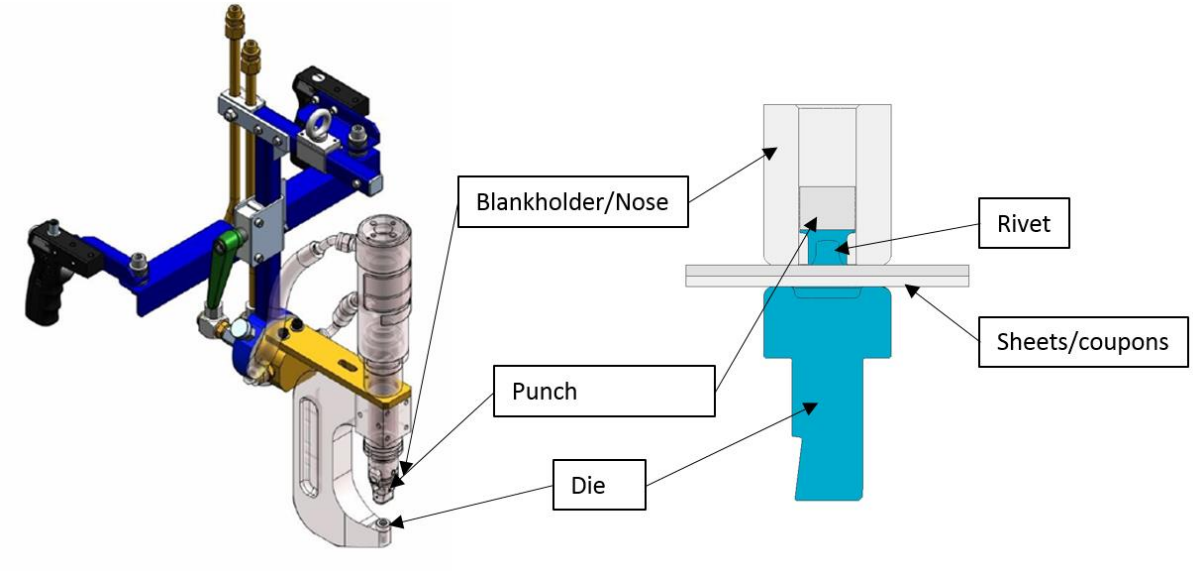

Figure 81, (left) SPR insertion equipment, (right) Simplified model of insertion equipment

Then blank holder, die and punch are used as rigid bodies without heat conduction whilst the rivet and sheet are regarded by the software as deformable bodies, for which stresses and strains are calculated. The movement of the components is defined individually for each component. Since the die is defined as rigid, without any further information it will remain fixed in space. Whilst the punch and nose are also defined as rigid bodies, they are attached to a press with a pre-specified movement which means this is the only direction they will move in. Deformable dies are positioned between the rigid die and without any specific movement restriction.

4.1.2.2 Press

As explained in the literature review chapter 2.3, there are several ways to insert an SPR rivet. Atlas Copco's most preferred insertion method is using a setter using inertia which is referred to as Servo setter. With this type of setter, the rivet is punched with a pre-determined velocity which then slows down upon piercing through the individual sheets and more energy is added throughout the process by the servo motor. Hydraulic setter is another available option and is also employed in certain scenarios. This type of setter introduces a uniform speed of insertion throughout the process with no extra energy added. Some other SPR suppliers use direct drive squeeze rivet insertion which uses a lot slower speeds.

To model a simplified version of the two options of rivet insertion methods used in this research, the software offers several options which are referred to as 'presses'.

4.1.2.2.1 Hydraulic press

Hydraulic press is available in the software with a constant velocity, a regularly (linearly) slowed down velocity or a force controlled velocity.

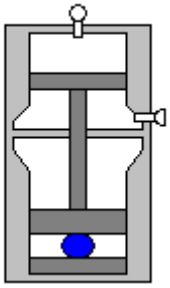

Figure 82, Schematic illustration of the hydraulic press

4.1.2.2.2 Hammer press

This is an energy based press and requires three values as an input; maximum energy, efficiency during stroke and mass.

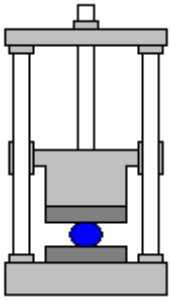

Figure 83, Schematic illustration of the hammer press

4.1.2.2.3 Screw press

Similarly to hammer press, screw press is an energy based press and requires three input values; gross energy maximum ram speed and efficiency during stroke.

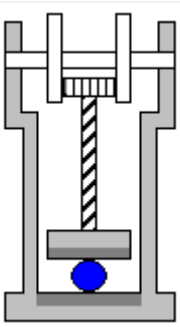

Figure 84, Schematic illustration of the screw press

4.1.2.2.4 Crank press

The crank press uses a crank to convert the rotation of a combined shaft to the translation of a piston by an arm connected to the crank. The parameters to be input are revolution, crank radius and rod length. (Simufact, 2015).

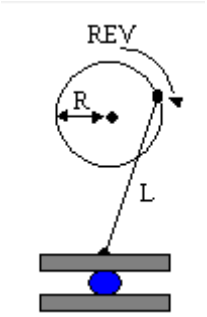

Figure 85, Schematic illustration of the crank press

4.1.2.2.5 Orbital forging press

Orbital forging (previously named "Radial press") is an incremental cold forming process, in which the centre axis of the upper die is slightly tilted with a specific angle and then rotated around the vertical axis. This reduces the contact area between the die and the work piece and thus the forming force as well as friction force are substantially reduced.

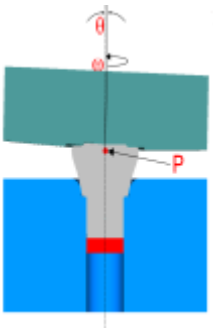

Figure 86, Schematic illustration of the orbital forging press

4.1.2.2.6 Scotch yoke drive press

Another press option is Scotch yoke mechanism which also known as eccentric press. This is a mechanical type of press and requires maximum stroke and revolutions as data input.

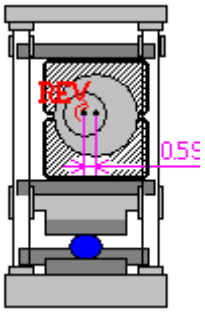

Figure 87, Schematic illustration of the Scotch yoke drive press

4.1.2.3 Clamping

Another aspect that needs to be pre-set in SPR is clamping. This is done by done using a component called nose (also referred to as blank holder) which consists of a number of components. The main purpose of this component is to hold the riveted sheets down to prevent dishing as well material flowing out of the die and generation of gaps between the sheet during the insertion process (TechSpec, 2019).

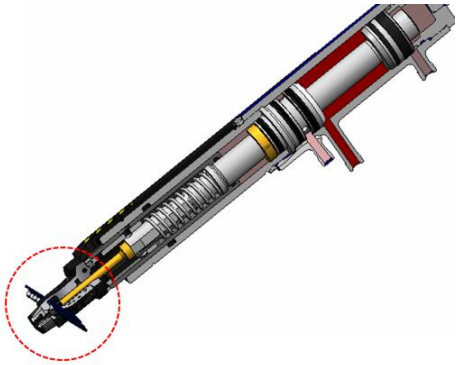

Figure 88, Clamp mechanism on servo setter

The part of the nose that comes directly in contact with the joint is a shape of hollow cylinder with external diameter of 18.0mm and internal diameter 8.0mm. The side of the nose that comes in contact with the top sheet has a radius on both internal and external diameter.

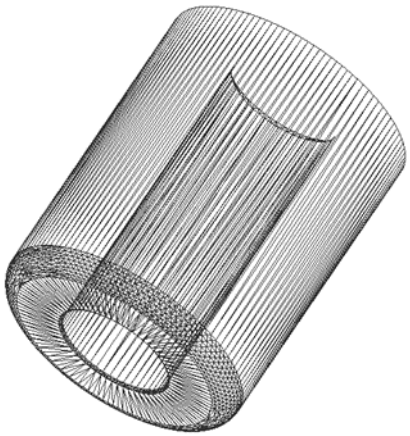

Figure 89, Model of blankholder/nose

The nose is put into action by use of spring mechanism attached to it and there are several methods in which the clamping can be executed in Atlas Copco – all related to the timing of the spring mechanism engaging, i.e. Pre-clamp or intermediate clamp. Each of these have their pros and cons (TechSpec, 2019).

4.1.2.3.1 Pre-clamp

In the pre-clamp scenario, the nose is pressing down on the sheets with a constant force of 5KN from the beginning of the insertion and is released along with the punch at the end of the insertion process. This method of clamping provides a stable and robust joints as the sheets are completely fixed in place throughout the entire process allowing the die to fully fill. However, in some specific instances such as when the die is too small, this restriction may cause immobility of the material which cannot temporarily flow out of die to accommodate the rivet legs being inserted. In some circumstances, this can lead to need for increased velocity and consequently increased force which can negatively impact the length of the life cycle of the setter as well as the rivet can be more prone to cracking. Another theoretical disadvantage, although not completely confirmed, of the pre-clamp is that by being restricted, the materials around the rivet might experience more local hardening than in for example post-clamp where this does not happen. This may lead to further stress added to the rivet and increase the capacity for cracks further still. Setters with pre-clamp are currently not used very frequently in Atlas Copco (TechSpec, 2019). Pre-clamp is only available in hydraulic setters.

4.1.2.3.2 Intermediate clamp

With this method of clamping, the spring mechanism is pressing on the sheet with force of 200N from the start of the process and this is followed by engagement of the clamp mechanism with 8 kN of additional force at a pre-set time near the of the end of insertion. This is meant to prevent sheets from dishing when they are about to be pulled downwards by the rivet which is at this point in the last

stages of compression when the highest force is being exerted, as shown in the image below. The point of the clamp engagement is dependent on several parameters – size of the rivet (3.0 or 5.0mm), type of actuator (250mm or 150mm) and the length of the stroke (or the length of the nose). On average, the clamp is engaged when the rivet is 0.525 - 0.55mm away from flush position for 5mm rivet and between 0.35mm and 0.40mm away from flush position for 3mm rivet (TechSpec, 2019).

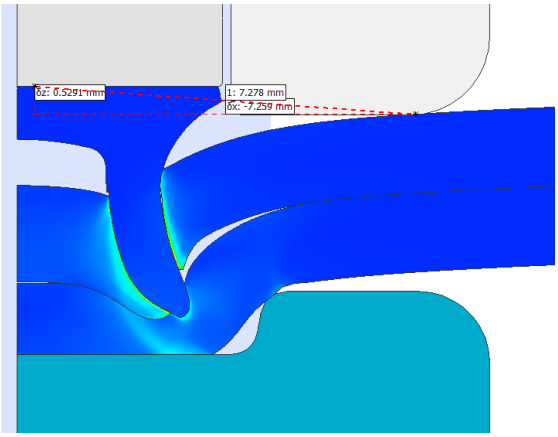

Figure 90, Point at which the clamp comes on and the nose is pressed down with 8kN.

The most frequently used timing is the clamp engaging 0.525mm before the rivet head is at the same level as the top sheet i.e. flush. Whilst this method of clamping gives the material more room to flow into by not restricting the movement of the sheets from above, it is also suspected that the die may not be fully filled due to the substrates temporarily flowing out of the die before they are squeezed back in by the nose pressing them down with 8 kN force. It is suspected that this is creating internal gaps inside the rivet in process leading to lower interlock. This clamping method is only used with servo setter.

4.1.2.3.3 No clamp

The last method is when there is no clamp used, which is available, however, this method leaves large gaps between the sheets and hence is used only in very limited scenarios.

4.1.2.3.4 Modelling clamping in simulations

To replicate this process in simulation, the software uses die springs which are used to control the movement of dies and in this specific instance the nose (blank holder).

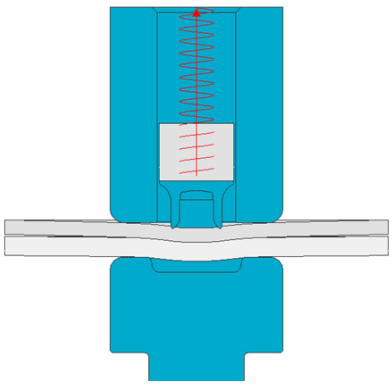

Figure 91, Die spring replicating the clamp mechanism

The springs available in the software are categorised according to their directions, as shown in the image below. A released spring counteracts in the direction D whilst with the compressed spring, the springs acts in direction D.

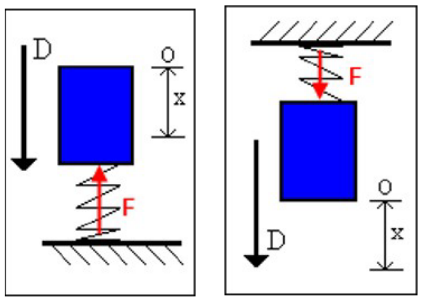

Figure 92, Released spring (left) and compressed spring (right) (Simufact, 2015).

A 'released' spring has been used to model the default clamp model which starts counteracting with full force as soon as the nose touches the top sheet. This is equivalent of the pre-clamp in the physical tests.

4.1.3 Material characterization

The type of material to be joined will determine what rivet and die needs to be used and so has an immense influence on SPR. The type of material will also influence how the material will behave during insertion and one of the main processes that take place during this, i.e. cold forming. Therefore the material characterization is one of the most crucial parts of simulation.

To create material property for simulations using Simufact software, the following data can be input in order to fully characterize the material:

- Chemical composition
- Thermal properties
- Mechanical properties
- Flow curves
- Anisotropy
- Damage
- Electromagnetic properties
- Microstructure
- Diffusion
- Creep

In context of SPR, some of these are optional entry i.e. simulation can run without them and in some cases SPR simulation does not use them.

- Chemical composition – applicable only in process type Casehardening in the application module heat treatment.
- Anisotropy – optional input, mainly used in deep drawing process with consideration for anisotropy. Unless specified, all simulations assume isotropic elasticity.
- Damage – optional input, damage based mesh separation can be used instead of Damage models.
- Electromagnetic properties – applicable in calculations of heat generated either from an electrical current or from an electromagnetic field passing the material (e.g. induction heating).
- Microstructure – optional input, used when microstructural evolution is required.
- Diffusion – optional input, applicable in case hardening process in order to equalize the carbon profile in materials.
- Creep – applicable when using process Simufact Additive and Simufact Welding.

The compulsory properties without which an SPR the simulation will not run are as follows:

- Thermal properties – include thermal conductivity, specific heat capacity, dissipation factor and latent heat (more explanations on this are in chapter 4.1.1.4.2).
- Mechanical properties – include Young's modulus, Poisson's ration and density.
- Flow curves

The former two, thermal properties and mechanical properties (which are used to model the elastic deformation) can usually be obtained from material properties records freely available from multiple sources, such as engineering publications or material suppliers' info sheets.

However, it is the latter that is the most important part of the material characterisation process needed for SPR simulation. Flow curves are graphs that describe strain hardening of metals (Alves et al, 2011) and they dictate how the materials behave once the plastic deformation starts.

To understand how these support the simulation it is important to know the concept of material forming. The next few sections will therefore look at what is happening to materials during forming and what is needed to create flow curves that describe the material in sufficient detail for the software to provide accurate results.

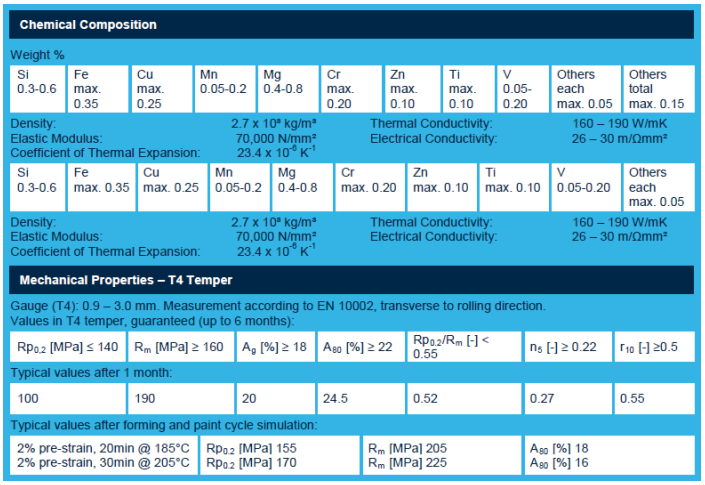

Chemical Composition

Weight %

Si	Fe	Cu	Mn	Mg	Cr	Zn	Ti	V	Others each	Others total
0.3-0.6	max. 0.35	max. 0.25	0.05-0.2	0.4-0.8	max. 0.20	max. 0.10	max. 0.10	0.05-0.20	max. 0.05	max. 0.15

Density: 2.7 x 10³ kg/m³ | Thermal Conductivity: 160 – 190 W/mK
Elastic Modulus: 70,000 N/mm² | Electrical Conductivity: 26 – 30 m/Ωmm²
Coefficient of Thermal Expansion: 23.4 x 10^{-6} K^{-1}

Si	Fe	Cu	Mn	Mg	Cr	Zn	Ti	V	Others each
0.3-0.6	max. 0.35	max. 0.25	0.05-0.2	0.4-0.8	max. 0.20	max. 0.10	max. 0.10	0.05-0.20	max. 0.05

Density: 2.7 x 10³ kg/m³ | Thermal Conductivity: 160 – 190 W/mK
Elastic Modulus: 70,000 N/mm² | Electrical Conductivity: 26 – 30 m/Ωmm²
Coefficient of Thermal Expansion: 23.4 x 10^{-6} K^{-1}

Mechanical Properties – T4 Temper

Gauge (T4): 0.9 – 3.0 mm. Measurement according to EN 10002, transverse to rolling direction.
Values in T4 temper, guaranteed (up to 6 months):

$Rp_{0.2}$ [MPa] ≤ 140	R_m [MPa] ≥ 160	A_g [%] ≥ 18	A_{80} [%] ≥ 22	$Rp_{0.2}/R_m$ [-] < 0.55	n_5 [-] ≥ 0.22	r_{10} [-] ≥0.5
Typical values after 1 month:						
100	190	20	24.5	0.52	0.27	0.55

Typical values after forming and paint cycle simulation:

2% pre-strain, 20min @ 185°C	$Rp_{0.2}$ [MPa] 155	R_m [MPa] 205	A_{80} [%] 18
2% pre-strain, 30min @ 205°C	$Rp_{0.2}$ [MPa] 170	R_m [MPa] 225	A_{80} [%] 16

Figure 93, Example of material property data available from material supplier Novelis.

4.1.3.1 Process of metal forming

During an extensive forming such as one that occurs during SPR, two types of deformation occur, elastic and plastic.

To illustrate these concepts better, it might be helpful to introduce the tensile test as a basic away of obtaining material properties. This test involves a T bone specimen pulled apart in a tensile test machine and its elongation under the tensile stress is recorded to document the material behaviour (Kelly, 2012).

The initial stages of the tensile test consist of elastic deformation. If the load continues to increase, the material reaches what is referred to as Yield point and this is when the deformation reaches the plastic region and material starts to undergo plastic deformation. Further increases in loading

(referred to as Flow stress) are required to continue the plastic deformation; this is termed work hardening Palaniswarmy, Billur, 2012).

What is happening during the deformation to the sample can be best demonstrated by the following the image.

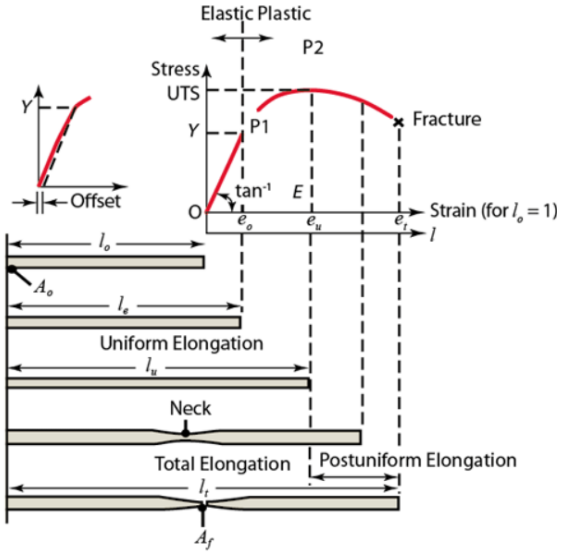

Figure 94, Deformation of tensile test sample (Altan, 2011)

It has been noted that at relatively low temperatures the force displacement curve generally follows the same pattern regardless of the rate at which the sample is pulled apart (Kelly, 2012).

The above force-displacement curve can now be looked at from perspective of stresses and strain relationship which is a starting point of a flow curve.

There are two methods used for describing this relationship. The first one is engineering stress (or nominal) and strain and the other one is true stress and strain.

At small elongations, predominantly in the elastic region, the differences between the engineering and true stresses and engineering and true strains are insignificant, however, where high contact stresses are involved and the deformation starts reaching the plastic region, the two calculations can produce different results as shown in Figure 95.

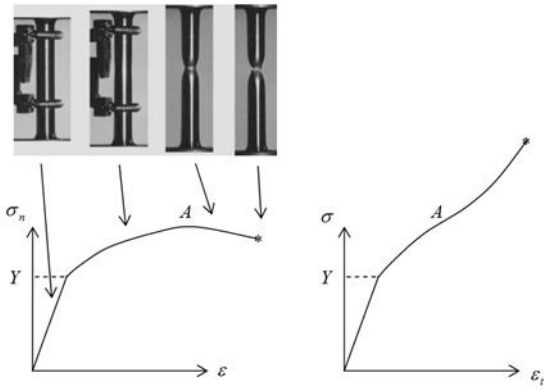

Figure 95, Engineering stress and strain curve and (b) True stress and strain curve

It can be noted that the force displacement curve shown in fig. is essentially an engineering stress-strain curve. The related image of the sample in Figure 95 shows that at point A necking starts which is a reduction in cross sectional area and shortly after this the sample breaks. Point A is referred to as Ultimate tensile strength of the material which is the maximum strength the material can withstand before breaking (Kelly, 2012, Palaniswarmy, Billur, 2012). Practicalities of measuring true stress and stress are very complex, involving cross sectioning sample at every stage which is unreasonable and therefore it is engineering stress and strain that is always measured and they can be converted to true stress and strain by using the following equations (MSC.Marc, 2013):

$$\varepsilon_t = ln(1+\varepsilon) \qquad \text{Eq. (28)}$$

$$\sigma_t = \sigma(1+\varepsilon)$$

ε_t – true strain

σ_t - true strain

ε – engineering strain

Using the above information it is possible to determine the stress and strain relationship in order to describe the behaviour of a material specifically for purposes of FE analysis using Simufact software. This process results in creation of a flow curve which is the main descriptor of materials' behaviour in engineering processes involving forming of metals and more and more increasingly, numerical modelling (Alves et al, 2011, Simufact, 2015).

4.1.3.2 Flow curves

The starting point for flow curves is the true stress strain curve, however, the total strain of the curve is made up of elastic strain and plastic strain (University of Babylon, 2018, ASTM standard, Simufact, 2015).

Eq. (29)

$$\varepsilon_{total} = \varepsilon_{elastic} + \varepsilon_{plastic}$$

Since the software will be using Poisson's ratio and Young's modulus to linearly relate the stress and strain during the elastic deformation and these values are set as constants in the software for each material to model the elastic deformation, the elastic portion of strain needs to be removed.

To do this, it is required to know where the elastic deformation ends. This is at what is referred to as yield point which is when the material is exposed to large enough stress to start deforming plastically. This level of stress is referred to as yield point $\sigma_{y.}$ If the stress level exerted on the material after this point are high enough to keep the material deforming, this is referred to as flow stress (Benham, 1996).

In some instances, the yield point can be clearly pinpointed on the true stress strain curve as a sudden sharp change of direction of otherwise linear curve. This is typically behaviour of some steels (University of Babylon, 2018, ASTM standard) and can be seen in Figure 96 below – curve C. However, with a lot of the materials, there is no a clear point in the curve to indicate the end of elastic deformation and the curve deviates rather gradually into a non-linear plastic deformation – as shown in image below, curve B. In this case, an estimation of the yield point is made. This is called proof stress, $R_{p0.2.}$ To obtain this value, a point is placed at an offset value of strain of 0.002 or (0.2% strain) and a parallel line is drawn along the linear part of the curve and the intersection of this line and the stress and strain curve is the yield point – as shown in image below. Curve A is an example of a very brittle material that proceeds to a fracture directly following the linear deformation stage without any non-uniform deformation (University of Babylon, 2017).

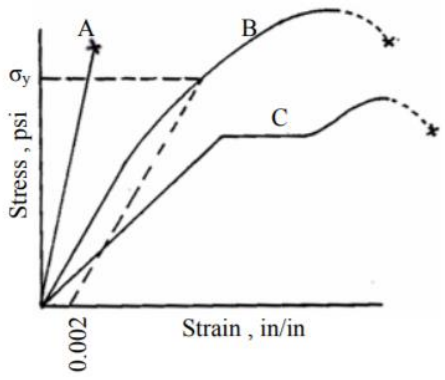

Figure 96, Example of stress and strain curves (ASTM standard 370)

Further demonstration of determining yield stress to created a flow curve is shown in Figure 97

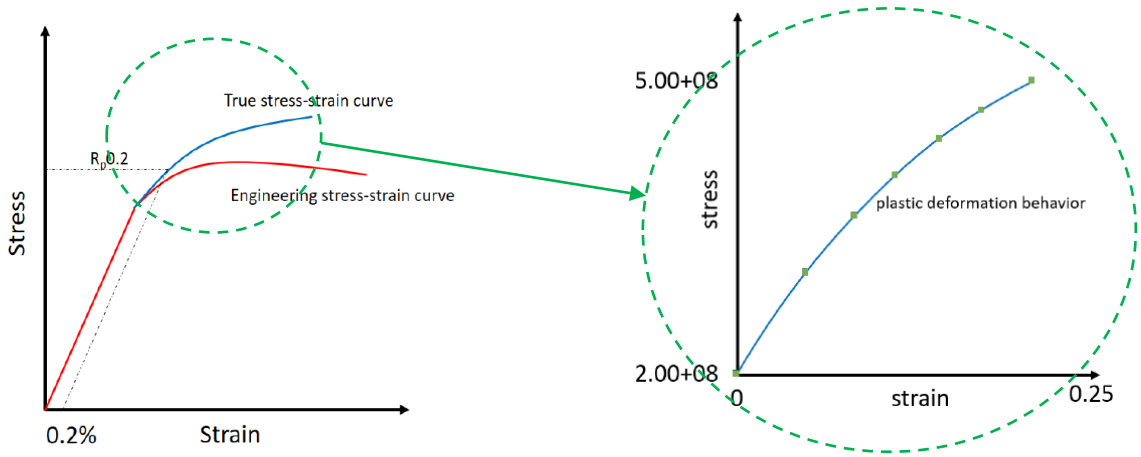

Figure 97, Illustration of determining yield point

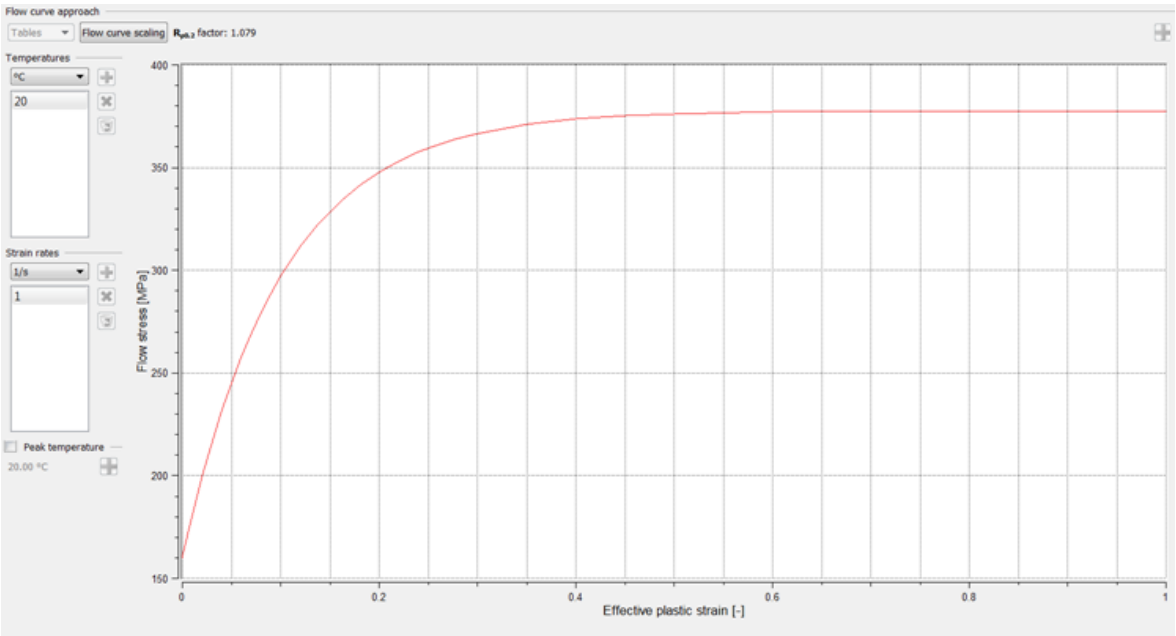

Figure 98, Example of a flow curve in the software

The flow curve can now be used, however, at this stage, most instances of materials completed using tensile test might show behaviour only up to a very limited strain. This is due to the fact that the material data from physical tensile test is only available up to the onset of non-uniform deformation in form of necking and does not capture material's behaviour at a strain higher than that. With some softer materials the strain can be measured up to 0.2 but with harder materials, such as high grades

of press hardened steels, the strain measured in a tensile test can be as little as 0.035 before the necking starts due to its brittleness (Eller, 2015). This means that in a simulation where material needs to deform further, the available data may not cover the whole range of strain required for the deformation in SPR (TechSpec1, 2019).

One way to resolve this is to extend the strain is to use different type of material testing that evaluates the strains to a higher extent such as compression testing or combine the tensile testing with another test that can reach higher strains or create extra support points.

Another common way is to extrapolate the flow curves to unknown values using equations that have proven to deliver realistic results (Simufact, 2015). Typical Equations for cold forming are Hollomon's, Ludwik's, Swift's, Hocket-Sherby's, Voce, Extended Voce etc. If temperature and strain rate effects need to be specifically considered, a more complex equations can be used such as Johnson Cook, Hensel Spittel, GMT. An extrapolated flow curve may look similar to the one below (Figure 99).

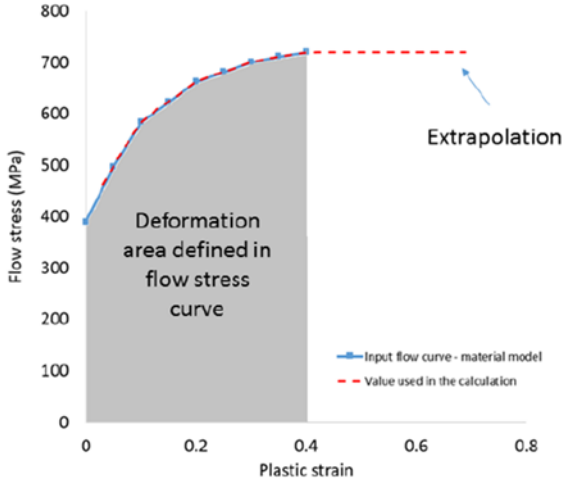

Figure 99, Example of extrapolated flow curve

Apart from methods of obtaining the flow curves (i.e. mechanical testing) and methods of extrapolating them, there are a couple of more aspects to be considered when creating flow curves:

- Conditions of testing – such as temperature and strain rate
- Material variations – materials might vary from batch to batch in material properties due to manufacturing variations as well as natural aging of materials.

All four aspects will be explained in the next few sections.

4.1.3.3 Type of testing

The first one to look at is the source of flow curves. There are several means of obtaining these flow curves (Traphöner at al ,2018, Bruschi, 2014). Amongst others, these include:

- Tensile testing
- Compression testing
- Stack compression testing
- Bulge testing
- In-plane torsion testing

4.1.3.3.1 Tensile testing

The already previously explained, tensile technique of obtaining flow curves is deemed the most readily available method and is also the most widely used (Campos, 2014, ASTM E8, 2013). As previously explained in the literature review, tensile test consists of sample of a flat specimen cut out from metal sheet or a cylindrical tubular specimen (Figure 100). The specimen is gripped at each end by specially designed grips and stretched in opposite directions in a tensile test device (Figure 101) usually at an agreed stretching rate. The force required to hold the specimen in its place at different rate of stretching is recorded. The extensometer is used to measure and record elongation in real time (Palaniswarmy, Billur, 2012).

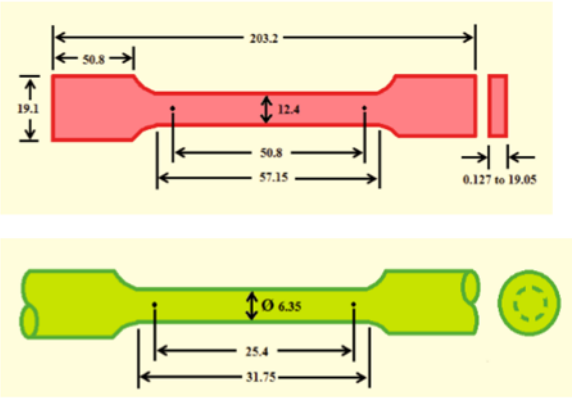

Figure 100, Types of specimens for tensile tests flat or tubular

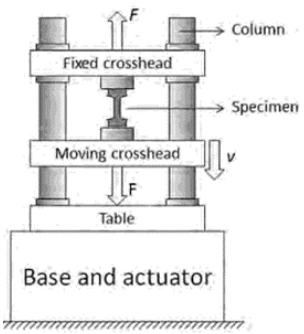

Figure 101, Tensile test machine

Whilst tensile tests are frequently completed using quasi-static strain rate at room temperature, the tensile test can be done at various strain rates and temperatures.

The resulting measurements reveal fundamental parameters of the material eg. deformation, stresses and strains and further parameters such as Young's modulus, elastic and proportional limit, tensile, yield and ultimate strength can be calculated (Fallahiarezoodar et al, 2015).

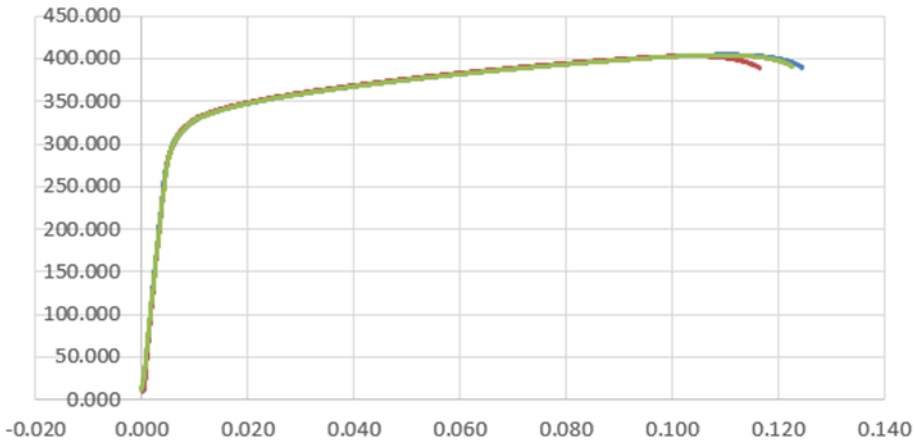

Figure 102, Tensile testing stress v strain curve for AA6111-T4 with engineering strain on x and engineering stress on y

The disadvantage of this method is that the material does not achieve a particularly high strains before the onset of necking (Traphöner at al, 2018). The additional concern is that the uniaxial motion of stretching the sample is less representative of the SPR process which is exerting high compression forces on the rivet and materials. As the data is to be used to predict how the material will behave in other applications, and specifically SPR, it might be more preferable to use testing that measures higher strains and use a method that is more representative of the SPR process. This leads on to the next method, which is compression testing.

4.1.3.3.2 Compression testing

The compression testing is essentially the opposite of tensile testing so instead of the sample being pulled apart, it is crushed by two opposing plates exerting compressive loads across the surfaces of

the top and bottom of sample interface (Hamidon, 2019). The sample shape is, unlike in tensile test, is a cylinder with a specific ratio of height and diameter. During the test, the sample experiences an elastic deformation first, followed by plastic deformation which causes the sample to become flatter and shorter in the direction of the force and expand by bulging out on in a direction parallel to the force (Hamidon, 2019, Testresources, 2019).

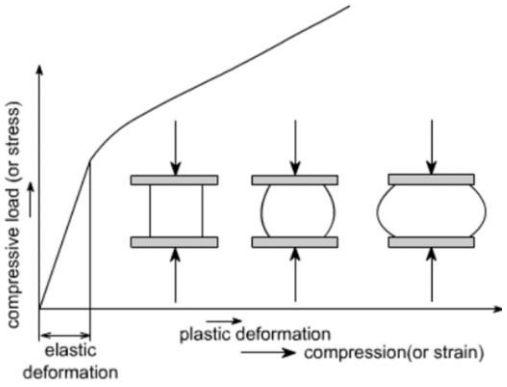

Figure 103, Schematic of compression test (Alves, 2011).

Similarly to the tensile test, deformation stresses and strains can be measured, the results report parameters such as elastic limit, yield, ultimate and compressive strength.

The most common set up of a compression test is with the two forces opposing each other, there are other ways to do this testing such as directing the pressure to multiple axes of the sample in order to change the usually uniaxial test to be biaxial or triaxial. Similarly to the tensile test, the compression test can also be carried out at higher temperatures in order to determine the behaviour of material under different conditions (Hamidon, 2019, Testresources, 2019, Hochholdinger et al, 2009).

Due to the absence of necking and hence ability to record higher strains than for example tensile test as well as similarities to a lot of forming processes using compressive forces, the compression test is the second most widely used testing method (Alves, 2011).

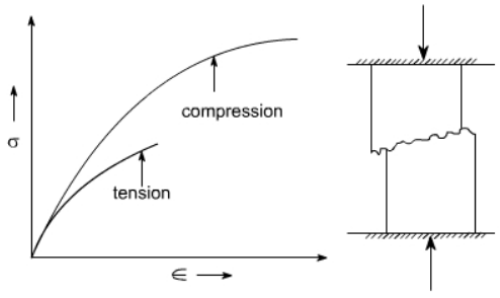

Figure 104, Comparison of tensile against compression test results (NPTEL, 2016)

There are of course concerns with this type of test too, with friction adding extra force into the process, which may interfere with the stress and strain responses of the material. The friction can also

cause bulging out of the sample in the middle due to the restricting the movement on the interface between the sample and plate (Alves, 2011). There are ways to curb the effect of the latter by measuring the barrelling and correcting the friction based on these measurements but even despite these measures both of these might cause a degree of error in the flow curves (Alves, 2011).

Further issue can be cause by the fact that the process relies on the measurements of transducers and there are also technical difficulties associated with operating extensometer directly on the specimen. These can all lead to inaccuracies in flow curve calculations too (Alves, 2011).

4.1.3.3.3 Stack compression test

As mentioned above, used despite some discrepancies that may occur in result flow curves. the compression test is one of the most widely used method of obtaining data for flow curves. However, producing the required cylindrical sample is not always a possibility when the material is exclusively supplied as sheet or plates. In this instance, it was suggested by Pawelski (1967) that the sheet material could be cut into discs and stacked on top of each other to form a cylinder of size ratio similar to that used for compression testing. The machinery used for this testing is the same as that used for conventional solid sample testing.

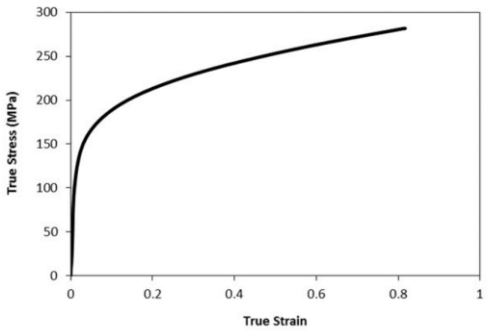

Figure 105, Typical result of stack compression test (Alves, 2011)

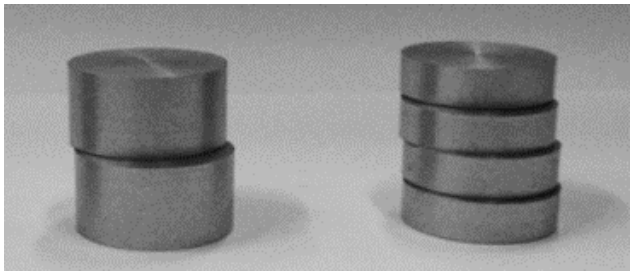

Figure 106, Sample used for stack compression test by Alves (2011)

This method of testing is not used as widely, due to belief that it might not be as effective as compression testing due concerns regarding friction between the individual stacks. There is some research available comparing conventional compression and stack compression tests which does

indeed confirm that if sliding friction occurs between individual stacks, an inhomogeneous flow follows (figure …) which can lead to a rise in stresses and strains closer to the boundary.

However, when the researchers extracted the load displacement curve this did not seem to be affected by the inhomogeneous flow which theoretically means that the flow curve is not affected by the inhomogeneous flow either. To ensure that the test is as accurate as possible and recreate similar condition achieved by compression testing, however, creating sticking friction conditions between the individual sheets would be recommended. This could be achieved by applying glue between individual sheets. (Alves et al., 2011). However, even this is not without concerns as shown in researcher by Hochholdinger et al (2009) who have glued three discs to create a cylindrical specimen for their stack compression tests and bulging, typical for compression tests has occurred in the sample.

Figure 107, Bulging behaviour in stack compression test with glued stacks. (Hochholdinger, 2009)

They have accounted for friction in their research and compared against scenario without friction consideration as shown in image below.

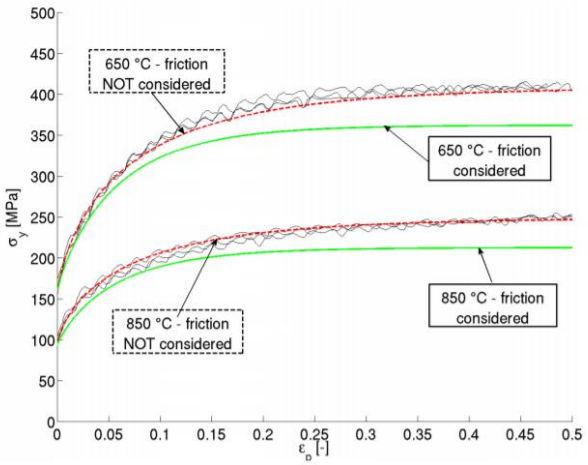

Figure 108, Flow curves created by compression testing with and without accounting for friction. (Hochholdinger, 2009)

Another concern related to the preparation of the sample was cutting the blanks which has proven to be a difficult task and several methods had to be tried out. Stamping the left the samples slighly bent

whilst laser cutting was likely to alter the properties of the material by heating them. The wire cutting has proven the least intrusive and most efficient way of blanks cutting. (Kraus, 2018).

Based on the above, previous research has confirmed that the results from stack compression testing are similar to the conventional solid testing which means that when cylindrical solid sample is not available, sheets of the testing material can replace this test. One however, must be aware of the aspect ratio of the sheets – very low aspect ratio might increase sensitivity to friction leading to breakdown of the lubricant between sheets and platens and build up pf pressure, thus leading to inhomogenous flow once again. (Alves et al, 2011).

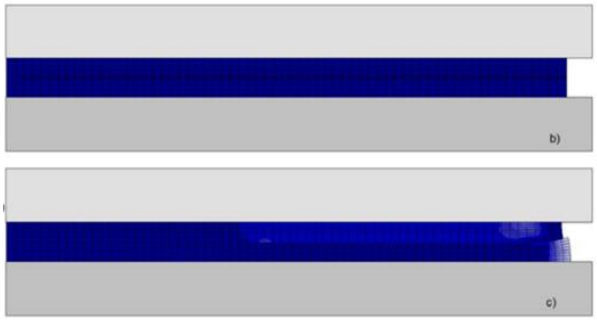

Figure 109, Example of inhomogenous flow in stack compression test (Alves, 2011)

4.1.3.3.4 Hydraulic bulge testing

Hydraulic bulge test in another alternative that has been suggested for sheet materials (Alves, 2015). The test involves a circular blank clamped around the edge in the bulge machine and application hydraulic pressure below the sample by using oil controlled by a punch. The upwards motion of the punch causes the material to bulge out and thin on the dome part (Junhe et al, 2013). The measurements are completed using am attached laser and camera to analyse geometry and strain respectively (Uthaisangsuk, 2009).

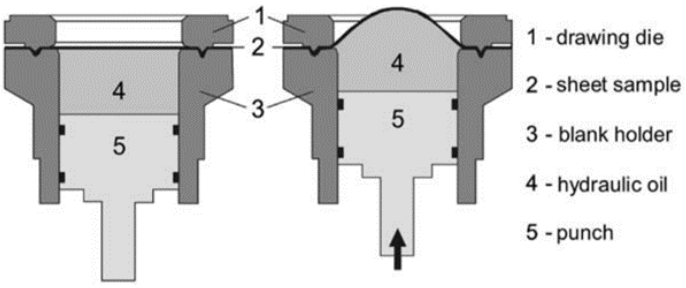

Figure 110, Hydraulic bulge testing set up (Junhe et al, 2013)

In comparison to other forms of testing such as tensile, this method has several advantages. This includes biaxiality and absence of necking which means that the strain can reach large strains seen in sheet metal forming processes (Campos, 2014).

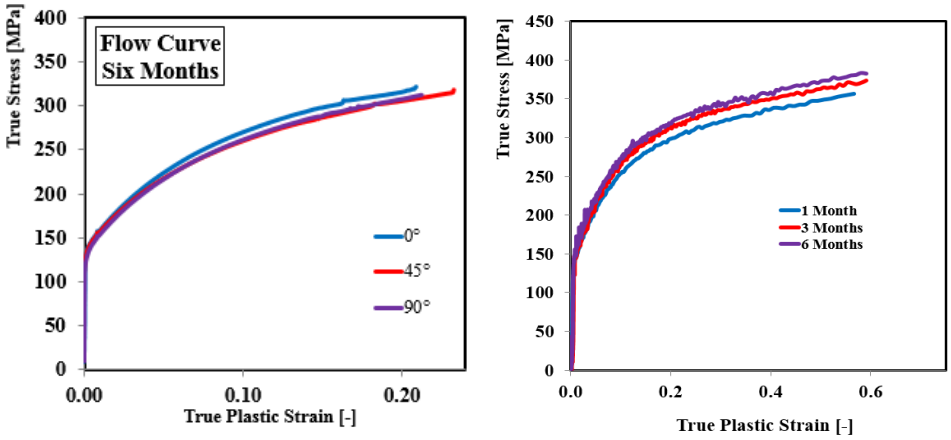

Figure 111, Tensile testing strains reaching 0.2 (left), hydraulic bulge testing up to strain vakue of 0.6 (right) (Novelis, 2017)

Fallahiarezoodar et al (2015) suggests that bulge test is more accurate than extrapolated tensile tests at higher strains. Furthermore, unlike in the compression testing, there are also no concerns related to friction. Based on this, it could be suggested that the bulge testing might be superior to all other methods of obtaining flow stress data. However, the bulge tests require a set up with bulge testing machine which may not always be an available option and, as Fallahiarezoodar et al (2015) also asserts, the bulge test does not supply flow stress data for the elastic stage of the process. Lack of data in this initial stage can lead to inaccuracies in simulations as the yield point may not be precisely defined.

To remedy this, Fallahiarezoodar et al (2015) goes on to suggest that a good approach would be a combination of tensile and bulge test which should combine good quality data for elastic deformation with good quality data in plastic range up to high strain values. Some adjustments will need to be made such as converting the uniaxial tensile test into a biaxial stress using the below:

Eq. (30)

$$\sigma_{biaxial} = \sigma_{uniaxial} \sqrt{\frac{(l + r_0)r_{90}}{r_0 + r_{90}}}$$

This process results in the combination of the best of both tests, the flow curve includes sufficient levels of strains but also an accurate determination of yield point.

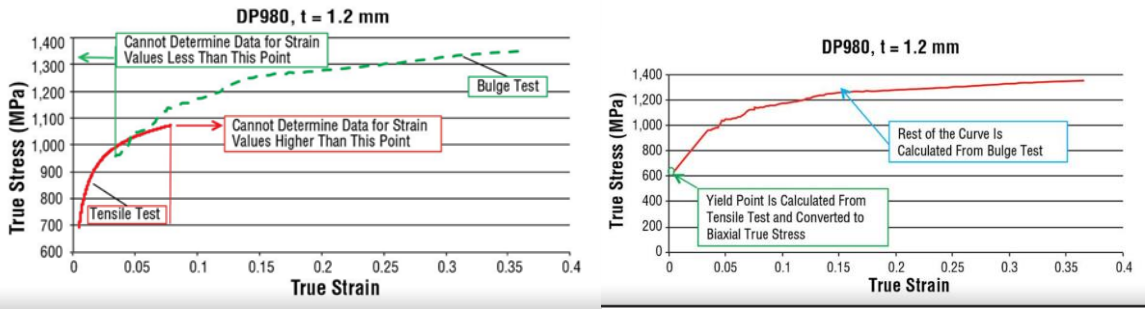

Figure 112, Combination of tensile and bulge test for producing flow curves (Fallahiarezoodar 2015)

4.1.3.3.5 In-plane torsion test

To characterize materials behaviour at larger strain, specifically aimed at sheet metals under shear stress, in plane torsion testing can be used (Yin, 2015, Bruschi, 2014). This method was first introduced by Marciniak (1961) in order to characterize the Bauschinger effect of copper sheets. Tekkaya et al. adapted the test in order to and generate flow curves of an aluminium alloy (1982). The test set up involves a planar circular blank fixed along the outer edge and at the centre. Torsion of the inner clamps against the outer out clamps leads to shear stresses in the free unclamped area of the specimen and the resulting shear stress can be calculated from the measured torque as a function of the radial distance and thickness of the sheet (Traphöner et al, 2018).

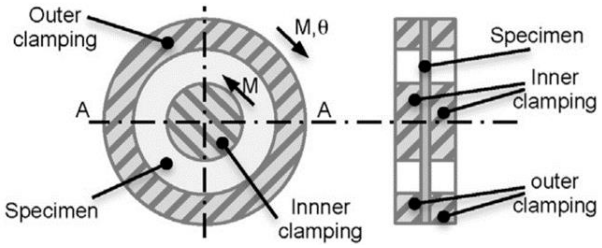

Figure 113, Sample set up of in-plane torsion test

The advantage of this test is that it is not subject to necking or buckling and is not exposed to any frictional behaviour either (Bruschi, 2014). The downside are the need to average the planar anisotropic properties as the orientation of the rolling direction to the shear load changes during the process of the test, however, the normal anisotropy r_n can be considered, using for example Hill's model (Traphöner et al, 2018). Furthermore, exceeding torque can lead to slipping between sheet and clamping tools, which mainly occurs with thicker sheets (Tekkaya et al, 1982).

4.1.3.3.6 Assessment of testing methods based on literature

There is a great amount of data in literature completed via various testing and evaluation methods in recent years (Carandente, 2016, Nutor et al, 2017, Eller et al, 2016, Hua et al, 2014, Chen, 2009, Li et al, 2016, Wi et al , 2017, Fallahiarezoodar et al 2015, Traphöner, 2018, Yin, 2015, Bruschi, 2014 and

many more). Armstrong (1982) asserted that a compression and torsion tests should provide sufficient levels of strains for ductile materials. Traphöner et al (2018) suggests that in-plane torsion tests are suited excellently to describing characteristics of sheet materials. Raabe's (2017) evaluation seems to suggest that from perspective of simulations, tensile test is the most suited for sheet metal description and simulation, followed by compression and torsion testing methods as alternatives. However, the variability of these methods in terms of testing conditions can lead to limited reliability of simulations. One of the latest research exercises by Jäckel at al (2019) indicates that despite the increased use of simulation there are no known standards or technical guidelines for generating flow curves suitable for purposes of simulating joining process.

4.1.3.4 Methods of extrapolation

As explained before, due to limited strains achieved in mechanical testing, strains may not always reflect the range of strains needed in the simulated process. An expansion of the mechanical testing results is therefore needed and a way to do this is extrapolation, also referred to as fitting which involves applying equations that capture the strain hardening and extending the flow curves to reach higher strains.

Although tests other than tensile tests, can reach higher strains, the FE software would benefit from all methods of testing being extrapolated to certain degree as in large plastic deformation in forming strains up to 5 can be required. As mentioned in the chapter 4.1.3.1, there are number of methods of doing so and these will be introduced in the next few paragraphs.

A simple equation describing the non-linear relationship between stress and strain in the plastic region is Hollomon's equation (Palaniswarmy, Billur, 2012, Chandramouli 2015). This serves well for materials that have been annealed (heated above recrystallization temperature and slowly cooled to remove any internal stresses) and are undergoing deformation at room temperature.

$$\sigma = K\varepsilon^{n} \qquad \text{Eq. (31)}$$

σ – Stress

Ɛ – Strain

K – Material's coefficient of strength

n – Strain hardening exponent

The stress that is calculated by this equation is extremely important for forming and simulation alike as it denotes the stress that is needed to maintain plastic deformation at a given rate i.e. This is also referred to as flow stress or equivalent stress in the plastic state. Unlike the stress in the elastic region

this stress is not linear as a complex process of strain hardening become part of the equation. Strain hardening is caused by dislocations (i.e. defect in materials) moving during forming which cause the material to harden which in turn requires more force to keep it deforming (Chandramouli, 2015).

Another well-known method which can generate extrapolation of flow stress is the Ludwik's equation which takes into consideration the yield stress.

$$\sigma = \sigma_y + K\varepsilon_p^n \quad \text{Eq. (32)}$$

σ – Flow stress

σ_y – Yield stress

ε_p – Plastic strain / effective strain

K – Material's coefficient of strength

n – Strain hardening exponent

For pre-strained materials, Swift's law might produce more accurate approximation as it takes into consideration pre-strain of the material (Palaniswarmy, Billur, 2012).

$$\sigma = K + (\varepsilon_0 + \varepsilon)^n\sigma \quad \text{Eq. (33)}$$

σ – Flow stress

Ɛ – Effective Strain

ε_0 – Pre-strain

K – Material's coefficient of strength

n – Strain hardening exponent

In addition to the above equations, there are more complex hardening laws available that require more specific material parameters such as (Zhu, 2018, Simufact, 2015, Kahrimanidis, 2015) Voce (and modified Voce, Hockett and Sherby and Gosh. If temperature and strain rates are considered in the flow curves, the hardening law such as Hansel and Spittel can be considered where coefficients such as temperature, strain, strain rate and material consistency coefficients are used. A summary of the frequently used hardening laws compiled by the author is presented below.

Voce	$\sigma = \sigma_sat - (\sigma_{sat} - \sigma_0).\exp(-k\varepsilon_p)$
Modified Voce	$\sigma = A - Be^{-C\cdot\varepsilon_p}$
Hockett and Sherby	$\sigma = \sigma_sat - (\sigma_{sat} - \sigma_0).\exp(-k{\varepsilon_p}^n)$
Gosh	$\sigma = k(\varepsilon_0 + \varepsilon_p)^n - p \cdot \varepsilon_p$
Hansel and Spittel	$\sigma = A\, e^{m_1 T}\, \varepsilon^{m_2}\, e^{\frac{m_4}{\varepsilon}}\, \varepsilon^{m_3}$

Eq. (34)

Table 4, Further power models for extrapolation of flow curves

In addition, Zhu et al (2018) suggested that reliable results have been provided by a combination of two of the hardening laws, Swift and Modified Voce:

$$\sigma = 0.5\,.K(\varepsilon_0 + \varepsilon_p)^n + 0.5\,.(A - Be^{-c\varepsilon_p}) \quad \text{Eq. (35)}$$

$K = 350$
$\varepsilon_0 = 0.01$
$n = 0.22$
$A = 162$
$B = 72$
$C = 4.3$

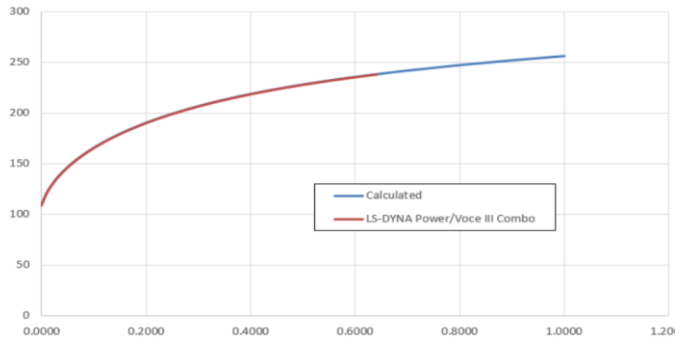

Figure 114, Combination of two of the hardening laws (Zhu et al, 2018)

This has been confirmed by Eller et al (2015) who used combination of the Swift and modified Voce hardening law for extrapolation of press hardened steels. Eller initially used the two laws separately, however, it has been noted that at high strains these behaved very differently as can be seen for the graph below. The assumption was that the hardening curve is somewhere between the two so he introduced the combination to address the two extreme scenarios.

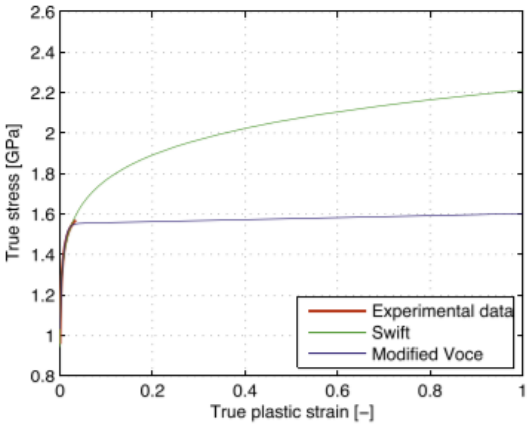

Figure 115, Example of using Swift and Modified Voce separately (Eller, 2015)

Two other researchers (Sung et al, 2010 and Roth and Mohr, 2014) introduced the same idea and combined the two models in their respective research cases.

$$\sigma_y(\bar{\varepsilon}_p) = (1-\lambda)\sigma_S(\bar{\varepsilon}_p) + \lambda\sigma_V(\bar{\varepsilon}_p) \qquad \text{Eq. (36)}$$

Assessment of extrapolation methods based on literature

A number of researchers, have produced data and simulations using different hardening laws in the context of SPR. Eckstein asserts that experimental tests have shown that flow curves for large scale forming operations (experiencing similar strains to SPR) with aluminous tend to be relatively flat. This has been confirmed by his earlier work which included extrapolation of semi-hollow punch riveting process as well as Gese (2004) who also documents better results with flatter extrapolations rather than higher extrapolations such as Gosh.

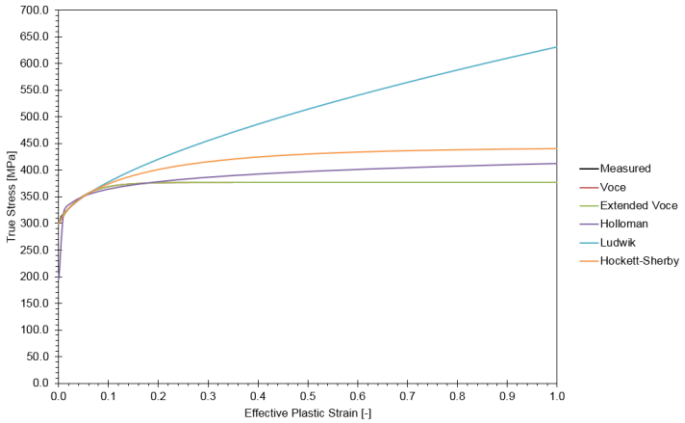

Figure 116, Comparison of Hockett and Sherby flatter flow curves with higher extrapolations such as Ludwik and Voce.

Marr (2014) concurred with this notion based on his research in which Hockett and Sherby hardening law gave an improved correlation over Hollomon and Ludwik. This was the case in research work of Du et al (2013) which considers Hockett and Sherby along with Voce the most realistic hardening law. Kahrimanidis (2015) has arrived at the same conclusion in his work on use of precipitation hardenable aluminium alloys which were heat treated in order to optimize their mechanical properties. Whilst he acknowledges that there are other advanced hardening model, his research was centred around using Hockett and Sherby as this gave the best correlation with experimental data whilst Gosh overestimated the hardening behaviour and Voce underestimated it. Kahrimanidis (2015) also suggested Swift as second most suitable alternative. Furthermore, Banabic (2012) gained highly accurate results with combination of Hockett and Sherby combined with Swift hardening law.

4.1.3.5 Mechanical tests under different conditions

The above mentioned mechanical tests are mainly all used at small strain rate and ambient temperatures and generate one flow curve per test with these parameters. This is considered sufficient for simulations, in that the simulation can proceed even with just one flow curve and will generate results. However, throughout the process being modelled, apart from level of stresses and strains, other the conditions might change, for example speed of deformation (i.e. strain rate) might vary and friction might create heat within the workpieces. Whilst the software will adapt this mathematically, this is an estimation. Therefore, where possible, it is ideal to have accurate data that captures as wide a range of material behaviour as possible. An example of one vs multiple flow curves are shown in the image below – both are flow curves for a rivet, xxx with just one flow curve, xxx with a number of flow curves that have been mechanically tested at a number of strain rates (0.1, 1.0, 10.0, 100.0 1/s) and temperatures (20, 100, 200, 250, 300 °C) and mathematically extrapolated.

What follows if such curve is available, is that as the speed and temperature throughout the process increase and decrease, the software is interpolating between the individual flow curves, finding average between two nearest to the given temperature and speed, and thus adding accuracy to the calculations that are otherwise conducted only based on mechanical properties.

However, creating such extensive flow curves for a large number of materials that are used in automotive industry can prove prohibitively costly and impossible to carry out on every manufacturing variation that is delivered. Whilst the multiple flow curves would improve accuracy, good results can be seen even with a single flow curve at room temperature and one suitable strain rate. It remains to be determined whether an accurate single flow curve is sufficient for a simulation and whether flow curves with a high number of temperatures and strain rates options do bring the desired benefit.

The types of testing that can obtain multi strain rates and multi temperature flow curves are briefly explained below.

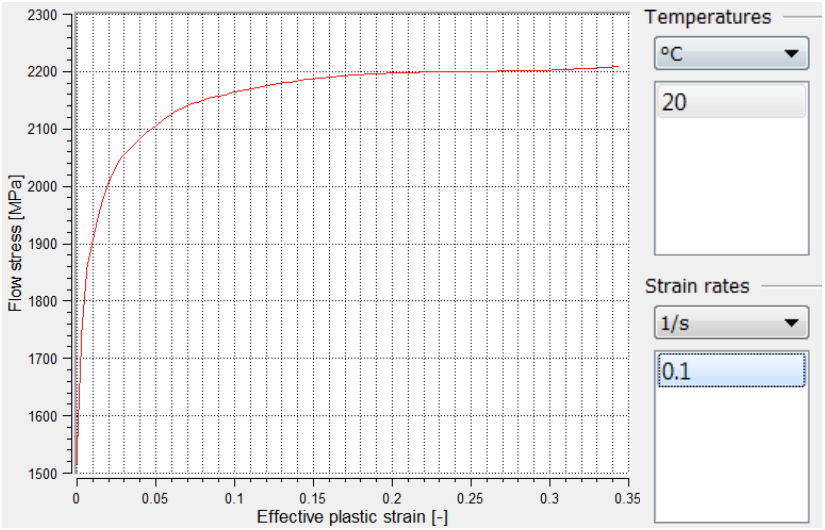

a

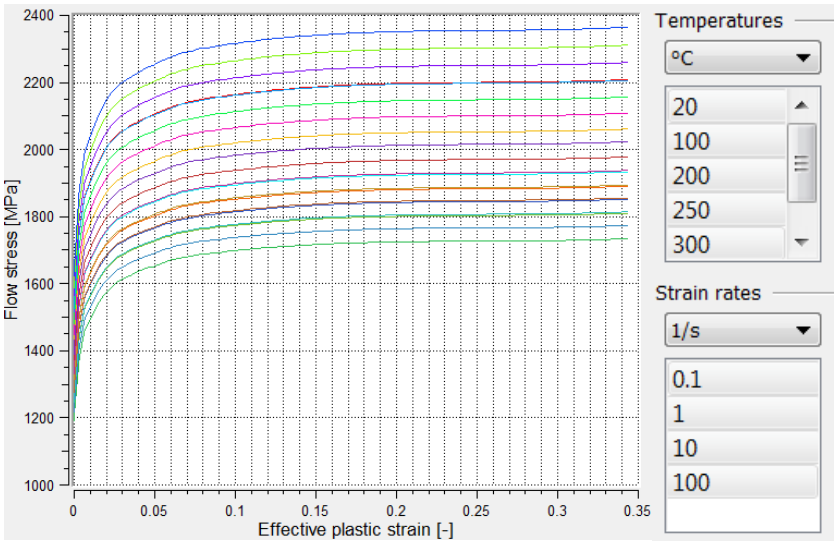

b

Figure 117, Flow curves for the same rivet material, a - single flow curve (top) and b - flowcurves that a combination of five different temperature and four different strain rates (bottom) (Simufact software, 2015)

4.1.3.5.1 Mechanical testing at elevated temperatures

With this type of testing, the tests samples are heated up to the desired temperature which is then kept constant along with the strain rate (Bruschi et al, 2014) during the test. Both tensile and hydraulic bulge tests can be completed using elevated temperatures.

The tensile tests have been used for example in research by Pellegrini (2011) when magnesium alloy flow curves were generated up to 300°C to prove that a significant increase of formability is reached

at this temperature. This was proven by a resulting stress-strain curve which showed material achieving increased strain rates.

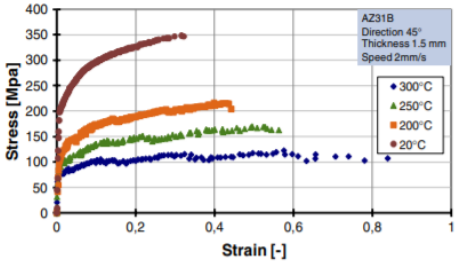

Figure 118, Increased formability shown at higher temperatures. (Pellergrini et al 2011)

Another way of the conducting these tests is using a Gleeble machine which heat the samples to very high temperatures such as that in example of tensile testing usibor (22MnB5) conducted by Turetta et al (2006). This high strength steel was, with aid of Gleeble machine, heated up to 900°C to evaluate the effects of strain rate, temperature and cooling off process.

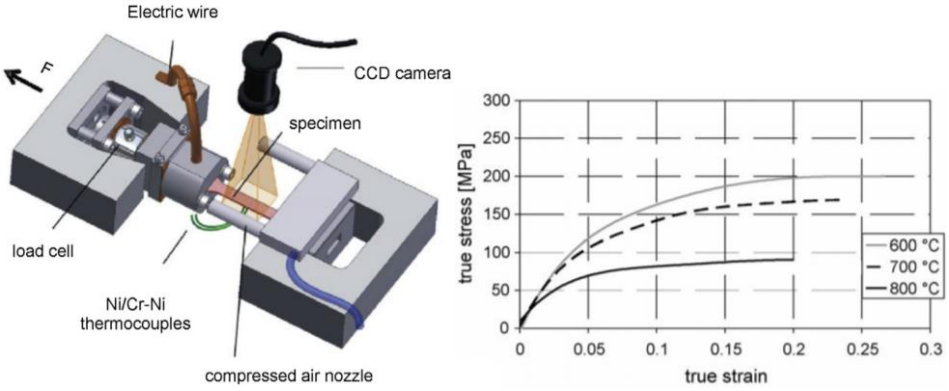

Figure 119, Set-up of Gleeble machine left. Right – Boron increased formability with increased temperature.

Similar test to that of Pellergini, measuring effect of temperature on magnesium alloys, was conducted by , however, using hydraulic bulge test with tempetatures elevated to 250°C. This has shown that temperature increase coupled with different strain rates can cause variation in yield stress values up to 50% (Rauch, 1992).

4.1.3.5.2 Mechanical tests at high strain rates

Along with temperature, speed of deformation, i.e. strain rate has an effect on how materials behave during forming. To evaluate the behaviour of material at high strain rates, devices such as drop towers and Split Hopkinson Pressure bars can be used which can test the materials at very high strain rates such as 1800 1/s.

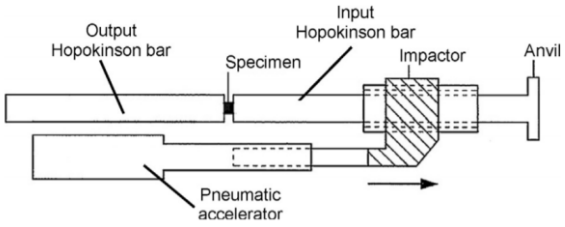

Figure 120, Set- up of a Split Hopkinson pressure bar

The strain rate tests on tensile tests have shown that there are different strain rate regimes which impact the behaviour of steel materials (Bruschi et al, 2014). When testing high strain rates, the response of material differs from the one at static strain rate. Image below shows a summary of strain rate regimes and their characterisrics (Field et al, 2004, Bruschi et al, 2014).

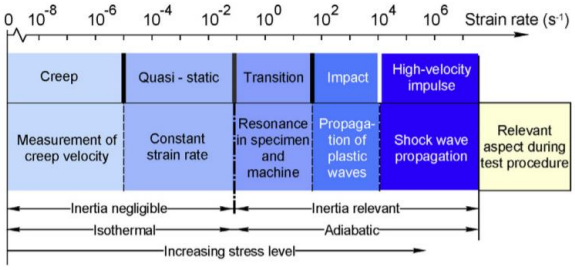

As the graph below shows, with high strain rates, the material shows higher strength initially, which is lowered by the changing strain rates in the test as well as softening effects of the heat generated in the system.

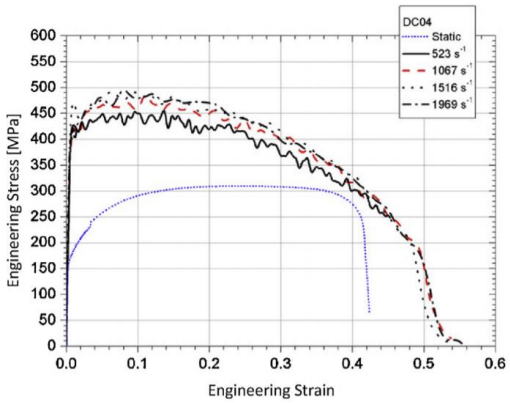

Figure 121, Comparison of static and dynamic stress strain curves for DC04 material. (Verleysen, 2011)

The split Hopkinson pressure bar can also be installed with hydraulic bulge test set-up (Ramezani, 2010) and was successfully used to generate flow curves for electromagnetic forming (Chu et al, 2012).

The disadvantage of both elevated temperatures and high strain rates tests is the inability to keep the both parameters constant throughout the test which makes it harder to identify the yielding criteria later on (Bruschi et al, 2014).

4.1.3.6 Material variation

An addition to all issues associated with creating flow curves, materials themselves can be subject to production and other variations. Testing materials and creating a quality set of flow curves can be quite a costly process and it is not possible to account for all manufacturing variables as no supplier will have the financial means to create a number of variations of each batch purposefully.

As material properties are a great factor in accuracy of simulations, it is crucial to be aware of any manufacturing or other variations to the materials which might lead to and potentially explain any differences between the simulations and physical joints.

There are usually two aspects of materials that can be affected by manufacturing variations:

Hardness

Hardness can be is described as resistance to penetration (UOB, 2018) and therefore it is effectively a measure of how readily will a material start permanently deforming. Therefore, once measured, hardness values can be correlated with ultimate tensile strength (UTS) of the metal and typically, the higher the hardness of metal, the higher the UTS ultimate strength will be (UOB, 2018). Conversion tables have been developed to predict UTS based on measurements of materials' hardness.

This can be measured by standard indenter testing equipment such as Brinell, Rockwell or Vickers hardness testing machines. Any hardness testing completed for this thesis has been completed by Vickers hardness machine which is the preferred option for sponsoring company Atlas Copco.

The Vickers hardness test was designed in 1921 and has one of the widest scales amongst the hardness tests and it can be used for all metals.

The test, similarly to other types of hardness tests, assesses material's ability to resist plastic deformation caused by a standard source. This is done through a method of pressing an indenter in a shape of a square based pyramid into a material sample with a defined load and time of loading (dwell time).

The indenter should be highly resistant to self-deformation and the shape should have the ability to produce geometrically comparable impressions. It was found that a diamond in the form of a square-based pyramid with 22° angle on either side fulfilled these requirements. The model of the indenter and the resulting indent are shown in Figure 122.

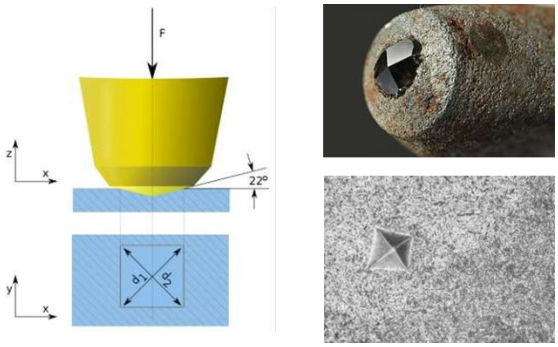

Figure 122, a) Indenter shape b) indenter tip c) indent in the sample

The size of the indentation is measured using diagonals (d1 and d2, as shown in figure …..) and the Vickers hardness (HV) is calculated as a ratio of force applied to the inenter (F) and the surface area of the indentation left by the indenter (A).

A is the surface area of the resulting indentation in square millimeters. A can be determined by the formula:

$$A = \frac{d^2}{2\,sin(136° \frac{2\,sin(136°)}{2}} \quad \text{Eq. (37)}$$

d - is the average length of the diagonal left by the indenter in millimeters

This formula can be approximated by evaluating the sine term to give:

$$HV = \frac{F}{A} \approx \frac{1.8544F}{d^2} \quad \text{Eq. (38)}$$

The depth of the indent can be calculated using the formula below:

$$h = \frac{d}{2\sqrt{2\,tan\frac{\theta}{2}}} \approx \frac{d}{7.0006} \quad \text{Eq. (39)}$$

An aspect to be considered during testing is the thickness of the samples. Generally, it is recommended that the sample thickness is greater than 2.5mm indent diameter.

The result of the test are Vickers hardness number which are in the following format:

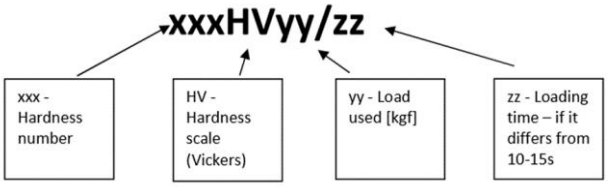

Figure 123, Naming convention for hardness test results

Ductility

Ductility is a capacity of a material's ability to undergo a plastic deformation before breaking (Budynas, 2015). There are two parameters that measure ductility of metal, a percent enlongation and percent reduction in area from and both can be determined using a tensile test (ASTM Standard A370, 2018).

Percent elongation is the increase in length of the sample and can be obtained by marking the tensile test sample and then measuring it after breakage.

$$percent\ elongation = \%\ El = \frac{L_{br} + L_0}{L_0}\ x\ 100\% \qquad \text{Eq. (40)}$$

L_o – original length between marks on the sample

L_{br} – length between marks on the broken specimen

The percent reduction in area is the decrease in the cross-section of the sample which is measured after testing.

$$Percent\ elongation = \%\ R\ in\ A = \frac{A_0 + A_{br}}{A_0}\ x\ 100\% \qquad \text{Eq. (41)}$$

A_o – original cross-sectional area

A_{br} – cross-sectional area at the point of breakage (ASTM Standard A370, 2018)

If changed by a significant value as part of manufacturing variations, both of these properties can have a negative effect of the robustness of a mechanical joining. Variations of both of these properties can occur for several reasons, with two most likely ones being:

- Manufacturing production - Batch to batch variation
- Age hardening

4.1.3.7 Manufacturing variations

4.1.3.7.1 Sheet materials

In an ideal scenario, materials provided for testing have a certificate showing hardness, batch number and various other additional information. However, it is more likely that the materials arrive with not much information other than a name and thickness.

There is usually some general tacit knowledge available on the material such as Aluminium alloys are generally quite soft suggesting that lower hardness rivets should be used such as (H1, H2 with H4 the highest) and with steel the name often implies hardness e.g. DP600 material is supposedly reaching 600 MPa, Usibor1500 1500MPa. However, this is usually just in indication.

The strength of a material is this is usually a range as opposed to a single value which might cover hardness and ductility etc. Values of these material parameters might differ to various extent in each batch due to manufacturing variations and yet still be within the specification.

However, in some instances, values too far towards the end of the range can have some undesirable effects on the joint.

An alternative to this could be hardness testing every material, cross referencing this with material property tables with UTS (Only available for steels, not aluminium) and the flow curves adjustment option to increase or decrease hardness (explained in chapter 4.1.3.6).

4.1.3.7.2 Rivet materials

Rivet materials are similar to the sheet material in that that despite the best intentions, variations in hardness do occur in production and hardness tests are carried out routinely as part of a quality check. Rivets have tolerances within their individual hardness levels.

Heat treatment level	Hardness range (Hv 10kgf)
0	As forged
1	255-305
G	290-350
H	330-390
2	380-440
3	420-480
4	450-510
5	480-540
6	530-580
7	550-600

Table 5, Rivet Hardness Levels

4.1.3.7.3 Age hardening variations

Whilst some materials need to be exposed to elevated temperatures (i.e. heat-treated) to increase their hardness properties, for some other materials this happens by merely being exposed to ambient temperatures. This is referred to as age hardening and was first discovered accidentally by Alfred Wilm.

Wilm created the first hardening curve in 1906 after attempting to develop an alloy to be used for manufacturing ammunition. Wilm used Al-Cu-Mn alloy and although the strength of the material was close to the value that was needed, the hardness property was rather behind the required value. He added Mg to the mix and after heating and quenching the sheet, he measured the hardness and left the sheet for a couple of days. When he measured the hardness following few days, the material was clearly showing increase on the previous values of hardness. This material has been subsequently patented by Wilm and is sold as Duralumin (Polmear, 2004). Many researchers have tried to explain the cause of this and it is now accepted that age hardening is a type of precipitation hardening which, however, occurs at room temperatures rather than elevated temperatures. There are usually several stages to this complex process involving formation of precipitates over time, an act which in turn affects mechanical properties of the material such as increase in hardness and tensile strength.

The development of Duralmin led to many experimental studies in the aerospace industry, adding and removing elements in order to develop new and better alloys. For example in Japan, this led to development of Extra Super Duralmin which has reduced the weight of the Zero fighter aircraft in 1938 (Murakami, 1998). When this plane crashed during the world war 2, the opposition has learned about this alloy by way of a detailed material analysis and subsequently UK and US have manufactured

planes out of similar material – 75S. This material has been later renamed to 7075 (Dix, 1950) and has been recently taken up by automotive manufacturers.

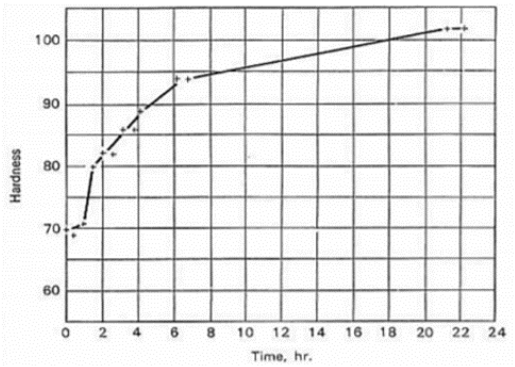

Figure 124, The first hardening curve (Polmear, 2004)

In recent days this behaviour is typical for aluminium alloys with the group referred to as 6xxx series (such as, AC160, AC170, AC200, AC300, AC600 and AA6111 etc) which are very frequently used by some automotive manufacturers such as Jaguar Landrover (Litherland, 2017). In context of SPR, this may be problematic as SPR relies on ductility of metals (Briskham, 2017) and by naturally hardening, the materials might lose a portion of this and give results different to those expected when riveted.

As an example, alloy AC600 T4 is a 6xxx series alloy which has not been heat treated so it is softer than the next hardness grade up of the same material, AC600 T6, which was heat treated to increase its hardness. If AC600 T4 is left to age for a sufficient time, it can over time achieve level of hardness equivalent to that of AC600T T6. This can cause issues such as a robust joint becoming a marginal or failing joint instead and subsequently in need of change of insertion velocity in the best case scenario or a change of rivet and die selection in the worst case, the latter being which is highly undesirable once in production.

4.1.3.7.4 Measures to mitigate material variations

Prevention

Natural age hardening can be prevented by placing materials in the freezer which will stop the natural ageing. This is particularly important for any long term projects as the effect of natural ageing can invalidate the results by making them incomparable over time.

Hardness tests

If the materials are already hardened by not being placed in a freezer or a new batch of materials is supplied with unknown spec, it is beneficial at least being aware of the spec by testing the materials. The machine used for this in Atlas Copco is Vickers hardness machine (as described in chapter 4.1.3.5).

4.1.3.8 Flow curves adjustment

Ideal scenario is that all flow curves for each of the material used in SPR are available for each manufacturing variation of this material, i.e. they capture a number of different stress-strain states. Most material manufacturers supply materials, especially steels, only as a bottom specification rather than one single definitive value. In reality this means that of for example a batch of steel sheets specified as having strength of 1500 MPs, may be supplied having 1800 MPa and this would still be considered to be within the spec but flow curve might be available only for material with UTS of 1500 MPa. These differences can negatively impact the automotive manufacturing process if joints are falling over due to not having anticipated a harder batch from the perspective of rivet selection.

To consider this material variability, the software has an option of adjusting flow curves to desired values of hardness which is a common approach in some engineering labs (Simufact, 2015). This function can be further used for updating and improving materials properties based on information given by supplier. These changes can be done via the scaling option where a scaling factor is set. The scaling factor is essentially a ratio by which a value can be increased or decreased and it is possible to set. The scaling factor can be applied to both ends of the flow curve, the beginning i.e. yield stress, or ending i.e. ultimate strength (Simufact, 2018).

4.1.3.8.1 Offset yield point scale factor - $R_{p0.2}$

The scaling is based on the yield stress or proof stress which is the initial stress value in the flow curve and it is applied to the elastic deformation and plastic deformation up to the $R_{P0.2.}$. It can be input as a stress value (for example Rp0.2 = 7.5e+7 Pa) or a factor (for example 1.1).The default factor is always 1 as shown in the image below where the original Rp0.2 is considered 1.

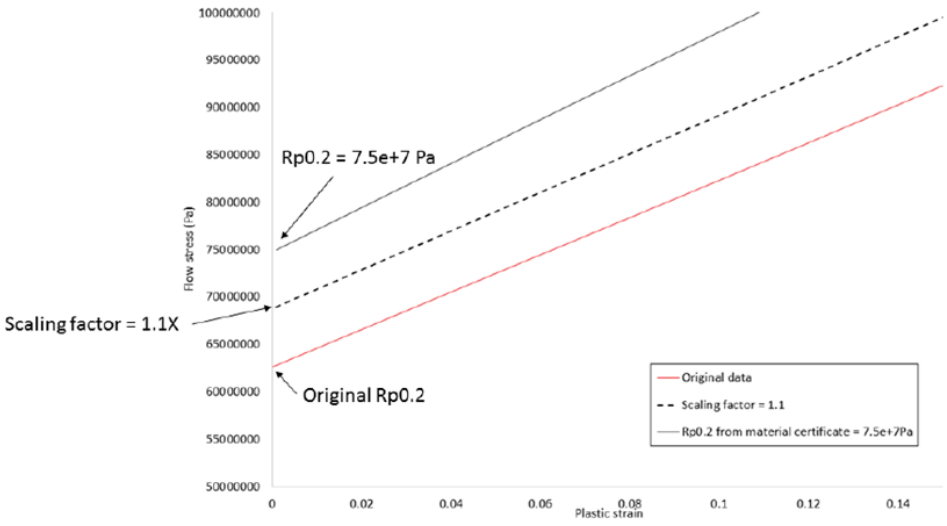

Figure 125, Offset yield point scale factor - $R_{p0.2}$

4.1.3.8.2 Hardening scale factor - R_m

The scaling adjusts the ultimate strength R_m (or UTS) of the flow curve whilst the yield stress remains constant. As with the Rp0.2, two methods of input are available, the stress value (for example R_m = 135E+9 Pa) or scaling factor (for example 0.91), but the calculations are applied only to the plastic deformation.

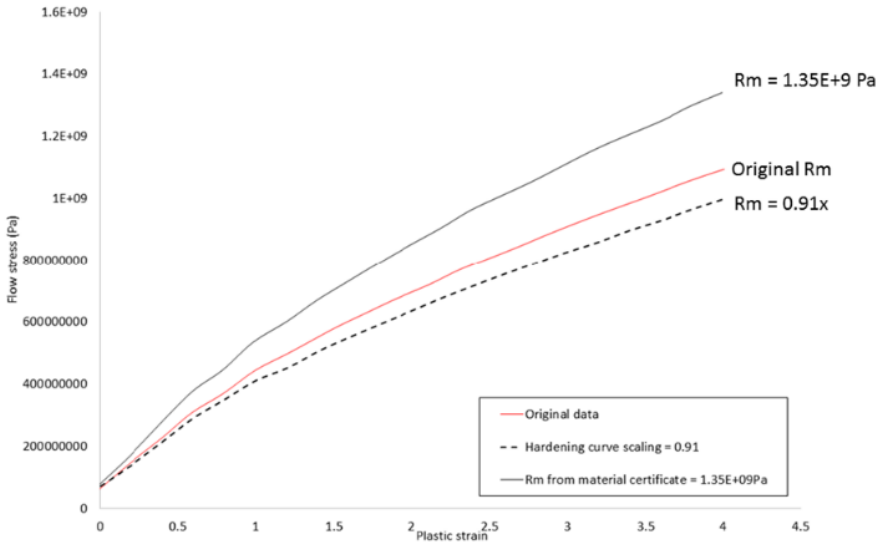

Figure 126, Hardening scale factor - R_m

Both scaling factors are independent from each other but can be combined to create a flow curve with amended yield point as well as ultimate strength of the material. In general they are mainly applied in cold forming processes. It is also important to highlight that these changes should be applied with caution as they can significant impact on the materials. It is recommended not to go above factor 1.5 or below 0.8 (Simufact, 2015). R_m factor is the parameter that directly leads to change of hardness of the material flow curve by increasing or decreasing it. This allows for simulating different hardness of materials which is a frequent scenario in physical testing due to manufacturing variables of materials but without the option to test any materials other than those supplied.

4.1.4 Rivets', dies', sheets' and tools' geometries

Before talking about what geometry means in simulation, a small distinction should be made between the term geometry used in Simufact and in AC. Whilst geometry in SPR means mainly the shape of the inside of the rivet and tips, the simulation software considers as geometries are the 3D CAD models used for each component of the simulation model.

For SPR this includes the following models:

- Punch
- Blankholder/ Nose
- Die

Tooling/ Dies

- Top sheet
- Middle sheet
- Bottom sheet
- Rivet

Workpieces

Whilst the sheets, rivets and dies are the models are the same as the part in reality, the punch and blank holder are a lot more simplified than their counterparts in reality owing to the fact that both are small parts of a larger equipment, simulations of which would not be feasible. Below picture shows the simplified versions of these.

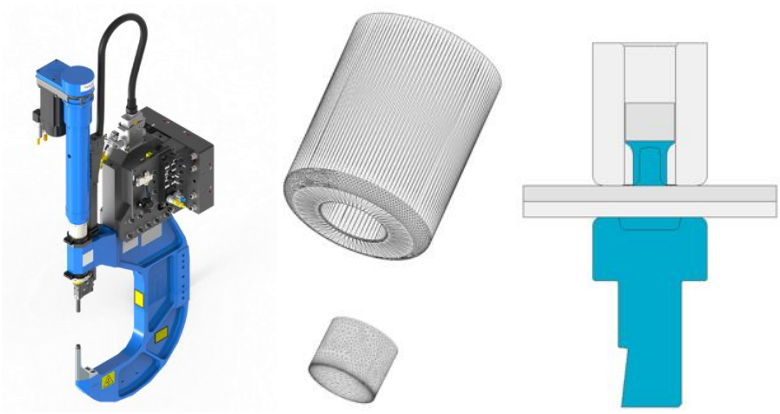

Figure 127, Complete C frame on the left, simplified versions middle and right.

In SPR, the rivet geometry plays a crucial role and specifically rivet tip geometry can have a significant effect on flaring of the rivet. The two radiuses on the rivets are carefully designed to take into consideration the normal stress exerted by punch and the counter pressure on the sheets introduced by the die geometry. Even slight deviation in the tip geometry might sometimes lead to less strong joint (Briskham, 2016).

The geometry of rivets, sheets and dies is one of the many variables in the process of SPR and whilst the models are drawn up with precise measurements, in reality some of the models are not an exact reproduction of the real part due to production variables or life cycle.

Whilst equipment has its lifecycle and it certainly is subject to fatigue over the time due to the high force exerted during insertion, the two main components coming in direct contact with rivets and sheets, the punch and blankholder are not very likely to change and therefore their variations will not

be considered for purposes of this thesis. This is also applicable to die which although are a subject to wear.

However, the rivets, sheets and die are both likely to be affected by production variables (this includes rivets and sheets) as well as life cycle (die). Resulting changes due to these production variables might in turn affect the agreement the simulations might have with the physical testing. These will be explained in the following sections.

4.1.5 Friction, lubrication and coatings

Friction between solid objects is a very complex phenomenon as it involves a wide variety of processes such as elastic and plastic deformation of the top layers of touching materials, microfractures, chemical reactions, excitations of electrons, transfer of particles and restoration of continuity of materials (Popov, 2010). This becomes even more complex in metal forming where a number of factors are at work (Fig. ….) and modelling this becomes an extremely difficult task. Therefore, the friction will form a big part of the sensitivity testing. The following section will introduce general concept of friction with focus on friction in metal forming and SPR.

There are two types of friction, static and kinetic.

4.1.5.1 Static friction

Static friction occurs when two bodies, pressed together by normal force, are in contact but there is no motion between them. The friction force in this case will not exceed a value of normal force timed by coefficient of static friction (Ashby, 1996).

$$F_s = \mu_s P \qquad \text{Eq. (42)}$$

Fs - Static friction force

P - Normal force (weight of the object)

μ - Coefficient of static friction (COF)

4.1.5.2 Kinetic friction

Kinetic friction occurs when two bodies are sliding over each other. The friction force is equal to a value of normal force timed by coefficient of static friction (Ashby, 1996).

$$F_k = \mu_k P \quad \text{Eq. (43)}$$

$F_k = \mu_k P$

Fk - Kinetic friction force

P - Normal force (weight of the object)

μk - Coefficient of kinetic friction (COF)

For the body to start moving the static friction force must be overcome. Once the sliding has started the resisting friction force is kinetic and the work done in sliding demonstrates itself as heat (Ashby, 1996, Simufact, 2015).

A relevant factor of friction worth highlighting at this point is the contact area. All materials – no matter how well polished, are said to have microscopic peaks and troughs on the surface which are called asperities. Illustration of this is in Figure 128.

Figure 128, Asperities on surfaces of materials

When materials are in touch (as shown in Figure 129) the real contact area are these asperities as opposed to the entire surface of material. This can be described by equation.

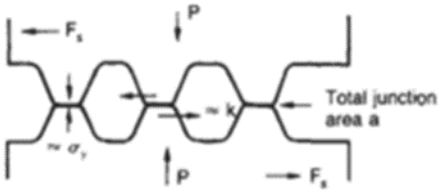

Figure 129, Asperities in contact

$$P \approx a\sigma_y \quad \text{Eq. (44)}$$

P – normal pressure

a – real contact area

σ_y – compressive yield stress

When materials start to slide over each other, shear stress appears on these asperities which form junctions with the opposing material.

$$\tau_f = \frac{F_s}{A} \quad \text{Eq. (45)}$$

T_f - Shear stress

F_s - Shear force

A - Contact area

Looking at friction from a perspective of metal forming, there is a large number of factors affecting this as seen in Figure 130 (Kardes, 2012, Simufact, 2015).

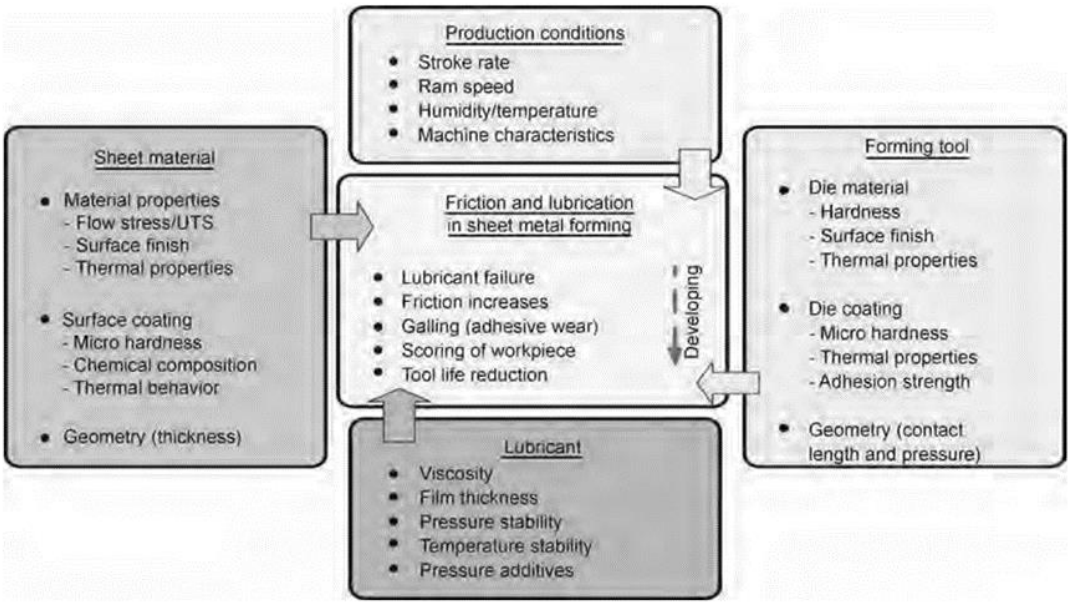

Figure 130, Factors affecting the friction in metal forming (Kardes, 2012).

There are three friction models that are currently used to describe friction in the software. The first one is referred to as Coulomb friction model.

4.1.5.3 Coulomb's friction model

This law can be described using the following equation:

$$\tau_f = \mu p \quad \text{Eq. (46)}$$

T_f - Frictional shear stress

μ - Coefficient of friction (COF),

p - Normal pressure

This model serves well to describe the friction with low contact stresses and is well suited to calculating dry friction conditions. However, it is only suitable if normal stresses exerted on the part are small. In some processes the interface shear stress can exceed the yield strength of the material, k.

$$\frac{F_s}{a} = k \qquad \text{Eq. (47)}$$

F_s - Shear force

a - Contact area

k - Shear yield strength

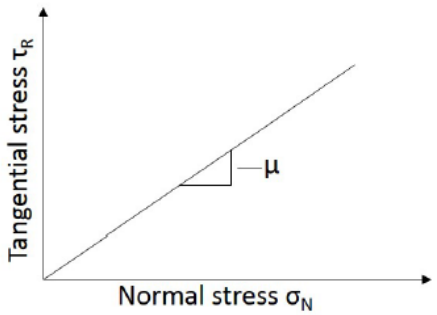

Figure 131, Coulomb friction model schematic presentation

This causes a problem for Coulomb friction model which uses the linear relationship between μ and p and if the yield strength of material is exceeded, coefficient of friction becomes meaningless (Kim, Kardes, 2012) and the software will calculate physically implausible friction stresses using this model only.

This is means that the Coloumb friction can be used in scenarios where the contact stress/pressure does not exceed the yield stress (the stress that is required to be exerted to continue the plastic deformation of a material), however, it has limitations in cases when the flow stress exceeds the contact stress.

4.1.5.4 Shear friction model

These limitations are addressed by another friction model proposed by Orowan, which is often referred to as Shear friction law. This law can be described by equation below:

$$\tau_f = f\sigma = m\,\frac{\sigma}{\sqrt{3}} = mk \qquad \text{Eq. (48)}$$

f - Friction factor

m - Interface friction factor

k - Shear yield strength

τ_f - Frictional shear stress

σ - Flow stress of deforming material

Interface friction factor, m, is always between the following values 0 < m < 1 with m=0 for no friction/ perfect lubrication and m=1 for sticking friction (a condition when the workpiece surface adheres to the surface of the tool rather than slides against it; it occurs when the friction stress is greater than the shear flow stress of the metal (Kim, Kardes, 2012, Simufact, 2015) as shown in the image below.

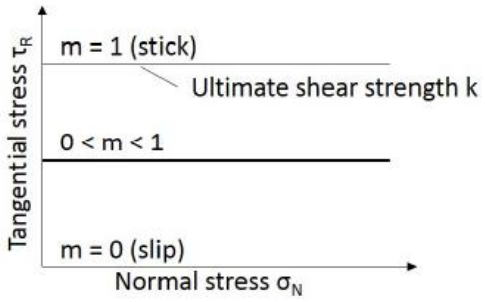

Figure 132, Shear friction model schematic presentation

The ultimate shear strength k is directly proportional to the yield stress of the material. As soon as the material hardens, due to its deformation during the forming process, the maximum friction stress rises as well. Therefore, in contrast to the Coulomb friction law, the Shear friction law is well suited for processes where the material experiences very high normal stresses. However, if the normal stresses are very small it will lack refinement in the calculation of the friction (Kardes, 2012, Simufact, 2015).

4.1.5.5 Combined friction model

The ideal friction model is one that combines the both Coulomb and Shear Friction Model i.e. uses Culomb friction law for low contact stresses and the shear friction law for high contact stresses as shown in the image below:

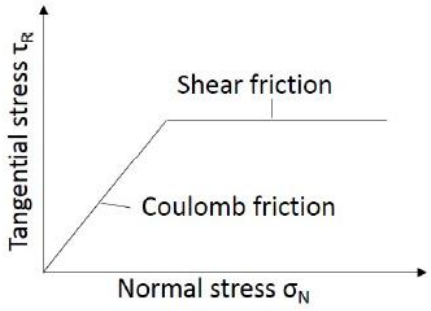

Figure 133, Schematic demonstration of Combined friction model

The Combined friction law is a combination of both the Coulomb and the Shear friction law. For low normal stresses the calculation of the friction stresses is done according to the Coulomb friction law.

As soon as the friction stress reaches a critical value which is the product of the user-defined Interface friction factor m and the current ultimate yield strength k, further calculations of the friction stress will be done according to the Shear friction law. The combination of these two friction laws ensures that the friction stress is calculated with sufficient detail for low normal stresses and that it is unable to surpass any physical boundaries for high normal stresses.

In SPR, determining the right friction is very important for rivet setting process as well as joint strength (Han et al, 2006) and knowing how it affects the joints might make a difference between a poor and a good quality joint (Briskham, 2016).

The friction can occur between the sheets and between the rivet and the sheets, the sheets themselves and between the bottom sheet and the die. The friction between these components of the model is determined by materials pairings and subsequently the condition of the surface of the two materials. Generally, there are four types of conditions in metal forming (Kim, Kardes, 2012):

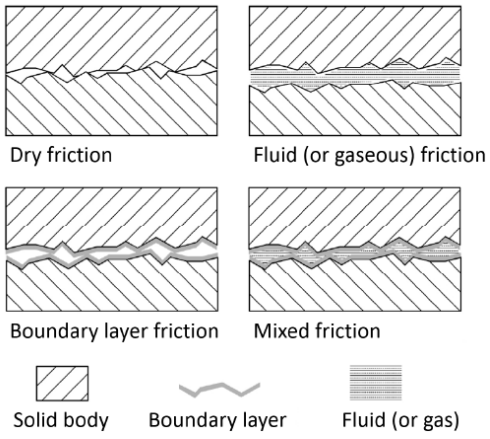

Figure 134, Four types of friction state (Simufact, 2015)

Dry condition

The friction partners are in direct contact with each other there is no lubrication between and so the friction is high. This condition is desired only in a few forming processes such as air bending or hot rolling of slabs or plates (Kardes, 2012, Simufact, 2015).

Fluid condition

The friction partners are separated by a fluid film. This condition is applicable in a few forming processes such as high speed sheet rolling where the large velocities at the interface between the tool and materials create hydrodynamic environment for example where oil based lubricants are used (Kardes, 2012, Simufact, 2015).

Boundary condition

In this case, the friction occurs between two boundary layers. These can be products of surface treatments of different parts or a results of reactions of the material with its surroundings (e.g. oxide layers) or the lubricant. In most metal forming process this is the preferred condition (Kardes, 2012, Simufact, 2015).

Mixed-film lubrication

This is another frequently used condition in metal forming which combines different states of friction.This means that for example, the micro peaks of the metal surface have characteristics of the boundary condition whilst the micro valleys of the metal surface (Kardes, 2012, Simufact, 2015).

Some research has been conducted on the surface conditions and how these affect the SPR process. Han and Chrysanthou (2008) who studied the effect of coatings on the sheet materials on the joint strength and quality. The research was completed on a joint with AA5754 aluminium and HSLA350 steel at the bottom. The HSLA350 was used with three different conditions – uncoated, e-coating coated and zinc plated. The results showed that there was a significant difference in effect these conditions had on quality of the joint and its strength.

Different research was also conducted by Han et al (2006) on sheet to sheet interfacial conditions. The study used two different coatings; a wax based solid lubricant and PTFE insert between the sheets and assessed their impact by measuring the fatigue performance of the joints. It was shown that the wax based solid lubricant slowed down the fretting damage on the aluminium surface which had a positive effect on fatigue performance. The PTFE insert eliminated the fretting damage but also resulted in a decrease of fatigue performance. This was caused by the fact that PTFE decreased the interfacial

friction between the sheets but consequently the load was concentrated on the rivet which consequently failed by fracturing significantly sooner than without PTFE.

4.1.5.6 Coatings and lubricants used in SPR in Atlas Copco

Rivet coatings in SPR have two main functions, to lubricate the rivet insertion and to protect the rivet from corrosion.

There are four main types of rivet coating employed in Atlas Copco SPR:

- Mechanical plating
- Electro plating
- Dry lubricant top coating
- Painting

It is common practice to use a base layer of plating to provide corrosion resistance in service, and to combine the base layer of plating with a top coating of dry lubricant or lubricative paint to provide lubrication for the rivet insertion.

At the start of this project we learnt that the simulations being done by other companies using the Simufact software were generally using the same rivet friction level for every rivet coating type. However, we know that different rivet coatings have different friction levels and these affect the rivet insertion result, for example a higher friction coating causes the rivet to flare more, and a lower friction coating causes the rivet to stake more. Therefore developing an understanding of which friction settings to use in the simulation software for different rivet coatings is an important aspect of advancing the field of SPR simulation to enable more accurate simulation results.

The following table details all the coatings currently offered on rivets by Atlas Copco.

Coating Code	Description	Notes
H00	Zinc/Tin (70/30) Mechanical plating.	Most popular coating for semi-tubular rivets (C, A, K, P, PG, R, J).
Y00	Zinc/Tin/Aluminium (40/50/5)(Almac™) Mechanical plating. Oven baked immediately after plating to remove hydrogen.	Widely used on semi-tubular rivets (C, A, K, P, PG, R, J).
M00	Zinc Mechanical plating.	Use for steel/steel joining, do not use for steel/aluminium joining.
HL0	Zinc/Tin (70/30) Mechanical plating with ultra low friction dry lubricant.	Used on T-rivets and BG-rivets.
H06	Zinc/Tin (70/30) Mechanical plating with trivalent passivation.	For applications where rivet is overpainted but not ecoated.
Y06	Zinc/Tin/Aluminium (40/50/5)(Almac™) Mechanical plating with trivalent passivation.	For applications where rivet is overpainted but not ecoated.
M06	Zinc Mechanical plating with trivalent passivation.	For applications where rivet is overpainted but not ecoated.
W03	Zinc/Nickel Electroplating 8 to 12 microns with trivalent passivation. Oven baked immediately after plating to remove hydrogen.	This coating is only available for SPR studs. Use for studs with hardness level 1 (280Hv) & level H (360Hv).
WLA	Zinc/Nickel Electroplating 5 to 10 microns with trivalent passivation. Oven baked immediately after plating to remove hydrogen.	Used for anodised aluminium assemblies that are bonded together with structural adhesive where the adhesive bond is the primary joining method.
W36	Zinc/Nickel Electroplating 5 to 10 microns with medium friction B18 paint top coating. Oven baked immediately after plating to remove hydrogen.	VW Audi Group patented coating. Only available on semi-tubular rivets to VAG or VAG suppliers. Contact us for information.
W39	Zinc/Nickel Electroplating 5 to 10 microns with ultra low friction paint top coating. Oven baked immediately after plating to remove hydrogen.	Only available on T-rivets. Use with structural adhesive due to reduce risk from HE. See electroplating page about using ZnNi on fasteners over 390Hv and risk of HE.
K01	H00 plating with multi-layer lubricative and protective black paint coating.	Suitable for low volume general industry applications.
YCB	Two coats of zinc/aluminium flake paint plus low friction dry lube top coating.	Not recommended for rivets, this type of coating is mainly used for bolts.
Z00	Zinc/Tin/Aluminium (40/50/5)(Almac™) Mechanical plating. Oven baked immediately after plating to remove hydrogen.	Oven baking after plating to remove hydrogen is rarely used on water based plating due to low risk of hydrogen embrittlement.
V00	Electro-Brass (bright decorative finish) with clear lacquer.	For general industry applications. Nickel or Copper also available.

Table 6, Types of rivet coating available from Atlas Copco (AC SPR coatings overview 2019)

4.1.5.7 Measuring friction

There are several methods available to quantify friction, such as a sliding test or ring compression test.

4.1.5.7.1 Ring compression test

This method uses changes in measurements of height and internal diameter of a test sample in a shape of a hollow cylinder with prescribed dimensions under compression as shown. These changes have been noted as being representative of various extents of sensitivity to contact friction by Kunogi (1954).

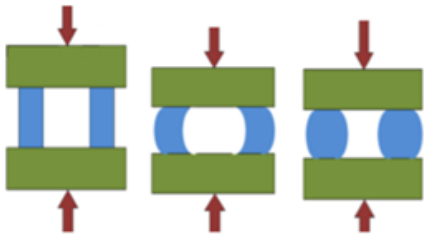

Figure 135, Ring compression test before & after compression, with low friction & high friction.

Interesting research has been completed on this type of testing by Rajesh et al (2013) using a prescribed cylindrical sample with three different coatings.

Figure 136, Cylinder sample for ring compression test

In this test, both coefficient of friction and interface friction factor can be determined using the following equations (Rajesh, 2013):

$$m = \frac{-1}{2\frac{Ro}{T}\left(1+\frac{Ri}{Ro}-2\frac{Rn}{Ro}\right)} \times \ln\left[\left(\frac{Ri}{Ro}\right)^2 \times \frac{\left(\frac{Rn}{Ro}\right)^2+\sqrt{3+\left(\frac{Rn}{Ro}\right)^4}}{\left(\frac{Rn}{Ro}\right)^2+\sqrt{3\left(\frac{Ri}{Ro}\right)^4+\left(\frac{Rn}{Ro}\right)^2}}\right]$$

$$Rn = Ro\sqrt{\frac{(Ri/Ro)+(\Delta Ri/\Delta Ro)}{(Ro/Ri)+(\Delta Ri/\Delta Ro)}}$$

$$\mu = \frac{m}{\sqrt{3}}$$

Rn – Radius of sample

Ri – Inner radius of sample after deformation

Ro – External radius of sample after deformation

Δ Ri – Change in internal radius of the sample after deformation

Δ R_n – Change in external radius of the sample after deformation

T – Height of sample

M – Friction factor

μ - Coefficient of friction

Rajesh (2013) compared several lubricants against unlubricated sample and the results of this study are clearly demonstrating that the interface friction factor as well as coefficient of friction can differ with different lubricants.

Lubricant condition	Load, Tonne	Friction factor		Coefficient of friction	
		Exp	The	Exp	The
Dry condition	80	0.88	0.82	0.52	0.48
Zinc stearate	80	0.48	0.34	0.14	0.19
Graphite	80	0.6	0.44	0.16	0.25
MoS2	80	0.52	0.33	0.14	0.19

Lubricant condition	Friction coefficient	total deformation, mm	stress, N/mm2
Dry condition	0.52	0.40268	818.02
Graphite	0.16	0.40552	833.88
MoS2	0.14	0.40613	837.86
Zinc stearate	0.14	0.40613	837.86

Table 7, Results of study comparing different lubricants in a ring compression test and their effects on μ and m.

4.1.5.7.2 Translational sliding

Kraus (2018) has completed measurements of friction specifically aimed at SPR by a translation sliding test. In this test a test rig was set where a normal force is applied by pneumatic actuator and a speed and displacement controlled friction force is applied by an electromagnetic cylinder.

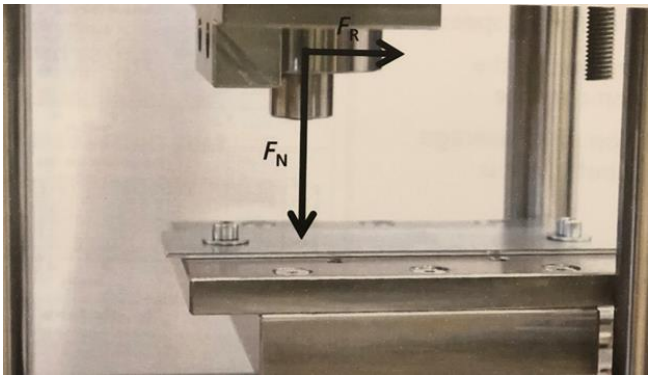

Figure 137, Test rig for translational sliding

Figure 138, Sample rivet measured using translational sliding test

Using this method, Kraus measured values for Almac coating which is a coating frequently used on Atlas Copco standard rivets. The values were as follows:

$\mu_{mean} = 0.157$

$\mu_{max} = 0.207$

$\mu_{min} = 0.101$

4.1.5.8 Assessment of advancements of friction in context of SPR simulation based on literature

A number of researchers have looked at determining friction in context of simulating SPR (Melander, 2003, Khezri et ala, 2000, Atzeni et al, 2005, 2009, Xu, 2006, Kato, 2007, Krishnappa, 2008, Abe, 2009, Mucha, 2011, Caradente et al, 2016, Honsch et al, 2018). However, these were mainly small studies in which friction was tightly configured to small number of joints (1-3). Furthermore, determining friction was one of many steps in order to complete the simulation and not the main aim of any of these studies. More recently, Kraus (2018) attempted to measure friction by using ring compression test, but experienced difficulties with the correct dimensioning of the ring sample. Only two of the above authors (Honsch et al, 2018 and Kraus, 2018) have also used the combined model whilst the rest used Coulomb model only which is great during elastic deformation of the process but not as reliable during plastic deformation part of the process (Kraus, 2018). Huang et al (2018) also attempted to simulate SPR using LS-Dyna and specified friction coefficient of 0.2 using Coulomb model in his work. However, the simulation results were not in a good agreement in terms of appearance and a typical material behaviour of a metal displayed within the physical joint was missing. Another research was completed by Varela et al (2018) which used software Forge and friction coefficient of 0.003. As before, the simulation of the joint did not display a typical behaviour captured in a cross section of the physical test. No research to date has attempted to simulate different coatings. Moraes et al (2018) confirms this state of art of friction, and asserts that an in-depth study related to friction does not currently exist.

4.2 FEA of SPR to date – Current state of the art

Now that main concepts of modelling of SPR have been introduced, it is possible to analyse available literature to establish the state of art in this field. Available literature suggests that a number of researchers have attempted to use FEA software packages in order to simulate an insertion of a self-pierce rivets as well as tensile and crash tests of self-pierce rivets. Amongst the initial studies is that of King (1995) which created a basic model of an indentation of SPR using DEFORM-2D. This model facilitated the initial set up and calculations of different aspects of the process such as displacements,

forces and component deformations which were then to be compared to physical results of the equivalent model.

A different software was used for a similar study by Hahn and Dolle (2001) – MSC AutoForge. Using this software, the researchers achieved a good agreement between the force-displacement curves and the respective simulations. This was shortly followed by research conducted by Westgate (2001) which used FE software package ABAQUS which was a basis for design of lightweight self piercing riveting equipment. This study proposed that 2D models were adequate for the initial design evaluation and 3D models would be needed to calculate stresses and to optimize designs.

The research was expanded on by Westberg who conducted a crash test simulation (2002) using software ABAQUS on DP600 steel. The study using peel specimens revealed that the setting up the model as precisely as possible is extremely important and that direct application of the velocity load caused high peak loads which was not deemed realistic behaviour. This was improved by adopting a ramped or smooth approach. It also suggested further research compares simulations with real tests completed at high displacement velocities and further investigates influence of rivet size, geometry, material grade, gauge of sheets, cracks and internal stresses on the simulation.

A comparable study was also completed by Stromstedt (2002) which conducted FE analysis of lap shear joints riveted by SPR method. Tang (2002) developed an FE method for simulating SPR using aluminium parts and structures which are subject to impact. The method was used to conduct analysis of a side impact on a vehicle and was reported to have achieved good agreement with the deformed mode. Sui et al (2004) focused on a non-linear FE model and pinpointed hoop residual stress as having the biggest influence on the mechanical behaviour of a joint. Another study concentrating on fatigue testing was by Kim et al (2005) which aimed to assess the structural stiffness and fatigue life. The experimental and numerical study found that fatigue life is higher in SPR joints in comparison to other joint types such as resistance spot welding.

Further research into various parameters of SPR was conducted by Atzeni et al who via a number of studies (Atzeni et al 2003, Atzeni et al 2004 and Atzeni et al 2005) evaluated factors such as friction coefficients and rate of kinetic energy by simulating joining of aluminium alloy and using ABAQUS software. Both rivet insertion and tensile tests completed as part of the study showed good agreement between experimental and numerical trials in deformed geometry and force-displacement curve.

Further study by Stuhmeyer (2005) looked in detail at rivet insertion simulations and highlighted further interesting aspects such as importance of remeshing in obtaining a more accurate result as

well as the importance of extrapolation of the material properties which was considered to have a far more of an effect than for instance process parameter such as friction.

A study by Bouchard et al aimed to expand the research by transferring the 2D results into a 3D mesh by interpolation technique (2005). This found that the history of the mechanical changes the rivet and sheets are submitted to during the insertion process is a great importance in the prediction of final strength of the joint. A comparable study was completed by Porcaro et al (2006a and 2006b) which attempted to simulate the riveting process using LS-Dyna software initially in a 2D axisymmetrical model. An r-adaptivity implicit solution and geometrical criterion relating to thickness of plates were used for these studies. Following a number of simulations with different two different grade of materials and rivet geometries, good agreements were found between the force-deformation curves suggesting feasibility of simulation (2006b). This has then been expanded into 3D model which was compared with the experimental results to show correct deformation modes and force-displacement curves (2006a).

Similar study has also been conducted by Gardstram (2006) who worked on few different models on SPR and pierce nut and attempted both 2D and 3D simulations. 2D simulations were completed using DEFORM-2D and were used for the rivet insertion simulation and 3D using ABAQUS in order to simulate the tensile test. The 2D simulation has shown good agreements in the cross sections as well as force-displacement curves. A difference in the force-displacement curve was noted toward the end of the insertion which might be due to the limitation in terms of material description at a particular strain rate. The 2D results were then transferred into a 3D model, a process which highlighted the importance of transferring the strain level which occurred in the joining phase. The results in the 3D were not as close to the experimental as the 2D simulation but despite this it was deemed that rivet and material combinations could be assessed based on a simulation. The study has also highlighted the importance of friction in the process of simulation and simulation was considered to be instrumental in development of a new design of the rivet and die in order to decrease the risk of rivet fracture.

Furthermore, in addition to exploring aspects of joint behaviour using FEA some researchers have increasingly started utilizing FEA modelling to help them optimize riveting difficult material combinations such as steel and aluminium which have proved problematic to join due to difference of flow stress (Cacko et al, 2004). Abe et al (2006) have attempted joining mild steel and aluminium and used simulation using LS-Dyna in order to predict the defects of this process. The study found that there was an agreement between the experimental and numerical prediction and it showed two of the three anticipated defects, necking and separation. However, the third anticipated defect,

penetration, that occurred in the experimental samples was not noted in the numerical results. With most of the defects demonstrating as expected the study considered finite element method effective in optimizing the riveting conditions. This was shortly followed by research into joining aluminium and high strength steel which proved possible by using FEA to optimize die shape (Abe et al, 2009). Further advances in the field were made by Ruprechter et al (2006) who developed a node independent model in order to simulate stiffness and strength of the joint. They were able to calculate local stresses that are required to determine the fatigue life. The results were verified using experimental tests.

Following their study in 2005, Bouchard et al have continued and built on their research using Forge software and suggested that the simulations they have conducted as part of the latter study (2008) have accurately predicted the behaviours of the joints in both two and three sheet materials stacks. The simulation also highlighted that the compressive residual stress in the lower part of the rivet is an important factor in the strength of the joint and that optimizing the lower die might have a desirable effect on structural strength of the joint. As previously, the study further proceeds to also transferring the 2D SPR model into a 3D model and assessing the strength of the joint via a shear test. Here, positive results were also reported and the study confirmed findings of Gardstram (2006) in that the mechanical history the parts of the model underwent in the insertion stage is crucial to accuracy of results of the strength testing. This research was followed by a study completed by Atzeni et al (2009) who also built on their previous research and conducted a numerical and experimental tests using AL6082 Aluminium alloy and ABAQUS software. The focus of comparison was on force displacement curves for both insertion (2D simulation) and shear test (3D simulation) which were found to be in a fairly good agreement with the experimental results. This applied also to the shape deformation in both 2D and 3D.

Hoang et al (2010) used LS-Dyna in order to simulate the insertion of self-piercing rivet and the efforts were focused on recommending optimal values for process parameters such as friction and adaptive internal. They have also conducted a mesh sensitivity study and experimented with different element sizes. The results of the simulation using joining aluminium were found to be in good agreement with the experimental results.

A comprehensive and critical review of available research into FEA of SPR was carried out in 2011 by He et al which confirms the assertions made by Fu and Malik in 2001 to be still applicable currently i.e. although a much more in-depth understanding has been gleaned from research to date, a correct and accurate simulation of the complex process of SPR still remains an extremely difficult task since a number of variables influence this process and whenever aspects of process change, new problems arise each time and numerical model requires a recalibration. To gain a full understanding of this

process, the simulation model is required to include all aspects of the rivet process, failure and join defects for joints mechanical properties for both static and dynamic scenarios as well as relationships between materials. He at al attempted to improve this state by further research (2013) in which LS-Dyna software was used to produce a 2D axisymmetric model of riveting RC5754 Aluminium alloy. An implicit analysis was used along with r-self-adaptivity and the results of numerical analysis were validated by physical tests. The comparison was based on monitoring of the force used to set the rivets and good agreements were reported in terms of both, force and displacement as well as deformation within the joint.

An all-encompassing approach to simulation was also suggested by Grujicic (2014) who stated that although there are a lot of studies focusing on a specific process parameter or behaviour of a joint but there is a lack of an extensive computational simulations which would involve a whole vehicle crash testing.

Carandente (2016) suggested in his work using Simufact software with hydraulic press and and 5 kN clamp and iso-thermal model that there are difficulties with configuring rivets and dies for various stacks which, compounded by the need for reduced number of setters on the line, can lead to a costly exercise of physical testing. It has been suggested that FE might support this in future by reducing the number of physical tests if used correctly.

The most recent research attempts to continue advancements in the field FEA of SPR and contributions from researchers such as Moraes et al (2015), Carandente et al (2016), Honsch, (2018) and Kraus (2018) have shown good levels of agreement between the simulations and experimental results.

4.2.1 Software types

There are a number of FE codes and softwares available for simulations of SPR and a lot of them were used in the past by various researchers.

Casalino and Rotondo (2008) explored numerical model and particularly focussed on governing equations in order to describe the process of SPR using Ansys/LS-Dyna finite element code and material 6060T4 aluminium alloy. They have elaborated on problems such as crack propagation, mesh size and calibration of kill-element technique. With optimized the mesh size and effective plastic strain threshold they have achieved good agreement with cross section and force-displacement curve of the experimental test.

Moraes et al have used the LS-Dyna software in order to conduct an explicit analysis of insertion of rivet into AZ31 magnesium sheets. The innovative part of this research is the use of ISV plasticity damage model in order to evaluate the deformation that takes place during the insertion process. This model was deemed by the authors to be more effective in terms of the calculation time which is improved by the fact that this model can capture large scale deformation without remeshing reducing the computation time further still and potentially improve the simulations as remeshing algorithms were reported to cause errors in the accuracy (Moraes et al, 2014). However, the results, while visually similar to the experimental results, were not considered as accurate as other results in this field or other results using plasticity models other than ISV plasticity damage model

Whilst the main part of the body of research up to about 2015 was completed by LS-Dyna, the more recent research into FE in SPR has centred around software Simufact which has made a number of improvements to its product to address specific needs of SPR simulation.

This software has been noted by a couple of research papers recently. These were the above mentioned paper by Caradente (2016), followed by papers by Honsch et al (2018) and Kraus et al (2018). The two former papers looked into a simple replication of an aluminium to aluminium joint whilst the latter explored measuring friction in the context of SPR respectively (this is explained further in chapter of friction, number 4.1.6.).

4.2.2 Different types of materials in simulation

A number of researchers explored materials covering wide range of aluminium alloys from 5xxx series, through 6xxx to 7xxx (Jäckel, 2018) , steels, magnesium (Moreaes et al, 2014), as well as CFRP. One of the initial research avenues were attempted by Khezri who has worked on a number of studies on simulation in area of SPR with the first one (2000) exploring simulation of SPR joining of high strength steel (DP600+Z100). The study started with experimental set up of two specimens in order to obtain flow curves through a compression test. The specimens were prepared for both steel sheets and steel rivets by stacking up coupons into a sandwich bonded by glue and by removing the rivet head and the bottom flared out part respectively. The flow curves were then used for simulation of a number of different rivets and dies using DEFORM software and verified and reliable results were reported to have been obtained from this study. Melander (2003) has followed up this research with SPR simulation using high strength steel DP600 and further research was completed by Abe et al (2008) using boron steel and conventional rivet.

A study conducted by Carandente et al (2016) has used Simufact as a FE software of choice and performed a simulation of rivet insertion into AA5754 Aluminium alloy whilst taking into consideration

the temperature increase during the insertion and subsequent thermal softening that occurs within the joint. To that end, the flow curves required to guide the behaviour of the rivet during the calculations were created whilst taking into consideration the increased temperature and strain rate. The results of this thermomechanical model were compared with isothermal model where temperature remained the same and both were compared to the results of the physical testing. The study found that the results of all seven different joints simulated using both thermomechanical were in a slightly improved agreement with the experimental results than the results obtained using isothermal model. However, it has been argued that creation of flow curves at different temperatures is prohibitively expensive and a judgement needs to be made as to the cost analysis of this exercise vs the amount of improvement this contributes to the accuracy of the simulation (TechSpec, 2019). This was followed by another study conducted by Honsch et al (2018) who also looked at the next alumimium alloys series, 6xxx, which remains a frequent choice for the automotive manufacturers.

More recently, Jäckel et al (2018) have looked into modelling of SPR using 7xxx series aluminium) alloy which is gaining momentum with automotive manufacturers dueto its strength as well as innovative materials such as CRFP. This study was done using solid riveting as well semi tubular rivets.

4.2.3 Optimisation of rivet and die geometries

Jäckel has attempted optimisation of both rivet and die using numerical modelling, however, this referred to simply using a different geometries of both, rivets and dies (2018).

Using numerical modelling for optimisation of rivet and die geometries gains significance when used by SPR manufacturer, as this represents the option to explore different shapes of rivet and dies without the costly exercise of producing a batch of slightly amended geometries. He at al (2007) indicated in his review paper aimed at SPR that using numerical modelling for supporting R&D as well as exploring options for new geometries via creating a process window will be a possibility in the future. However, so far this has not been evidenced by a lot of research.

Khezri has worked on a number of studies on simulation in area of SPR with the first one (2000) exploring simulation of SPR joining of high strength steel (DP600+Z100). The study started with experimental set up of two specimens in order to obtain flow curves through a compression test. The specimens were prepared for both steel sheets and steel rivets by stacking up coupons into a sandwich bonded by glue and by removing the rivet head and the bottom flared out part respectively. The flow curves were then used for simulation of a number of different rivets and dies using DEFORM software using hydraulic press and 5 kN clamp. Verified and reliable results were reported to have been obtained from this study.

4.2.4 Areas for future development

It would seem that all the simulations to date have been carried out using a hydraulic setter and so far no researchers have attempted to design the insertion method in simulated version using an energy or inertia based setters such as servo setter. Due to the nature of the variable speed insertion, developing a model for servo setter might make the simulations mimic the process more accurately and hence lead to more accurate results. A concept related to the different types of press is also clamping which is the act of keeping the sheets pressed together by a nose prior or during the insertion which has not been given much consideration in literature.

It can also be noted that all the rivet designs modelled to date are those of the standard designs, semi tubular rivets, and no T-rivets have been simulated so far, which is the last innovation of Henrob. It would therefore be of use to simulate this particular rivet and explore how this the

Furthermore, whilst there are some studies that used simulation for geometry optimisation (Mucha, 2015), they generally concentrated on selecting different rivets and dies for a joint in question using existing geometries. To the author's knowledge, there are no attempts to develop a completely new design for a rivet with support of FE analysis which leaves space for contribution. This would particularly mean using FE analysis to support design of a new rivet to add to Atlas Copco range to address the continuously evolving trends in joining in automotive industry.

Another important area that did not seem to have a great amount of research accomplished on it in relation to SPR insertion simulation is the friction. Friction is an important area of interest in SPR and the software might have some limitations in this area. Researching friction further and collaboratively create a model within the software that would particularly capture the influence of velocity on friction rivet insertion which has been highlighted by the R&D department as lacking would be extremely advantageous.

Joint robustness testing via establishing a process window for manufacturing variables was another avenue that has not been focused on in available literature. He et al (2007) in his review paper asserted that simulation will in future have the capability to be used for addressing variables of the process and create a process window, however, not a lot of research has been completed in this area.

5 RESEARCH METHODS

The aim of this thesis is to investigate feasibility of using simulation as a predicative tool of SPR joint behaviour in order to optimize rivet and die selection by reducing physical testing, improve the design of existing rivets, and design new rivets. To meet the objectives of this research project, both physical tests and FE analysis will be used throughout the thesis and details of both will be noted in the following sections.

5.1 Physical SPR tests

Physical tests serve to validate the reliability of the numerical results predicted by the software.

Physical tests results used in this thesis come from several different sources:

1. Testing carried out for purposes of PhD by author
2. Testing carried out for purposes of PhD by AC technicians/ engineers (as requested by author)
3. Historical testing data completed for purposes of previous projects
4. Testing carried out as part of a research collaboration

Several physical tests used in the experimental part of the thesis were carried out as part of a collaboration and this will be specified in the method description in each individual case. In all other cases of SPR insertion testing that were carried out internally at AC, the following steps and procedures applied:

Material status:

- Material sources are as follows:
    - Novelis for Aluminium
    - Arcilor Mittal for steel
- Materials are supplied directly from the above suppliers or from the above suppliers but via customers.
- Materials (sheets or coupons) were placed in the freezer upon delivery if age hardening is a concern (specifically applies to 6xxx series of Aluminium).

Sample preparation:

- Unless materials are already supplied as coupons, cutting is required. The metal is cut into squares of 40mm x 40mm dimensions (coupons for SPR insertion testing) or 40mm x 120mm (for mechanical testing) using Hydraulic sheet metal guillotine.
- Coupons are given a sample reference number and assembled in the riveting order prior to testing.
- Random check of thickness of the coupon is carried out using Digital Gauge Micrometer (Vernier) to ensure that no large variations to sample thickness are present.
- Where possible, 5off samples are prepared for statistical reasons (shortage of materials or time constraints can be a reason for a 1off sample only).
- Conducted by a trained technician/ engineer due to health and safety regulations.

SPR insertion

- Unless otherwise specified, riveting is carried out by G1.5 AC setter with medium throat depth C-frame rated for 80kN max repetitive load.
- Conducted by a trained technician/ engineer due to health and safety regulations.
- Velocity is calibrated by a trained technician/ engineer based on the stack thickness and hardness.
- Unless stated otherwise, one rivet is inserted per one coupon stack.

Joint examination

Cross sectioning

- Riveted joints are cut through the centre to create a cross section using Struers sectioning cutter with coolant supply.
- Grinding is then conducted using 1200 grit size.
- Carried out by a trained technician/ engineer due to health and safety regulations.

Photographing

- Microscope Zeiss STEMI 508 with IDEA SPOT USB camera mounted above worktop are used to photograph the cut sample.
- Conducted by a trained technician/ engineer/ author.

Measuring

- A SPOT software 5.0 for Microscopy and Macro-photography is used with calibration as follows – 3264 sensor pixels = 20mm
- Conducted by the author.

Joint analysis

- For purposes of comparison with simulation in the experimental stage of this work, an average value for all measurements is calculated so the most representative values are compared with simulation.
- Conducted by the author.

Extraction of force-displacement curves

- When required, force-displacement curves are extracted from the setter software, Rivmon and recorded on the external drive.
- Conducted by technician / engineer.

5.2 FE analysis

- For FE analysis an FE software called Simufact by MSC Software Company will be used.
- All simulations are conducted by the author.
- Velocity of the press is always informed by the velocity of the physical test or historical data on similar joint when not former not available.
- In presented images where it is relevant to show a colour legend, this has been shown. In many images, the analysis is focused on cross section measurements and not on stress/strain distribution and in these images the colour legend is not included.

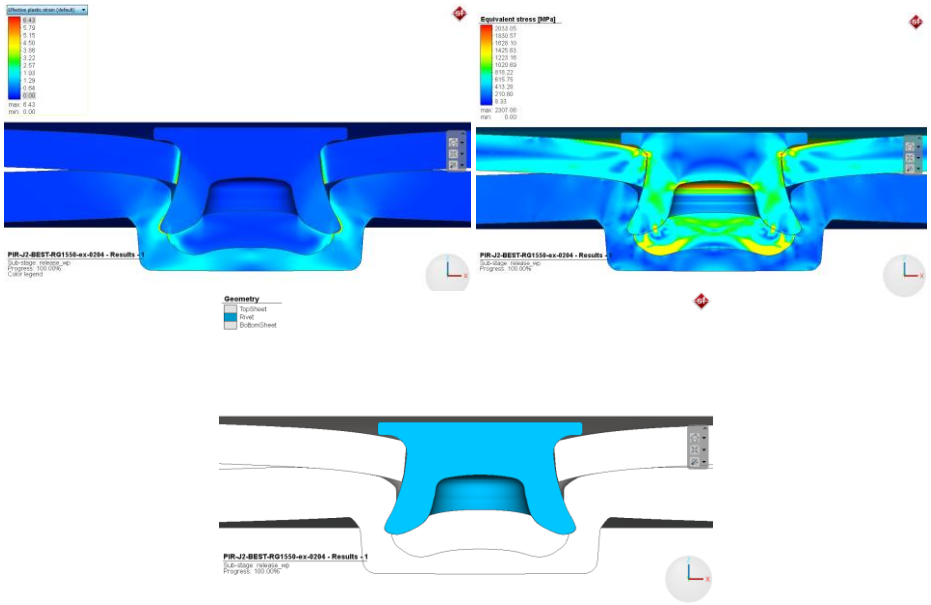

Figure 139, Examples of simulation presentation – Effective plastic strain (top left), equivalent stress (top right) and geometry (bottom)

- Additional external input will be required in form of geometries and materials:

Geometries

- This refers to CAD models of all parts used in simulation i.e.
  - Tooling - nose, punch
  - Deformable parts - rivet, sheets
  - Non-deformable parts – die
- All rivets, dies and nose CAD models have been supplied by AC.
- CAD models of punch and sheets have been created by author.

Material flow curves

Currently, AC does not have the capability to conduct material testing and therefore all flow curves used in this thesis have been supplied from the following sources:

- Simufact library – Simufact has extensive library of materials including materials frequently used in automotive industry.
- Material suppliers – Novelis have supplied majority of flow curves for Aluminium and Arcilor Mittal supplied flow curves for steel.
- Published literature – specialized literature sources such as Papers focusing on FE, Theses, Material forming research, Conference papers and many others.

- Research collaborations – namely collaborations with Fraunhofer IWU (Germany) and Tecnalia (Spain).

5.3 Validation of simulation by experimental tests

Most of the simulations go through a validation by experimental results to inform the user if the settings are correct. The flow chart below details the validation process.

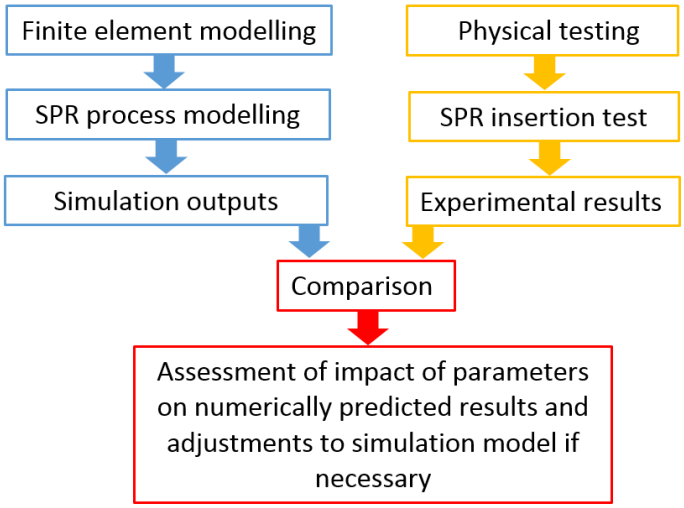

Figure 140, Simulation validation chart

6 EXPERIMENTAL STAGE

With fundamentals of SPR and FE covered in previous chapters, it is fitting to now take a detailed look at the software in order to evaluate the current capability of its default built-in SPR model, this is a model provided with the out of the box software and we need to determine if the built-in model works and if not how to modify it to make it work. The aim is to identify any further areas within this model that might need improvements and optimisation in order to develop an effective simulation base model using settings closely matching the rivet setting equipment used in the test lab at the sponsoring company. This base model is intended to then be used as a platform for a wide range of simulations in order to tackle the current issues the joining industry is experiencing such as reliance on costly physical testing and lack of ability to test manufacturing variability of rivets and subtrates alike.

The built-in SPR model will be tested in the following sections by changing various process parameters in sensitivity studies in order to understand the behaviours, trends and influence of individual parameters.

The variables to be examined in this chapter are those looked at earlier in the literature review, which have been selected as having an influence of SPR process.

- Material behaviour – flow and plasticity and material characterization
- Mechanics of damage Friction, lubrication and coatings
- Characteristics of the process – e.g. accurate process description e.g. boundary conditions, type of press, speed of insertion, temperature, clamping, mesh.
- Rivets, dies, sheets and tooling geometries

These variables, depending on their nature, are obtained either by a variety of experimental tests from different sources, as listed in section 5.2 and / or calibration exercises following sensitivity study, by calculations, or by using CAD system in the case of preparing the geometries. The following sections will look at these concepts in greater detail and aim to do the following:

- Examine their impact on the accuracy of simulation.
- Attempt to select settings that are closest to the SPR process in reality.

The result expected at the end of this chapter is to have a simulation model that has proven to give results that are deemed within the acceptance criteria and is ready to aid selection of optimal rivet and die combinations as well as the design of new rivets and dies.

6.1 Simulation assessment and accuracy tolerances

A converged solution is a term used for simulations that have ran their course and were completed as per criteria. In this software, it is the dynamic FE analysis Newton-Raphson iterations that carry out the assessment of the convergence and unless there are problems with mesh, excessive stresses or an incorrect set-up of simulation model, usually all simulations converge i.e. complete. However, whether they are in good agreement with a physical part is another important question. The solution might never be able to replicate joints with 100% accuracy but it is considered to be sufficient to achieve a solution that is within a certain tolerance of it, providing the tolerance is correctly set.

Therefore, the next logical step is to set out tolerances that would indicate whether the simulation has been successful or whether there are parameters that need to be addressed further.

There are a number of variables influencing the joints in reality, such as imperfections in materials (e.g. hardened spots), changing thickness (this can vary by up to 0.3mm in for example cast materials), alignment of the sheets, distance of rivet to the end of the sheets etc, age of material, manufacturing variables in material hardness, irregularities in application of adhesive (TechSpec, 2019).

Generally, it is good practice to carry out at least 5 off samples (in some specific projects this can go up to 20 off). This means that statistical data can be calculated such as coefficient of variance, standard deviation and doing so can point out any trends as to the stability of the joint. In reality, depending on the joint, even within the 5 off sample there can be variances which make it difficult to simulate accurately. There are joints that can be very stable, for example a joint with two reasonable thickness aluminium sheets (1.5mm and above). These stable joints can become less stable if mixed materials are introduced such as steel to aluminium, and thickness of the sheets is either too think or too thick.

The tolerances that will be adopted for the simulation results will also need to reflect the variability between samples of the same joints, since in real laboratory tests there is some variation from test to test.

6.1.1 Simulation assessment – Joint measurements

Before any research work starts, however, a set of criteria is needed to evaluate what is considered a successful and accurate simulation and what is not.

Following consultation of historical results as well as internal expertise on variability within 5 off samples, a tolerance of +/- 0.15mm (TechSpec1, 2019) has been established for all three measurements of interlock, Tmin and head height is sufficient for the simulation to be deemed as

sufficient. This can be reconsidered on an individual basis in instances where a material has a known variability and is likely to give results that are farther apart or under new circumstances such as adding adhesive into the joint.

The aforementioned variability of materials can be noted in two different areas:

- Variability within batch – this can be caused by general presence of imperfections in the metal and / or rolling of the sheet material for example, the material might not be the same thickness throughout the entire sheet, edges might be different thickness that the middle area, leading to different outcomes in a riveted joint (TechSpec1, 2019).
- Batch to batch variability – the material's ductility can be subject to manufacturing variability and can vary from batch to batch leading to materials being potentially harder or softer and subsequently to different outcomes in a riveted joint. This is specifically true for higher strengths of Aluminium (TechSpec1, 2019).
- In addition, some materials such as 6xxx series of Aluminium are subject to age hardening and if this is not frozen to keep at the same hardness this can also lead to differences in the riveted stacks (TechSpec1, 2019).

This tolerance will also need to be reviewed in a specific scenarios, such as a misaligned setter, or imperfections in materials, as these can cause asymmetry or variation in joints. Due to the balance between length and accuracy of the simulation, and the nature of the SPR process, a 2D axisymmetric model has been selected to enable rapid simulation, but a 2D model is unable to simulate scenarios which cause one side of the rivet insertion to differ from the other, as it only looks at a slice taken out of a halved cross section, and not both sides of a cross section, and not all the way around the rivet. The 2D simulation of a half cross section that is used to enable fast simulations is shown in the image below.

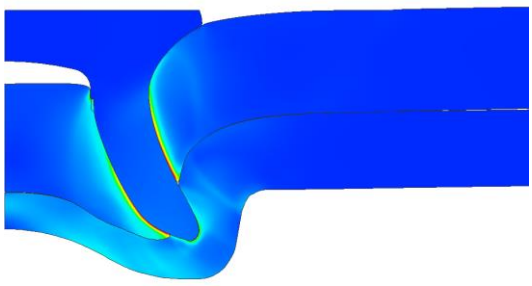

Figure 141, Example of a 2D axisymmetric result for a half cross section

6.1.2 Simulation assessment – Joint visual attributes

As noted in section 2.7.1, the visual appearance of the joint is also important and therefore, the simulation must achieve a joint that visually looks the same as a real joint. In some instances the measurements may be in agreement, however, the overall appearance of an inserted rivet may not display the same typical features seen in a real test of a specific hardness material, or other process parameters shown below. A difference might indicate that a simulation model is not set up correctly.

Therefore, a satisfactory simulation is required to show some signs of replicating of what is deemed to be the typical features seen in a real joint test. This can include different metal behaviours such as bore filling, such as those shown in Figure 142, drag-down of the material under the rive leg as shown in Figure 143, or the size of the triangular gaps' between the two sheets and rivet as shown in Figure 144.

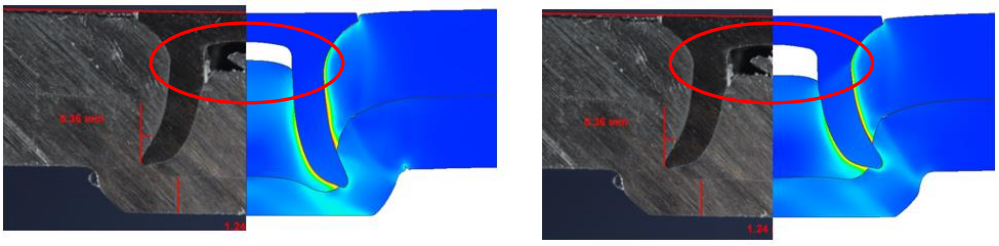

Figure 142, Example of same simulation using softer (left) and harder (right) material in the same joint.

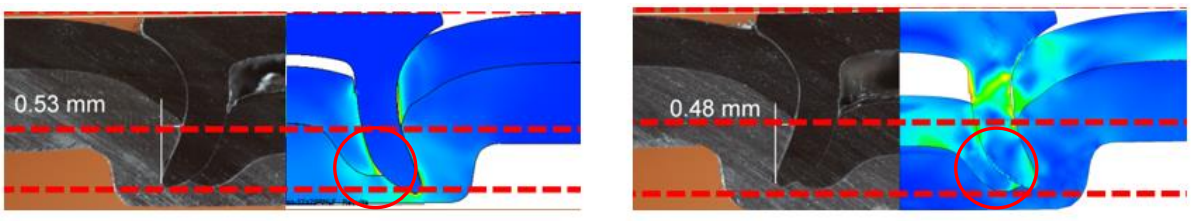

Figure 143, Example of same simulation using different friction settings, low (left) and high (right) in the same joint.

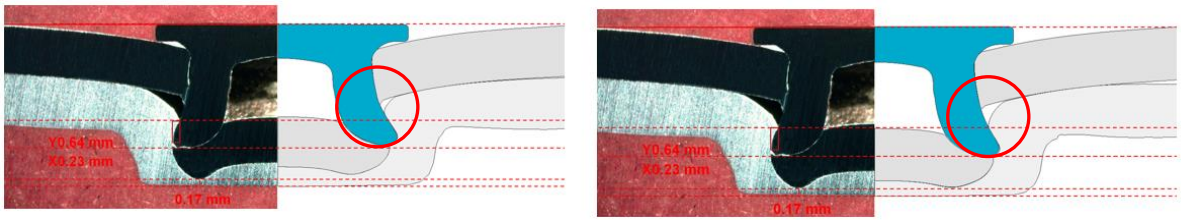

Figure 144, Example of same joint using different clamping methods, preclamp (left) and mid-clamp (right) in causing internal gaps in the same joint.

Further example of this include aspects such as buckling of the rivet legs (Figure 145a), internal gaps Figure 145b), flow pattern deformation feature under the rivet leg Figure 145c), excessive flaring (Figure 145d) or flow pattern deformation feature in the corner of the sheet (Figure 145e).

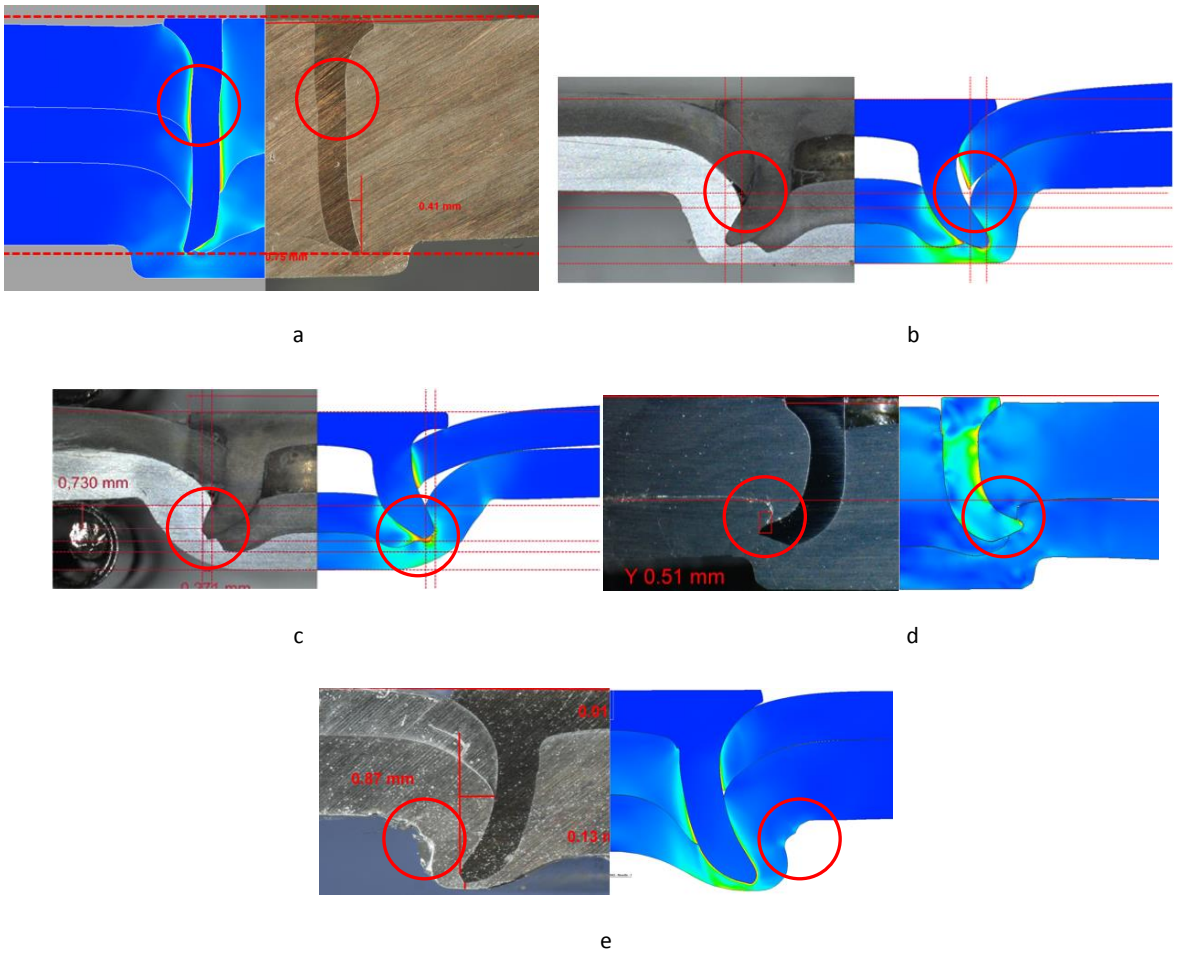

a b c d e

Figure 145, Individual examples of typical rivet and sheet behaviour.
Various examples of typical rivet and materials behaviour e.g. buckling (a), internal gaps (b), flow pattern deformation feature under the rivet leg (c), excessive flaring (d) and flow pattern deformation feature in the corner of the sheet and button (e).

6.1.3 Simulation assessment – Agreeability scorecard

To be able to determine whether a simulation is accurate and providing a realistic result, usually it is compared against a validation physical test on the basis of the two aspects discussed above in sections 6.1.1 and 6.1.2. This usually consists of:

1. Noting measurements and comparing them with physical result, if available, as shown in the Figure 146.

Joint:	1.5mm AC600T4 + 1.5mm AC600T4	
Rivet:	C50G41A	
Die:	DG09-160 (flat-bottomed, Width=9.0mm, Height=164mm)	
	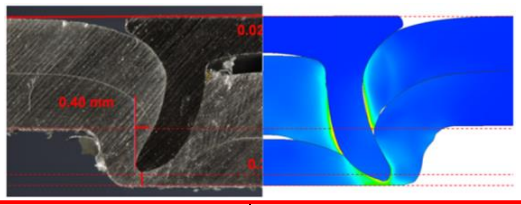	
Parameter	Physical test result [mm]	Simulation [mm]
Interlock:	0.40 (Avg)	0.32
Tmin:	0.35 (Avg)	0.10
HH:	0.02 (Avg)	0.09

Figure 146, Comparison of measurements of simulation and physical test results.

2. Overlaying simulation result over an image of a physical cross section (if available) and, often with the help of gridlines (as shown in Figure 147), looking out for resemblance of specific flow pattern deformation features between the two. In case of the below image for example, a very specific feature is the incomplete bore fill as this indicates that the material property used for simulation is of correct hardness and does not flow up the bore too easily, similarly to the physical joint.

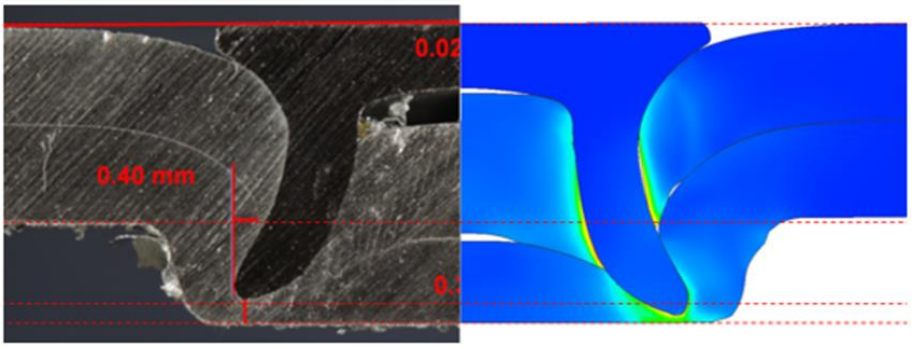

Figure 147, Example of comparison of simulation and physical results.

In order to ensure that all different features of the inserted level are assessed and nothing is omitted, a checklist has been created which has later evolved into a sorecard in order to quantify the results. This scorecard breaks down the two main areas of comparison – measurements (HH, interlock and Tmin) and visual attributes (such as shape of sheets and rivet). It then marks each aspect out of a total of 100%, with 20% weight of the marks allocated to each of the measurements and the remaining 40% split between the flow pattern deformation features. An example of the scorecard is shown below in figure Figure 148.

SCORECARD physical test & simulation agreement		Value	Input	Total Agreement
Measurements	Interlock	20%		
	Tmin	20%		
	HH	20%		
Visual attributes	Rivet leg compression	8%		0%
	Top / Mid sheet shape	8%		
	Bottom sheet shape	8%		
	Bore fill	8%		
	Under leg material drag-down	8%		

Figure 148, Example of a scorecard

Example of a completed scorecard can be seen in Figure 149, where a bad (a) and good (b) example of simulation can be seen compared to the same physical cross section subsequently receiving a different score in each instance.

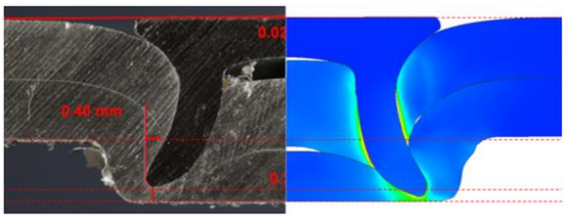

SCORECARD physical test & simulation agreement		Value	Input	Total Agreement
Measurements	Interlock	20%	20%	
	Tmin	20%	10%	
	HH	20%	20%	
Visual attributes	Rivet leg compression	8%	4%	66%
	Top / Mid sheet shape	8%	8%	
	Bottom sheet shape	8%	0%	
	Bore fill	8%	4%	
	Under leg material drag-down	8%	0%	

a

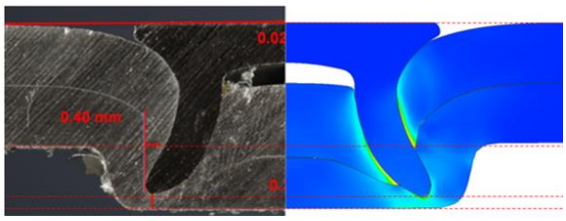

SCORECARD physical test & simulation agreement		Value	Input	Total Agreement
Measurements	Interlock	20%	20%	
	Tmin	20%	15%	
	HH	20%	20%	
Visual attributes	Rivet leg compression	8%	8%	93%
	Top / Mid sheet shape	8%	8%	
	Bottom sheet shape	8%	6%	
	Bore fill	8%	8%	
	Under leg material drag-down	8%	8%	

b

Figure 149, Completed agreeability scorecard example – Same physical joint replicated with two different materials showing two different levels of agreement.

In terms of measurements, if the measurement is within the +/- 0.15mm tolerance, it is given the full 20%. If for example, as shown in the Figure 149a, the interlock, albeit visually lower, is still within the +/- 0.15mm tolerance, which means it is given the full 20% mark. However, Tmin is outside the tolerance with measurement of 0.10mm as shown in Figure 146, and after taking subtracting the maximum tolerance it is about half that of the physical test and therefore it is given mark of 10% out if 20%.

In terms of some the flow pattern deformation features, if some of the features are missing completely then 0% mark is given. This can be demonstrated in Figure 150 where the bottom sheet is not showing the same downwards dishing as the bottom sheet in the physical test and it is, in-fact, dishing upwards which is the complete opposite of what should be seen.

It should be highlighted that these marks are usually only approximate as in most of the cases even the physical joints are not completely identical and small differences between measurements within a 5off physical sample are a certainty. Therefore, these measurements are not always an absolute number but rather an estimate only designed to roughly quantify the visual similarities of a a joint.

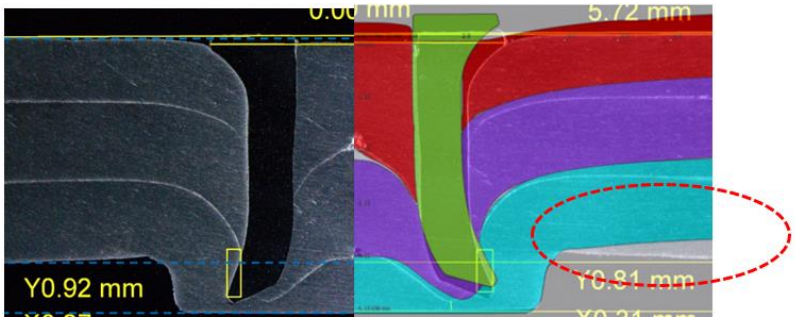

Figure 150, Example of a specific feature missing completely in a simulation

However, if the feature is there but not to the same extent, it can be marked up to its allocated weighting of 8% such as the bore fill in Figure 151, where the signs of partially filled bored are there, just not to the same extent.

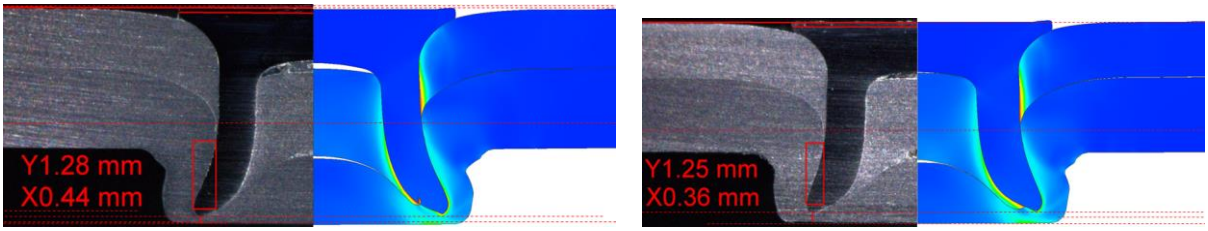

Figure 151, Examples of bore filled in less in a simulation then in the physical test.

Due to novelty of assessing of joints this way (as opposed to only using the measurements) the importance of some of the features need to be discussed with development engineers. An example of this can be seen in Figure 150, where the downwards dishing of the bottom sheet is crucial as this is a specific characteristic of a narrow flange joint where the die is also narrow and hence cannot support the sheets which in turn start dishing down – which is referred to as 'stiletto' effect amongst the development engineers (TechSpec, 2019). If this feature is not present, then this might be indicative of an incorrect clamping method used in simulation, for example one that might be making the joint stiffer than in reality.

This assessment will be used to compare all simulations against physical results. Based on the experience with this method throughout the work, generally, judgement has been made that a 75%

agreement and below (which included the +/-0.15mm tolerance on the measurements) has been established to point to an inaccurate simulation.

The distribution of the weighting of marks is currently measurement-centred with measurements having the highest allocations of the overall score. This is due to the fact that the measurements are the main indicator of quality of a joint in physical testing. However, throughout the progress of this thesis, it is becoming apparent that if the specific features of changed geometries are present and accurate then it is clear that the software is capturing the behaviour of materials correctly and the measurements may become on par with these in terms of the weightings allocation in future. Improvement of this method is something that will be further addressed in the future work.

6.2 Software selection

Based on the literature review research there are several FE software types on the market with various degrees of capability in SPR. As shown in section 4.2.1, according to the literature search, the main names in the field for material forming include Deform, Abaqus, LS-Dyna, Ansys, Forge, Simufact and MSC and a recent newcomer to the market , Sorpas by an established Welding FE software company, Swantec.

Of the above software packages, there are three that have specifically expanded into the field of SPR. These are Deform, Simufact and Sorpas, and all managed this expansion with various levels of success. Out of these three, the software that has been consistently coming to the forefront in recent years in form of recommendations was Simufact.

To author's knowledge, this software has been used by a number of companies including material suppliers (Magna, Arcilor Mittal), automotive companies (Renault, Audi, JLR and Nissan) as well as automotive suppliers (Gestamp) and research institutes such as Fraunhofer IWU (Germany) and IRT (France) with good recommendations (TechSpec, 2019). This is particularly useful as the ability to try a range of different software packages is limited by their extensive license costs.

To that end, the author attended a user presentation by Deform and requested a free trial version of Sorpas whilst the sponsoring company has purchased an academic license of Simufact. This enabled an insight into all three software packages in order to compare and select without this being prohibitively expensive.

Simufact offers a number of advantages such as allowing non-linear analysis (Carandente, 2016), using a combined friction model (beneficial when large strain deformations are modelled) and implementing segment-to-segment contact option (particularly useful in cases where complex contact

amongst different parts needs to be modelled). Simufact also uses a MSC.Marc solver which is a particularly well established and powerful FE software package and it has a very user friendly graphic user interface specifically for SPR which means it does not require a large amount of coding prior to being able to use it. All these aspects combine into a great potential for the software.

The fact that this software is also used by a number of automotive companies also played an important role as this ensures research compatibility without any further need for additional software in case of any potential collaborations are set up (such as a currently ongoing research project with Renault, French research institute IRT and Arcilor Mittal).

Based on this, the Simufact software has been selected as the most suitable choice for this work and the default 'out of the box' version will be assessed next.

6.2.1 Evaluation of the software

The initial software evaluation consists of two parts:

- Evaluation of accuracy of the 'out of the box' version of software's Simulation template
- Identification of influencing parameters in 'the out of the box' version of software's Simulation template

Evaluation of accuracy of the 'out of the box' version of software's Simulation template

METHOD

An initial assessment has been conducted by simply running simulations with an out of the box version of the software without any changes to any of the settings and comparing the results with physical tests to establish how reliable and accurate the software is in its current version.

TESTING PROCEDURE

AC procedure for sample preparation, rivet insertion and joint examination, as outlined in sections 5.1 and 5.2 has been followed.

RESULTS AND DISCUSSION

Whilst there were instances where the software has given some relatively accurate results, such as Figure 152, there were also quite a few examples where the results were a lot less accurate such as those in Figure 153.

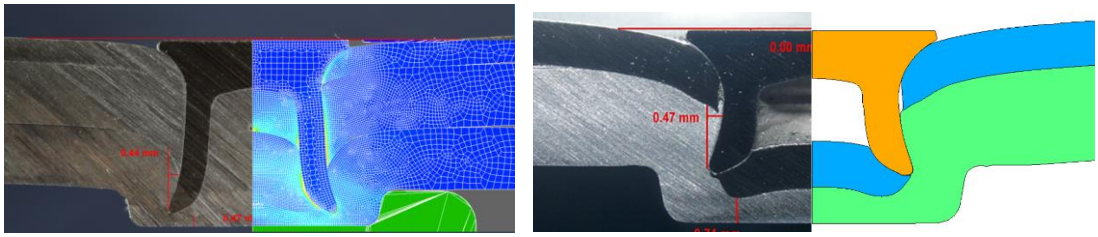

Figure 152, Examples of a simulation with out of the box software model with good agreement

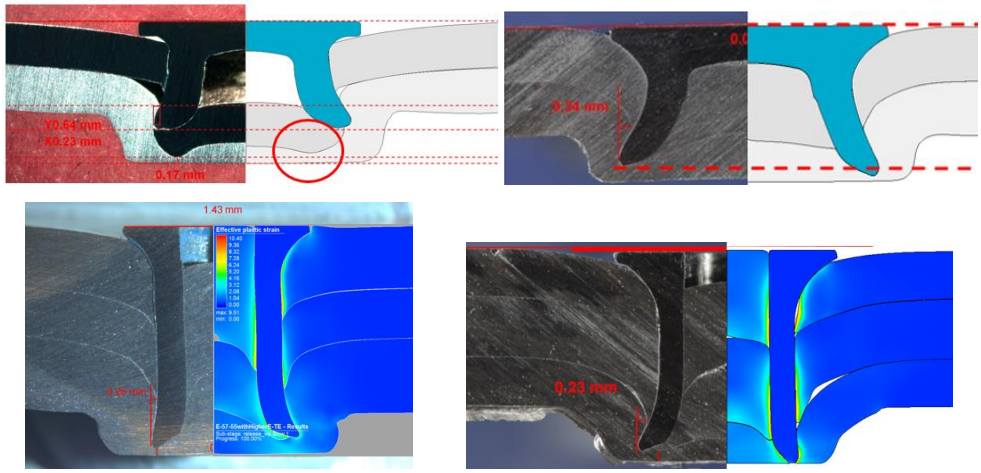

Figure 153, Example of a simulation with 'out of the box' software model showing poor agreement

Whilst some of the results are accurate, the software is not producing these consistently enough for the software to be considered reliable yet. Therefore, more research and more work is required. The initial step in this direction will involve conducting sensitivity studies with highest and lowest values to determine which parameters have a pronounced influence on the SPR insertion and its result.

Identification of influencing parameters in 'the out of the box' version of software's Simulation template

METHOD

A demo version of SPR insertion provided in the software has been selected for preliminary sensitivity study as a reference study. All models and materials are supplied by Simufact and no adjustment has been made to any of the demo version settings. The aim of this exercise is to solely assess impact of changes made to the reference simulation rather than an agreement with any physical results. Testing has been conducted on the following internal settings within the software

- Material properties – thermal and mechanical settings but excluding flow curves)
- Friction – testing the range
- Clamping – pre clamp and no clamp
- Press type – hydraulic, screw press, hammer press

RESULTS AND DISCUSSION

Testing revealed that of all tested parameters, the most significant effect on the results have clamping and friction.

Clamping

Clamp seems to affect the shape of the rivet on how the joint is formed during the insertion as shown in Figure 154where the same joint has been inserted with and without clamp. The sheets of the joint with clamp is held firmly together by the nose Figure 154 (left) whilst in the joint Figure 154 (right) the clamp is missing and the sheets display a much larger gap and the sheet are flowing out of the die. The is also a differnet in the level of Tmin, the joint with a clamp seems to have a visibly higher interlock than the same joint without the clamp. The effect on Tmin has been observed in a joint with a deeper die

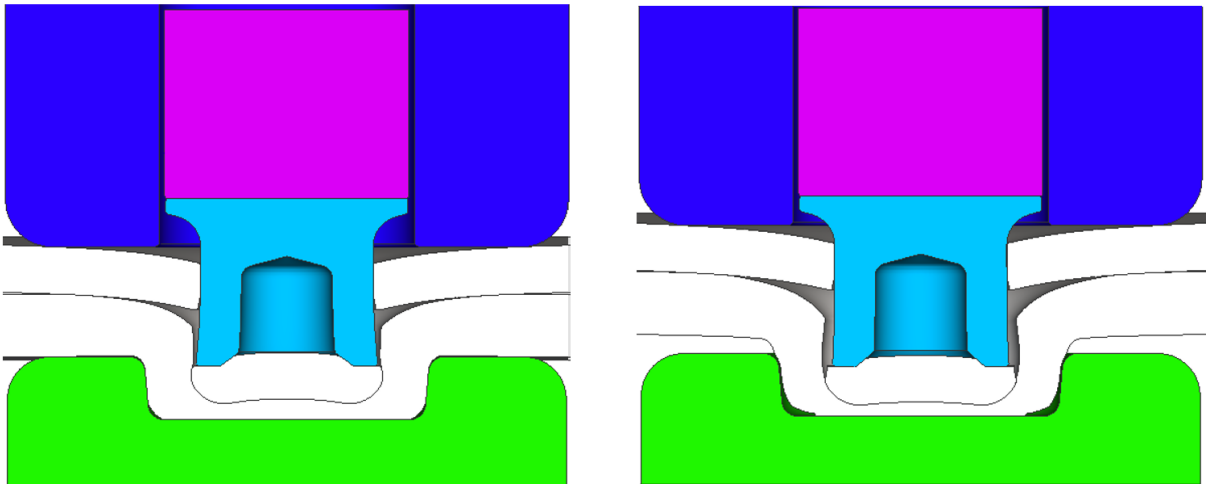

Figure 154, Joints using default clamp method (left) and no clamp (right)

Friction

The demo joint was tested with three various settings of friction with the same setting applied to all friction pairings of the joint.

a) $\mu = 0.01$
b) $\mu = 0.2$
c) $\mu = 1.0$

Differences are visible in compression of the rivet which is minimal with friction $\mu = 0.01$ but more obvious with $\mu = 1.0$. The most striking difference can be seen in the interlock of the joint with the

highest friction Figure 155c, where a wraparound interlock can be seen. The additional sign of the high friction is also a bore filled only partially when compared with the first two joints. This is not unexpected as the frictional opposing force is increasing with the increasing friction so this is a logical result.

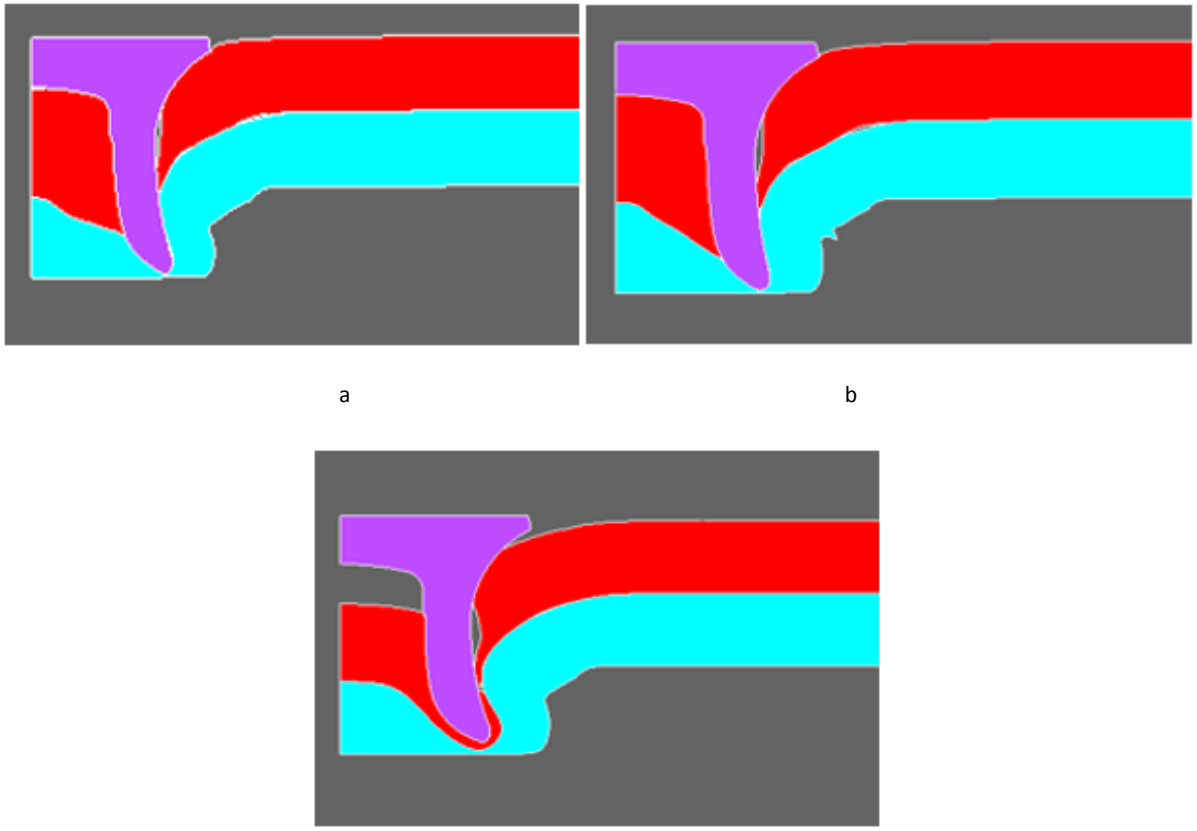

a b

c

Figure 155, Preliminary tests of friction $\mu = 0.01$ (a), $\mu = 0.2$ (b) and $\mu = 0.8$ (c)

Friction	Head height [mm]	Interlock [mm]	Tmin [mm]
$\mu = 0.01$	-0.005	0.294	0.067
$\mu = 0.2$	0.001	0.213	0.056
$\mu = 0.8$	0.119	0.18	0.083

Table 8, Test results – Three different levels of friction

A further simplified test was conducted to isolate the effects of friction from other complexities of SPR by inserting a rivet into a simple block of aluminium as opposed to multiple sheets using the same speed and energy. The two levels of friction were two extreme ends of the scale:

$\mu = 0.01$

$\mu = 1.0$

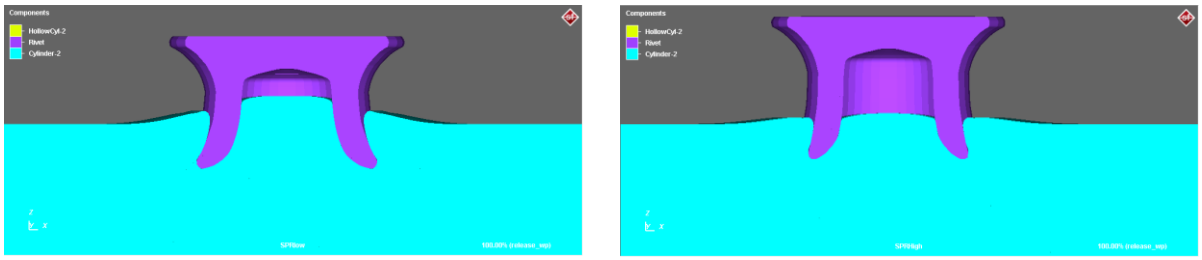

Figure 156, Simplified friction test – rivet inserted into a block of aluminium with friction $\mu = 0.01$ (left) and $\mu = 1.0$ (right)

From the result shown in Figure 156, it is obvious that friction has a very significant effect on forming process occurring in SPR and therefore more work will be done to investigate this effect.

error, whilst selection of Simufact has been a step in the right direction due to its advantages over the competitors, the software is currently not calibrated to be used for AC riveting process and more research work needs to be done to ensure accuracy and reliability of the simulations at all times before it can start being used in an effective manner. The two parameters with most influence on the outcome are friction and clamping and as such will be explored in more detail in this work in order to establish an effective set of values.

6.3 Simulation process description

These are parameters that need to be fed into the software based on the physical process that the simulation is trying to replicate. In order to attain a simulation model as close to a model of the physical process as possible, some tests are first needed to establish parameters, or to select the correct type of mechanism within the simulation software.

6.3.1 Friction

Owing to a number of complexities of variables detailed in literature review involved in friction in context of SPR, simulation of this concept is a rather challenging task. It is deemed that reverse engineering to match a physical sample might be a suitable approach to this. However, before embarking on a complex task of simulating friction in SPR, it is imperative that the software's capability

of friction simulation is verified on a simple indentation test. Once a simple test shows that the software can model friction correctly, a general study on trends and behaviour caused by friction in SPR and a larger study on identifying the precise friction values for SPR will follow.

6.3.1.1 Hardness tests

INTRODUCTION

As explained before, the hardness tests are a very simple process and the presumption is it can be shown that the FE software can replicate a basic process with very few variables correctly, it is probable that the same principles leading to a correct result are applied in a more complex process where verification is not as easy due to a large increase in variables influencing the result.

METHOD

The experimental testing has been carried out using Vickers hardness machine (Figure 157) using three different loads 5, 10 and 20 kgf in combination with three different materials most commonly used in automotive manufacturing (RC5754, AC600T4 and AC600T6). These were then simulated using FE software. The demonstration set-up of both is as per below.

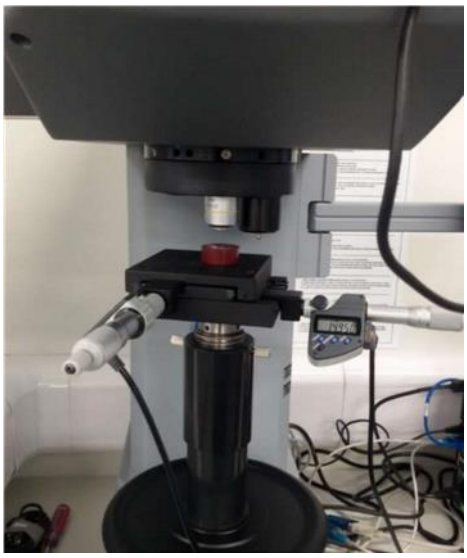

Figure 157, Test machine set up

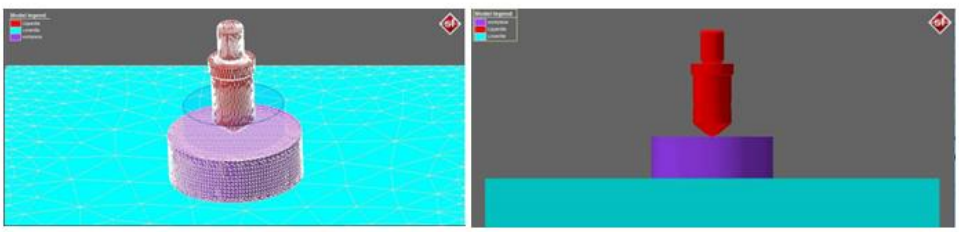

Figure 158, Simulation model set up

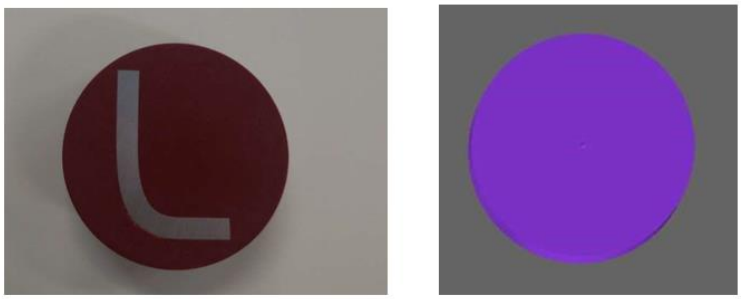

Figure 159, Experimental test sample and simulation sample

The testing matrix has been drawn up to follow on in two phases. The first phase looks at simple hardness test and its replication using numerical modelling for purposes of verification. This is then followed by application of different coatings onto the samples.

Sample material	Indenter material (tip)	Load [kgf]	Sample no.
RC5754	Diamond	5	Test 1
RC5754	Diamond	10	Test 2
RC5754	Diamond	20	Test 3
AC600T4	Diamond	5	Test 4
AC600T4	Diamond	10	Test 5
AC600T4	Diamond	20	Test 6
AC300T61	Diamond	5	Test 7
AC300T61	Diamond	10	Test 8
AC300T61	Diamond	20	Test 9

Table 9, Testing matrix – Hardness tests

TESTING PROCEDURE

Due to the planar shape and small thickness of coupons available for this testing and subsequent inability to polish these in order to test them, the 40mmx40mm coupons have been cut in a Struers cutter, de-burred, bent into a shape to fit the cylindrical sample holder, cut further if needed, polished, mounted and polished again. (as shown in Figure 159). Care has been taken to not to test in the part of the material as this would give incorrect reading of hardness due to work hardening occurring in this part of the sample. A mesh sensitivity study has been carried out for this test (detailed in chapter meshing, 6.2.1) to determine the correct size of elements.

Details of the tests along with the resulting measurements are shown in the following section.

RESULTS AND DISCUSSION

On comparison of the sample measurements taken from experimental and simulation results (tables 1-5), a good agreement was seen between the simulation and physical tests with all three materials.

Material	Load [kgf]	Force [KN]	Velocity [mms]	μ	Experimental results		Simulation results
					D1 [mm]	D2 [mm]	D1 [mm]
RC5754	5	0.049	20	0.1	0.363	0.335	0.349
RC5754	10	0.098	20	0.1	0.51	0.508	0.51
RC5754	20	0.196	20	0.1	0.736	0.734	0.721

Table 10, Comparison of experimental and simulation results for RC575

Material	Load [kgf]	Force [KN]	Velocity [mms]	μ	Experimental results		Simulation results
					D1 [mm]	D2 [mm]	D1 [mm]
AC600T4	5	0.049	20	0.1	0.329	0.327	0.329
AC600T4	10	0.098	20	0.1	0.461	0.471	0.473
AC600T4	20	0.196	20	0.1	0.655	0.64	0.656

Table 11, Comparison of experimental and simulation results for AC600T4

Material	Load [kgf]	Force [KN]	Velocity [mms]	μ	Experimental results		Simulation results
					D1 [mm]	D2 [mm]	D1 [mm]
AC300T61	5	0.049	20	0.1	0.337	0.34	0.33
AC300T61	10	0.098	20	0.1	0.471	0.486	0.478
AC300T61	20	0.196	20	0.1	0.666	0.661	0.66

Table 12, Comparison of experimental and simulation results for AC300T61

RC5754	RC5754	AC600T4	AC600T4	AC300T61	RC5754
Experimental	Experimental	Simulation tests	Simulation tests	Experimental	Experimental tests
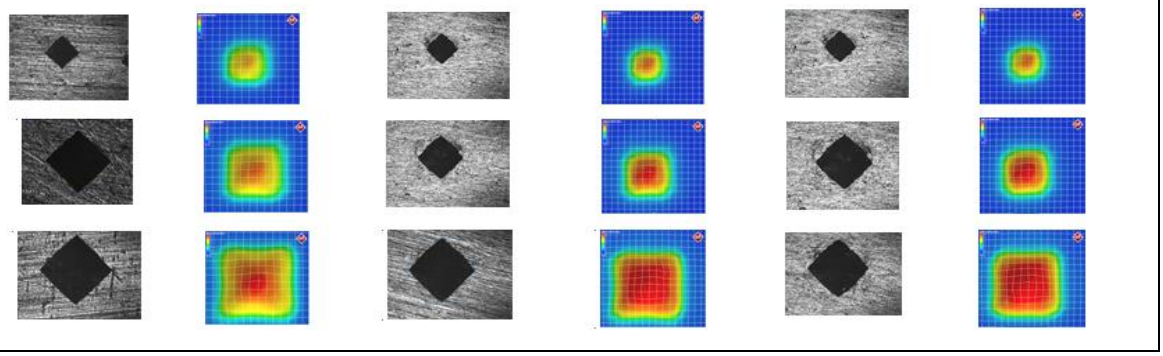					

Table 13, Visual demonstration of the experimental vs. simulation results.

Friction sensitivity study

As indicated above, the comparison study was extended to test friction, one of the main influencing factors in SPR, and the results are as per below. As with the first set of hardness tests, the comparison shows good agreement in measurements of all samples.

Material	Load [kgf]	Force [KN]	Velocity [mms]	μ	Experimental results		Simulation results
					D1 [mm]	D2 [mm]	D1 [mm]
RC5754	5	0.049	20	0.08	0.366	0.367	0.367
RC5754	5	0.049	20	0.1	0.368	0.365	0.367
RC5754	5	0.049	20	0.2	0.361	0.366	0.362

Table 14, Comparison of experimental and simulation results for RC5754 at load 5kgf

Material	Load [kgf]	Force [KN]	Velocity [mms]	μ	Experimental results		Simulation results
					D1 [mm]	D2 [mm]	D1 [mm]
RC5754	10	0.098	20	0.08	0.509	0.512	0.513
RC5754	10	0.098	20	0.1	0.514	0.517	0.508
RC5754	10	0.098	20	0.2	0.514	0.51	0.505

Table 15, Comparison of experimental and simulation results for RC5754 at load 10kgf

Material	Load [kgf]	Force [KN]	Velocity [mms]	μ	Experimental results		Simulation results
					D1 [mm]	D2 [mm]	D1 [mm]
RC5754	20	0.196	20	0.08	0.722	0.725	0.727
RC5754	20	0.196	20	0.1	0.725	0.73	0.726
RC5754	20	0.196	20	0.2	0.726	0.721	0.722

Table 16, Comparison of experimental and simulation results for RC5754 at load 20kgf

The results of both, hardness tests and friction sensitivity study suggest that the software is providing accurate results as a good agreement was seen between the experimental and simulation test results in both studies. The results of the simple hardness test suggest that the software arrived at the same solution as the experimental test provided and hence can be considered to provide reliable results for material flow in response to a hard indenter. Secondly, the effect of using differing levels of friction for the substrate surface by top coating the substrate seems to be negligible for the case of making a shallow indentation into a single sheet of material.

There were some limitations to this study as all the tests were carried out at a low velocity of 20mm/s and the SPR process uses velocity in the range of 40-360mm/s which means the results are not directly comparable to SPR. Therefore, whilst this study indicates the software is robust at low speeds, further testing is required to examine the reactions of the software at higher velocities to establish its capability for simulating the SPR process. Furthermore, the favourable conclusion in regards to friction might also be related to the use of a low velocity and a shallow indentation depth. This is not

comparable to the real SPR process which is a fast velocity and a deep insertion of what is essentially a partly ductile indenter. Friction effects in SPR are known to change with rivet insertion speed. This initial study was an exercise in learning to use the software and in probing its capabilities on a simple test.

6.3.1.2 Selecting friction model for SPR

Although different researchers have conducted tests on friction as far back as 2000s, as the literature review shows, the friction model used was always Coulomb model. In recent times, the research has advanced and FE codes have started to offer an option of a combined friction model however, to date, only two pieces of research have selected the combined model and both as recently as 2018.

As explained in the literature review, Coulomb model is essentially suitable for applying friction during the elastic phase of deformation – when the contact stresses are low and do not exceed the yield stress (Kraus, 2018), however, as soon as the yield stress is exceeded, the material starts deforming and shears off the asperities that have been previously causing the resistance. This is when the shear friction model starts applying friction in the software calculations. This model combines the static elastic deformation from the Coulomb model and the dynamic friction plastic deformation from the Shear friction model.

Based on this understanding, a combined model, which employs both of the above has been selected which is also in concurrence with the software supplier's advice (TechSpec1, 2019).

6.3.1.3 Selecting friction values

6.3.1.3.1 Verification joints

INTRODUCTION

To be able to understand the effect of the friction, a physical test is required as means of comparison. The two joints used for the previous trend observation studies have now been completed as a physical sample using servo setter.

Joint:	1.5mm 6016 + 1.5mm 6016
Rivet:	C50541A (5mm long, level hardness 1)
Die:	DG09-120 (flat-bottomed, Width=9mm, Height=1.2mm)

Joint:	3.0mm RC5754 + 3.0mm RC5754 + 3.0mm RC5754
Rivet:	T51144A (11mm long, level hardness 4)
Die:	DG11-180 (flat-bottomed, Width=11mm, Height=1.8mm)

TESTING PROCEDURE

AC procedure for sample preparation, rivet insertion and joint examination, as outlined in sections 5.1 and 5.2 has been followed.

RESULTS AND DISCUSSION

Both joints are deemed very stable with further 5 off samples all showing have fairly similar measurements. Due to this reason only one cross section representative of both joint combinations is compared against all simulations in future tests.

Joint:	1.5mm 6016 + 1.5mm 6016
Rivet:	C50541A (5mm long, level hardness 1)
Die:	DG09-120 (flat-bottomed, Width=9mm, Height=1.2mm)
Image:	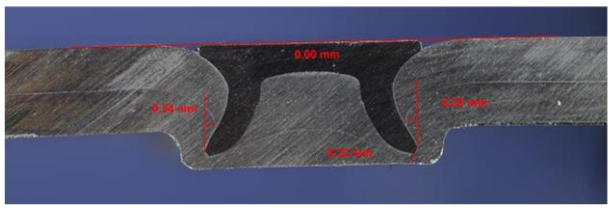
Parameter	Physical test result [mm]
Interlock:	0.37
Tmin:	0.32
HH:	0.01

Figure 160, Verification joint 1

Joint:	3.0mm RC5754 + 3.0mm RC5754 + 3.0mm RC5754
Rivet:	T51144A (11mm long, level hardness 4)
Die:	DG11-180 (flat-bottomed, Width=11mm, Height=1.8mm)
Image:	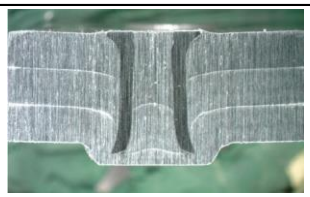
Parameter	Physical test result [mm]
Interlock:	0.21
Tmin:	0.67
HH:	0.04

Figure 161, Verification joint 2

6.3.1.3.2 Stage 1 – Application of previous research

INTRODUCTION

Although the hardness tests have given some insight into friction and confirmed that when using simple processes with low force the software replicates the reality very accurately, the friction involved in the indenter model is far off the complexities of SPR insertion. Therefore, at this stage it is beneficial to have tests completed directly on the SPR process to observe and understand how the friction affects the insertion of a self-pierce rivet.

Due to the fact that a number of researchers have researched friction as far back as 2000 and established friction levels for simulating SPR as part of their research, a short validation study has been completed to establish suitable values when applied to a different joint. This is to determine whether the correct set of values for simulating friction in SPR is already available as the joints completed in previously published papers have been presented as having a very good agreement.

METHOD

A joint used for this study is the standard rivet used for the study in chapter 6.2.3. Five different friction levels and models as found literature were applied to the simulation model. The joints will be compared to the verification joint.

Joint:	1.5mm 6016 + 1.5mm 6016
Rivet:	C50541A (5mm long, level hardness 1)
Die:	DG09-120 (flat-bottomed, Width=9mm, Height=1.2mm)

Friction between rivet and sheets	Coefficient of friction	Interface friction factor
Research paper by Mucha (2011)	0.05	-
Research paper by Carandente (2016)	0.09	-
Suggested by Simufact	0.1	0.2
Research paper by Kato (2007)	0.2	-
Research paper by Honsch (2018)	0.1-0.3	0.3-0.5

Table 17, Testing matrix – Previous friction research

Joint:	1.5mm 6016 + 1.5mm 6016
Rivet:	C50541A (5mm long, level hardness 1)
Die:	DG09-120 (flat-bottomed, Width=9mm, Height=1.2mm)
Image:	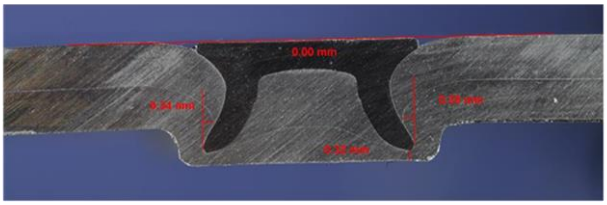
Parameter	Physical test result [mm]
Interlock:	0.37
Tmin:	0.32
HH:	0.01

Figure 162, Verification joint 1

TESTING PROCEDURE

AC procedure for sample preparation, rivet insertion and joint examination, as outlined in sections 5.1 and 5.2 has been followed.

RESULTS AND DISCUSSON

Measurements:

Friction between rivet and sheets	Coefficient of friction	Interface friction factor	Interlock [mm]	Tmin [mm]	HH [mm]
Nominal	-	-	0.364	0.352	-0.01

Friction between rivet and sheets	Coefficient of friction	Interface friction factor	Interlock [mm]	Tmin [mm]	HH [mm]
Research paper by Mucha (2011)	0.05	-	0.469	0.159	0.023
Research paper by Carandente (2016)	0.09	-	0.37	0.174	-0.021
Suggested by Simufact	0.1	0.2	0.4	0.116	0.012
Research paper by Kato (2007)	0.2	-	0.406	0.225	0.032
Research paper by Honsch (2018)	0.1-0.3	0.3-0.5	0.458	0.23	0.009

Table 18, Results – Previous friction research

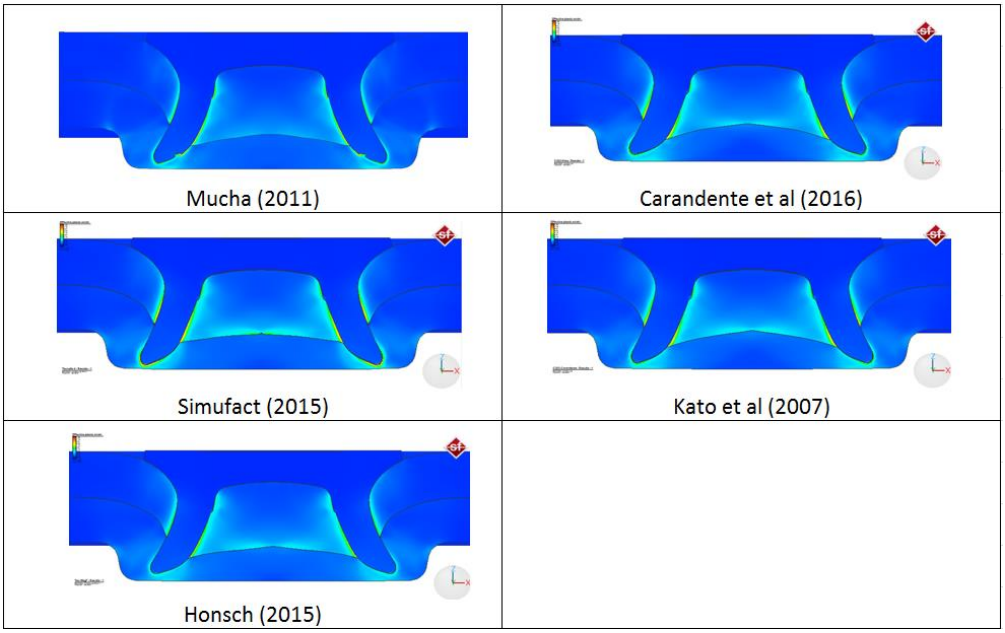

Figure 163, Visual attributes of joint – Previous friction research

Based on the results, it is possible to see that interlock achieved in all simulations is in good agreement with the representative measurement of 0.37mm on the physical section. However, Tmin is not in such a good agreement with the representative measurement of 0.32mm in instances where lower friction values were used such as those suggested by Simufact own template as well as Carandente's research (where $\mu < 0.1$ and $m < 0.2$). The agreement is better with higher friction values such as those suggested by Kato and Honsch which could be said are within the tolerances of successful simulation solution. However, in terms of the physical appearance of the joint, a physical feature that is regularly present in most of the joints in a bell like shape of the bottom sheet and a little bit of material drag down under the leg of the rivet is absent in the simulated joint which suggests that these values are not accurate enough and a better approach is needed, this is developed in the next section.

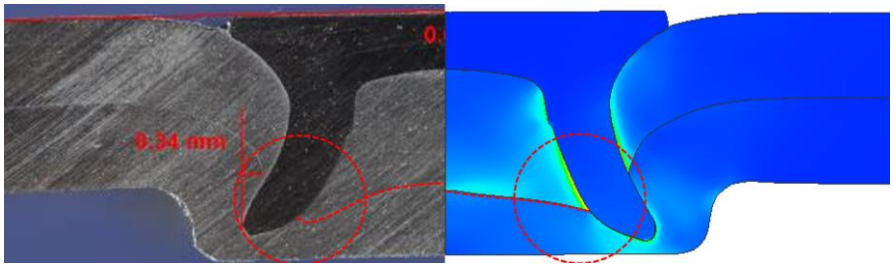

Figure 164, Comparison of cross section with simulation with low friction based in literature

6.3.1.3.3 Stage 2 – Initial observation of trends with changing friction

INTRODUCTION

As the friction values from previous research did not produce as good an agreement as expected visually, more work is required. A further study was then completed to attempt to understand joint behaviour trends at different friction levels.

METHOD

A combined friction model was applied to the verification joint 1 and 2 with seven different variations across all the friction partners

- Rivet – sheets
- Top sheet – bottom sheet
- Bottom sheet – die
- Punch – rivet
- Nose – top sheet

Joint:	1.5mm 6016 + 1.5mm 6016
Rivet:	C50541A (5mm long, level hardness 1)
Die:	DG09-120 (flat-bottomed, Width=9mm, Height=1.2mm)

Joint:	3.0mm RC5754 + 3.0mm RC5754 + 3.0mm RC5754
Rivet:	T51144A (11mm long, level hardness 4)
Die:	DG11-180 (flat-bottomed, Width=11mm, Height=1.8mm)

Joint 1 & 2

The values selected as starting point were increments of coefficient of friction ranging from 0.01 (mathematically, it is required to choose a value as opposed to zero, otherwise the software would calculate implausible results (TechSpec1, 2019)) to 0.5 which is the maximum value for μ. There is a large number of combinations of coefficient of friction μ with Interface friction factor m, but for simplicity, the calculation used in ring compression test has been used to calculate interface friction factor – 'm' (Rajesh, 2013). Further information on interface friction factor can be found in section 4.1.5.4 on Shear friction model. Each individual test used the its respective value for all friction interfaces in the model.

$$\mu = \frac{m}{\sqrt{3}} \quad \text{Eq. (49)}$$

μ - Coefficient of friction

m – Interface friction factor

The resulting values are as per below table:

Joint 1 & 2	μ	m
Friction Test 1	0.01	0.017
Friction Test 2	0.05	0.085
Friction Test 3	0.1	0.17
Friction Test 4	0.2	0.34
Friction Test 5	0.3	0.51
Friction Test 6	0.4	0.68
Friction Test 7	0.5	0.85

Table 19, Testing matrix – Assessing effect of friction levels, joint 1 and 1

At this point, it should be highlighted the idea of this exercise was not to reach a correct replication of a physical test, but rather to assess the behaviour of the metal caused by different levels of friction cause and identify any potential trends in terms of the rivet shape and the three main assessment criteria – interlock, Tmin and HH. Based on previous research and observations completed in Atlas Copco on a joint with two different coatings, the expectation is that the interlock and Tmin will increase with increased friction (TechSpec, 2019). This has been specifically noted in cases of Trivet which has a specially low friction coating applied to prevent premature flaring.

TESTING PROCEDURE

AC procedure for sample preparation, rivet insertion and joint examination, as outlined in sections 5.1 and 5.2 has been followed.

RESULTS AND DISCUSSION – JOINT 1

Joint:	1.5mm 6016 + 1.5mm 6016
Rivet:	C50541A (5mm long, level hardness 1)
Die:	DG09-120 (flat-bottomed, Width=9mm, Height=1.2mm)

Test no.	μ	m	Interlock [mm]	Tmin [mm]	HH [mm]
Friction Test 1	0.01	0.017	0.549	0.147	-0.011
Friction Test 2	0.05	0.085	0.524	0.156	-0.022
Friction Test 3	0.1	0.17	0.501	0.195	-0.011
Friction Test 4	0.2	0.34	0.44	0.27	-0.013
Friction Test 5	0.3	0.51	0.386	0.321	-0.015
Friction Test 6	0.4	0.68	0.307	0.401	-0.028
Friction Test 7	0.5	0.85	0.25	0.456	-0.045

Table 20, Test results – Assessing effect of friction levels, joint 1

Trends that are immediately visible when looking at the measurements are that the low friction decreases the interlock whilst increasing Tmin. From almost no friction with coefficient of 0.01 to maximum coefficient of 0.5, the interlock was reduced to less than half of its original value.

However, measurements are not the only factor to go by during this exercise (as also shown in the last section) and whilst measurements are very useful, it is also possible to assess the differences in the way the material is shaped throughout the simulation as well as the final appearance of the joint.

Figure 165 is capturing joints on after they have pierced the second sheet and are about to start flaring further. At this point, the bore is filled to various degrees – with increasing friction, the portion of bore filled by displaced aluminium is proportionately smaller, which was anticipated as the surfaces of the bore are resisting the substrate material sliding upwards over them. There is also an expected difference in the depth of the insertion at this point when all the simulations are the same amount of time into the insertion process as the rivets is working against various degrees of friction as it is being inserted. The rivet also appears to be a lot more compressed with increased friction which is caused by the increased heat generated by the increased friction work. This also explains the trends seen in measurements improving Tmin values are due to the fact that the rivet is shorter due to compression and so although it does flare more, the reduced length does not effectively improve the interlock.

Figure 165, Results – Assessing effect of friction levels, joint 1. Joints on after they have pierced the second sheet and are about to start flaring further

The results that were not anticipated were captured in the final stages of the rivet where the joints with high friction have created the previously noted bell-like shape in the middle of the bottom sheet as opposed to almost a straight line in the same location in joints with low friction. With higher friction levels the rivet also seems to drag some of the material with it whilst piercing through the second sheet. As mentioned before, this bell-like shape curvature and dragging of the material under the rivet leg is something that can typically be seen to a greater or lesser extent seen in almost all cross sections. The simulations with very low friction (up to and including coefficient of friction of 0.1) appear to be lacking this curvature and instead, the rivet leg stakes through the sheet without any of the material dipping around it. This could be explained by the fact that with low friction there is low resistance i.e. friction force which leads to coating not wearing off on the top of the rivet as quickly as when the friction force is high due to increased friction settings. This would mean that the rivet leg is 'gliding' through the material more easily whilst rivet leg where coating has worn off has creates a more of a rough surface, dragging the softer sheet with it.

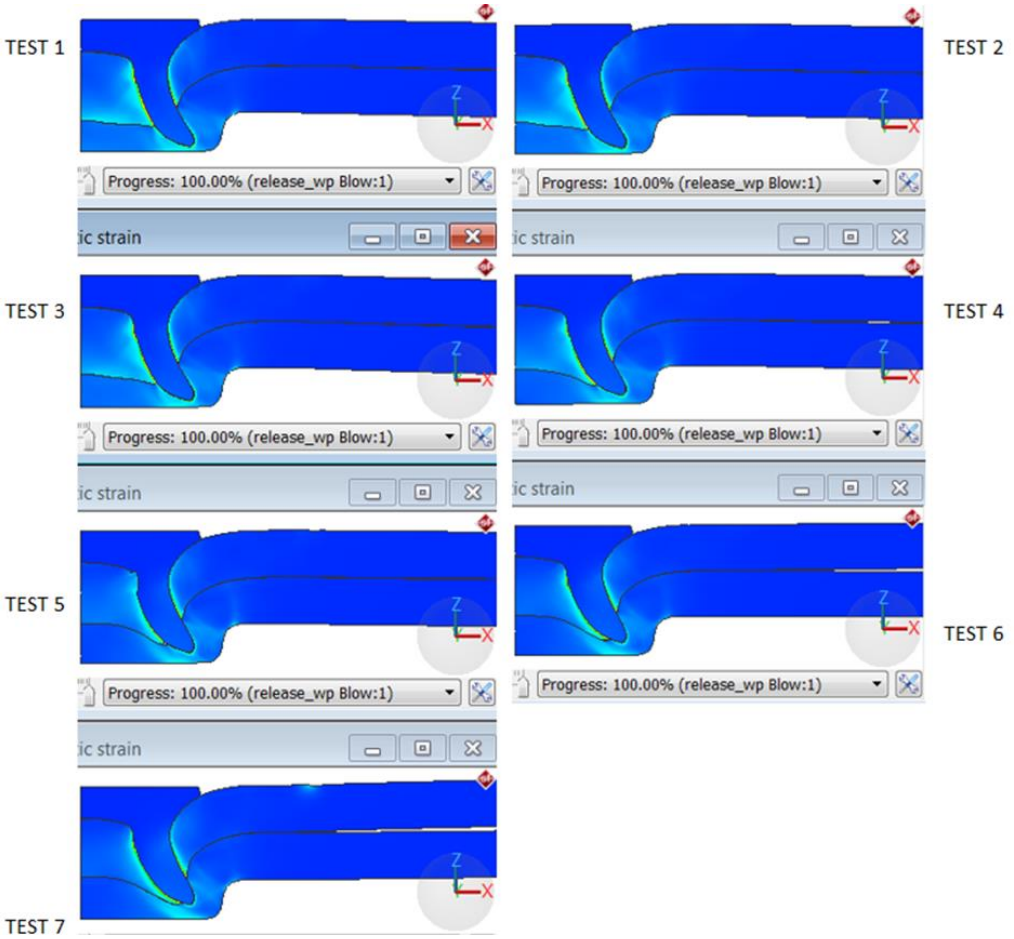

Figure 166, Assessing effect of friction levels, joint 1- Effects of applying low to high friction (left to right)

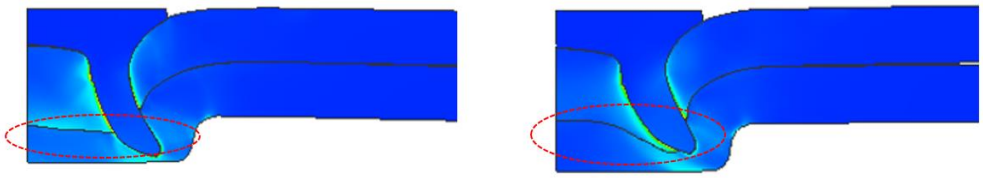

Figure 167, Friction levels comparison, joint 1. Contrasting lowest friction level (left) μ=0.01 and highest friction level (right) μ=0.5

RESULTS AND DISCUSSION – JOINT 2

Joint:	3.0mm RC5754 + 3.0mm RC5754 + 3.0mm RC5754
Rivet:	T511 (11mm long, level hardness 4)
Die:	DG11-180 (flat-bottomed, Width=11mm, Height=1.8mm)

Joint 2	μ	m	Interlock [mm]	Tmin [mm]	HH [mm]
Friction Test 1	0.01	0.017	0.36	0	-0.003
Friction Test 2	0.05	0.085	0.44	0.156	-0.004
Friction Test 3	0.1	0.17	0.439	0.231	-0.026
Friction Test 4	0.2	0.34	0.405	0.329	-0.005
Friction Test 5	0.3	0.51	0.392	0.516	-0.006
Friction Test 6	0.4	0.68	0.293	0.636	-0.007
Friction Test 7	0.5	0.85	0.172	0.786	-0.006

Table 21, Test results – Assessing effect of friction levels, joint 2

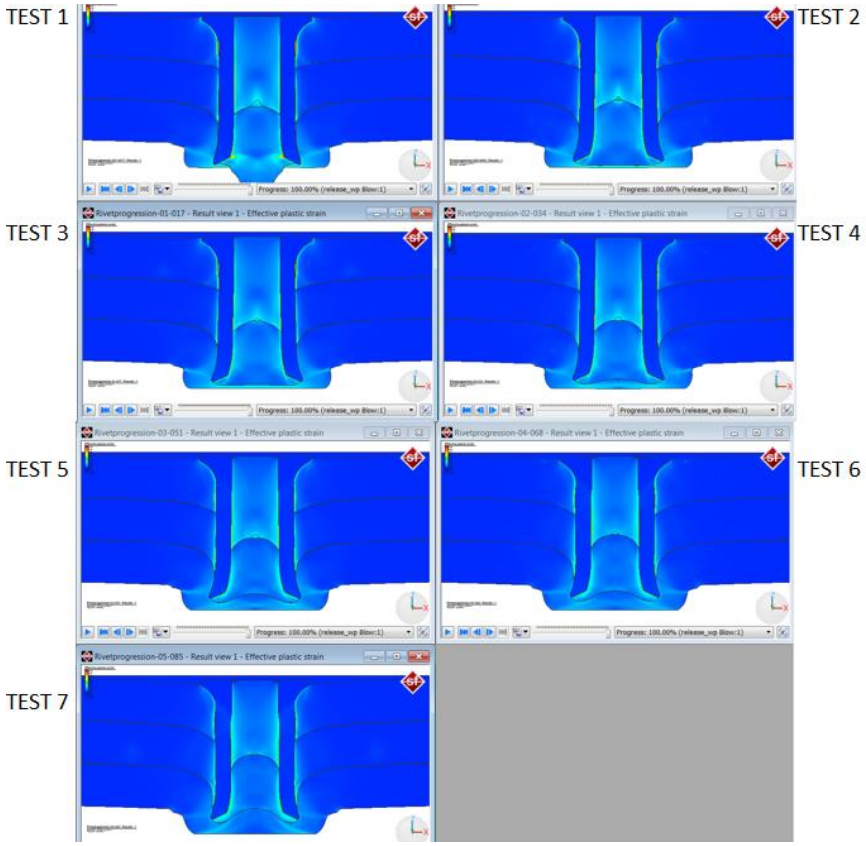

Figure 168, Assessing effect of friction levels, joint 2. Simulation of Trivet with 3 sheets of aluminium

Similar results have been confirmed with this type of rivet too. The interlock decreases with increased friction and at the same time Tmin increases. The bell-like shape of the bottom sheet with the drag-down of the material is also present in this instance. The remarkable difference between the two is that with the low friction with this joint, the Tmin is completely thinned out and it would likely break in physical test scenario. It is only because the contact has not been set up for interaction between the middle sheet and die that the material is spilling out into the die. What is also interesting is that

with this joint the interlock starts off rather low with low friction, then improves and then seems to circle back to low values.

Comparison with the physical samples of both joints has confirmed that friction values for SPR can be roughly anticipated to be in the higher range tested due to the presence of the curvature of the bottom sheet highlighted as one of the more obvious differences between high and low friction, as shown in the image below. The measurements of the physical section, when compared to the tests with various friction levels also seem to be closer to those tested with higher levels of friction in the range of coefficient of friction values of 0.2 – 0.3.

6.3.1.3.4 Additional validation of joint with very low friction

INTRODUCTION

An additional short test has been conducted to further inverstigate and confirm the presence of the curvature of the bottom sheet and drag-down of the material under the rivet leg as indicators of friction. This time on a different joint to check if this is happening in other circumstances. Two joints were made, one with standard Trivet lubricant on the rivet and another one with a largely excessive and thorough coverage of lubricant on the rivet.

Joint:	1.0mm RC5754 + 2.5mm RC5754 + 2.0mm RC5754
Rivet:	T51044A (10mm long, level hardness 1)
Die:	DG10-140 (flat-bottomed, Width=10mm, Height=1.4mm)

TESTING PROCEDURE

AC procedure for sample preparation, rivet insertion and joint examination, as outlined in sections 5.1 and 5.2 has been followed.

RESULTS AND DISCUSSION

Measurements:

Joint :	1.0mm RC57554 + 2.5mm RC5754 + 2.0mm RC5754	
Rivet:	T51044A (7.5mm long, level hardness 4)	
Die:	DG10-120 (flat bottomed, Width=10.0mm, Height=1.2mm)	
	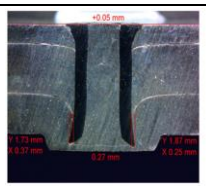 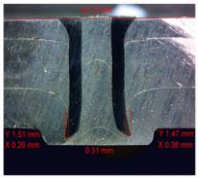	
Parameter	Excsessive coating [mm]	Standard coating [mm]
Interlock:	0.05	0.13
Tmin:	0.31	0.32 (Avg)
HH:	0.27	0.31

Visual attributes:

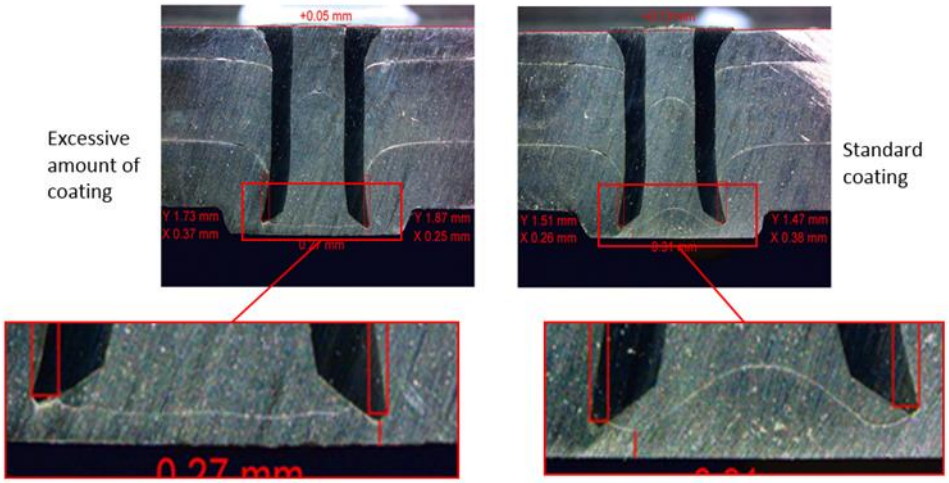

Figure 169, Same joint with excessive amount of lubricant on the left and with standard Trivet coating on the right.

The results in the joint with low friction are rather remarkably similar to what has been highlighted in the study with joint 1 where a straight line instead of the concave shape of the bottom sheet has been noted.

6.3.1.4 Design of experiment

INTRODUCTION

Equipped with the knowledge of the trends and behaviours understood from the above studies, next step is to attempt to isolate the individual friction partners' behaviour to examine their influence.

Subsequent steps are then to adjust their individual values to find a friction set-up that would be applicable across all joints.

METHOD

Individual friction partners were identified in a both joint with 2 sheets (2T) and joint with 3 sheets (3T) as shown in figure Figure 170 and number of simulations have been conducted to determine ideal friction parameters by means of reverse analysis using the physical testing on joints 1 and 2 used in the previous tests, as shown below.

Joint no.	Materials	Rivet	Die
Joint 1	1.5mm 6016 + 1.5mm 6016	C50541A	DG09-120
Joint 2	3.0mm RC5754 + 3.0mm RC5754 + 3.0mm RC5754	T51144A	DG11-180

Friction interfaces on 2T stack	
1	Punch and rivet
2	Nose and top sheet
3	Rivet and top sheet
4	Rivet and bottom sheet
5	Top sheet and bottom sheet
6	Bottom sheet and die

Friction interfaces on 2T stack	
1	Punch and rivet
2	Nose and top sheet
3	Rivet and top sheet
4	Rivet and middle sheet
5	Rivet and bottom sheet
6	Top sheet and middle sheet (set in contact table)
7	Middle sheet and bottom sheet (set in contact table)
8	Bottom sheet and die

Figure 170, Friction partners in 2T and 3T stacks

These tests were subject to 15 various combinations of all friction settings each combining the above friction partners in a testing matrix.

In addition to joint 1 and 2 as verification, the resulting parameters were then tested on a set of selected joints shown in the table below in order to validate this on range of different joints.

This included joints shown in the matrix below with varied:

- Layers – two and three joining partners (sheets)
- Rivets – standard 3.0mm and 5.0mm rivets, tubular rivets and newly designed BG rivet
- Dies – flat bottomed and profiled.
- Materials – stacks using aluminium to aluminium, aluminium to HSSS and UHSS sheets.

Joint no.	Materials	Rivet	Die
Joint 3	1.2mm RC5754 + 2.0 mm RC5754	C50641A	DP09-175
Joint 4	1.2mm RC5754 + 2.0 mm RC5754	C50641A	DG09-160
Joint 5	1.2mm 5182 + 1.2mm 5182 + 1.2mm 5182	J30542A	DG07-120
Joint 6	1.1mm 5182 + 1.0mm 5182 + 1.0mm BH300	C30E44A	DP06-100
Joint 7	1.5mm 5182 + 1.5mm 5182	C50641A	DP09-175
Joint 8	2.5mm RC5754 + 2.0mm RC5754 + 3.0mm RC5754	T50C44A	DG10-160
Joint 9	1.5mm RC5754 + 2.0mm RC5754 + 2.0mm RC5754	T50M42A	DG10-120
Joint 10	1.5mm Usibor + 1.5mm 6016	BG0446A	DG09-160
Joint 11	1.0mm DP600 + 2.0mm RC5754	C50541A	DG09-140
Joint 12	1.mm 5182mm + 3.0mm RC5754 + 2.6mm 5182	T50944A	DG10-180

Table 22, Testing matrix – Friction design of experiment

Following feedback from these tests, the friction settings were further validated by being used on every joint simulation carried out for the purposes of all research tasks in both experimental and all practical applications chapter completed in this work.

TESTING PROCEDURE

AC procedure for sample preparation, rivet insertion and joint examination, as outlined in sections 5.1 and 5.2 has been followed.

RESULTS AND DISCUSSION

Adherence to all trends in friction behaviour such as decreasing interlock and compression of the rivet with increasing friction, less of drag down of material with decreasing friction which were identified in the section 6.3.1.3.3 have been also represented in this larger scale experiment with all stacks tested. Based on the results obtained as part of this test, a set of friction parameters have been established – shown in the below image that have provided close agreement across a number of joints.

Friction interfaces on 2T stack		μ	m
Punch and rivet		0.1	0.2
Nose and top sheet		0.1	0.2
Rivet and top sheet	H00	0.3	0.6
	HL0	0.1	0.2
Rivet and bottom sheet	H00	0.3	0.6
	HL0	0.1	0.2
Top sheet and bottom sheet		0.3	0.6
Bottom sheet and die		0.25	0.6

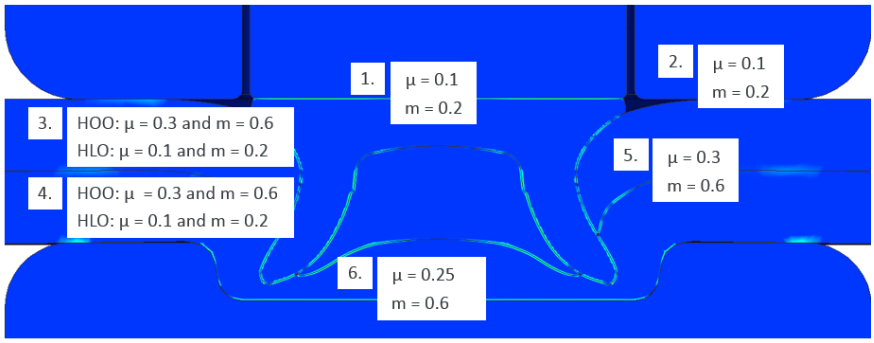

Figure 171, Results – Proposed friction settings for 2T stack

Friction interfaces on 3T stack		μ	m
Punch and rivet		0.1	0.2
Nose and top sheet		0.1	0.2
Rivet and top sheet	H00	0.3	0.6
	HL0	0.1	0.2
Rivet and middle sheet	H00	0.3	0.6
	HL0	0.1	0.2
Rivet and bottom sheet	H00	0.3	0.6
	HL0	0.1	0.2
Top sheet and middle sheet (set in contact table)		0.3	0.6
Middle sheet and bottom sheet (set in contact table)		0.3	0.6
Bottom sheet and die		0.25	0.6

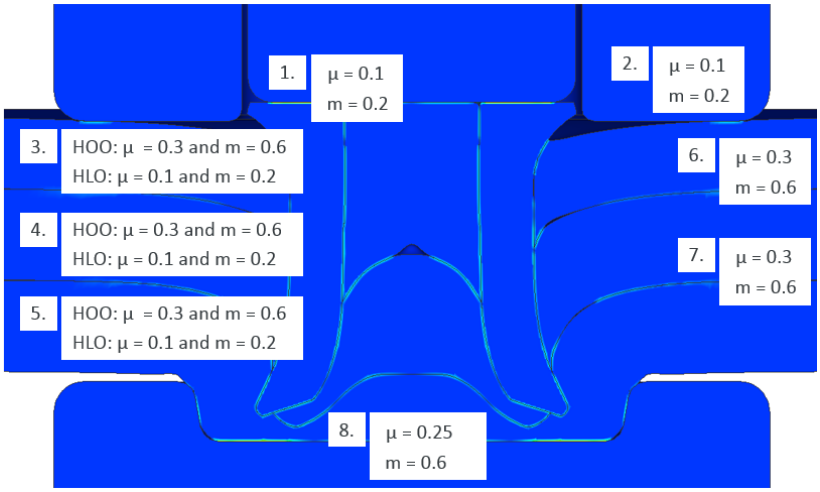

Figure 172, Results – Proposed friction settings for T stack

There are two levels of settings for friction partners 2 and 3. This is due to the fact that the rivet manufactured in Atlas Copco currently has two different types of coating, a standard one (HOO) used for C and K rivets and a low friction one (HLO) used for Trivet and BG rivet. The differences between the two coatings have been noted in the numerical analysis which confirmed the need for two different settings.

These newly established friction levels may appear to be much higher in comparison to settings used by other researchers in the past, however, the outputs of the simulations of all test joints with the proposed settings were scored using the agreeability score card, as shown in the below table, and seem to display a high level of agreement.

The setting recommended by the software supplier for SPR is using μ = 0.1 and m = 0.2 (both explained in section 4.1.5.5) for all friction interfaces and joints, this inaccuracy of this setting will be shown in the next few paragraphs to highlight difference when compared with the newly established friction settings developed in this study.

A number of patterns of material behaviour based on different friction levels were identified in this study as well as the extent of friction levels that are needed to correct these behaviours to reflect to the physical test.

The influence of the friction between the work pieces and tooling, i.e. friction between the punch and rivet and nose and top sheet, has been found very low in the simulation when tested increased in isolation. The friction partners with most influence on the agreement of simulation with physical test

were sheet to sheet, sheet to rivet and bottom sheet to die. The following section will aim to illustrate these.

One of the indicators of the correct friction level is the before mentioned bell-like shape of the bottom sheet as shown in the image below. The study pinpointed that this is mainly caused by increased friction between die and bottom sheet.

The low friction also causes the rivet to almost glide through the sheets and stake, causing very low Tmin (a). With increased friction between the top and bottom sheet and the rivet and sheets, to the levels shown above, the rivet is seen to compress considerably more and reflect the compression of the physical test more. This leads to decrease in the interlock as the rivet is shortened by compression which prevents further flaring. The compression of the rivet however also leads to improved Tmin. All four aspects are demonstrated in the image below comparing the results of a built-in SPR model with default low friction setting with the new friction model.

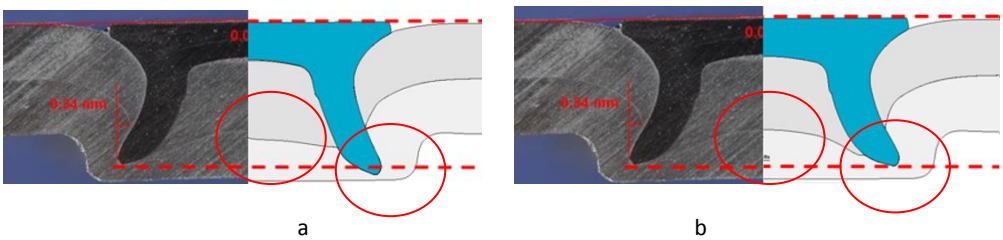

a b

Figure 173, Comparison of built-in SPR model friction and new friction settings in test joint 1.

Whilst reduction in interlock would be negative if improvement of the joint was being discussed, in this instance, the reduced interlock is more realistic as shown in figure b.

In addition to the bell like shape created by the high friction between the bottom sheet and die, the previously noted dragging of the material under the rivet leg is a very characteristic sign present in almost all of the joints. The extent of this characteristic is dependent on the geometry of the given stack, for example experience shows joints with shallow dies with thin stacks will display this characteristic less extensively as demonstrated in the image above. However, the following image of a physical cross section below is using a deeper die with a thicker sheet and is exhibiting this aspect a lot more extensively. Whilst the simulation completed with the built-in SPR model default friction, i.e. low friction (a) setting does reflect this aspect too, this is somewhat less pronounced than the simulation using the newly established, i.e. higher friction setting (b) which gives a more realistic match with the cross section. This behaviour has been found to reflect the physical cross section realistically when friction between both, rivet and sheets and sheets themselves is in correct balance.

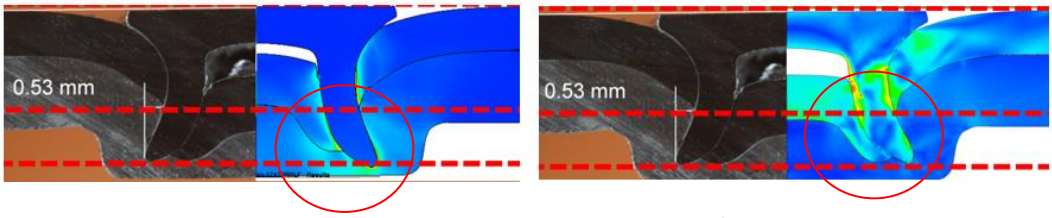

Figure 174, Comparison of built-in SPT model default friction and new friction settings in test joint 11.

Another aspect that this image is also demonstrating is bore fill. This interaction is influenced by the friction between the rivet and the sheets. As expected, there is a direct correlation between increased friction and less bore fill which is clearly shown in the image above.

Based on the results below, the trends clearly points to a higher friction as more suitable for numerical model of SPR which is specifically applicable to friction interface factor (m). This part of the combined friction model used for this study has been identified by this study as the main contributor towards this behaviour during the plastic deformation (μ is mainly employed prior to the plastic deformation stage) and is beneficial if this value is higher than μ. However, this study has also identified a limit to increasing the friction. Too high a friction causes the agreement of the numerical result with the cross section to eventually decrease. As shown in the example below, where the image on the left (a) is using the new friction setting and image on the right (b) is setting with friction too high (μ=0.4, m= 0.8). As can be seen, the drag down of the material under the rivet leg is excessive causing both Tmin and interlock to decrease unrealistically which does not match the physical cross section.

Bore fill is also indicative of an unnecessarily high friction. This will also cause lack of correlation with Tmin in physical cross section as although higher friction does improve Tmin as seen before, the excessive drag down of the material will thin out the Tmin as shown in the image (b).

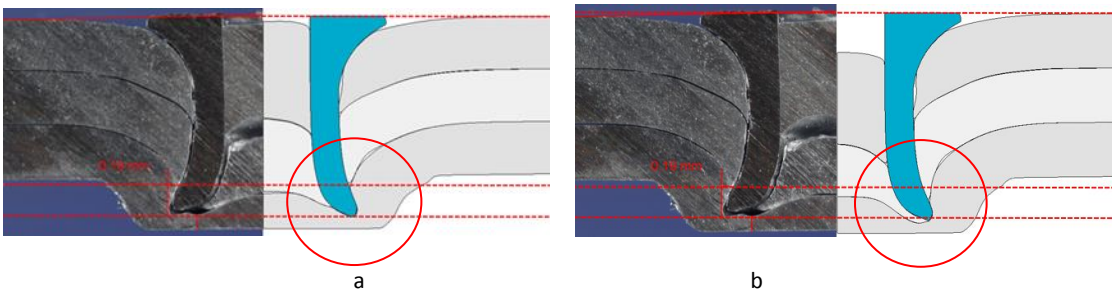

Figure 175, Comparison of new friction settings with setting with too high a friction in test joint 5.

Since a physical test successfully verifying behaviour of excessive coating to lower the friction has been completed previously (6.5.3.4), it has been decided that a test confirming behaviour of a higher than normal friction will also be completed. An additional test has been therefore completed on two joints,

one with standard coating and one without coating to purposefully increase friction. The study will be detailed in the next chapter.

As far as frictional influence of different materials is concerned, the study seems to indicate that no difference has been noted between use of aluminium and steel as the same settings provided sufficiently accurate results across joints with both aluminium to aluminium and aluminium to steel. This could be due to the speed of the process and coating acting as lubricant between the sheets and rivet and sheets during a part of the duration of insertion.

Additionally, the simulation has also independently highlighted that as well as tubular Trivet, the newly launched BG rivet for UHSS materials needs to use the friction settings for lower friction coating. The image below shows example of joint with lower ad higher friction levels compared to the physical cross section. Interestingly, the joint with lower friction created better interlock due to flaring out more despite showing more compression which, contrastingly, is usually a sign of a higher friction. This, however, has been repeated consistently across further simulations and physical tests of BG rivets which seems to suggest that this is correct.

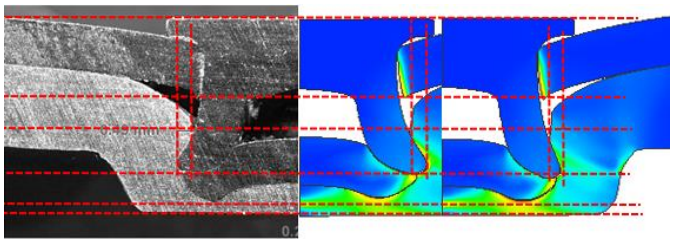

a b

Figure 176, BG rivet simulated with low (a) and high (b) friction settings in test joint 10

6.3.1.4.1 Additional validation of a joint with high friction

METHOD

The behaviour of rivet with varied friction levels was tested on the joint 9 from the above study with one joint tested with standard coating and the same joint with rivet without any coating to increase the friction.

Joint 1:	RC5754 1.5mm + 2.0mm RC5754 + 2.0mm RC5754
Rivet:	T50M42A (7.5mm long, level hardness 2)
Die:	DG10-120 (flat bottomed, Width=10.0mm, Height=1.2mm)

TESTING PROCEDURE

AC procedure for sample preparation, rivet insertion and joint examination, as outlined in sections 5.1 and 5.2 has been followed.

RESULTS AND DISCUSSION

The results of the additional physical test confirmed the behaviour documented above, whereby overly increased friction in rivet without coating leads to lowered interlock, decreased Tmin and lowered bore fill as can be seen from measurements and visual appearance of the joints as detailed in the table and figure below. This is in correlation with results of simulation with overly increased friction.

Measurements:

Joint:	RC5754 1.5mm + 2.0mm RC5754 + 2.0mm RC5754	
Rivet:	T50M42A (7.5mm long, level hardness 2)	
Die:	DG10-120 (flat bottomed, Width=10.0mm, Height=1.2mm)	
	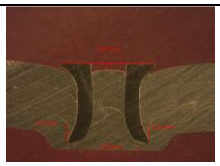	
Parameter	Standard coating HOO [mm]	No coating [mm]
Interlock:	0.41	0.24
Tmin:	0.32	0.29
HH:	-0.02	0.01

Table 23, Test results – Verification joint

Visual attributes:

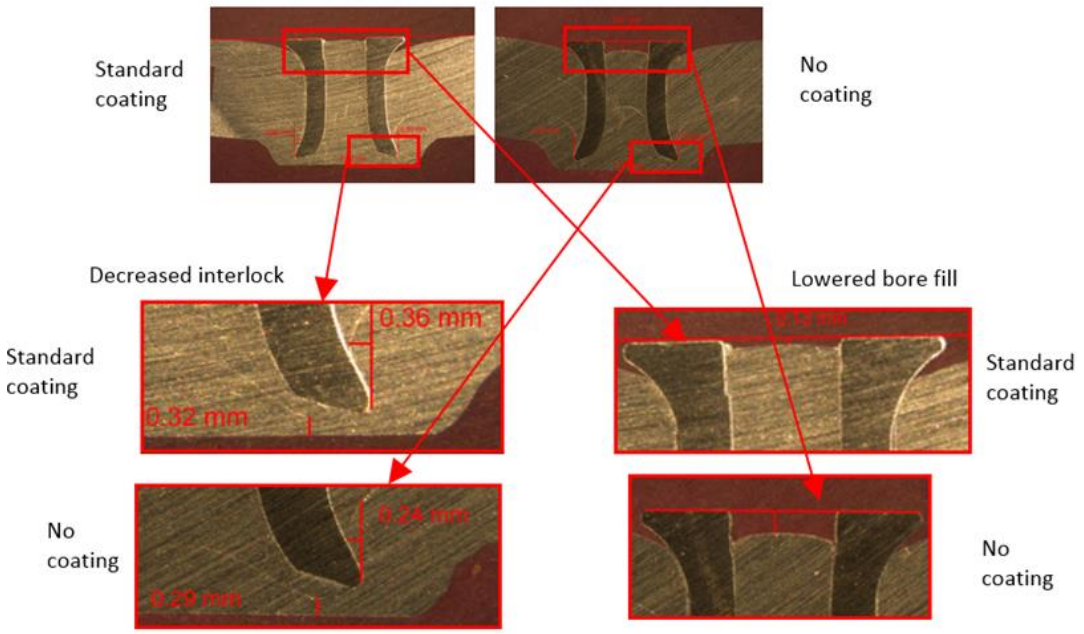

Figure 177, Comparison of low and high friction coatings

Whilst the established friction values do work well for most of the joints as can be seen throughout this work, there are joints in which these settings did not provide a result that was expected. In these instances, it is possible that other parameters such as material characterisation, geometry or coating variation in the physical test may be accountable for the difference.

As previously mentioned, it would seem that a high friction is needed consistently across all joints unless they are manufactured with particularly low friction coating such as Trivet and BG rivet. This is in contrast with the low figures used by other researchers as well as the settings suggested by the software for SPR which suggests using μ=0.1.

One possible explanation could be that friction is a matter of calibration and potentially in the software the μ of value 0.1 is designed to calculate less of a friction than it means in reality and the physical equivalent of this would be μ=0.2/0.3 instead. Another potential explanation of increased friction working better is that the fact that the coating is scraped off throughout the process of insertion which leads to an increased friction between materials.

In absence of ability to physically measure the friction during the insertion due to the speed as well as a number of other variables, an empirical example might be better suited to confirming this theory.

6.3.1.4.2 Validation of high friction via empirical testing

METHOD

To that end, two empirical tests have been conducted, one on the coating of the rivet and another on the sheets.

Rivet coating

A test comparing a rivet that has been inserted, cross sectioned and then taken out of the joint with several rivets prior to insertion has been conducted. Both the cross sectioned and intact rivets were photographed under ultraviolet light to show the coating.

Sheets coating

A non-cross sectioned joint has been disassembled to reveal in order to examine how sheets are affected by the insertion.

TESTING PROCEDURE

AC procedure for sample preparation, rivet insertion and joint examination, as outlined in sections 5.1 and 5.2 has been followed.

RESULTS AND DISCUSSION

Rivet coating

As can be seen from the image, the coating on the rivets is applied evenly and in sufficient amount to entirely cover the areas around the tips as well as the underhead radius of the rivet and shank. On the other hand on the cross sectioned rivet, there is no coating on the rivet tips and very little on the under head radius. More coating has been retained on the shank than expected. However, this confirmed the use of high friction values as correct.

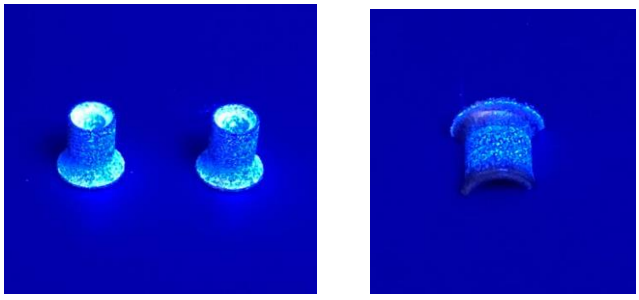

Figure 178, Comparison of coating levels under ultraviolet light before and after insertion

Sheets coating

The disassembled joint, as shown in the image below, clearly shows a resolute change in surface of the sheets with areas that have been clamped by the joint looking are exhibiting a visibly rougher surface than the parts of the sheets outside of the joint which look polished and shiny by comparison.

Figure 179, Rivet removed from joint to show wear of the coating

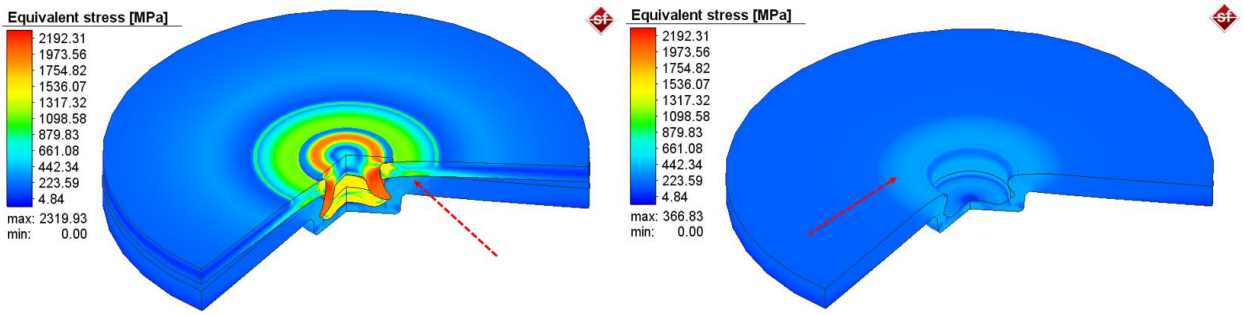

Figure 180, Simulation corresponding with physical test in Figure 179, to confirm the extent of stress in this area and probability of sheet coating being worn off

Whilst this does not precisely pinpoint friction, it does confirm that the coating that is supposed to lower the friction between raw metals throughout the insertion is worn off in a very short time which justifies the use of high friction in the new friction settings established by this study.

In summary, the exercise has achieved the objective by identifying specific behaviours various levels of friction can lead to and then used these to adjust the friction for a desired outcome in process obtaining a set of values. A set of friction values established in this way has so far worked well and yielded realistic results (such as specific deformation flow features in a riveted joint). However, there certainly is a scope for improvement and future work should also include options to include variable friction window applicable to different parts if the rivet to reflect the variability in coating for example the rivet bore might be as well coated in lubricants as the outside.

6.3.2 Clamping

When setting up the simulation model for an SPR insertion, amongst other things, clamping needs to be considered. As explained in the literature review (chapter 4.1.2.3) there are two main types of clamping that are used in Atlas Copco SPR insertion process, pre-clamp or intermediate clamp.

The built in software model uses pre-clamp mechanism, and before the effects of clamp were considered in this research work, only this clamping set-up was employed in the simulations, this approach gave generally satisfactory results. The same can be said for real joint testing as many joints look the same whether they are set on a pre-clamp or an intermediate clamp, the clamping arrangement does however have an effect on some types of joint stack, so it was considered important to develop an intermediate clamp for the development of the base simulation model (objective 1).

6.3.2.1 Set-up of the intermediate clamping model

INTRODUCTION

To develop a model that would reflect the insertion process in reality as close as possible, a new model was needed to replicate the intermediate clamp.

METHOD

An intermediate clamping model was set using data about the clamping setup on the servo setter.

TESTING PROCEDURE

AC procedure for sample preparation, rivet insertion and joint examination, as outlined in sections 5.1 and 5.2 has been followed.

RESULTS AND DISSCUSION

In order to replicate the intermediate clamping used in the servo setter, a clamping force displacement curve was extracted from the servo setter, as shown below.

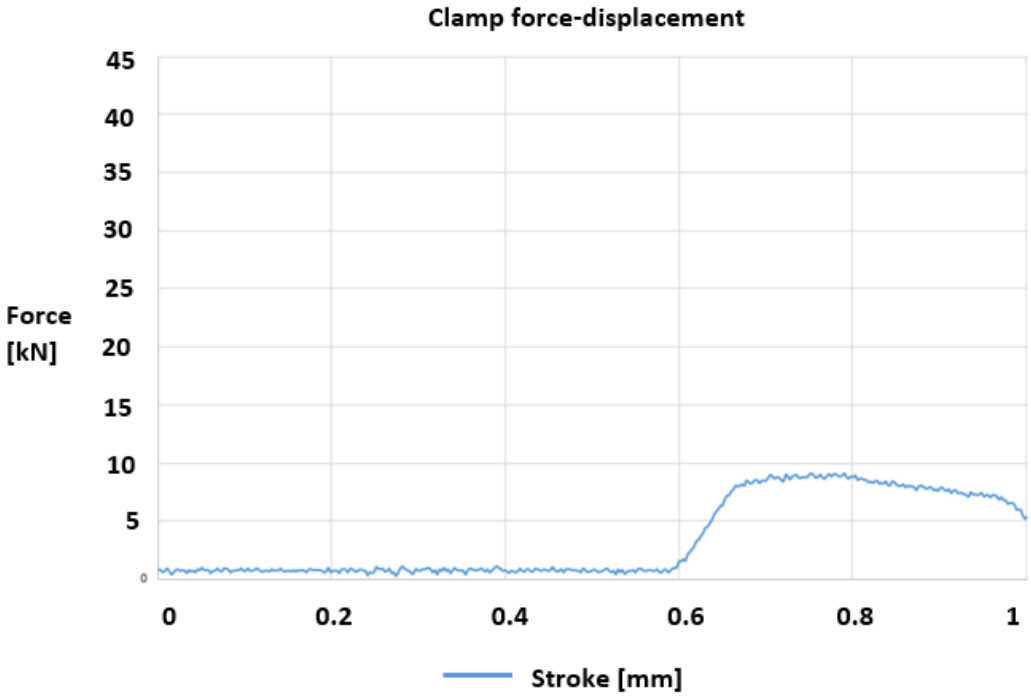

Figure 181, Force-displacement for clamp

The model employed the same spring size used for the original pre-clamp setting, however, instead of being applied with a fixed force, a graph was used to chart the movement of the nose. This was set to start at the 200N, which the initial (also referred to as 'tripper spring') spring clamp load, followed by an 8 kN force which starts when the rivet is 0.525mm away from being fully inserted (flush head), as shown in Figure 182. This was determined by a simple calculation subtracting the mentioned figure of 0.525 from the length of the stroke which is determined by the length of the rivet.

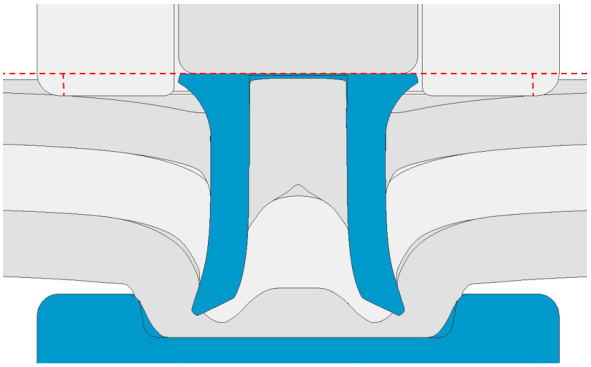

Figure 182, The red line illustrates the approximate point when the nose starts pushing on the sheets with 8kN force

As an example, if K50742A rivet is used, which is 7.0mm long rivet, the clamp would be set to engage at 6.475mm. This values applies to 5mm diameter rivets, for smaller 3.0mm rivets, the 8kN clamp is engaged 0.4mm away from full insertion. It has been decided that for the new 4.0mm diameter rivets

currently being designed, the clamp will engage at the same time as for 5.0mm rivets. Currently, this setting needs to be adjusted individually for each joint.

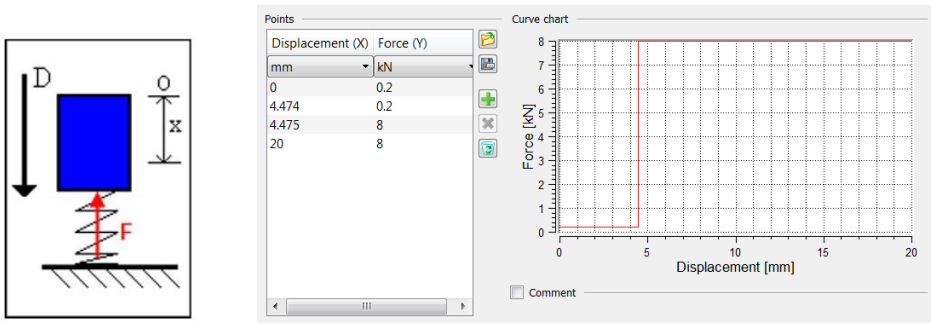

Figure 183, Intermediate clamp model set up - use of 'released' spring (left), exaple graph controlling movement for a nose with intermediate clamp with rivet fully inserted at 5.0mm.

The model was validated on a joint made with the original pre-clamp model and a new intermediate clamp model. Displacement graphs extracted from the software confirmed that the clamp model was working as intended.

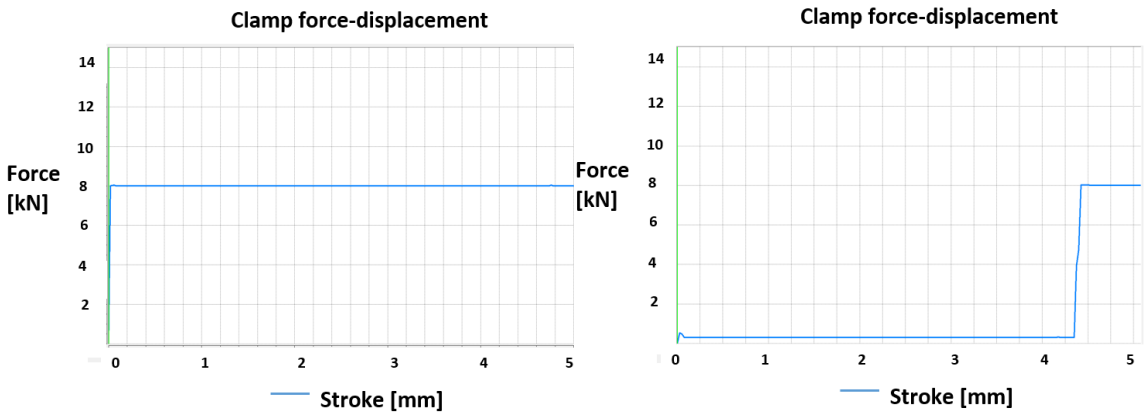

Figure 184, Example of pre-clamp and intermediate clamp force-displacement curves.

6.3.2.2 Pre-clamp vs intermediate clamp comparison

INTRODUCTION

The initial premise regarding clamping is that using one or the other causes significant differences in physically tested joints. However, there was no significant difference noted between the joints simulated with the initial set-up with pre-clamp and joints completed with the new intermediate model. Therefore a bigger range of joint types must be tests to include joints where the clamping method usually has more of an effect.

Based on this, a new model including intermediate clamp model was set up within the simulation. This was followed by testing the new model on three different joints to validate this model and determine whether it had an effect in simulations.

METHOD

A comparison of both models was tested on three different joints, these were selected specifically to reflect the evolution of material usage; going from aluminium alloy only, to high strength steel and aluminium, and then to ultra high strength steel to aluminium. All three joints were completed with pre-clamp and with intermediate clamp that with the main force coming on at 0.525mm before flush.

Joint 1:	1.5mm 5182 + 1.5mm AA5182
Rivet:	C50G41A (5.5mm long, level hardness 1)
Die:	DG09-180 (flat-bottomed, Width=9mm, Height=1.8mm)

Joint 2:	1.5mm DP600 + 1.5mm AA5182
Rivet:	C50G44A (5.5mm long, level hardness 4)
Die:	DG09-180 (flat-bottomed, Width=9mm, Height=1.8mm)

Joint 3:	1.2mm Fortiform + 1.5mm AA5182
Rivet:	BG0E46E (5.5mm long, level hardness 6)
Die:	DG09-160 (flat-bottomed, Width=9mm, Height=1.6mm)

TESTING PROCEDURE

AC procedure for sample preparation, rivet insertion and joint examination, as outlined in sections 5.1 and 5.2 has been followed.

RESULTS AND DISCUSSION

Joint 1

Measurements:

Joint no.	Type of clamp	Physical test			Simulation		
		Interlock [mm]	Tmin [mm]	HH [mm]	Interlock [mm]	Tmin [mm]	HH [mm]
1	Preclamp	0.39	0.25	0.00	0.37	0.33	0.06
	Int. clamp	0.41	0.26	0.00	0.38	0.32	0.04

Visual attributes

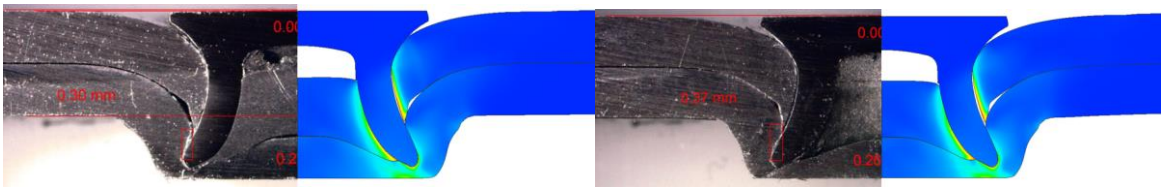

Figure 185, Joint 1 visual results

Joint 2

Measurements:

Joint no.	Type of clamp	Physical test			Simulation		
		Interlock [mm]	Tmin [mm]	HH [mm]	Interlock [mm]	Tmin [mm]	HH [mm]
2	Preclamp	0.48	0.15	0.09	0.64	0.33	0.10
	Int. clamp	0.45	0.21	0.02	0.60	0.35	0.08

Visual attributes:

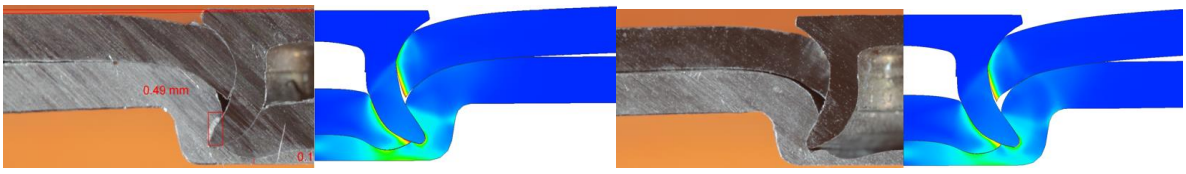

Figure 186, Joint 2 visual results

Joint 3

Measurements:

Joint no.	Type of clamp	Physical test			Simulation		
		Interlock [mm]	Tmin [mm]	HH [mm]	Interlock [mm]	Tmin [mm]	HH [mm]
3	Preclamp	0.57	0.36	0.08	0.60	0.40	-0.20
	Int. clamp	0.20	0.19	-0.18	0.34	0.35	-0.11

Visual attributes

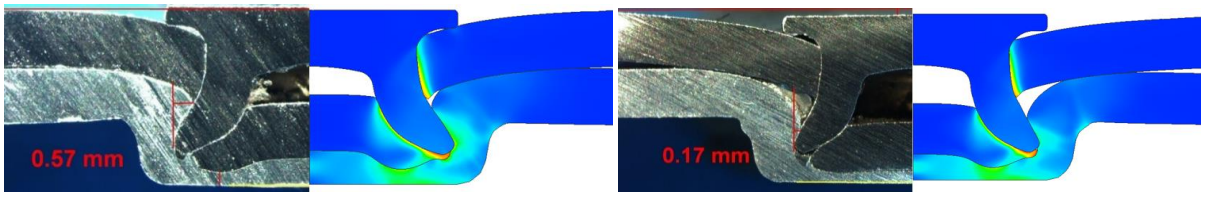

Figure 187, Joint 3 visual results

It has been determined by physical testing and by simulation that the differences between pre-clamp and intermediate clamp methods are mainly seen in joints with ultra high strength steel materials such as Usibor 1500MPa. In this instance, the use of intermediate clamp sees increased large internal gaps between the sheets, due to sheets not being tightly clamped together until just before the end of the insertion as shown in the image below. This leads to lowered interlock when compared with use of pre-clamp. This is demonstrated by the below image capturing joint 3 with both preclamp and intermediate clamp during in the process of insertion, roughly 4.4mm into the stroke. It can clearly be seen that the position of the nose is significantly lower with pre-clamp which is keeping the sheets firmly on top of the die, whereas with intermediate clamp the sheets are lifting off of the die as the nose is not pressing on them with any clamp load yet. This is what is causing the lowered interlock.

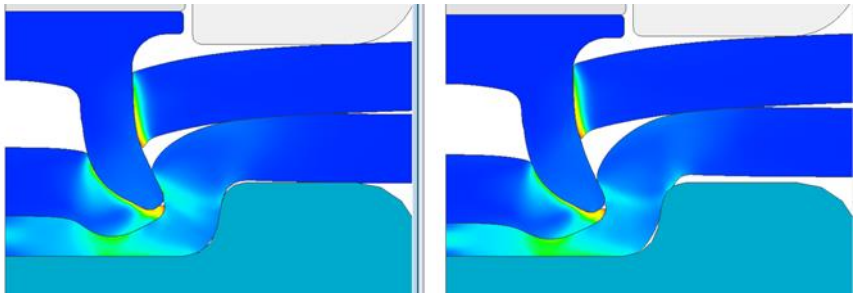

Figure 188, Joint 3 with pre-clamp (left) and intermediate clamp (right) captured at 4.4mm into the stroke.

The intermediate clamp also tends to cause increased dishing of the UHSS steel sheets, lowered Tmin and another characteristic feature, which is a slight step in the bend at the foot of the button (caused by the sheets lifting off of the die as shown in the Figure 189.

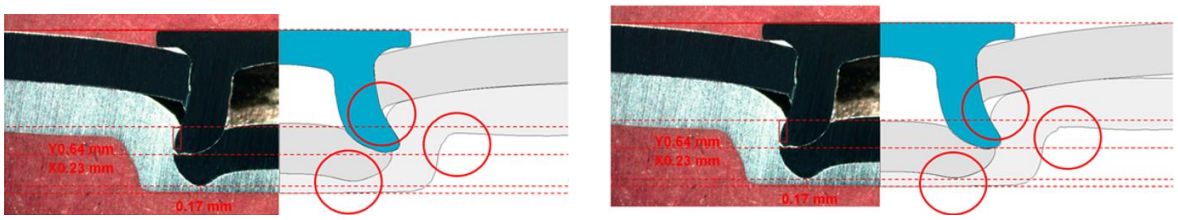

Figure 189, Examples of joints completed with pre-clamp on the left and intermediate clamp on the right.

This step can be more or less pronounced and is due to the fact that for most part of the process the sheets are not clamped and therefore under certain circumstances can flow out of the die. An example where this is happening coupled with too small a die is shown in Figure 190.

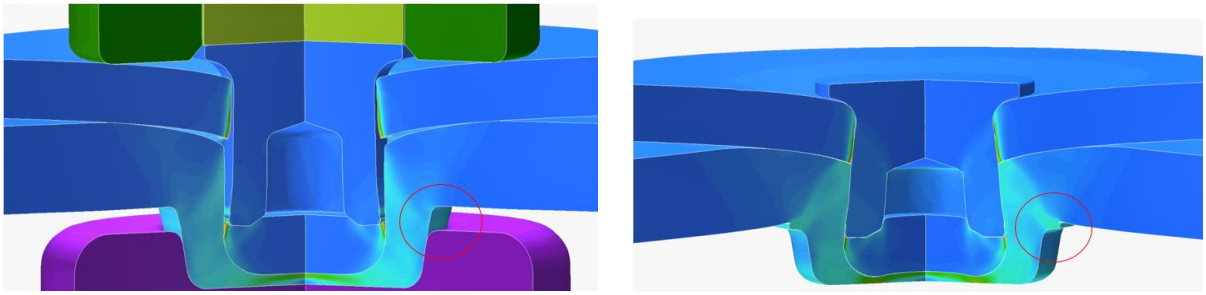

Figure 190, Example of a small die used with intermediate clamp

These differences have been noted in simulation as well as in physical testing which suggests that the model of the new intermediate clamp is correct.

There is a less pronounced effect of use of pre-clamp vs intermediate clamp in the joint with dual phase steel DP600, and almost no effect on softer and more ductile aluminium. The latter would explain the earlier success in simulations which were all joining aluminium to aluminium using a pre-clamping model that was not accurately replicating the intermediate model mostly used in Henrob.

However, during application of the intermediate clamp model with clamp engaging at 0.525mm before flush across a wide range of joints, that the results may not always reflect accurately the joint but that some changes in time of the clamp engaging such +/- of 0.5-1.0mmmm usually improves this. Upon further investigation, it has been clarified that there are tolerances for the clamp mechanism assembly which means that clamp does not always necessarily engage at the exactly prescribed position. Access to a small study conducted in the R&D laboratory has shown that the clamp has been activated between +/-1.6mm earlier or later than the specified time on the tested setters. Therefore,

whilst the set-up of an intermediate model is really beneficial, in addition to using this model, it would be recommended to test a process window of +/-1.6mm tolerance on the position of clamp activation.

This study confirmed that intermediate clamp was beneficial in the early days of SPR when mainly ductile aluminium sheets were joined and intermediate clamp did not cause significant differences between the two clamping methods, whilst having the benefit of allowing the sheet material to flow into the joint from further away reducing localised work hardening (as explained in chapter 4.1.2.3.1).

However, the constant evolution of materials is increasingly heading into direction of using UHSS steels and thus is a reason to consider using pre-clamp servo setters for these joints due to the improved results seen when pre-clamp is used on UHSS steels.

In summary, a new model of intermediate clamp was proposed to replicate AC clamping method more accurately. This means that unlike the in the default out of the box version of the software where the sheets are clamped from the beginning, the clamp does not come on until the rivet head is 0.525mm away from the top sheet.

To validate the proposed model, three different joints with various hardness materials (Aluminium, HSS and UHSS) were physically tested as well as simulated with both methods and good agreement could be seen between simulations and physical testing in all instances.

The difference between the two clamping methods is mainly visible in joints with high strength steels and less so in softer aluminium only joints which was also confirmed in simulation.

The proposed model is a variable parameter, hence the settings of this will be a function of another process parameter - rivet length. In physical testing, the intermediate clamp is also subject to variation depending on the stiffness of the C-frame and overall hardness of the substrate materials and the simulation settings should account for this by adding a process window and testing the clamp.

6.3.3 Press selection

INTRODUCTION

A vital part of the process of simulation involves selection of the insertion method (termed ‘press’) within the software. As outlined in literature review chapter (4.1.2.2), a number of press types are available in the software, the default is hydraulic. The physical lab process of insertion has two main insertion methods available these are hydraulic or servo systems (as explained in chapter 2.5).

From the point of view of the software, the hydraulic press is a straightforward option to match to a real hydraulic setter. However, the more frequently used setter type is servo and there is currently no well-matched equivalent press option available in the out if the box software.

Based on the description of the servo setter, the press type within the software that matches the servo most closely is called the 'Screw press', the reason it is a reasonable match is because it allows input of velocity to be set prior to the rivet impact on the top sheet, and because it is an energy based press which varies the speed slowing down during the rivet insertion process. This is very different to the hydraulic which provides a constant speed throughout the rivet insertion process.

The specifications that are required for input with this type of press are 1.) gross energy, 2.) maximum ram speed and 3.) efficiency during stroke.

METHOD

A simulation was completed on a selected physical sample of a joint in order to test the suitability of screw press and its aspects:

- Calibration of press parameters and comparison of physical test and simulation results.
- Comparison of force and levels of HH at different depths of insertion in physical test vs simulation
- Comparison of force-displacement curves in physical joint and simulation.

The joint selected for physical testing is described below:

Joint:	1.2mm DP600 + 1.5mm AA5182
Rivet:	BG50546E (5mm long, level hardness 1)
Die:	DG09-180 (flat-bottomed, Width=9mm, Height=1.8mm)

The HH and force reading achieved by simulation was compared to HH of rivets physically inserted at six different head height levels in a strip of metal. Two cross sections were completed at HH aiming for two different levels of HH – 0.00mm (flush) and 0.1mm. A force displacement curve was extracted from servo setter for the joint with flush HH.

TESTING PROCEDURE

AC procedure for sample preparation, rivet insertion and joint examination, as outlined in sections 5.1 and 5.2 has been followed.

RESULTS AND DISCUSSION

Calibration of press and comparison of physical test and simulation results

Data is required for the three main input parameters,

Gross energy

Maximum ram speed

Efficiency during stroke

Gross energy

Input of gross energy is subject to calibration in relation to the stroke and the software automatically calculates force which is required to insert the rivet. If a sufficient value for energy is set, the simulation will fully complete the required stroke. However, if the energy value and subsequently force value is too low, the simulation may not complete the pre-determined stroke. A practical example of how this is affecting the simulation is shown below. The joint on the left in Figure 191, Example of rivet inserted with high energy (left) and low energy (right).has been given enough energy to be fully inserted (software notifies user that the simulation 'finished on stroke') whilst for the joint on the right, the energy input was reduced, leading to only a partial insertion (the simulation is 'finished on energy'). The correlating force was also lowered in case of the second joint whilst for the fully inserted joint the force was similar to that calculated by the setter for the physical test.

If high enough velocity is used to pierce through all sheets but not enough gross energy is input, then the rivet will not be inserted fully. If both are sufficiently high, but efficiency if stroke is a lower than 0.3, again, the rivet will not be inserted fully.

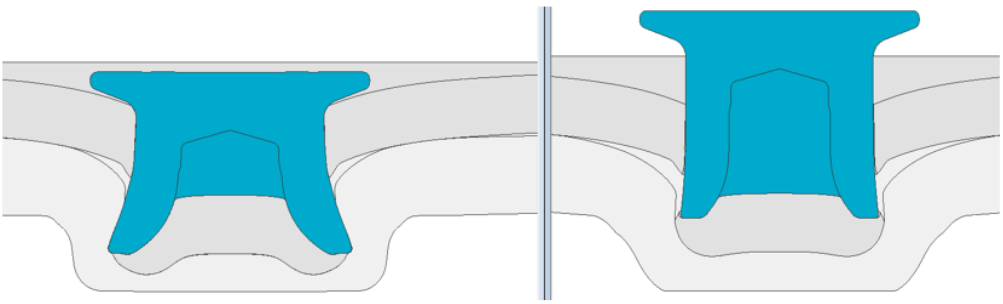

Energy [J]	177	93
Force[kN]	38	27
Simulation ended	On stroke	On energy

Figure 191, Example of rivet inserted with high energy (left) and low energy (right).

Maximum ram speed

The maximum ram speed is the velocity with which the punch is moving on the impact of the rivet. With physical samples, this figure is calibrated for each joint individually as part of testing by changing velocity until intended level of insertion is achieved. If no guide figure is advised by physical test, simulation shall calibrate this by means of similar sensitivity study i.e. incrementally altering velocity until the fill or intended level of insertion is achieved. In this particular instance, a velocity of 300mm/s was advised by physical test in order to achieve flush HH. Unlike in hydraulic press, where velocity is constant throughout the insertion, velocity in this process is variable and decreases with advancement of the stroke.

Efficiency during stroke

The efficiency specifies how much of the energy of the press is used for the forming of the workpiece. The maximum of this value within Simufact software is 1.0 which is never exceeded (Simufact, 2015).

To replicate the process of insertion using AC setters, the efficiency of stroke was set at a constant value of 0.3 in order to achieve 30% efficiency.

The simulation of the joint using the above parameters (along with friction values from sensitivity study) has provided results that are in 95% agreement with the physical cross section (based on the score card) of the joint at flush head height which includes characteristic gaps between the sheets with this joint. The screw press therefore can be tested further on this joint.

Joint:	1.2mm DP600 + 1.5mm AA5182	
Rivet:	BG50546E (5mm long, level hardness 1)	
Die:	DG09-180 (flat-bottomed, Width=9mm, Height=1.8mm)	
	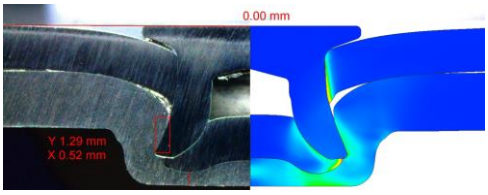	
Parameter	Physical test result [mm]	Simulation result [mm]
Interlock:	0.52	0.51
Tmin:	0.45	0.44
HH:	0.00	0.01

Table 24, Test results – verification joint

Comparison of force and levels of HH at different depths of insertion in physical test vs simulation

METHOD

As shown in the image below, the above joint has been inserted with varying force which results in joints that are inserted only partially; the below table shows results achieved in terms of head height.

TESTING PROCEDURE

AC procedure for sample preparation, rivet insertion and joint examination, as outlined in sections 5.1 and 5.2 has been followed with a variation on a number of rivets inserted in one coupon due to shortage of materials, in this instance six rivets were inserted in a row into 40mm x 120mm coupon.

Figure 192, Physical test of differing forces

RESULTS AND DISCUSSION

Results of physical tests are as per below:

Physical test	
Force [kN]	hh [mm]
25	0.20
30	0.15
35	0.09
40	0.06
45	0.00
50	-0.10

Table 25, Results - physical test of differing forces.

This exercise has been repeated via simulation, which, to achieve similar outcomes has to generate similar values of force. The table below shows results that are in correlation with the physical test.

Simulation	
Force [kN]	HH [mm]
32	0.21
37	0.16
38	0.09
41	0.06
43	0.04
55	-0.12

Table 26, Result - simulation of differing forces

An additional cross section of a joint at head height of 0.1mm has been completed to check the measurements correlate with the same joint if the HH level changes.

Joint:	1.2mm DP600 + 1.5mm AA5182	
Rivet:	BG50546E (5mm long, level hardness 1)	
Die:	DG09-180 (flat-bottomed, Width=9mm, Height=1.8mm)	
	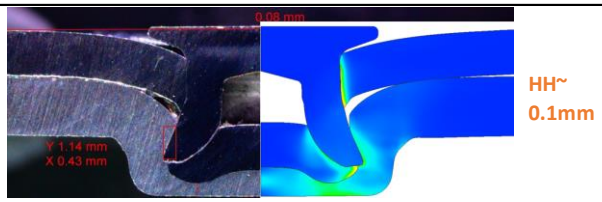	
Parameter	Physical test result [mm]	Simulation result [mm]
Interlock:	0.43	0.47
Tmin:	0.44	0.43
HH:	0.08	0.09

Table 27, Test results for verification joint with 0.1mm HH

The agreeability scorecard points to 95% agreement between the simulation and the physical cross section also at HH=0.1mm, with the software replicating the typical feature of use of post clamp in the model i.e. gaps between sheets. With both levels of levels of HH simulated accurately, the next step is to compare the force-displacement curves.

Comparison of force-displacement curves

METHOD

A force-displacement curve has been extracted from the servo setter for the joints with HH=0.0mm and HH=0.09mm, and then collated with the corresponding outputs from the software HH=0.01mm and at HH=0.085mm.

TESTING PROCEDURE

AC procedure for sample preparation, rivet insertion and joint examination, as outlined in sections 5.1 and 5.2 has been followed.

RESULTS AND DISCUSSION

The collated curves can be seen below:

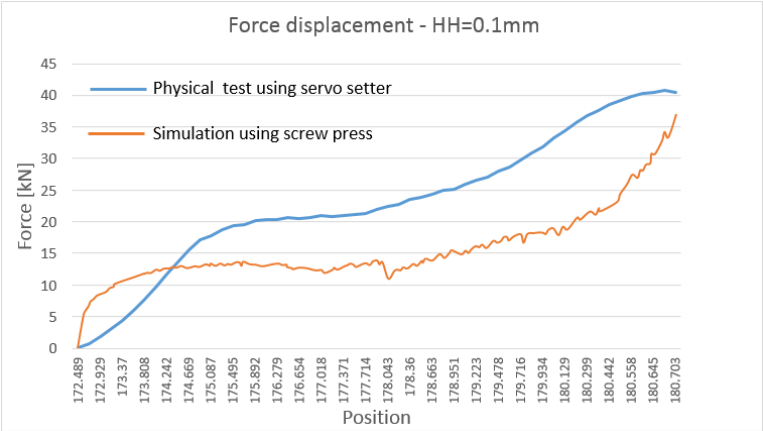

Figure 193, Force-displacement curve for joint with 0.10mm head height

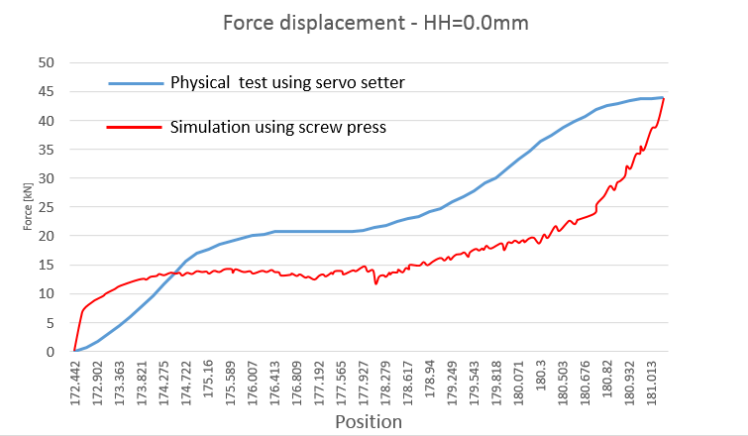

Figure 194, Force-displacement curve for joint with 0.00mm head height

The trends that can be seen in the force-displacement extracted from the simulation are similar to the force-displacement curve for the physical test of particular joint extracted from the software in some parts. The force is initially rising to pierce the steel top sheet, then temporarily reaching a plateau before rising again during the compression phase of the insertion. There is also good agreement in maximum force values exerted to insert the rivet in reality, as well as in simulation in both instances. However, although the curve extracted from simulation does reach the same force by the end of the insertion, it can be seen that the screw press seems to overestimate the force in the initial part of the

stroke, and on reaching around 14kN it then seems to overestimate it in the subsequent parts of the insertion.

This can be explained by the differences between the servo and screw press insertion method. Screw press in simulation is given a certain amount of energy at the beginning and once this runs out, the stroke ends. Whilst this is applicable to a basic connected drive servo setter, on the Henrob servo setter the punch is given extra energy throughout the insertion process by the servo motor which probably is the reason for the difference in the two curves – the difference between the real equipment where extra energy is added during rivet insertion and the simulated curve for a screw press where no extra energy is added during rivet insertion, is highlighted in the coloured in green area in the image above.

Despite the differences in supply of energy, there is good correlation achieved between the physical results and simulation equivalent cross section results as shown in Figure 195.

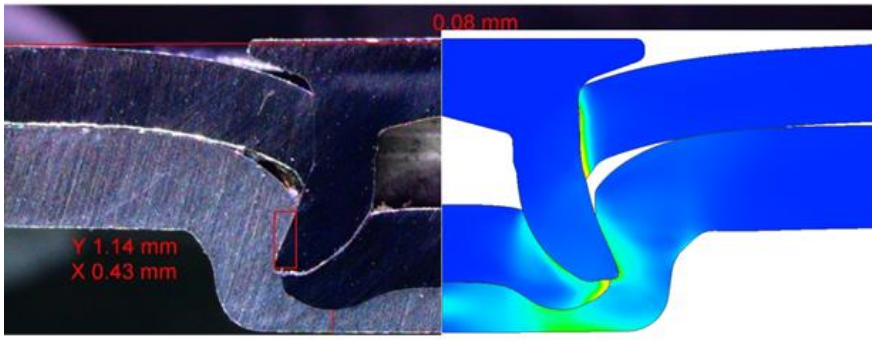

Figure 195, Comparison of physical and simulation cross section results

This is perhaps not surprising as the bulk of the every is provided from the inertia give to the rivet before it hits the top sheet, and only a small amount of extra energy is added during the rivet insertion. The screw press has therefore been confirmed as a suitable press type to use to simulate the servo joining process, until a new press type with added energy during insertion is added to the software by the software supplier. In the long-term, the intention is to work with the software developers to develop an additional press type that would allow the press to start with inertia fly press which would bring the punch up to the fast starting speed and then add some extra energy during the rivet insertion. This development request has already been presented to Simufact and a collaboration project has been started to create and validate a new press type.

6.3.3.1 Speed of insertion

A related concept to press selection is speed of insertion. In simulation the speed selection is usually informed by some previously conducted physical testing on some similar joints using historical test

data. However, the speed used has a proven effect on insertion of the rivet; for example a very slow insertion has a very different outcome to a very fast insertion. It is therefore imperative to assess whether the speed setting aspect is reflected correctly in the software using the following study.

METHOD

The selected joint has been set at three different velocities – 0.1 mm/s, 100 mm/s and 10 m/s. A hydraulic press was used to ensure the same speed was applied throughout the insertion process.

Joint:	2.0mm A6111T4 + 2.5mm A6111T4
Rivet:	C50642A (6mm long, level hardness 2)
Die:	DG10-140 (flat-bottomed, Width=10.0mm, Height=1.4mm)

A verification physical sample joint was been made to validate the simulation, which was run using the same speed settings as the physical tests.

TESTING PROCEDURE

AC procedure for sample preparation, rivet insertion and joint examination, as outlined in sections 5.1 and 5.2 has been followed.

RESULTS AND DISCUSSION

Simulation of the joint shows 94% agreement with the physical cross section at 250mm/s.

Joint:	2.0mm A6111T4 + 2.5mm A6111T4	
Rivet:	C50642A (6mm long, level hardness 2)	
Die:	DG10-140 (flat-bottomed, Width=10.0mm, Height=1.4mm)	
	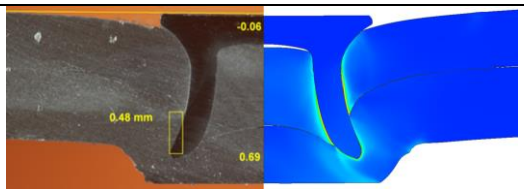	
Parameter	Physical test result [mm]	Simulation [mm]
Interlock:	0.47 (Avg)	0.43
Tmin:	0.75 (Avg)	0.82
HH:	-0.06	0.09

Table 28, Test results – verification joint

Measurements:

Test no.	Velocity [mms]	Interlock [mm]	Tmin [mm]	HH [mm]
Physical test	250	0.47	0.75 (Avg)	-0.06
A1	0.1	0.434	0.928	0.051
A2	100	0.43	0.883	0.055
A3	10000	0.43	0.809	0.054

Table 29, Results –Speed of insertion

Visual attributes:

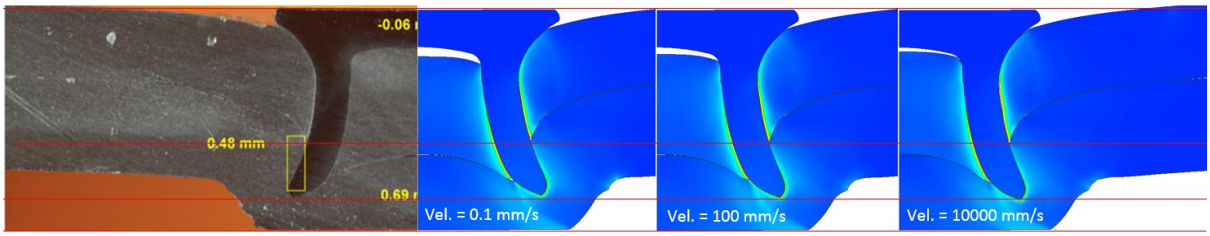

Figure 196, Axisymmetric view of joints tested at different velocities with single flow curve compared to a physical result.

There are slight differences between the three different speeds and there seems to be a pattern of Tmin lowering marginally with increasing speed, the joint images suggest this is because the rivet compresses slightly less with higher speed meaning the rivet is longer. Interlock and HH remain unchanged. The changes seen are very minor which could be due to the fact that the sheet material data was a single flow curve at one strain rate. If there are more strain rates available within the flow curve data, the software can then interpolate between the curves to calculate the most suitable curve for each particular stage of simulation to improve the simulation accuracy. However, if there is only one strain rate available, the interpolation process does not occur and strain rates are only calculated as part of the mechanical calculations. This theory will be examined in an additional test that follows.

METHOD

The same test will be repeated on the same joint as above, however, the sheet material data has been amended to a data set with several strain rates to determine whether the speed of insertion will have a more pronounced effect when more material data is provided.

Joint:	2.0mm A6111T4 + 2.5mm A6111T4
Rivet:	C50642A (6mm long, level hardness 2)
Die:	DG10-140 (flat-bottomed, Width=10.0mm, Height=1.4mm)

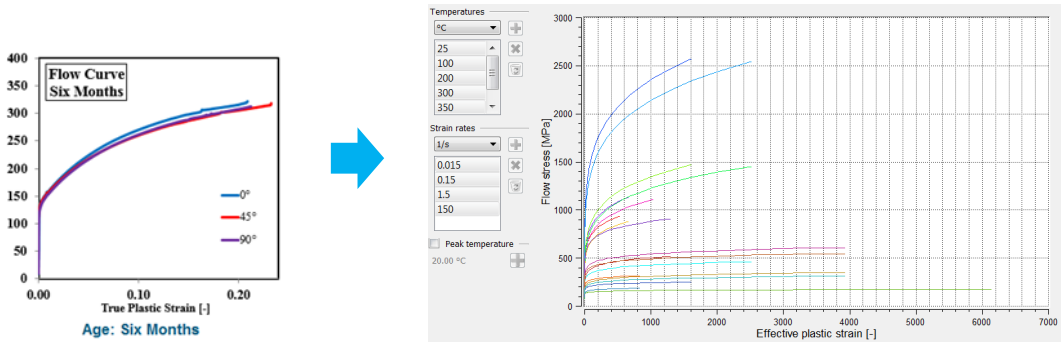

Figure 197, Single flow (left) curve vs multiple flow curves (right)

RESULTS AND DISCUSSION

Measurements:

Test B				
Test no.	Velocity [mms]	Interlock [mm]	Tmin [mm]	HH [mm]
Physical test	250	0.47	0.75 (Avg)	-0.06
A1	0.1	0.386	0.711	0.011
A2	100	0.44	0.873	0.032
A3	10000	0.646	1.269	0.001

Table 30, Test results

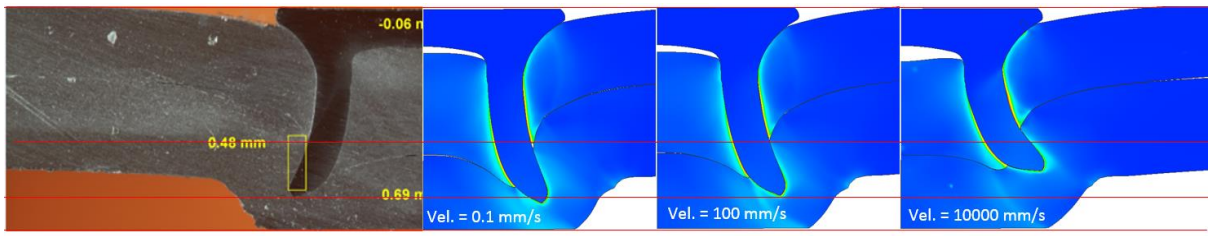

Figure 198, Axisymmetric view of joints tested at different velocities with multiple flow curve compared to a physical result.

As expected, there is a significant difference between the slowest and fastest insertion rate as shown in the image above. This has confirmed the theory that the software is sensitive to different insertion speeds so long as it is given enough data to interpolate between. The result with the most significant difference cannot be verified using the riveting equipment as Atlas Copco equipment is not able to go up to such high speeds, however, this exercise has confirmed that if sufficient data at different strain rates is fed into the software, this will be reflected in the outcome.

Obtaining flow curves at different strain rates and temperatures is not an easy or cheap process and hence cannot be done for all materials. Therefore some simulations might need to be run with a single flow curve that is not giving the most accurate effect to changes of speed. However, considering that the insertion speed range used in Atlas Copco is very narrow (typically between 250mm/s to 360

mm/s) and will never achieve the extreme speeds at either ends of the scale used for this study of 0.1 mm/s or 10,000 mm/s, using a single flow curve with one strain rate is likely to be sufficient for simulations where an approximate result is all that is required. The suggested plan for the company is to obtain accurate sets of flow curves for small number of commonly riveted materials, and the use single flow curves for the rarely riveted materials where the high cost of flow curve testing cannot be justified in relation to the small improvement likely in the accuracy of the simulation result. How to obtain the material flow curve information is described elsewhere in this thesis, some more material testing will be described in section 6.4

6.3.4 Mesh

Within this section, mesh size will be established for two processes – hardness tests carried out for friction study and SPR method itself.

As mentioned previously, a small mesh provides greater accuracy as opposed to large mesh, however, a balance needs to be struck between the accuracy and sensible duration of simulation. The usual simulation approach uses a 2D axisymmetric model which reduces the time, which would be much longer if a 3D simulation was used.

To ensure the best possible accuracy of the simulation a sensitivity study needs to be conducted and most suitable size of the mesh for all deformable elements has to be established. This exercise will apply to all deformable parts of any simulation model. In the instance of the hardness tests conducted to test the friction this will apply to the sample of metal being hardness tested, whilst in SPR simulation this will include the workpiece i.e. rivet and also the sheets.

6.3.4.1 Hardness tests mesh sensitivity study

INTRODUCTION

Hardness tests using Vickers hardness machines are simple to simulate and therefore an ideal opportunity to use for a mesh sensitivity study on the small end of the scale in order to become familiar with and learn this process before moving onto simulate more complex tests.

METHOD

The mesh size sensitivity study consists of running a number of simulations of the same model using an increasingly smaller size mesh in the deformable parts and can be concluded when the values of specific results start appearing to be the same from one iteration to another. The first sensitivity study

was conducted on the sheet sample tested using the Vickers hardness testing machine. The sensitivity study commenced with relatively large elements.

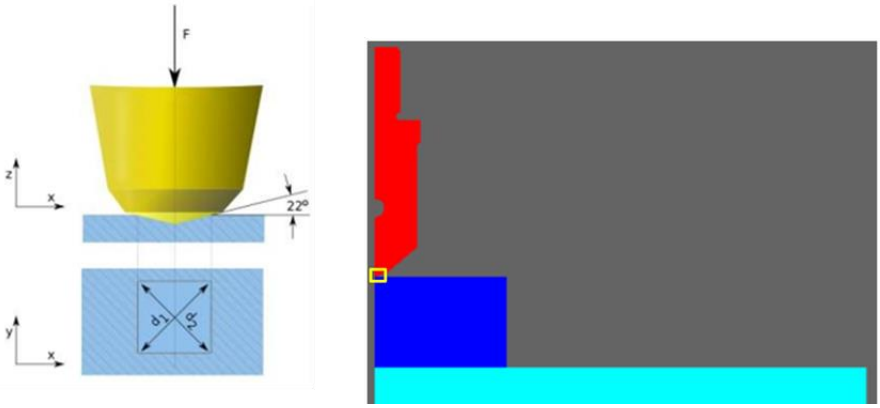

Figure 199, Location of the mesh area used for sensitivity study for hardness tests.

TESTING PROCEDURE

A simulation process, as outlined in section 5.2, has been followed.

RESULTS AND DISCUSSION

The results of the mesh size sensitivity study for hardness tests are below. The study started with quite large element size but was quickly reduced to a smaller size based on the results.

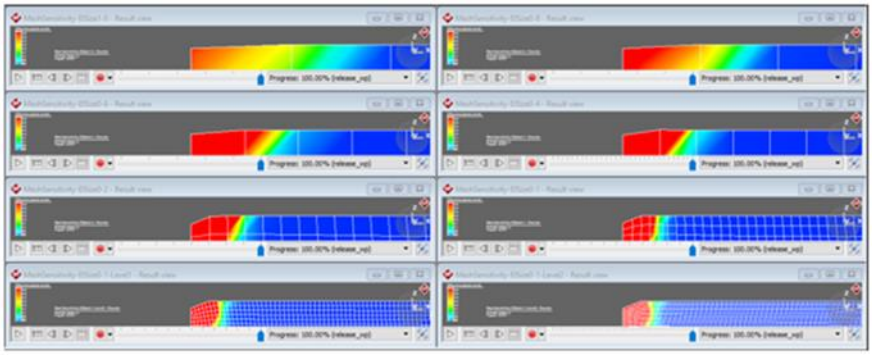

Figure 200, Visual results of mesh sensitivity study on coupons for hardness testing

Test no.	Element size [mm]	Diagonal measurement of indent [mm]	Depth of indent [mm]	Comment
Test 1	1.00	1.15	0.39	Not feasible
Test 2	0.80	0.89	0.41	Not feasible
Test 3	0.60	0.62	0.43	Not feasible
Test 4	0.40	0.43	0.44	Not feasible
Test 5	0.20	0.22	0.96	Not feasible
Test 6	0.10	0.21	0.84	Not feasible
Test 7	0.05	0.21	0.78	Feasible
Test 8	0.04	0.20	0.79	Feasible
Test 9	0.03	Simulation not completed, terminated after two hours		Not feasible

Table 31, Results – Mesh sensitivity study for hardness testing

6.3.4.2 SPR mesh sensitivity study

6.3.4.2.1 Rivet mesh

Given that no intense deformation of the rivet is expected, it is recommended that the rivet uses the mesher Simufact refers to as 'Quadtree' which has good refinement capabilities. The first step is to ensure that the mesh fills out the entire model without any gaps or parts of it missing. The software offers an option to check the correlation of mesh against the model outline as well as measurements of deviation of the mesh from the outline of a model. Both options have been used, as demonstrated in the following images. When comparing the mesh against the model outline, it can be seen that the mesh is not completely matched with the curvatures of the model until it is reduced to element size 0.07mm or 0.06mm.

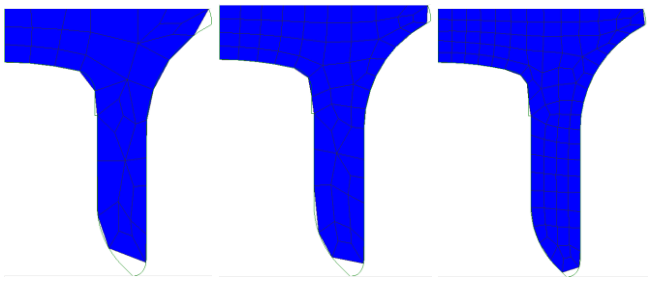

a b c

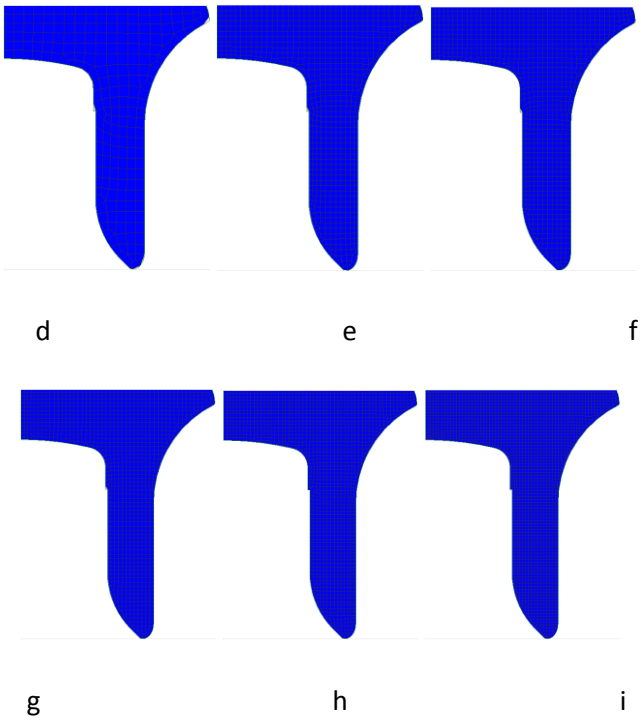

Figure 201, Outlines of mesh at different sizes

Direct comparison of mesh and model outline at different sizes - (a) 0.5mm, (b) 0.4mm, (c) 0.3mm, (d) 0.2mm, (e) 0.1mm, (f) 0.09mm, (g) 0.08mm, (h) 0.07mm and (i) 0.06mm.

This has then been checked for deviation from the shape as illustrated in the image below, and this has shown that the deviation reached zero value at 0.05mm and below. A summary of all values can be seen in the table below.

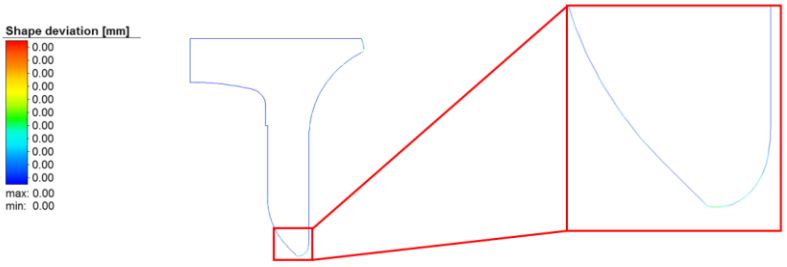

Figure 202, Deviation from the shape

Element size [mm]	Shape deviation [mm]
0.5	0.12
0.4	0.11
0.3	0.08
0.2	0.03
0.1	0.01
0.09	0.01
0.08	0.01
0.07	0.01
0.06	0.01
0.05	0
0.04	0

Table 32, Summary of element sizes checked by mesh comparison and shape deviation checks.

Having arrived at figures 0.06mm to 0.04mm, which will be applied throughout the entire rivet, a standard element size sensitivity study can now take place, whereby element size is decreased until no visible changes are occurring in the results. Remesh will retain the same characteristics as the initial mesh in terms of the element size.

To reduce the CPU time of simulation, it is possible to use a coarsening tool to decrease the size of elements in the parts of the rivet that are not in contact with smaller mesh size of the sheets as shown in Figure 203.

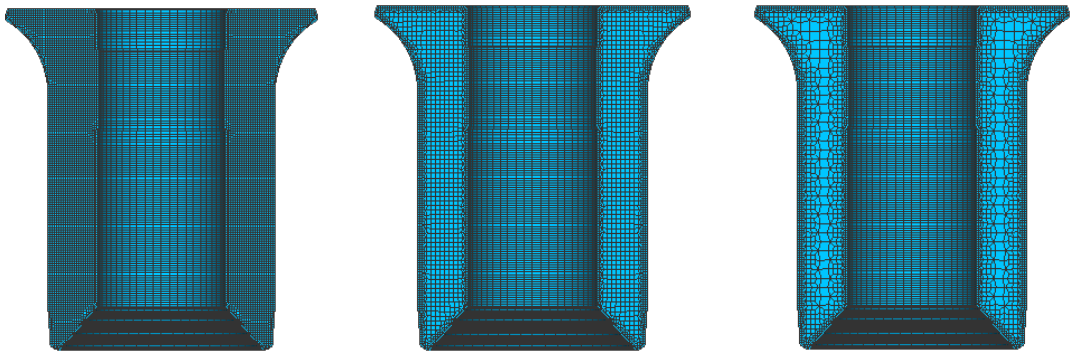

Figure 203, Coarsening of the internal part of rivet mesh, no coarsening (left), level 1 (middle) and level 2 (right)

This has found to have no/ or negligible effect on the results of simulation due to small extent of rivet deformation but introduced shorter calculation time.

Because the simulation of sensitivity study has to be to be run using sheets at the same time, it is required to set up the mesh of the sheets at the same time, this was done as described below.

6.3.4.2.2 Sheet mesh

Because the sheet needs to deform excessively to the point of splitting into two parts, the Advanced front quad mesher is used which has the option of splitting sheets. It is recommended that the rivet

and sheets are of the same or very similar size of elements so as not to cause unrealistic stresses by combining contacts of larger and smaller meshes.

This is made possible by using the segment to segment contact method which is used where there are no element size dependencies. Therefore, the sheet mesh will match that of the rivet in terms of the element size. The only difference is that this size element will be applied in the sheet only in refinement windows as opposed to the entire sheet. This is due to the fact that most of the deformation takes place around the rivet and meshing the whole sheet with a fine mesh will increase computational time. Remesh for sheets will also follow the same pattern as the initial sheet mesh.

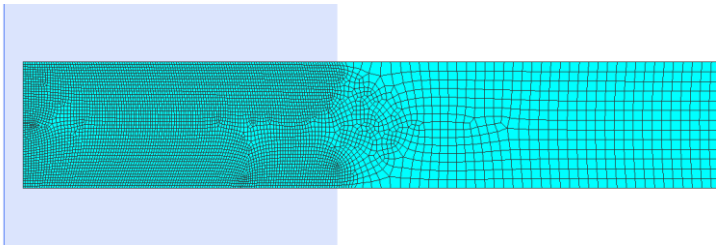

Figure 204, Axisymmetric view of mesh with refinement windows

With all three elements of the model – rivet and the two sheets having an approximate idea of element size a testing matrix can be drawn up for further sensitivity study:

Test no.	Rivet element size [mm]	Sheet element size [mm]	Sheet refinement level [element / 0.5]
Test 1	0.06	0.24	2.00
Test 2	0.05	0.20	2.00
Test 3	0.04	0.16	2.00
Test 5	0.03	0.12	2.00
Test 6	0.02	0.08	2.00
Test 7	0.01	0.04	2.00

Table 33, Test matrix – Mesh sensitivity study for sheet mesh

A physical cross section of the same joint will be used to validate any results of the sensitivity testing.

Joint:	1.5mm 6016 + 1.5mm 6016
Rivet:	C50541A (5mm long, level hardness 1)
Die:	DG09-120 (flat-bottomed, Width=9mm, Height=1.2mm)
Image:	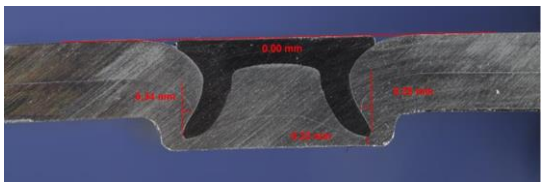
Parameter	Physical test result [mm]
Interlock:	0.37
Tmin:	0.32
HH:	0.01

Table 34, Physical joint test results

RESULTS AND DISCUSSION

Resulting measurements of simulations of incrementally changing element size as shown below.

Sample no	Rivet element size [mm]	Sheet element size [mm]	Sheet refinement level [element / 0.5]	Interlock	Tmin	HH
Test 1	0.06	0.24	2.00	0.366	0.299	-0.015
Test 2	0.05	0.20	2.00	0.359	0.31	-0.018
Test 3	0.04	0.16	2.00	0.357	0.318	-0.023
Test 5	0.03	0.12	2.00	0.382	0.385	-0.018
Test 6	0.02	0.08	2.00	0.375	0.415	0.031
Test 7	0.01	0.04	2.00	-	-	-

Table 35, Test results – Mesh sensitivity study for sheet mesh

The measurements showed a plateau in terms of similarity of measurements has been reached at value of 0.04mm element size. At the next step lower, 0.03mm, these measurements have registered a noticeable increase in value, diverging from the first few simulation results as well physical cross section. This could be potentially due to the fact that the extremely fine mesh increases the stiffness matrix causing derived unbalanced forces which can in turn lead to divergence (Markou, 2014). At this stage the simulation also took an uncharacteristically long time to complete i.e. approximately 60 minutes in comparison to the standard 30-40 minutes. The next lower increment, 0.02mm has shown the same pattern with Tmin value increased even further and simulation lasting 7 hours. The smallest last increment, 0.01mm has been terminated after 10 hours or running, classes as unfeasible.

Further complications with the simulation handling the internal small step (shown in the image below) were noted in the higher increments of the rivet geometry. The modelling was not correct in this area until it reached element size 0.04mm as shown in Figure 205.

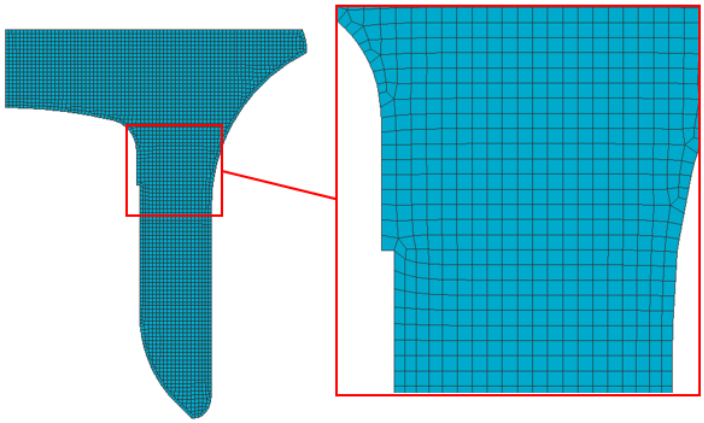

Figure 205, Internal step in geometry of the rivet

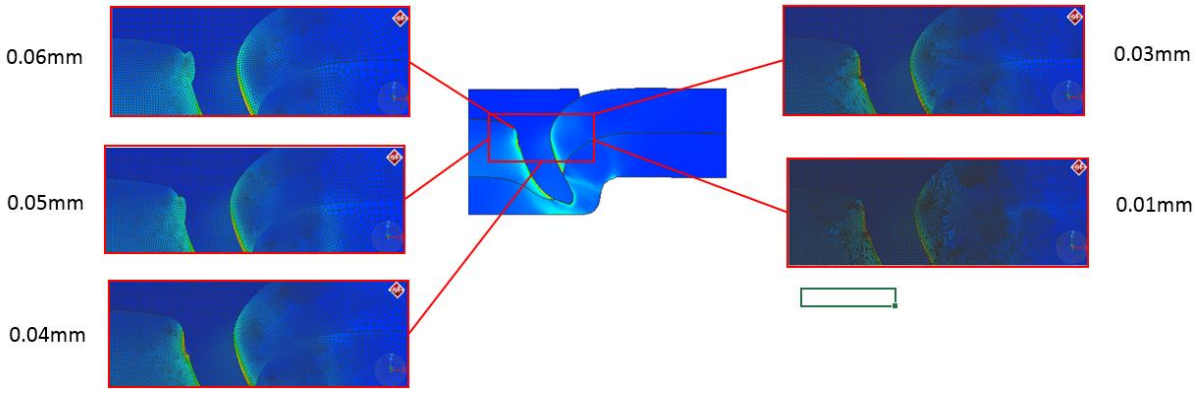

Figure 206, Modelling of the internal step in the rivet geometry

These results indicate that the ideal element size is 0.04mm which provides a good balance between the length of the simulation process and accuracy of modelling of the internal step as shown in Figure 205 and Figure 206. The issues with modelling the internal step have not, however, occurred in every joint simulation tested subsequently with element size 0.05 and 0.06mm. Therefore, element sizes 0.05 and 0.06mm would also be acceptable for using in simulation, if reducing process time takes priority.

6.3.5 Damage mechanics

INTRODUCTION

As explained in literature review, there are a number of models for modelling damage, however, most of these require additional material data which is not easy to obtain. The approach to damage taken therefore is to utilize the minimum thickness criteria mesh separation which specifies when splitting of a sheet should occur. Due to the model type selection of 2D axisymmetric mode, the simulation is

not expected to model cracking (merely areas of elevated stresses and strains potentially pointing to where cracks may be likely occur) so the minimum thickness criteria mesh separation should be sufficient for purposes of this work. The values to be used will be determined based on sensitivity study.

METHOD

A sensitivity study has been conducted involving testing increments of minimum thickness criteria at on a wide scale to see how this impacts the result of a simulation and to determine a value to be used across all simulations going forward. The study has been carried out on the joint shown below due to the fact that the moment of splitting of the sheets was been experimentally captured for this joint, this every useful evidence provides a guide to the selection of the suitable value for simulations.

Joint:	3.0mm RC5754 + 3.0mm RC5754 + 3.0mm RC5754
Rivet:	T51144A (11mm long, level hardness 4)
Die:	DG11-180 (flat-bottomed, Width=11mm, Height=1.8mm)

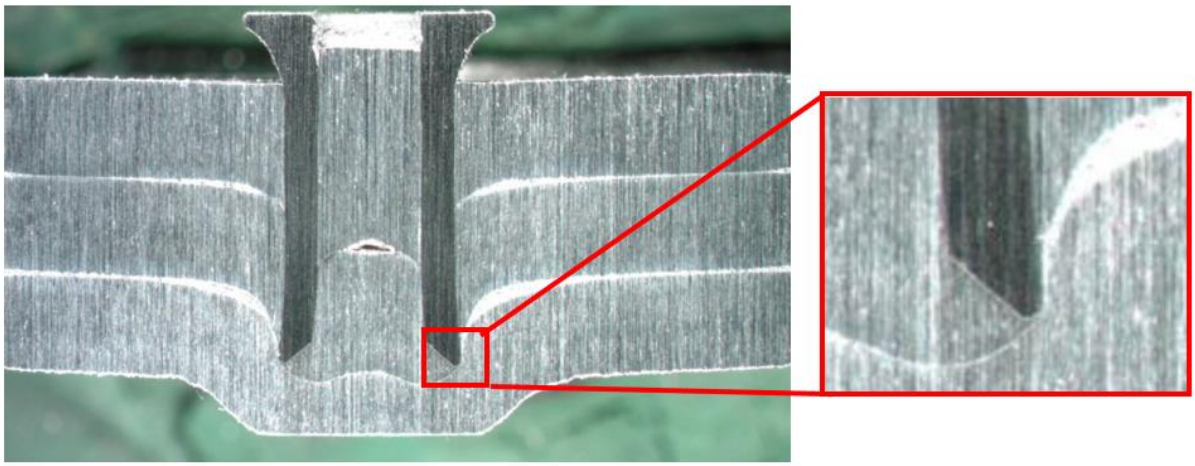

Figure 207, Example of completion of sheet piercing

The testing matrix has been drawn to include a high value of 0.5mm through to 0.1mm and then zeroes in on smaller increments from 0.04mm onwards which is the size of the element.

Test no	Thickness [mm]
Test 1	0.500
Test 2	0.100
Test 3	0.040
Test 4	0.035
Test 5	0.030
Test 6	0.025
Test 7	0.200
Test 8	0.015
Test 9	0.010
Test 10	0.005

Table 36, Testing matrix – Damage mechanics

TESTING PROCEDURE

AC procedure for sample preparation, rivet insertion and joint examination, as outlined in sections 5.1 and 5.2 has been followed.

RESULTS AND DISCUSSION

The results of tests are as per below:

Test no	Thickness [mm]	Interlock [mm]	Tmin [mm]	HH p[mm]
Test 1	0.500	0.455	0.44	0.02
Test 2	0.100	0.436	0.387	-0.036
Test 3	0.040	0.426	0.395	-0.02
Test 4	0.035	0.429	0.394	-0.017
Test 5	0.030	0.427	0.395	-0.024
Test 6	0.025	0.437	0.393	-0.021
Test 7	0.200	0.435	0.404	-0.018
Test 8	0.015	0.458	0.405	-0.022
Test 9	0.010	Simulation did not complete		
Test 10	0.005	Simulation did not complete		

Table 37, Test results – Damage mechanics

The general guideline suggested by the software of not using less than 1/3 of the element length as minimum thickness criteria has been confirmed as correct. Based on the sensitivity study on mesh size, the ideal element dimension is 0.04mm meaning that the minimum thickness criteria should be no less than 0.013mm. The two simulations with values below this figure (Test 9 and 10, 0.01 and 0.005mm respectively) did not complete and have shown signs of mesh instability prior to early termination – as shown in Figure 208.

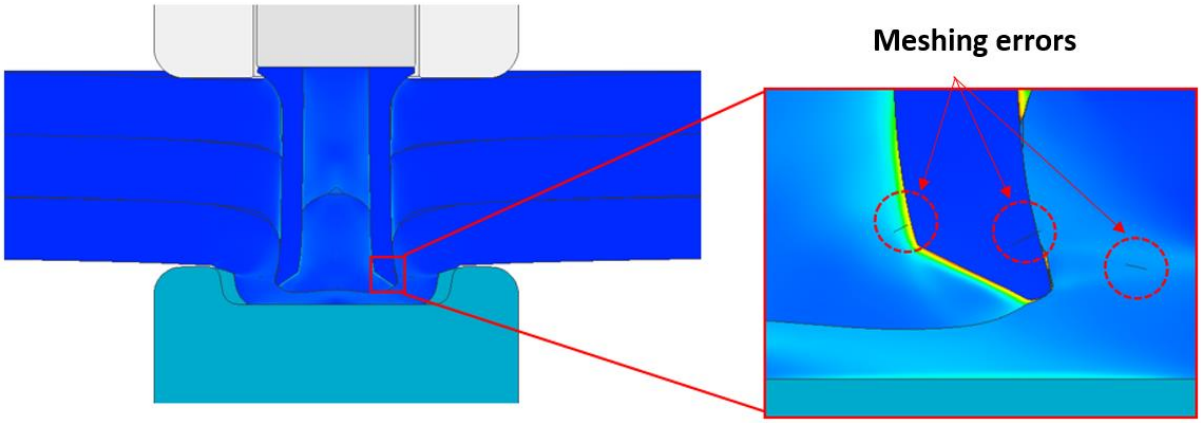

Figure 208, Mesh instability example

In terms of measurements, the results show not much variation outside the amount that would occur in a typical 5off sample, especially where Tmin is concerned. There are, however, some trends to be identified within the interlock measurements. The simulated joint with the highest thickness criteria (0.5mm) seems to have slightly a higher interlock in comparison to the lower values of the minimum thickness criteria. This is expected, since this parameter does seem to affect how the joint is shaped – as shown below, the piercing of the material starts a lot earlier in the process and the rivet has more space to flare – as shown in Figure 208. However, the point at which the sheets are separated is unrealistic when compared to the physical joint. This kind of crack initiation as shown in image below on the left occurs in less ductile materials and is not representative of ductile behaviour of soft aluminium alloy – as shown in images Figure 209 and Figure 210

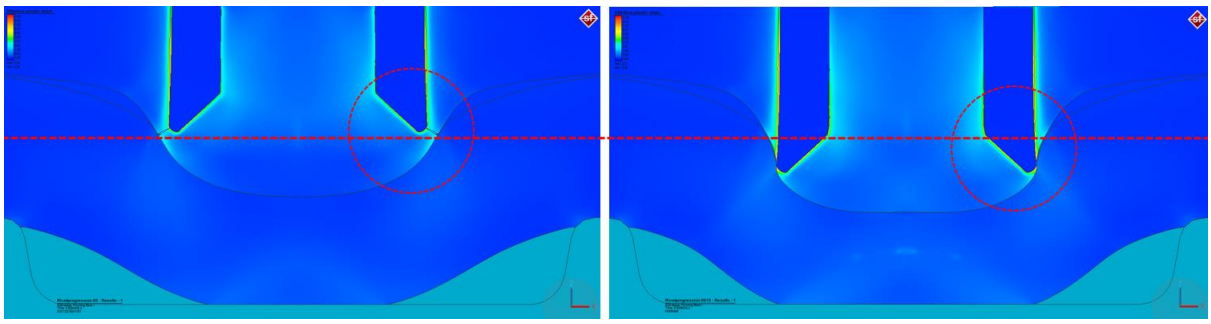

Figure 209, Comparison of minimum thickness set at 0.5mm (left) and 0.015mm (right)

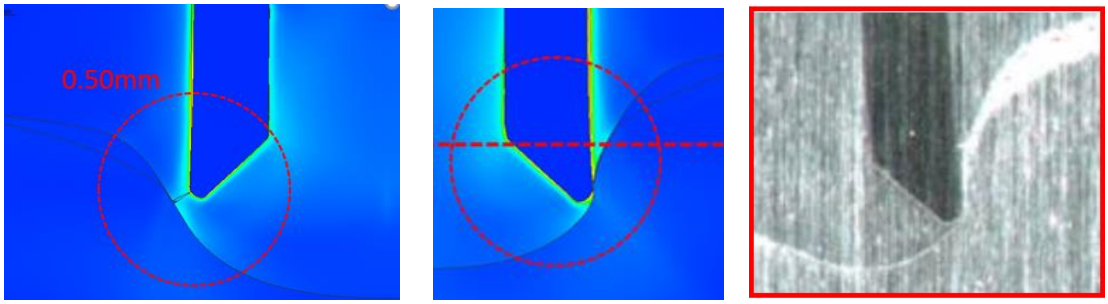

Figure 210, Zoomed in view of comparison of minimum thickness of material vs physical test

Based on this requirement for ductility, the smallest possible minimum thickness value that the software is able to handle, 0.015mm has been has been selected to be used from here onwards.

This has been tested on two standard joints which provided similar results.

The images completed with higher value for minimum thickness criteria and their resemblance to behaviour of steel have raised a question as to whether a different setting should be set to steel sheets as the level of ductility is not considered to be the same as in aluminium and the image above.

Therefore another test was completed on a joint with a steel DP600 as bottom sheet to determine the minimum distance. The resulting image has shown that the material has cracked at 0.08mm which will be used as minimum setting for the less ductile steels in simulations from here onwards. This is in line with suggestions from Simufact that this parameter be set based on physical testing.

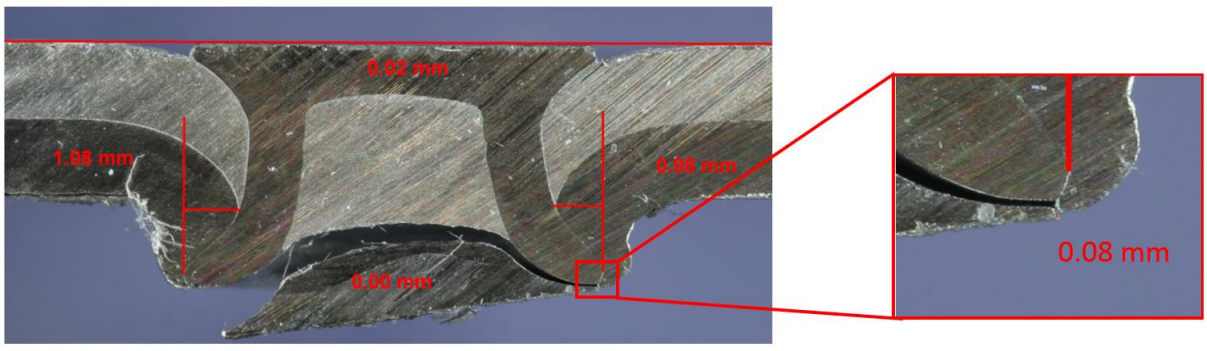

Figure 211, Example of lower ductility displayed by DP600.

6.3.6 Temperature effects

Although SPR is a cold forming process, the work the materials do during the insertion, such as forming and piercing, is translated into heat. Alongside with friction, this is an underexplored subject as the extreme speed of the process and size of the joint make it very difficult to measure the temperature. The assumption is that the rivet tip and legs might reach quite high temperature during the insertion,

however, this is not supported by the fact that the coupon can be easily touched by hand during and straight after insertion without burning fingers. It is only when setting at least 20 joints in a quick succession in a strip next to each other that the metal starts feeling slightly warm. A single joint (riveted with small 40mmx40mm coupons) does not register any difference in temperature. It is suggested that this can be explained either by the fact the heat quickly dissipates into the surrounding areas or the joint that do not heat up or this is a process of adiabatic heating (Baylin, 1994).

Due to verification of the thermal properties' values described earlier in this work such as dissipation factor, specific thermal capacity and thermal conductivity with the software engineers and the subsequent verification of sources of these, an assumption has been made that these thermal properties' values are correct for modelling purposes and therefore no sensitivity study has been conducted on these. The focus of testing is instead on:

- Measuring the temperature in the joint and comparing this with the temperature provided by software to determine in how close an agreement these are.
- Determining effect of using flow curves obtained at different temperatures on the calculation of the temperature in the joint. Ultimately, if the flow curve part of calculations does not improve accuracy, it can be neglected as obtaining flow curves at high temperature is a very costly process.

It is not feasible to generate full strain flow curves for all materials and their individual batches as this would be an incredibly expensive process.

The simulations were completed for a randomly selected joint with a model that is the closest to the Henrob physical insertion process, as established in previous chapters. The details of the joint parameters set up are below:

Joint:	1.2mm AA5182 + 2.0mm AA5182	
Rivet:	C50641A (5mm long, level hardness 1)	
Die:	DP09-175 (profiled, Width=9mm, Height=1.75mm)	
	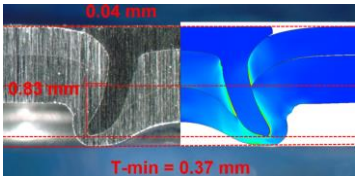	
Parameter	Physical test result [mm]	Simulation result [mm]
Interlock:	0.83	0.782
Tmin:	0.37	0.384
HH:	0.04	-0.021

Table 38, Test results – Verification joint

The joint is in a good agreement with a physical cross section (as per below image) so the joint can be analysed for temperature.

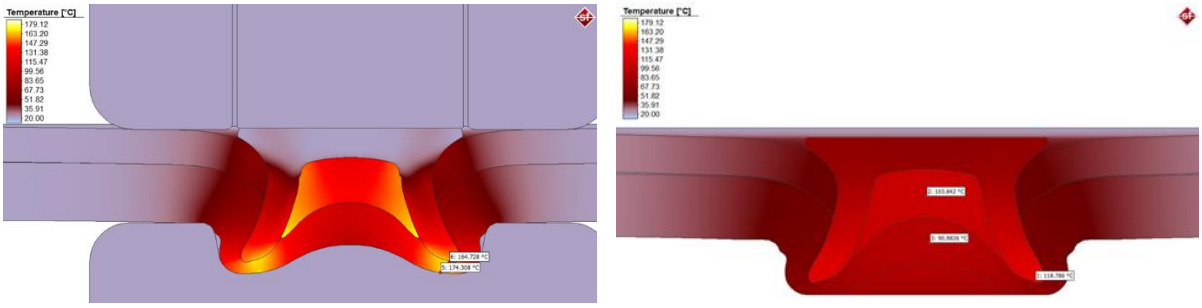

Figure 212, Highest temperature shown in the joint is showing at 179° in the hotspots.

A check of temperatures in various areas of the simulated joint has confirmed the presumptions made by engineers in Atlas Copco, by showing a rather high temperature in some parts of the insertion process and specific parts of the rivets – as shown in Figure 212.

The joints seems to reach the highest temperature (174°C) in the bottom sheet and the tip of the rivet at the point of almost full insertion. The chart seems to indicate that the highest temperature indicated is 179°C which however could not be pinpointed – presumably this is a small hotspot within the area of the high temperature.

These results are insightful, however, it is impossible to know if they are realistic as they have not been verified against a temperature measurement of a physical result. The simulations results could easily be over or under estimating the temperature of a real joint. Therefore some attempts at testing the temperature of the joint have been conducted and will be detailed in the next few paragraphs.

Measuring temperature inside a joint is a rather difficult aim since the process of insertion is extremely fast. A few methods of measurements were considered:

- Thermal strips
- Non-contact digital thermometer
- Thermocouple

6.3.6.1 Thermal strips

This option would be ideal to measure the temperature inside the joint by being applied to the surface of one of the sheet and placed between the sheets.

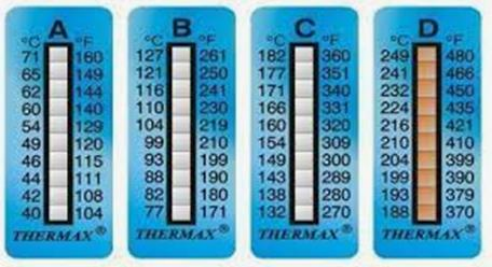

Figure 213, Thermal strips

However, to be able to measure inside the joint, the strip would have to be pierced and subsequently damaged which would not provide any measurements. By attempting to save them from damage they could be placed farther away from the centre of the joint which, however, would not capture any results as that part of the sheet stays cool throughout the insertion. This option has therefore been disregarded.

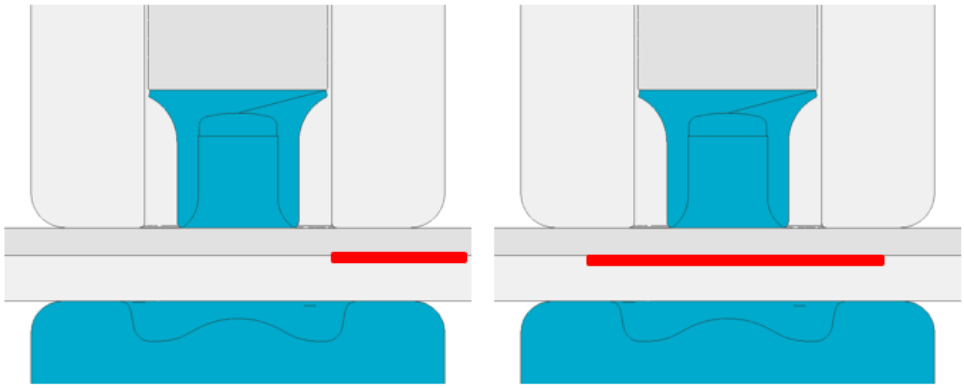

Figure 214, Examples of where thermal strips might be placed.

6.3.6.2 Non-contact digital thermometer

The second option was to use the non-contact digital thermometer. Due to ease of use and availability, this option has been tested on a number of joints being riveted in the lab but unfortunately no change of temperature has been registered on the thermometer and the reader remained at 20°C at all times.

Figure 215, Illustration of the non-contact handheld thermometer

6.3.6.3 Thermocouple

The next option was to use thermocouple, which is another type of temperature measuring device. However, simply affixing the thermocouple on the outside of the top coupon yielded similar results to the non-contact thermometer, i.e. no change in temperature.

Figure 216, Thermocouple

METHOD

The idea was to insert a thermocouple inside the joint, this would lead to inevitable damage of the thermocouple as it would be cut half way through the insertion. However, the thermocouple would be saving data until the moment it is destroyed and some insight could be gained from this exercise.

The parameters of joint selected for this exercise are as per below:

Joint:	1.5mm 6016 + 1.5mm 6016
Rivet:	C50541A (5mm long, level hardness 1)
Die:	DG09-120 (flat-bottomed, Width=9mm, Height=1.2mm)

A J-type thermocouple was embedded horizontally inside the middle of the bottom sheet (as shown in the image below) and the temperature was recorded using a 100 data/sec as speed data logger. The logger recorded the data until the flow of the die material flowing into the die cut off the wire leading to the thermocouple.

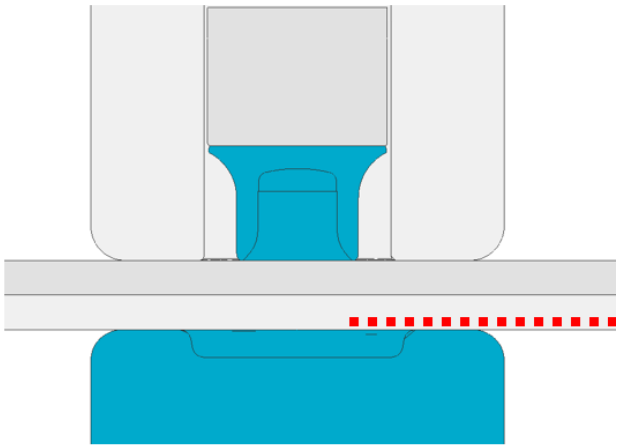

Figure 217, Schematic view of placement of thermocouple

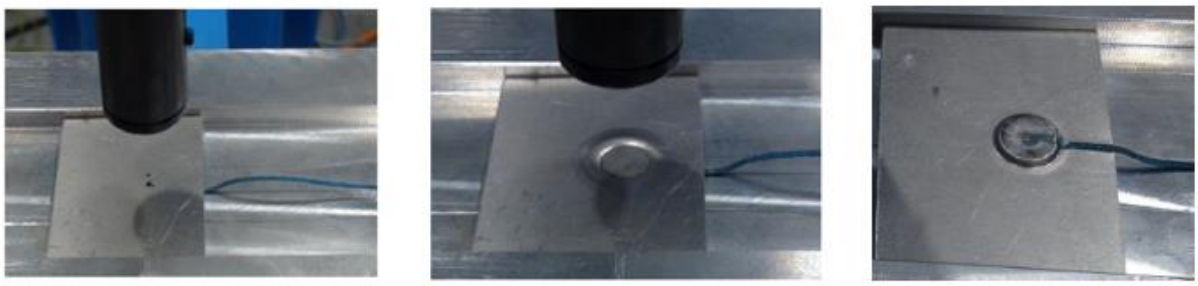

Figure 218, Thermocouple embedded in the sheet

A simulation of the same joint was made. As before, this was done with the simulation model using the settings resulting from the test conducted by author in previous stage of establishing the closest simulation model to the AC process. The simulation result is in a good agreement with the physical test in terms of the appearance as well as measurements.

Joint:	1.5mm 6016 + 1.5mm 6016	
Rivet:	C50541A (5mm long, level hardness 1)	
Die:	DG09-120 (flat-bottomed, Width=9mm, Height=1.2mm)	
Image:	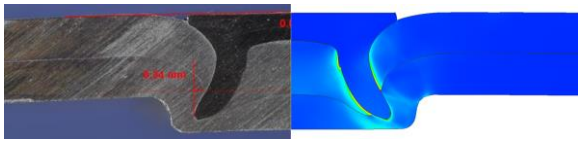	
Parameter	Physical test result [mm]	Simulation result [mm]
Interlock:	0.37	0.364
Tmin:	0.32	0.352
HH:	0.01	-0.009

Table 39, Test results - Verification joint

The temperature of the physical test with thermocouple joint has been recorded in a graph and compared with a graph of temperature evolution in two different locations within the joint where the thermocouple has likely been taking measurements from during the insertion.

The physical test results have confirmed that despite the joint feeling cool to touch during and straight after the insertion, the inside of the joint does reach quite high temperatures. The highest temperature recorded by the thermocouple was over 100°C which seems to be in close agreement with the highest temperature achieved in simulation in that specific part of the simulation model which was the bottom sheet. It should be noted the legend in Figure 219 is showing much higher temperatures such as 185°C, this is a location closer to the rivet tip than the thermocouple.

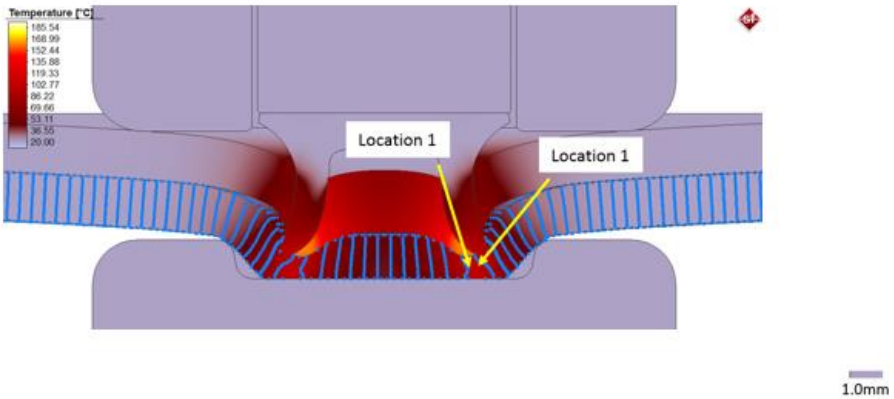

Figure 219, Temperatures captured in simulation

TESTING PROCEDURE

Due to its complexity, physical test has been carried out by Spanish research Institute Tecnalia. The testing procedure is compliant with AC procedure for sample preparation, rivet insertion and joint examination, as outlined in sections 5.1, following purchase of AC equipment by Tecnalia and training received on SPR riveting.

A simulation process, as outlined in section 5.2, has been followed.

RESULTS AND DISCUSSION

Temperature measurements of the experimental joint as well simulation have been compiled into a graph for easy comparison - as shown below. Although the evolution of the temperature is not identical, the trend seems to be similar and it is considered that this exercise has proven that the temperatures the software is calculating for that particular are within a range that could be expected in a physical test and is not extremely over or under estimated. Some differences could be attributed to characterisation of the material and a number of other variables within the simulations.

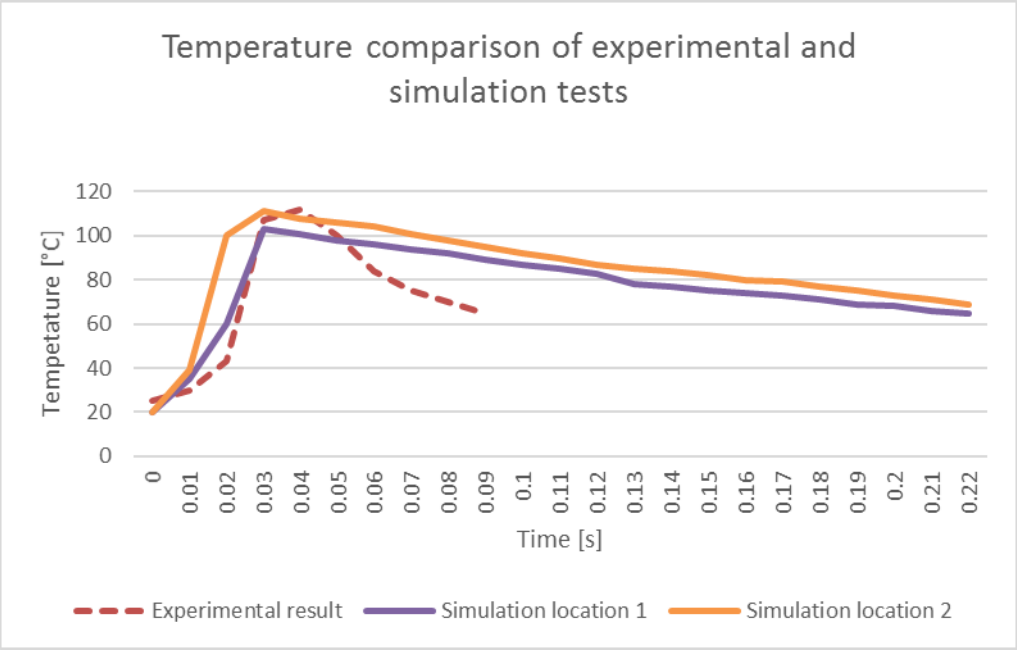

Figure 220, Test results – Temperature comparison of experimental and simulation tests

A cross check of the recorded temperature (T~100°C) with effective stress (σ=245MPa) and plastic strain (ε=0.12) readings of 6016 material in the simulation shows that the material is roughly representative of stress and strain behaviour at this point which provides a further confirmation (Simões et al, 2018).

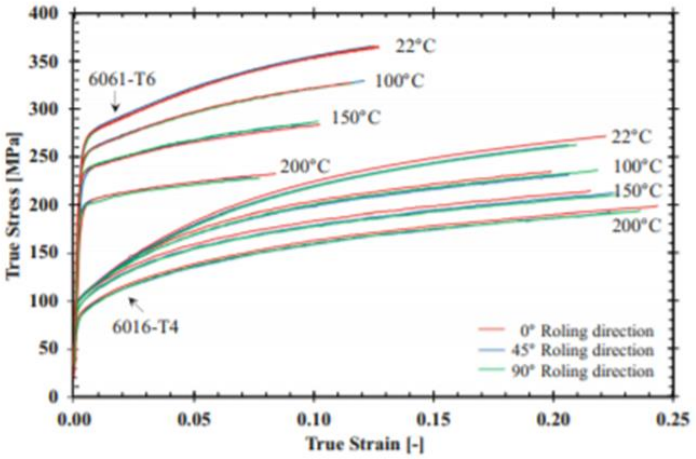

Figure 221, Flow curves captured at various temperatures (Simões et al, 2018)

Having achieved partial measurements of the temperature, a test attempting measuring the temperature for longer was designed. This was done by using a thermocouple wire coming in from below the joint by making a hole for feeding the wire in the die cavity.

TESTING PROCEDURE

Physical test has been carried out by Spanish research Institute Tecnalia. The testing procedure is compliant with AC procedure for sample preparation, rivet insertion and joint examination, as outlined in sections 5.1, following training given to Tecnalia on SPR riveting.

A simulation process, as outlined in section 5.2, has been followed.

Details of joint selected for this study is per below:

Joint:	1.5mm 1500 MPa Usibor + 1.5mm 6016
Rivet:	BG0446A (4mm long, level hardness 6)
Die:	DG08-200 (flat-bottomed, Width=8.0mm, Height=2.0mm)

The joint was selected due to the fact that joining of dissimilar materials such as steel to aluminium and specifically use of usibor (22MnB5) are increasingly requested by automotive manufacturers and therefore are very likely to be frequently used. It would be useful to know what are the temperature would be in a joint using one of the hardest materials currently used in the industry.

Usibor is a hot formed grade of steel specifically designed for automotive industry by Arcilor Mittal and due to its high mechanical strength allows 30% to 50% weight saving as opposed to other cold rolled grades (Matweb.com, 2019).

In this instance, the thermocouple was embedded vertically inside the die (as illustrated in the below image) by machining a hole in the die. This allowed the data logger to record data for longer before the wire leading to the thermocouple is damaged by the flow of material.

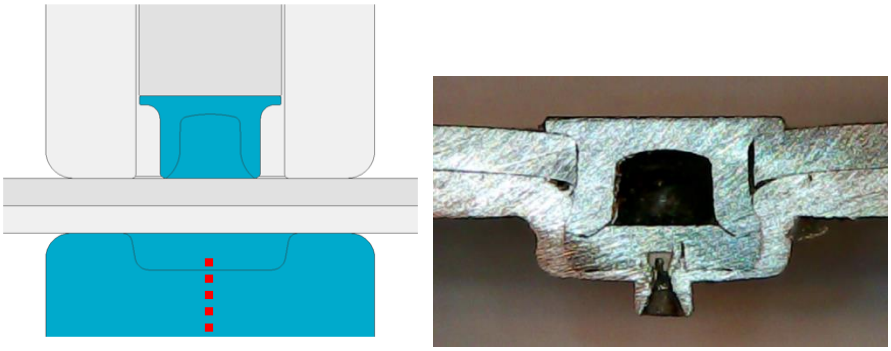

Figure 222, Schematic view of the sample (left) and a completed physical sample (right)

As before, the joint was reproduced in a simulation using the following parameters. The initial agreement between physical and simulation tests for this joint was unsatisfactory when values of friction for a standard rivet were applied. However, we then found out that the BG rivet used had the same low friction coating that has been used for T rivets, the friction values in the model were then adjusted which resulted in a much improved agreement – as per below results table:

Joint:	1.5mm 1500 MPa Usibor + 1.5mm 6016	
Rivet:	BG0446A (4mm long, level hardness 6)	
Die:	DG08-200 (flat-bottomed, Width=8.0mm, Height=2.0mm)	
	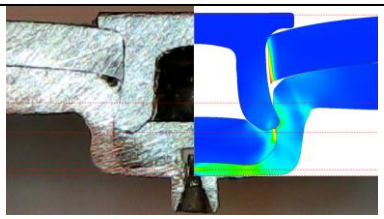	
Parameter	Physical test result [mm]	Simulation result [mm]
Interlock:	0.30mm	0.257mm
Tmin:	0.21mm	0.332mm
HH:	0.30mm	0.243mm

Table 40, Test results – Verification joint

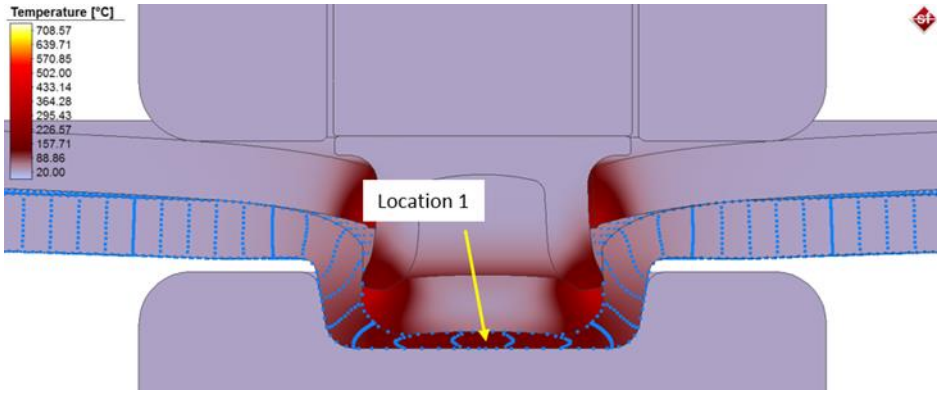

Figure 223, Temperatures captured in simulation

RESULTS AND DISCUSSION

As with the previous test, the data has been compiled into one graph for easy comparison. Again, the trends of rising temperature and cooling down seems to be similar. The software is showing temperature spike higher roughly by 30°C, this may be an over estimation, but a 30 degrees difference is close enough to be useful as we are looking to see if we can detect temperature increases of hundreds of degrees.

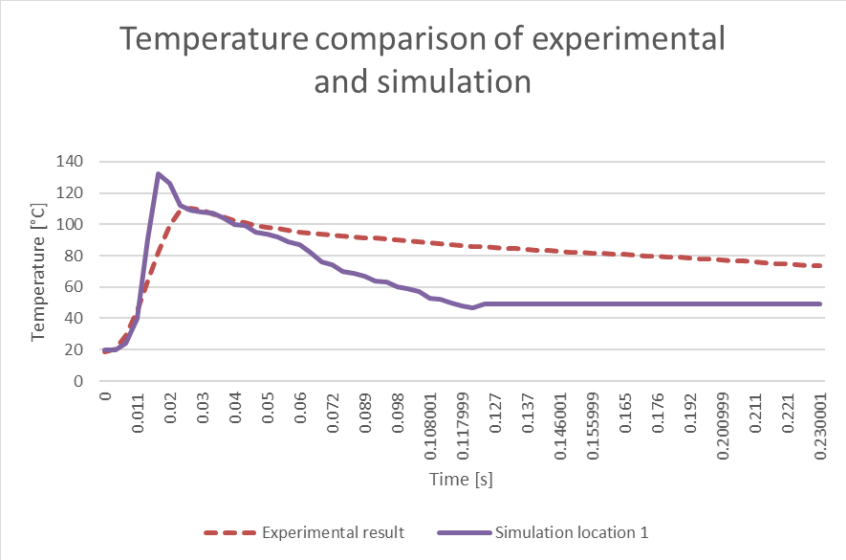

Figure 224, Test results – Temperature comparison of experimental and simulation tests

Having confirmed that the software is giving a reasonably close estimation of temperature throughout the insertion process it is now possible to move onto the next topic for the sensitivity study.

- Velocity of insertion
- Friction

Studying the effect of these two parameters may serve as confirmation that the model is correct, especially in case of friction.

6.3.7 Materials characterisation

As mentioned in chapter 4.1.3.2, material characterisation in context of SPR is predominantly centred on creation of flow curves as the main descriptor of material behaviour during plastic deformation. Importance of correct flow curves is therefore essential for accurate simulations as shown in the example of joint simulations. The flow curves are usually input as a .csv data sheet or the software's graph tracing option can be employed in cases where only a curve is available as opposed to a data sheet. Flow curves are individually added to each material entry used in the software.

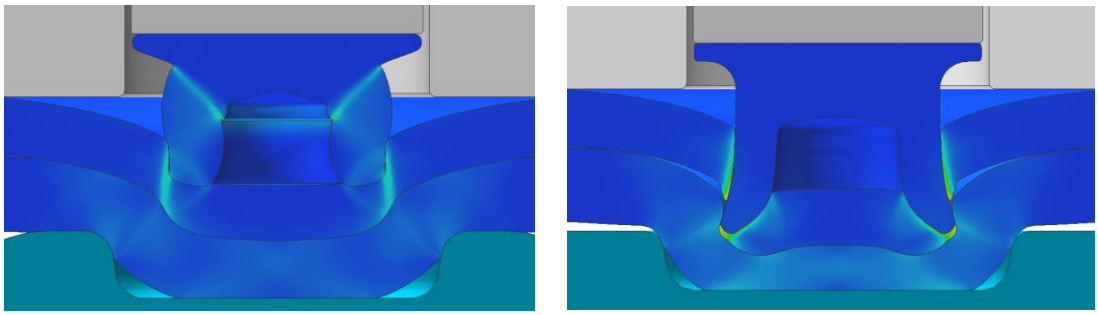

Figure 225, Joint with the same material, left – poorly defined flow curve, right – good quality flow curve.

It should be noted that any mechanical testing and extrapolation are considered in context of the sheet materials to be joined. The rivet materials for all seven currently produced rivet hardness levels have been mechanically tested at a number of strain rates (0.1, 1.0, 10.0, 100.0 1/s) and temperatures (20, 100, 200, 250, 300 °C) and mathematically extrapolated by a university research laboratory at Vienna University of Technology (2015) to the strain value of 0.35. This leaves only the planar sheet materials in need of material characterisation.

6.3.7.1 Comparison of flow curves from different types of mechanical tests

INTRODUCTION

As established in the literature review, there are a number of ways to generate initial data for flow curves. However, there are no guidelines currently available on what is the best data collection method for flow curve to be used for SPR (Kraus, 2018). Therefore a project has been set up to determine this data by a collaborative partnership which with a German research institute,

Fraunhofer IWU. As a first part of this research a number of tests were used to generate flow curves and they will be tested as part of this thesis to evaluate the available methods by being compared to physical tests.

METHOD

Five different flow curves for 5xxx series aluminium alloy AA5182 have been tested as part of this project and therefore are available to test in simulations so far. The flow curves were obtained by testing lab at Fraunhofer IWU and used following methods - compression, tensile, stack compression, in-plane torsion and hydraulic bulge test at quasi-static strain rates and ambient temperature of 20°C.

All flow curves are using Hockett and Sherby extrapolation method which was found in the literature review to be the most suitable for SPR. Five joints in total were tested, each with all five flow curves and compared to a physical sample of the same joint.

The simulations were run with the latest simulation model which uses the mesh, clamp, press and friction settings selected based on the sensitivity studies completed thus far and validated on numerous joints as part of this work.

The performance of the flow curves will be assessed based on the agreement they have with the verification physical test.

TESTING PROCEDURE

A simulation process, as outlined in section 5.2, has been followed with material definitions supplied by Fraunhofer IWU as per below:

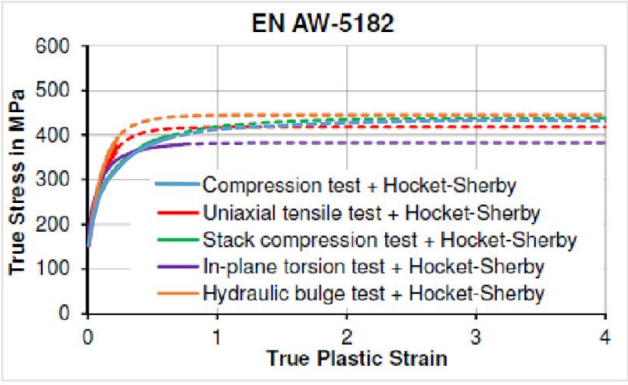

Figure 226, Flow curves generated as part of the flow curve standardisation of flow curves project (Jäckel, M. et al, 2018)

The flow curves will be tested on the following joints:

Joint 1:	1.2mm AA5182 + 2.0mm AA5182
Rivet:	C50641A (6mm long, level hardness 1)
Die:	DP9-175 (profiled, Width= 9.0mm, Height=1.75mm)

Joint 2:	2.0mm AA5182 + 1.5mm AA5182
Rivet:	C50641A (5mm long, level hardness 1)
Die:	DP09-175 (profiled, Width=9mm, Height=1.75mm)

Joint 3:	1.2mm AA5182 + 3.0mm AA5182
Rivet:	C50644A (5mm long, level hardness 4)
Die:	DG09-180 (flat-bottomed, Width= 9.0mm, Height=1.8mm)

Joint 4:	2.0mm AA5182 + 1.7mm AA5182
Rivet:	C50641A (6mm long, level hardness 1)
Die:	DP09-175 (profiled, Width=9mm, Height=1.75mm)

Joint 5:	1.0mm AA5182 + 1.5mm AA5182
Rivet:	C30441A (3mm long, level hardness 1)
Die:	DF07-130 (profiled, Width=7.0mm, Height=1.3mm)

RESULTS AND DISCUSSION

All five joints were simulated with the each of the flow curves with all results compiled below.

Measurements:

Joint no.	Test type	Interlock [mm]	Tmin [mm]	HH [mm]
Joint 1	Physical test	0.78	0.39	0.04
	Compression	0.618	0.454	0.011
	Tensile	0.646	0.53	0.009
	Stack compression	0.639	0.437	0.022
	In-plane torsion	0.717	0.445	0.026
	Hydraulic bulge	0.6	0.623	0.008
Joint 2	Physical test	0.62	0.53	0.02
	Compression	0.32	0.597	0.006
	Tensile	0.355	0.595	0.021
	Stack compression	0.292	0.599	0.021
	In-plane torsion	0.402	0.579	0.023
	Hydraulic bulge	0.292	0.599	0.021
Joint 3	Physical test	0.51	0.47	0.01
	Compression	0.472	0.49	0.019
	Tensile	0.505	0.507	-0.033
	Stack compression	0.462	0.471	-0.02
	In-plane torsion	0.446	0.409	0.018
	Hydraulic bulge	0.512	0.596	0.051
Joint 4	Physical test	0.52	0.55	0.03
	Compression	0.388	0.691	0.019
	Tensile	0.395	0.687	0.017
	Stack compression	0.391	0.688	0.015
	In-plane torsion	0.449	0.66	0.024
	Hydraulic bulge	0.343	0.697	0.022
Joint 5	Physical test	0.37	0.38	-0.03
	Compression	0.232	0.412	0.014
	Tensile	0.235	0.434	0.017
	Stack compression	0.234	0.386	0.022
	In-plane torsion	0.315	0.373	0.015
	Hydraulic bulge	0.1981	0.492	0.012

Table 41, Test results – Material definitions using results from different mechanical tests

Visual attributes:

Due to a large number of images only the best and worst case scenario are shown.

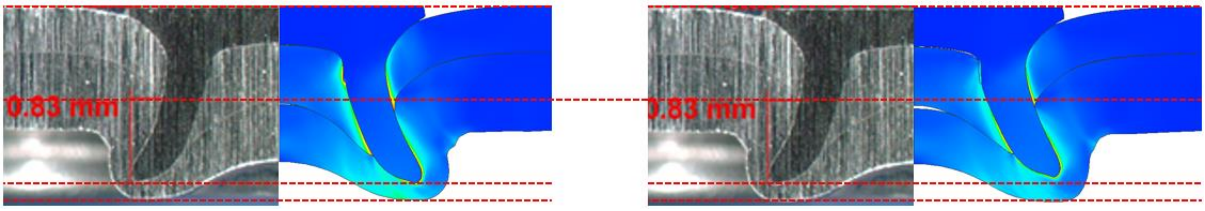

Figure 227, Joint 1 - In-plane torsion test visual results on the left, hydraulic bulge test results on the right.

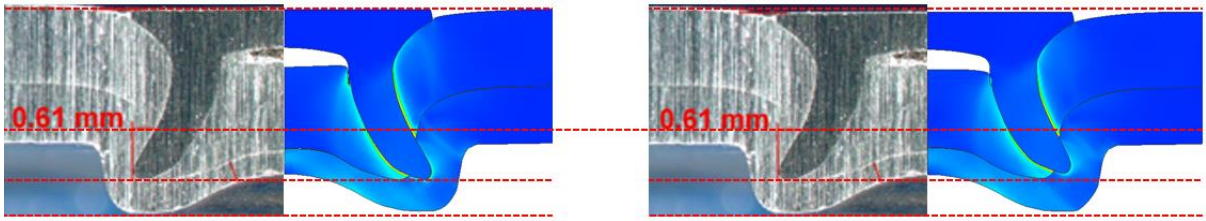

Figure 228, Joint 2 - In-plane torsion test visual results on the left, hydraulic bulge test results on the right.

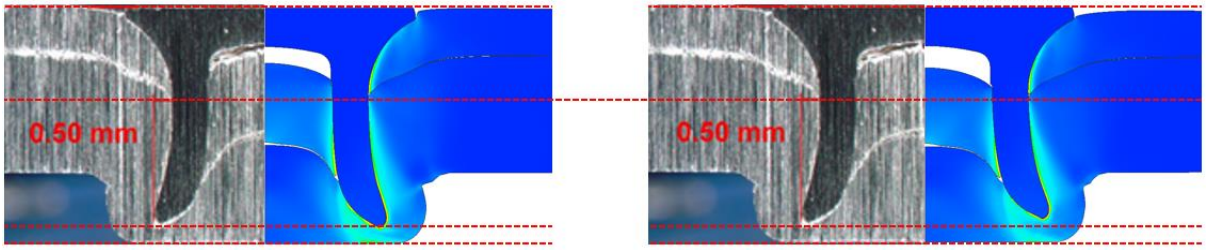

Figure 229, Joint 3 - In-plane torsion test visual results on the left, hydraulic bulge test results on the right.

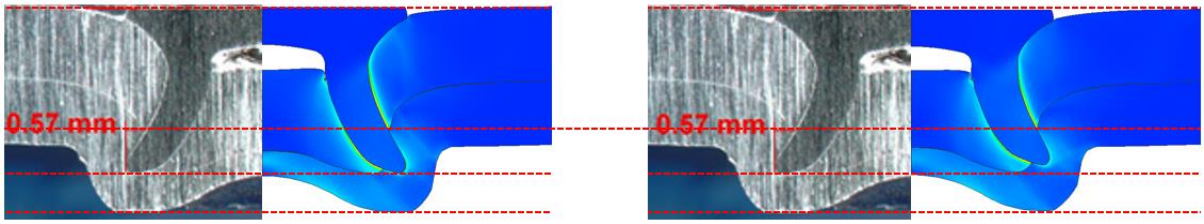

Figure 230, Joint 4 - In-plane torsion test visual results on the left, hydraulic bulge test results on the right.

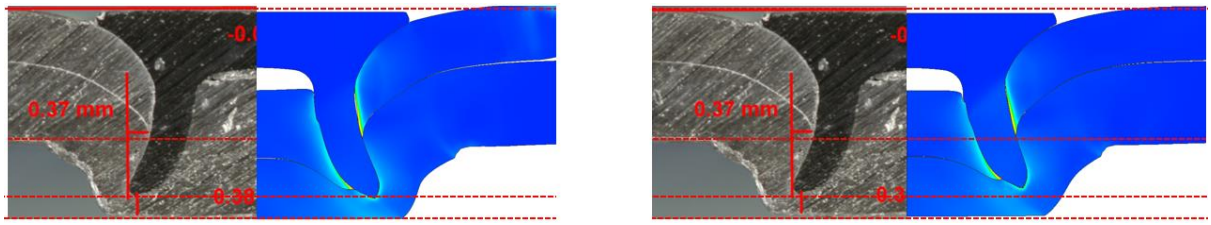

Figure 231, Joint 5 - In-plane torsion test visual results on the left, hydraulic bulge test results on the right.

Whilst all the flow curves generally provided some level of agreement with the respective physical tests and physical features, the flow curves from in plane torsion tests are on average appearing to be most similar, most consistently. This is the case across all joints except joint 2, where in-torsion plane test interlock varies by 0.2mm which is outside the tolerance of the simulation vs physical test agreeability score. However, in this instance, the remaining methods were even further away from the physical joint measurements than in-plane torsion test. This error was seen to be consistent across all methods in case of this specific joint due to which it is deemed to be caused by some other variable involved in the process. The exact cause remains unclear at this point in time. The results provided by compression, stack compression and tensile tests were close behind the in-plane torsion test when compared to the physical sample, which is a positive result since these two methods are most commonly available and can be executed by an Instron machine with the correct fixtures.

The confirmed suitability of the in-plane torsion method would concur with opinions of some researchers in the field of material forming and characterisation such as Armostrong, Hockett and Sherby (1982) and Raabe (2019).

The method that gave the least agreeable results most consistently is the hydraulic bulge testing with an upwards step change in rivet compression across all five joints. When looking at the individual flow curves provided for each test, it is clear the hydraulic bulge testing would appear to be the hardest of the materials with flow curve reaching the value of 440 MPa at its highest point which would explain the compression of the rivet. When compared to the in-plane torsion which is reaching the lowest value of all flow curves, 370 MPa at its highest point, it is clear that these two flow curves are at the extreme ends of the scale.

With any flow curves, a difference of 70 MPa is expected to have an impact on the result. It could also be due to the fact that was mentioned earlier in the literature review, suggesting the hydraulic bulge test does not identify the starting point of the flow curve, i.e. yield stress with great accuracy which can be compounded by extrapolation and reach higher hardness levels.

In conclusion, whilst the in-plane torsion type of test might be correct for this particular material, more research might need to be done to further validate this result, especially with other, dissimilar types of materials such as for example UHSS. Unfortunately, research of this scale is out of scope of this work and therefore, further simulation tests of most suitable material test methods will be subject to future research.

Furthermore, even the flow curves generated by less suitable testing methods have proven to give relatively good results for simulation when used with various extrapolations methods which leads to the next set of testing on power laws.

6.3.7.2 Comparison of flow curves with different methods of extrapolations

As with the mechanical tests, there also a number of laws available to extrapolate the flow curves, i.e. extent the strain rates cover the range of strains occurring in SPR insertion. As part of material characterisation examination, two additional power laws have been applied to the resulting flow curve of the in-plane torsion test discussed above, Swift and Voce. These have been compared to the power law used for the previous exercise, Hockett and Sherby.

METHOD

Same five joints have been tested as in section 6.4.1 each tested with three different power laws – Hockett and Sherby (tested as part of the above exercise, used for comparison), Swift and Voce.

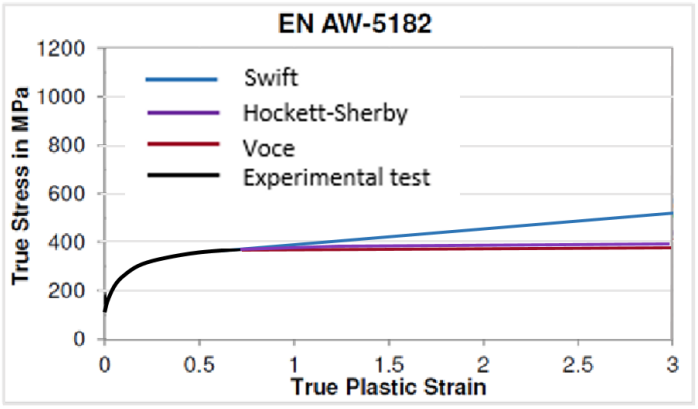

Figure 232, Extrapolation of in-plane torsion test using Swift, Hockett-Shery and Voce models

In addition, a test has been run for each joint using the un-extrapolated flow curve – noted as experimental in the graphs. This is a flow curve that has been captured up to strain rate of value 0.7. This has been included as previously it has been noted that even if a flow curve with very small range of strains has been input in the software, the simulation has ran its full course with a fairly good agreement to the physical sample. It is unclear how this happen and therefore a further examination of this aspect has been included in the test.

The simulations were run with the latest simulation model which uses the mesh, clamp, press and friction settings selected based on sensitivity studies completed and validate on numerous joints as part of this work.

The flow curves will be tested on the following joints:

Joint 1:	1.2mm AA5182 + 2.0mm AA5182
Rivet:	C50641A (6mm long, level hardness 1)
Die:	DP9-175 (profiled, Width= 9.0mm, Height=1.75mm)

Joint 2:	2.0mm AA5182 + 1.5mm AA5182
Rivet:	C50641A (5mm long, level hardness 1)
Die:	DP09-175 (profiled, Width=9mm, Height=1.75mm)

Joint 3:	1.2mm AA5182 + 3.0mm AA5182
Rivet:	C50644A (5mm long, level hardness 4)
Die:	DG09-180 (flat-bottomed, Width= 9.0mm, Height=1.8mm)

Joint 4:	2.0mm AA5182 + 1.7mm AA5182
Rivet:	C50641A (6mm long, level hardness 1)
Die:	DP09-175 (profiled, Width=9mm, Height=1.75mm)

Joint 5:	1.0mm AA5182 + 1.5mm AA5182
Rivet:	C30441A (3mm long, level hardness 1)
Die:	DF07-130 (profiled, Width=7.0mm, Height=1.3mm)

TESTING PROCEDURE

A simulation process, as outlined in section 5.2, has been followed.

RESULTS AND DISCUSSION

Joint no.	Hardening law type	Interlock [mm]	Tmin [mm]	HH [mm]
Joint 1 In-plane torsion test	Physical test	0.78	0.39	0.04
	Experimental	0.725	0.41	0.03
	Swift	0.595	0.473	0.021
	Hockett and Sherby	0.717	0.445	0.026
	Voce	0.71	0.472	0.012
Joint 2 In-plane torsion test	Physical test	0.62	0.53	0.02
	Experimental	0.403	0.607	0.019
	Swift	0.27	0.591	0.02
	Hockett and Sherby	0.402	0.579	0.023
	Voce	0.41	0.585	0.018
Joint 3 In-plane torsion test	Physical test	0.51	0.47	0.01
	Experimental	0.43	0.41	0.02
	Swift	0.299	0.283	0.015
	Hockett and Sherby	0.446	0.409	0.018
	Voce	0.462	0.449	0.008
Joint 4 In-plane torsion test	Physical test	0.52	0.55	0.03
	Experimental	0.423	0.695	0.008
	Swift	0.318	0.691	0.017
	Hockett and Sherby	0.449	0.66	0.024
	Voce	0.462	0.665	0.026
Joint 4 In-plane torsion test	Physical test	0.37	0.38	0.01
	Experimental	0.288	0.442	-0.092
	Swift	0.2	0.487	-0.076
	Hockett and Sherby	0.315	0.373	0.015
	Voce	0.298	0.496	0.025

Table 42, Test results – Material definitions using results from different extrapolation methods

The previous results obtained by Hockett and Sherby hardening law has been compiled along with other two hardening laws as well as the experimental result. It is not surprising to see from the tables that Voce and Hockett and Sherby have provided similar results given that the flow curves seem to be reaching similar values. The surprising aspect of this exercise was the results of the experimental flow curve with a very short strain range. Upon further examination of this, the discussion with the software engineer revealed that if the flow curve does not reach the necessary level of strains, it is automatically expanded in a straight line and capped at the highest value achieved. A flow curve expanded in this way is very similar to Hockett and Sherby and Voce in this particular instance which would explain the similar results. This, however, is not considered a reliable result and extrapolation should always be used. The visual aspects of all joints tested were largely similar with joint completed with Swift power law showing signs of being consistently slightly more compressed – as shown in example of joint 5 below.

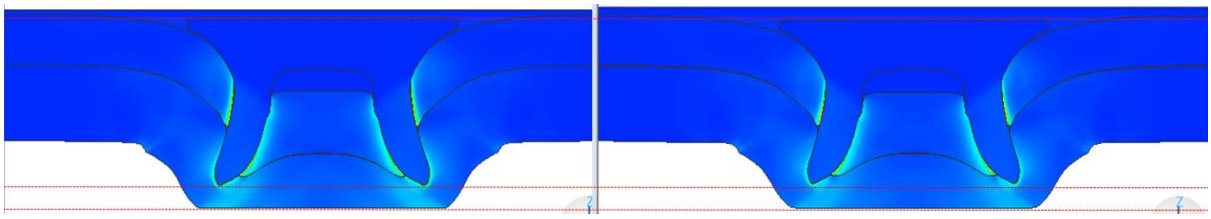

Figure 233, Example of visual result – comparison of Hockett-Sherby (left) and Swift (right) hardening laws

However, as with mechanical tests, this is a very vast area which for sure needs to be subjected to more research in the future.

6.3.7.3 Comparison of flow curves obtained under different strain rate and temperature conditions

As mentioned before, obtaining flow curves under conditions other than room temperature and relatively low strains available on tensile test machine, can provide additional accuracy for the simulation but is also prohibitively costly (figures in region of 13K per material for testing high strains and temperatures) so this option is not always available. The extent of improvement when using flow curves with a number of strain rates and temperatures (from here onwards referred to as multiple flow curves) is currently unclear as reasonably good results have been generated by using flow curves with single strain rates and temperatures (single flow curves). This chapter will therefore aim to explore this area and investigate the differences between using flow curves with multiple strain rates and temperatures. The two main intentions are to examine the effect of strain rate and temperature when used individually and to determine the contribution the multiple flow curves bring to the process in comparison to the flow curve obtained at single strain rate and temperature. To that end, the following tests will be conducted:

- Verification joint test
- Test A – examining varying strain rates
- Test B – examining varying temperature
- Test C – comparison of multiple strain rates and temperature flow curves vs single flow curve from a different source.

It should be highlighted that whilst rivet materials are just as important as sheet materials, the focus of this exercise is mainly on the sheet materials as this is currently the area of shortage for quality flow curves. The rivet materials for all currently available hardness levels have been tested by a specialist

laboratory by tensile and compression testing at up to 300 °C and 100 1/s and are unlikely to change apart from if rivets are manufactured at lower or higher hardness at upper or lower tolerances.

METHOD

The below joint has been selected for this study:

Joint 2:	2.0mm A6111T4 + 2.5mm A6111T4
Rivet:	C50642A (6mm long, level hardness 2)
Die:	DG10-140 (flat-bottomed, Width=10.0mm, Height=1.4mm)

The sheet material AA6111T4 was selected for the testing due to the fact that flow curves at different strain rates are available for this material, including a high strain rate flow curve of 150 1/s and high temperatures up to 350°C. The flow curves were generated by tensile test and the variable strain rates and temperature have been calculated using analytical models for strain rates and temperatures shown in the image below.

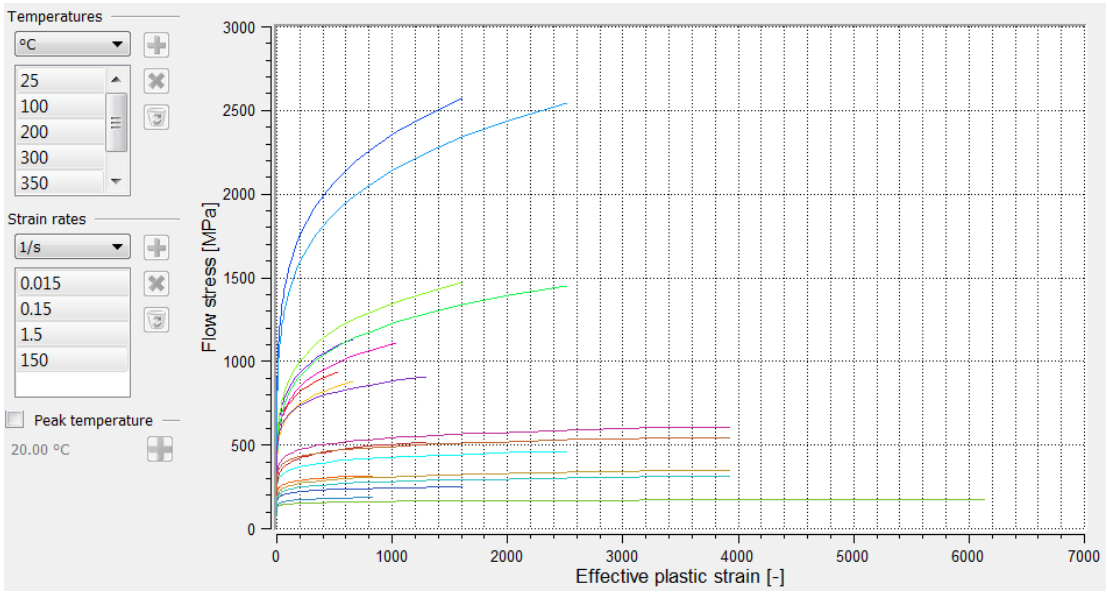

Figure 234, AA6111 material – multiple flow curve

In order to understand the effect of temperature and strain rate effect and show the impact they have on the final outcome in isolation the above flow curve has been disassembled and strain rates and temperatures were tested individually

Due to too many combinations to test, most likely combinations were selected to be tested. This involves testing flow curves at the most easily available testing temperature, i.e. room temperature with all strain rates (Tests A1 – A5) and then reversing this order and testing the most common testing strain rate, quasi-static rate, with all temperatures (Test B1 – B6) .

For purposes of comparison of single and multiple flow curves (Test C), the same flow curve used for Tests A and B has been used, however, in two reiterations – with the highest and lowest strain rate and temperatire (test C1) and with all available combined temperatures and strain rates combined (test C2). This was compared against a simulation using a single flow curve provided by a material supplier (test C3).

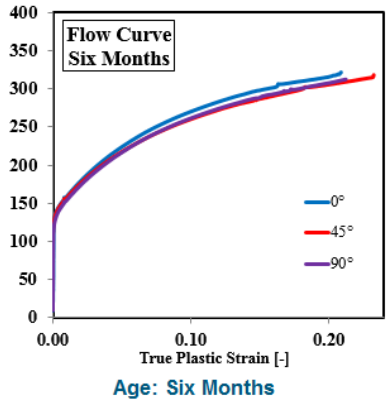

Same speed of insertion has been used for all joints used in the testing i.e. velocity 250mm/s.

TESTING PROCEDURE

A simulation process, as outlined in section 5.2, has been followed.

Testing matrices:

Test A - varying $\dot{\varepsilon}$		
Test no.	T [°c]	$\dot{\varepsilon}$ [1/s]
A1	25	0.015
A2	25	0.15
A3	25	1.5
A4	25	150
A5	25	Combined

Test B - Varying T		
Test no.	$\dot{\varepsilon}$ [1/s]	T [°c]
B1	0.015	25
B2	0.015	100
B3	0.015	200
B4	0.015	300
B5	0.015	350
B6	0.015	Combined

Table 43, Testing matrix - Material definitions using varying strain rates

RESULTS AND DISCUSSION

Verification joint

A physical cross section of a selected joint is as per below:

Joint:	2.0mm A6111T4 + 2.5mm A6111T4
Rivet:	C50642A (6mm long, level hardness 2)
Die:	DG10-140 (flat-bottomed, Width=10.0mm, Height=1.4mm)
	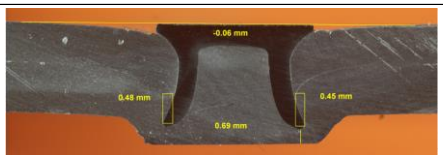
Parameter	Physical test result [mm]
Interlock:	0.47 (Avg)
Tmin:	0.75 (Avg)
HH:	-0.06

Table 44, Test result – Verification joint

Test A - Strain rate testing

Table below shows compiled measurements of tests with varying strain rate against the physical sample.

Test A - varying $\dot{\varepsilon}$					
Test no.	T [°c]	$\dot{\varepsilon}$ [1/s]	Interlock [mm]	Tmin [mm]	HH [mm]
	Physical test		0.47	0.75 (Avg)	-0.06
A1	25	0.015	0.387	0.682	0.048
A2	25	0.15	0.373	0.657	0.051
A3	25	1.5	0.361	0.576	0.017
A4	25	150	0.145	1.583	0.054
A5	25	Combined	0.264	1.178	0.042

Table 45, Test results - Material definitions using varying strain rates

Visual attributes:

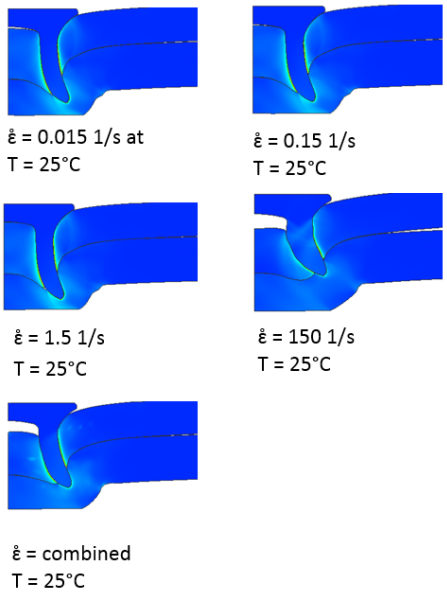

Figure 235, Axisymmetric view of results with varying strain rates.

Test B – Temperature testing

Table below shows compiled measurements of tests with varying temperature against the physical sample.

Test B - Varying T					
Test no.	$\dot{\varepsilon}$ [1/s]	T [°c]	Interlock [mm]	Tmin [mm]	HH [mm]
	Physical test		0.47	0.75 (Avg)	-0.06
B1	0.015	25	0.387	0.682	0.048
B2	0.015	100	0.361	0.497	0.047
B3	0.015	200	0.317	0.24	0.35
B4	0.015	300	Not possible to run as cold forming		
B5	0.015	350	Not possible to run as cold forming		
B6	0.015	Combined	0.341	0.357	0.035

Table 46, Test results - Material definitions using varying strain rates

The individual flow curves at 300°C could not be tested due to the software not allowing using single flow curves with temperatures over 250°C in cold forming operations such as SPR. This is because the software is written for cold forging and not for hot forging.

Visual attributes:

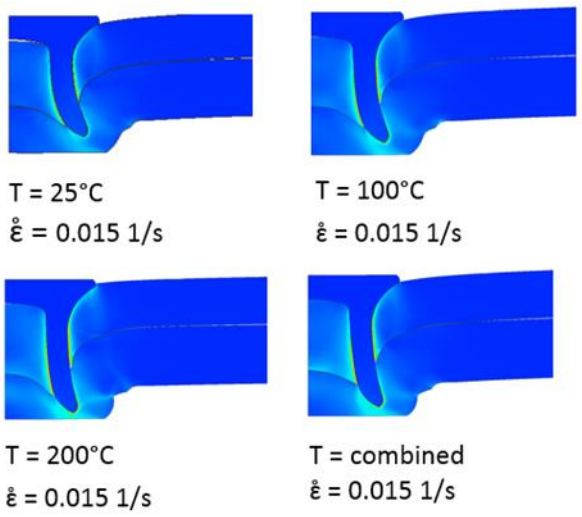

Figure 236, Axisymmetric view of results with varying temperatures.

A visual comparison has been compiled with use of grid lines for ease of comparison of the physical sample with results from simulation testing:

Strain:

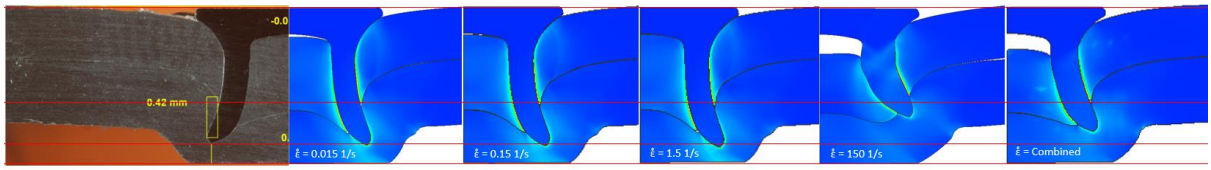

Figure 237, Varying strain rates at 25°C

Temperature:

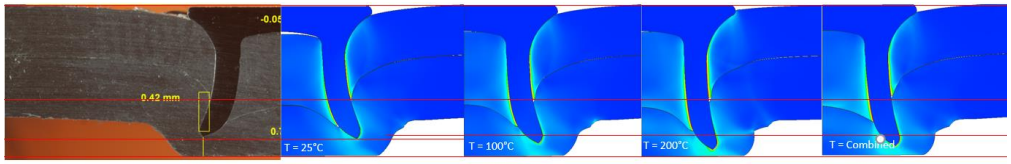

Figure 238, Varying temperatures at 0.015 1/s

In terms of the strain rate, based on both, the measurements as well as visual outputs, it would appear that should individual flow curves be evaluated, quasi-static strain at 25°C rate (test A1) provides the best match for the physical test with a variation that would be easily seen in the 5off sample. The results start to deviate further with slightly higher rates 0.15 and 1.5 1/s although still give relatively good agreement with physical cross section. However, the joint with flow curve obtained at room temperature and high strain rate of 150 1/s seems to exhibit severe buckling and compression. The joint with all strain rates combined at 25°C does not display the severe buckling the single flow curve at 150 1/s does, however, in comparison to low strain rates it displays high compression of the rivet as well as some unusually distributed strains in the sheets around the leg.

From the perspective of the temperature testing, it is interesting that the same joint with quasi-static strain rate and room temperature (A1 / B10) has presented itself as the best result when compared with higher temperatures as shown in Figure 239. The decline in agreement occurs as soon as temperature increases to 100°C and it decreases further still at 200°C, noting no improvement in the version run with all temperature flow curves combined.

Test C – comparison of multiple flow curves

Test C - Multiple flow curves vs single						
Test no.	Flow curve source	$\dot{\varepsilon}$ [1/s]	T [°c]	Interlock [mm]	Tmin [mm]	HH [mm]
Physical test		n/a		0.47	0.75 (Avg)	-0.06
C1	Multiple flow curve from test A and B	0.015 - 150 (All)	0.015 - 150 (All)	0.378	0.872	0.075
C2	Multiple flow curve from test A and B	0.015 and 150 (only)	25 and 350 (only)	0.377	0.874	0.082
C3	Single tensile test from mat. Supplier	0.001	25	0.426	0.82	0.09

Table 47, Test results - Material definitions using multiple flow curves

Visual attributes:

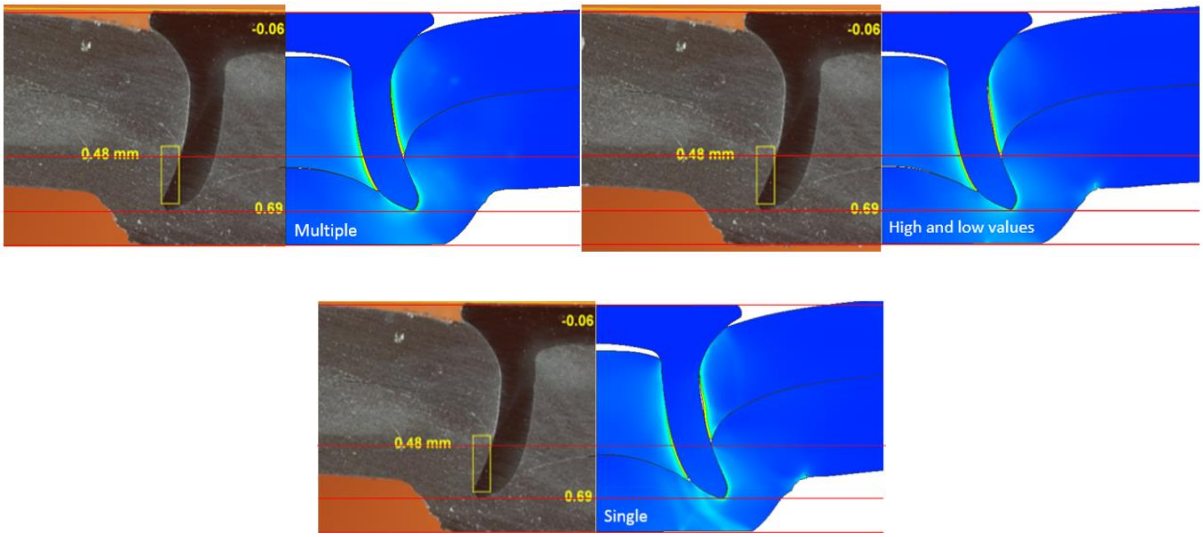

Figure 239, Comparison of multiple vs single flow curves – test C1 (top left) and highest and lowest strain rates and temperature values – test C2 (top right) and single flow curve - test C3 (bottom)

All three results appear to be within the tolerance of a simulation considered in agreement with the cross section in regards to measurements with variations similar to those in 5off samples. All display typical visual attributes of the joint where similar features seem to be replicated accurately. It should be noted that although the measurement of the Tmin is higher in simulation they still appear similar in the image because of the common differences between Tmin under each leg of the rivet in the physical sample, where the Tmin was measured in the narrowest part of the bottom sheet as shown on the visible part of the picture.

Although further testing will be completed as and when more multiple flow curves will be available to verify this outcome, based on this particular test it would appear that similarly accurate results can be achieved by both multiple a single flow curves, which is a positive results in light of cost saving. It is also interesting to see that the result at extreme ends of strain rate and temperatures scales is very

similar to using a number of flow curves which might suggest that it might be possible to reduce the high cost of making flowcurves by reducing amount of testing required.

This exercise has further pinpointed a suitable strain rate and temperature for conducting any potential in-house material testing in absence of specialist equipment such as Hopkinson split bar.

Nevertheless, obtaining material data remains a very complex area with many questions still to be yet researched in future.

6.3.7.4 Comparison of flow curves obtained at different material ages

INTRODUCTION

Another aspect that will influence the flow curves is the age of the materials as outlined in section 4.1.3.7.3 with some materials prone to age hardening. From both, physical testing and simulation point of view, this presents a problem due to changing hardness of samples (for example the project might be deferred until other materials arrive) as well as during testing itself. Some projects can stretch over several months and this can lead to inconsistent results over the time due to material age hardening. A fresh supply of AC600T4 alloy will give different results when compared to joints completed with AC600T4 that has been stored in a laboratory over few year.

Consequently, if a combination of rivet and die has been suggested to an automotive supplier based on testing with 1 month old AC60T4 but in production six months old AC600T4 is used (or vice versa), this might have undesirable effects on marginal joints.

Another concern is shipping of materials such as the real life scenario of transport of AC600T4 from location of manufacture (UK) to location of use (eg. Singapore) where due to logistical complexities, the transport can take up to several months. Depending on how old are the sheets before the shipping commences, it is quite possible that the sheets will significantly age harden.

An awareness of how the age of material impacts the resulting joints would be beneficial and therefore, an exercise of simulation of aged hardened materials has been conducted.

METHOD

Three different flow curves of material AC600T4 have been provided by a material supplier upon request:

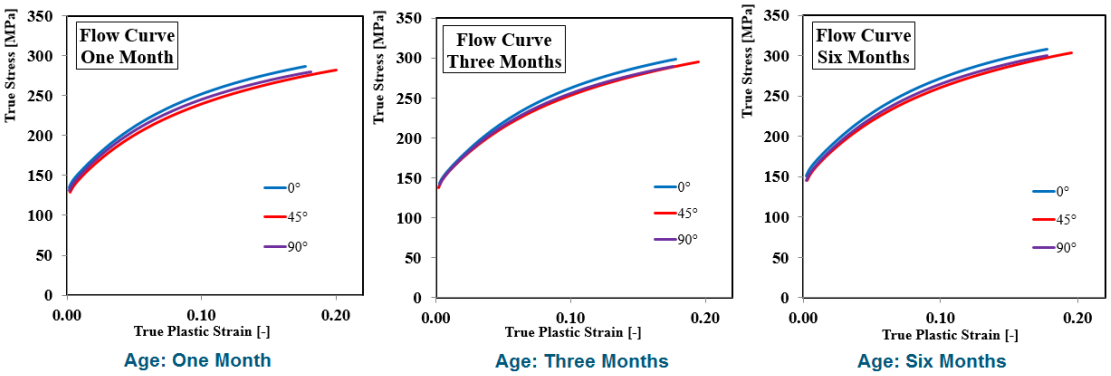

Figure 240, AC600T4 flow curves provided by the material supplier (Novelis, 2016)

The yield stress and UTS of materials is as follows:

Material age	Rp02 [Mpa]	Rm [MPa]
1 month	134	238
3 months	143	248
6 months	150	257

Table 48, Yield stress and UTS of AC600T4 alloy

These were used to simulate the below joint which was made with AC600T4 of an unknown and untraceable age:

Joint:	1.5mm AC600T4 + 1.5mm AC600T4
Rivet:	C50G41A (5.5mm long, level hardness 1)
Die:	DG09-160 (flat-bottomed, Width=9mm, Height=1.6mm)
	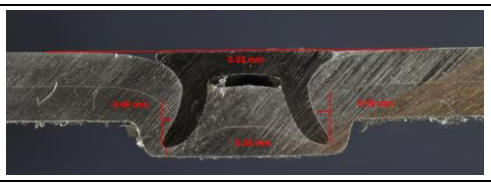
Parameter	Physical test result [mm]
Interlock:	0.40
Tmin:	0.35
HH:	0.02

Table 49, Test result – verification joint

TESTING PROCEDURE

AC procedure for sample preparation, rivet insertion and joint examination, as outlined in sections 5.1 and 5.2 has been followed.

RESULTS AND DISCUSSION

Measurements:

Material age	Rp02 [Mpa]	Rm [MPa]	Interlock [mm]	Tmin [mm]	HH [mm]
1 month	134	238	0.455	0.115	0.029
3 months	143	248	0.446	0.141	0.03
6 months	150	257	0.387	0.275	0.037

Table 50, Results – Testing different levels of hardness or aged AC600T4 alloy

Visual attributes:

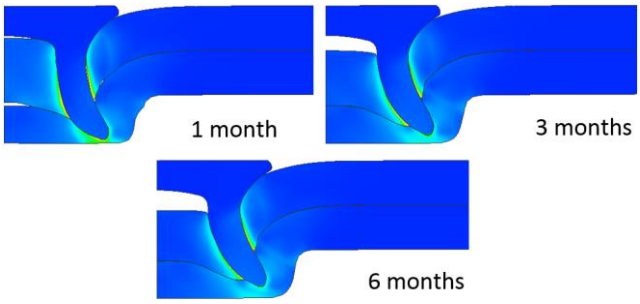

Figure 241, Axisymmetric view of joints with 1, 3 and 6 months old AC600T4 alloy

The three simulated joints and have displayed rather different measurements for each age, with Tmin starting unsurprisingly low with the very soft 1 month old material and improving as the material became older and subsequently harder. (Interlock decreased marginally when Tmin reduced)

These were then compared to the same joint completed as a physical sample. The comparison has clearly highlighted similarities between physical test and simulation completed with flow curves at six months. This demonstrates age of material can lead to a robust joint made with harder material changing to a failure condition when made with softer materials.

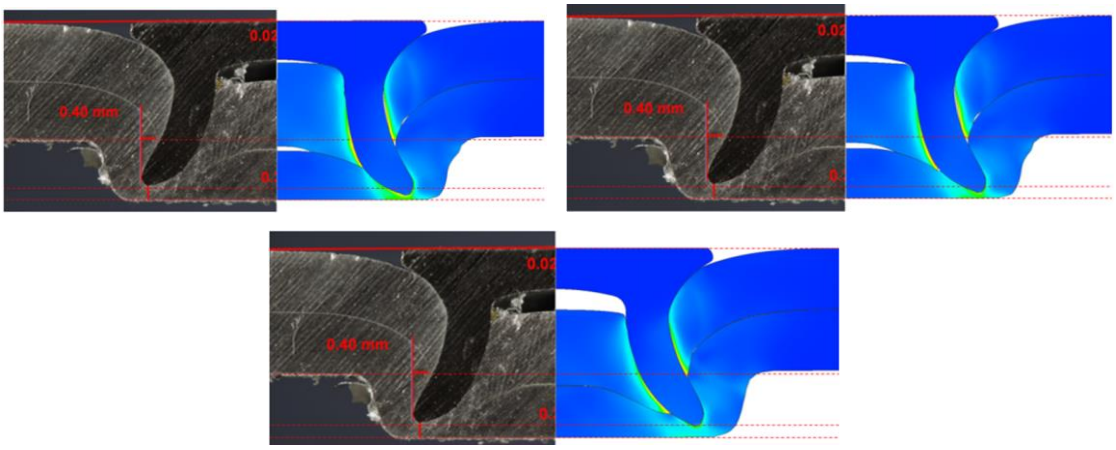

Figure 242, Comparison of joint with 1 month old (top left), 3 months (top right) and 6 months (bottom) old AC600T4

This result suggests that one of the benefits of the simulation might also be creating a process window test for age hardening of materials. In addition, if material flow curves are proven to be accurate, simulation of different ages could prove beneficial to estimating age and subsequently hardness of 6xxx aluminium alloys which are usually supplied by companies requiring testing with very little information accompanying. In case of steel this is salvageable by hardness testing the coupons and relating the hardness value to UTS in using material properties tables in order to remove guesswork on what rivet to use. However, with aluminium, Vickers testing machine is not sufficient due to its inaccuracy for measuring softer materials and the results cannot be related to UTS.

6.3.8 Influence of geometries

The simulation is usually deemed accurate upon validating it by a physical testing at least in one instance. If this verification has been supplied, then the same simulation can be run with small variations such as changing thickness of a sheet/s, die or a rivet on a presumption that agreement should not veer off too far. This can be a case of for example a material of a specific thickness being unavailable in which instance a simulation can be run with the same material of a different thickness that is available which should be available to give an estimation on how the joint would fare with the material that is unavailable.

However, the agreement of the simulation result with the physical sample is amongst many things dependable on the quality of geometries fed into the software. If a simulation is completed with an optimally configured geometry however, but the physical test is done with a part that has been subject of some manufacturing variations, the agreement may be poor. This section therefore looks at how potential small variations in physical geometry of the part can result affect the simulation.

6.3.8.1 Rivet geometries

INTRODUCTION

As mentioned before, the geometry of the rivets is their USP and changes depending on what each individual joint is meant to achieve. For example, the A-rivet is purposefully sharp so as to penetrate thin sheets, T-rivets are purposefully blunter so as not to flare prematurely before piercing all the way through a thick stack which they were designed for etc.

Despite best efforts at the forging stage of rivet production, rivets are subject to production variation to an extent that tolerances have to be determined and monitored for each type of a rivet on a number

of parameters – as listed in the below table. The image following the table shows an example of where on the rivet a variation might occur. Currently the tolerance ranges on the tip size are quite wide as can be seen from the table, at 0.15 +/-0.07, which is +/- 50% of the tip size.

Feature	Dimension [mm]	Tolerance ± [mm]	Upper Spec [mm]	Lower Spec [mm]
Under Head Radius	1.8	0.15	1.95	1.65
Shank	4	0.1	4.1	3.9
Bore	2.3	0.1	2.4	2.2
Length	5.5	0.1	5.6	5.4
Nominal Tip	0.15	0.07	0.22	0.08

Table 51, Possible production variations areas of the rivet and their limiting tolerances

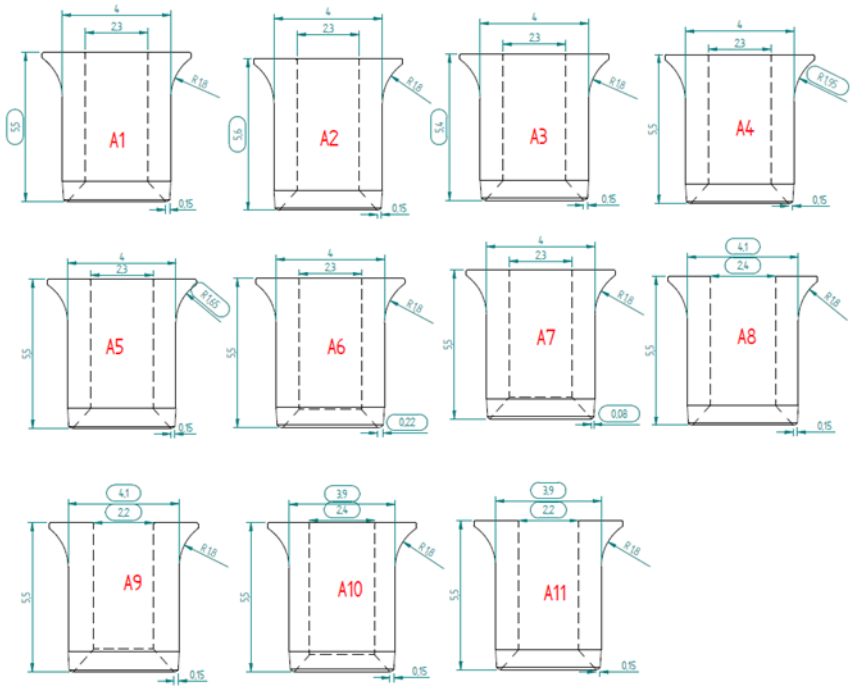

Figure 243, Illustration of the rivet production variation

As a way to evaluate the FE software's sensitivity to change in geometries of rivet as well as to assess the impact of variation within the tolerances on the geometry and subsequently the actual rivet, a sensitivity study was conducted.

METHOD

A benchmark joint was physically tested with a new development rivet currently in process of being designed to provide a calibration for materials for the simulations.

Joint:	2.5mm 5182 + 1.5mm 5182
Rivet:	TX0G44A (5mm long, level hardness 1)
Die:	DG07-08 (flat-bottomed, Width=7.0mm, Height=0.8mm)

Various version of the same rivet were then drawn up a CAD models in addition to the usual nominal CAD model, one at each of the tolerance band and compiled into a testing matrix.

Test No.	Shank [mm]	Bore [mm]	Tip [mm]	UHR [mm]	Length [mm]
A1	4	2.3	0.15	1.8	5.5
A2					5.6
A3					5.4
A4				1.95	5.5
A5				1.65	
A6			0.22	1.8	
A7			0.08		
A8	4.1	2.4	0.15		
A9		2.2			
A10	3.9	2.4			
A11		2.2			

Table 52, Testing matrix – Rivet geometry variation

TESTING PROCEDURE

AC procedure for sample preparation, rivet insertion and joint examination, as outlined in sections 5.1 and 5.2 has been followed.

RESULTS AND DISCUSSION

Physical test and comparison of the benchmark joint:

Joint:	2.5mm 5182 + 1.5mm 5182	
Rivet:	TX0G44A (5mm long, level hardness 1)	
Die:	DG07-08 (flat-bottomed, Width=7.0mm, Height=0.8mm)	
Image:	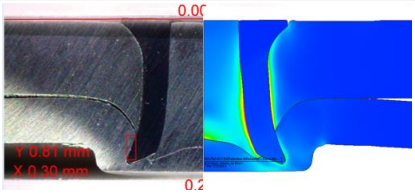	
Parameter	Physical test result [mm]	Simulation result [mm]
Interlock:	0.30	0.375
Tmin:	0.25	0.293
HH:	0.00	0.021

Table 53, Test result – Verification joint

Simulation is in 93% agreement with the verification nominal physical joint in terms of measurements and visual features including the sheet material dishing downwards due to the narrow die which is not supporting the sheets as much as standard die would do so sensitivity study can go ahead as planned.

As with other tests, a comparison of measurements and joint appearance has been compiled. The plus and minus variation in each feature/ parameter has been compared to the benchmark joint.

Joint ref no.	Variable	+/- tolerances [mm]	H - Int [mm]	Tmin [mm]	HH [mm]	Force [kN]
A1 (REF)	Length	5.5	0.323	0.226	0.017	34.8874
A2		5.6	0.353	0.215	0.09	34.457
A3		5.4	0.317	0.252	-0.09	35.643
A1 (REF)	UHR	1.8	0.323	0.226	0.017	34.8874
A4		1.95	0.358	0.249	0.01	34.7081
A5		1.65	0.348	0.249	0.011	35.1779
A1 (REF)	Rivet tip radius	0.15	0.323	0.226	0.017	34.8874
A6		0.22	0.305	0.175	0.012	35.0698
A7		0.08	0.391	0.762	0.027	31.1251
A1 (REF)	Shank	4.0 – 2.3	0.323	0.226	0.017	34.8874
A8		4.1 - 2.4	0.349	0.289	0.008	35.0032
A9		4.1 - 2.2	0.344	0.357	-0.028	37.5116
A1 (REF)	Bore	4.0 - 2.3	0.323	0.226	0.017	34.8874
A10		3.9 - 2.4	0.37	0.172	0.012	32.3315
A11		3.9 - 2.2	0.39	0.311	0.018	31.6194

Table 54, Test result – Rivet geometry variation

For most part, the variations of the geometry did not lead to staggeringly different results in terms of measurements, most of which would routinely be noticed within the 5off samples and would not impact the quality of this particular joint. Where the variation has had an impact was in test A10 and test A6. In test 10, the wider bore allows more material to be displaced into it so the rivet can be inserted further in process thinning out the Tmin which is consequently below spec of 0.20mm in this particular joint combination. In regards to the tip geometry, based on the measurements it would appear that the rivet with radius of 0.08mm (Test A7) has improved the Tmin which sees a large increase from 0.226mm in the reference joint to 0.762mm in the variation A7. However, this is due to the fact that the rivet has very visibly over-flared. This is not beneficial to the joint as the rivet is under considerable residual stress and might be prone to cracking. The simulation has confirmed the assumptions that sharper rivet tip is more prone to early and excessive flaring (this is a basis for A rivet, which has been designed to have balance between overflaring but also flaring early enough to create interlock in a very thin sheet, more detail on this chapter 2.2).

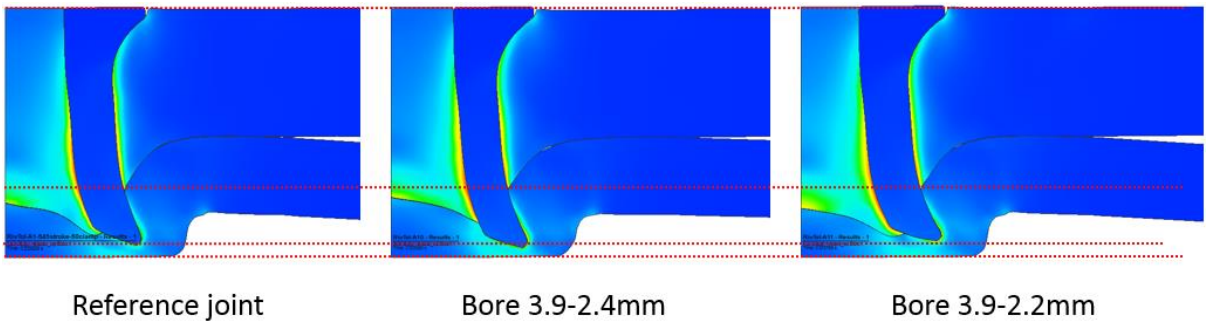

Axisymmetric view of results of Test A10 - Bore

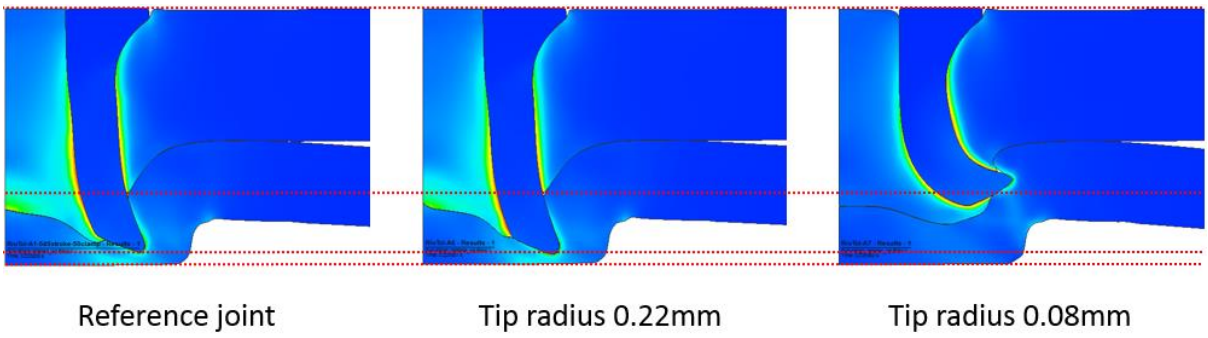

Figure 244, Axisymmetric view of results of Test A10 - Rivet tip radius

There are several things that can be concluded from this exercise. The simulation model is sensitive enough to model differences between geometries and it has confirmed assumptions held for the sharp end of the tolerance of the rivet geometry where the rivet is prone to early and excessive flaring. This parameters has been affected by the variation the most in comparison to the other parameters.

Based on the good agreement with the physical cross section, it is also assumed that the simulated behaviour of the rivet might reflect the behaviour of the physical rivet should it be manufactured with the sharpest tip radius. This variation also highlights the fact that simulations can only be as accurate as the CAD model that is supplied. If for instance, a nominal model is tested but compared against a joint that has been manufactured at the lower end of scale of the tip rivet geometry, it may be regarded as inaccurate when in fact the opposite is true.

From the perspective of assessing of the impact of manufacturing variation in geometry on performance of the rivets, this exercise has given insight into how simulation can add a great value in informing the rivet design.

6.3.8.2 Sheet geometry

Unlike in the rivet, where every angle and radius serves a purpose, the sheets are of considerably simpler geometry and only have the two areas where any variation in physical samples is likely to cause differences. These are

- Width and length of the coupon – X and Y dimensions
- Thickness of the coupon – Z dimension

6.3.8.2.1 X and Y dimensions

INTRODUCTION

It is recommended that the coupons for testing SPR insertion on different materials in laboratory conditions are of size 40x40mm and the CAD models of sheets have been created accordingly. However, it is not always guaranteed that this is how the coupons will arrive. In some cases, they might arrive pre-cut in stripes of 20mm width and in other cases the materials are very hard to obtain and therefore need to be conserved. In these instances, the laboratory technicians might cut the usual size coupons into halves in order to create more samples. This is an acceptable practice, however, with high strength steel materials, the smaller coupons might be prone to dishing (i.e. ends of the sheet rising). This is a less frequent occurrence in soft aluminium alloys unless this is cast aluminium such as 7075 which is extremely brittle. In cases where these two types of materials are used, the technicians would advise where possible to have 30x40mm as smallest possible size where possible, although sometimes size 20x40mm is unavoidable as no other option is available for testing.

It was unclear whether size of the sheets is going to affects a simulation and therefore a small study has been simulated in order to replicate the two possible outcomes.

METHOD

Two joints were simulated, steel to aluminium and aluminium to aluminium in order to see if dishing occurs in the same way as it does in physical testing. Sheets of dimensions were 20mm diameter and 40mm diameter were used in both types of simulated joints.

Joint:	1.2mm 1500 MPa Usibor + 2.5mm 6111 T4
Rivet:	BG0544A (5mm long, level hardness 6)
Die:	DG10-180 (flat-bottomed, Width=10.0mm, Height=1.8mm)

Joint 1 – steel to aluminium

Joint:	1.5mm 6016 + 1.5mm 6016
Rivet:	C50541A (5mm long, level hardness 1)
Die:	DG09-120 (flat-bottomed, Width=9mm, Height=1.2mm)

Joint 2 – aluminium to aluminium

TESTING PROCEDURE

A simulation process, as outlined in section 5.2, has been followed.

RESULTS AND DISCUSSION

Joint 1 results:

Joint:	1.2mm 1500 MPa Usibor + 2.5mm 6111 T4	
Rivet:	BG0544A (5mm long, level hardness 6)	
Die:	DG10-180 (flat-bottomed, Width=10.0mm, Height=1.8mm)	
	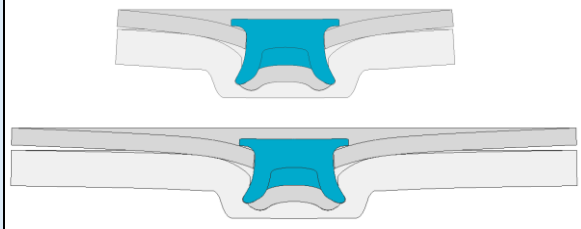	
Parameter	Simulation result 20mmx20mm sheet [mm]	Simulation result 40mmx40mm sheet [mm]
Interlock:	0.48	0.52
Tmin:	0.52	0.56
HH:	0.38	0.26

Table 55, Results - Joint 1

From the results, it is visible that the end of the smaller 20x20mm sheet is positioned slightly higher by 0.206mm in comparison to the same position on the 40x40mm sheet. This difference is further reflected in the measurements of the joint where interlock is improved by 0.04mm by the larger sheet and the Tmin follows the same pattern. HH has been measured at 9.0mm as per Atlas Copco specification and a difference 0.12m can be seen. Dishing, albeit with a very small effect, has been captured by the simulation with high strength PHS steel as top sheet which is known to cause dishing in laboratory conditions.

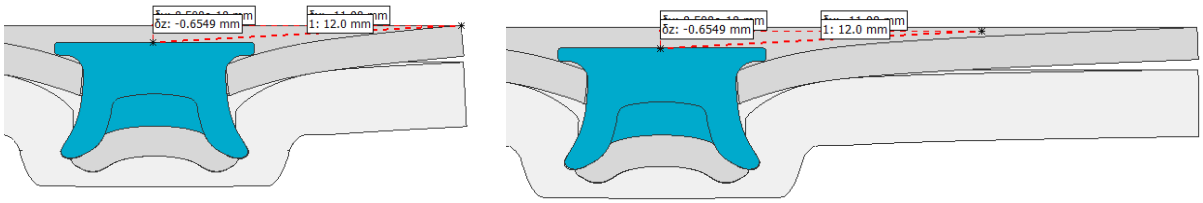

Figure 245, Joint 1 - Close up of results

Joint:	1.5mm 6016 + 1.5mm 6016	
Rivet:	C50541A (5mm long, level hardness 1)	
Die:	DG09-120 (flat-bottomed, Width=9mm, Height=1.2mm)	
Image:	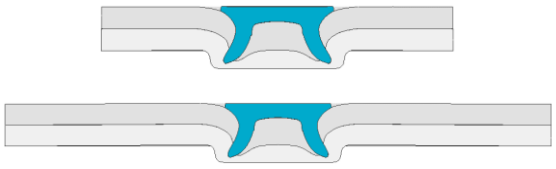	
Parameter	Simulation result 20mmx20mm sheet [mm]	Simulation result 40mmx40mm sheet [mm]
Interlock:	0.38	0.36
Tmin:	0.33	0.35
HH:	0.02	0.00

Table 56, Results – Joint 2

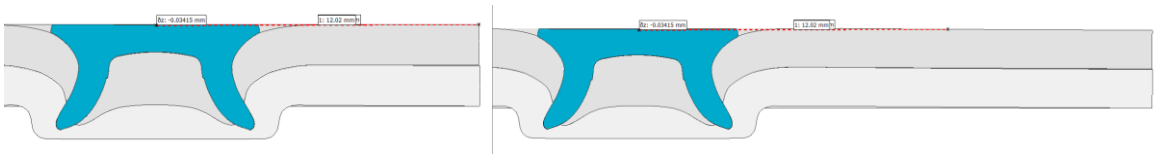

Figure 246, Joint 1 - Close up of results

Although measurements different slightly, no visible dishing has been demonstrated by the aluminium to aluminium joint. The end of the smaller sheet as shown in the image above is exactly in the same position in

Whilst the differences in results of the two size sheets can be deemed negligible, both results are what would usually be expected to be seen in the physical testing of both of these materials. Because the simulation will always only be an approximation, it is ideal to strive to replicate the process as closely as possible as even though there are small differences, if coupled with other, potentially incorrectly calibrated parameters, this can lead to larger differences and unnecessary adjustments in the model. Therefore, the size of the sheets should be always clarified before simulations take place.

6.3.8.2.2 Thickness of the coupon

INTRODUCTION

In the sheet, the variation in shape is a slightly less complex than the rivet as their geometries are most likely to vary in thickness and occasionally draft angles. Whilst the former is less likely to occur in cold rolled materials, in the cast materials the variations in thickness up to 0.3mm is common.

METHOD

A check of thickness across a selection of most frequently used materials has been completed in order to see a snapshot of variation between sheet thickness.

RESULTS AND DISCUSSION

Alloy	Thickness [mm]	Batch/ source	Mean	Max	Min	δ	Standard deviation	Coefficient of variation
AA5182	1.0	BLA4	1.01	1.03	0.98	0.05	0.02	1.64
AA5182	1.0	Novelis	1.02	1.02	1.01	0.01	0.01	0.52
AA5182	1.2	BLA4	1.21	1.22	1.20	0.02	0.01	0.72
AA5182	1.2	Novelis	1.21	1.22	1.20	0.02	0.01	0.61
AC170PX	1.0	Novelis	1.00	1.00	0.99	0.01	0.00	0.42
AC600T4	2.0	18903	2.00	2.05	1.99	0.06	0.02	0.89
AC600T4	1.5	18549	1.51	1.52	1.50	0.02	0.01	0.44
AC600T4	2.5	20809	2.50	2.50	2.49	0.01	0.01	0.21
AC600T4	2.0	18903-a	2.01	2.02	1.99	0.03	0.01	0.42
AC600T4	1.5	18549-a	1.52	1.53	1.50	0.03	0.01	0.56
AC600T4	2.5	18700	2.49	2.50	2.48	0.02	0.01	0.25
AC600T4	2.0	18903	2.00	2.01	1.99	0.02	0.01	0.37
AC600T4	1.5	18549	1.50	1.50	1.49	0.01	0.00	0.28
AC600T4	2.5	20809	2.49	2.50	2.47	0.03	0.01	0.51
AC600T4	3.0	JLR	3.06	3.08	3.04	0.04	0.02	0.52
RC5754	2.0	18614	2.02	2.03	2.00	0.03	0.01	0.48
RC5754	1.5	21325	1.49	1.50	1.47	0.03	0.01	0.69
RC5754	2.5	18936	2.51	2.54	2.48	0.06	0.02	0.77
RC5754	1.0	19464	1.00	1.01	0.99	0.02	0.01	0.79
RC5754	2.0	JLR	2.02	2.05	2.02	0.03	0.01	0.48
RC5754	2.5	JLR	2.52	2.53	2.51	0.02	0.01	0.27

Table 57, Snapshot of variation between sheet thickness

It seems that there is some degree variation between the sheets albeit very small in most evaluated examples. Whilst variation is upwards is not a great concern there are, however, instances where an already thin sheet is made thinner by 0.03mm by the variations. This can see an already thin sheet reduced by 0.03mm in the best-case scenario and by 0.09mm in the worst case (in three sheet stack).

Considering that rivet is often selected based on the overall thickness of the stack (rivet should be between 2.0 to 3.0mm longer than the overall stack thickness) it is worth to considering the worst case scenario on that particular thickness joint.

METHOD

A thin stack joint and validated by physical test, as per below. They were simulated with the correct thickness as determined by the label on the box as well as the highest and lowest thickness as measured in the previous exercise. The selection of the two stacks from the opposite ends of the thickness scale was purposefully aimed at compounding

Joint:	1.5mm RC5754 + 1.5mm RC5754 1.47mm RC5754 + 1.47mm RC5754
Rivet:	C50G41A (5.5mm long, level hardness 1)
Die:	DP09-175 (profiled die, Width= 9.0mm, Height=1.75mm)

Joint:	3.0mm AC600T4 + 3.0mm AC600T4 3.09mm AC600T4 + 3.09mm AC600T4
Rivet:	K50742A (7.0mm long, level hardness 2)
Die:	D10-160 (flat-bottomed die, Width= 10.0mm, Height=1.60mm)

RESULTS AND DISCUSSION

Good agreement can be seen in both joints upon comparison of the physical test and simulation with the correct thickness. The Tmin in the thin stack joint (1.5mm RC5754 + 1.5mm RC5754) is a little marginal in comparison to the average Tmin in physical cross sections, however, the 5 off physical sample for this joint displays large differences even within one joint where material under one leg is very thin whilst the material under the other leg is much thicker. This is unfortunately the nature of thin sheets as bottom sheet but for purposes of this comparison this will be sufficient.

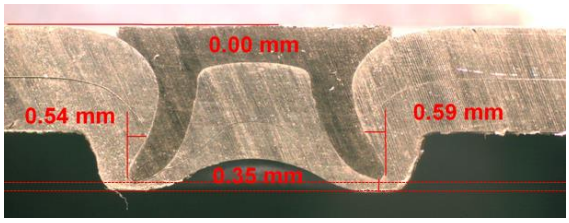

Figure 247, Inconsistencies within rivet

6.3.8.3 Nose geometry

As part of a review of geometries in order to create an Atlas Copco simulation model, it has been noted that the built in software template used a narrower, 16.0mm diameter nose. For this work this

has been replaced by a CAD model of an 18.0mm diameter nose that the same as the nose used for the physical tests with the same corner radii.

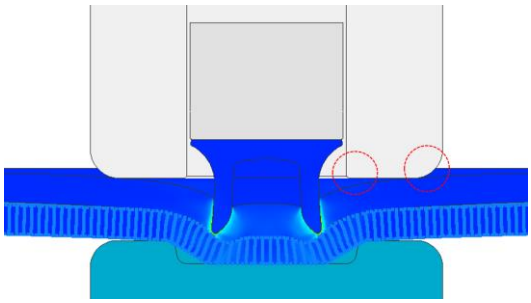

Figure 248, Standard 16mm dia Nose CAD model was replaced with a 18mm Nose diameter.

6.4 Summary

Following a large amount of testing carried out for purposes of this chapter, the next few paragraphs will aim to summarize the findings and best practices established by the research.

In section 1 of this chapter, the research established tolerances for simulation i.e. when is the simulation considered accurate and subsequently developed a method of assessing this via an 'Agreeability scorecard (section 6.1.1 to 6.1.3) that has been used to assess of subsequent joints.

Next, attention has been given to selection of the software. Based on the comparison of competing software packages offering SPR and their current technical capability, graphic user interface and number of users in the industry, Simufact has been selected. Several sensitivity studies have been completed which highlighted the shortcomings of the software's 'out of the box' version and these have become priority for the project of developing an improved base model (section 6.2).

Friction is one of the parameters that has been shown to have a great influence of the simulation accuracy and therefore a number of studies have been conducted to examine this aspect. The resulting values are as per below and have been validated by a number of physical tests (section 6.3.1).

Friction interfaces on 2T stack		μ	m
Punch and rivet		0.1	0.2
Nose and top sheet		0.1	0.2
Rivet and top sheet	H00	0.3	0.6
	HL0	0.1	0.2
Rivet and bottom sheet	H00	0.3	0.6
	HL0	0.1	0.2
Top sheet and middle sheet (set in contact table)		0.3	0.6
Middle sheet and bottom sheet (set in contact table)		0.25	0.6

Friction interfaces on 3T stack		μ	m
Punch and rivet		0.1	0.2
Nose and top sheet		0.1	0.2
Rivet and top sheet	H00	0.3	0.6
	HL0	0.1	0.2
Rivet and middle sheet	H00	0.3	0.6
	HL0	0.1	0.2
Rivet and bottom sheet	H00	0.3	0.6
	HL0	0.1	0.2
Top sheet and middle sheet (set in contact table)		0.3	0.6
Middle sheet and bottom sheet (set in contact table)		0.3	0.6
Bottom sheet and die		0.25	0.6

Table 58, Friction model

The clamping was something highlighted as lacking in the default set up of the SPR model and the research established a model for this (6.3.2). A clamping model has been set up for a mid-clamp method, specific to AC, which was not previously available in the software and which ensures that the clamp does not engage until rivet is 0.5mm away from full insertion. As with press, some settings in the clamp are variable parameters and will depend on the rivet length, the below example is shown based on 4.5mm long rivet.

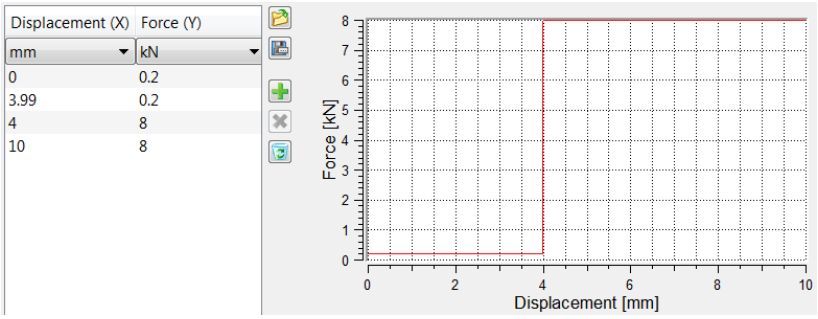

Figure 249, Clamp model

As part of the process description section, the research confirmed that Screwpress is currently the closest approximation of the servo setter gun used in AC (section 6.3.3) despite not having the ability to add extra torque during the process of insertion which, however, will be addressed as part of the future work. Some parts of the screw press are variable parameters such as maximum ram speed and energy whilst stroke energy efficiency remains a constant.

Mesh size is particularly important in FE analysis and to that end a sensitivity study on both of the deformable bodies, rivet and sheets, was conducted (section 6.3.4). Values were established for the minimum edge length of the element. Theses value are as follows:

Sheets

- 0.16mm for sheet models outside of the area of refinement
- 0.04mm for sheet models in the area of refinement

Rivet

- 0.04mm for rivet model
- Coarsening level 2

Both were found to lead to a good agreement of the simulation with physical joint in subsequent simulations as shown in the Figure 250.

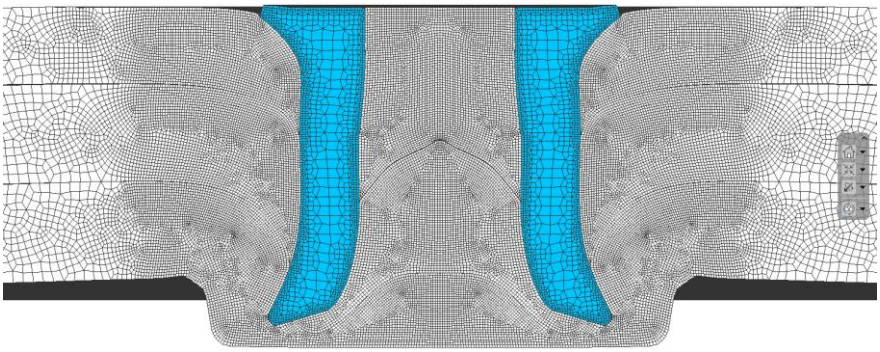

Figure 250, Example of rivet and sheet mesh

Damage mechanics (section 6.3.5) are closely interlinked with meshing options as currently the mechanism used to describe damage is Minimum thickness criteria which is set within the mesh settings. Minimum thickness criteria specifies the lowest value the element minimum edge length dimension can be deformed to before it is split into two to simulate cracking. It is recommended that this value is established for each material individually, however, when this is not possible due to lack of material for testing, two general values have been established based on the historical data and simulation testing, as shown in the table below.

Material type	Minimum thickness criteria ZXK
Aluminium	0.015
Steel	0.08

Table 59, General values for minimum thickness criteria

It should not be noted at that the value of 0.015mm is the lowest possible value for scenario of = 0.04mm. If this value is higher then minimum thickness criteria should be calculated as 1/3 minimum edge element length of a minimum edge element length.

Another way to model damage is use of damage models, however, this is not always avaible due ot lack of in depth material data required to use a damage model but remains in the list for future work.

Next, calculations of the temperature of the joint have been investigated via physical tests and it has been confirmed that the temperature the software calculates are correct (section 6.3.6.3).

Furthermore, various aspects of materials definitions required by the software have been examined and it seems that based on the research currently available, in-plane torsion test would be the most suitable method of obtaining material's mechanical data and Hockett & Sherby model is the most suitable method currently for extrapolating data. This is, however, a very fluid and highly researched area of FE and it is likely that new information about this topic will supersede these findings.

In the next section, influence of geometries has been examined for the two deformable components of the model, rivet and sheets (sections 6.3.8.1 and 6.3.8.2). Influence of rivet geometry has proven a particularly interesting topic as making small changes to the rivet geometry, particularly of the tip geometry, has led to some astounding differences between the reference rivet with 0.15 radius on the tip and a rivet with sharper tip geometry (0.08mm radius), as shown below.

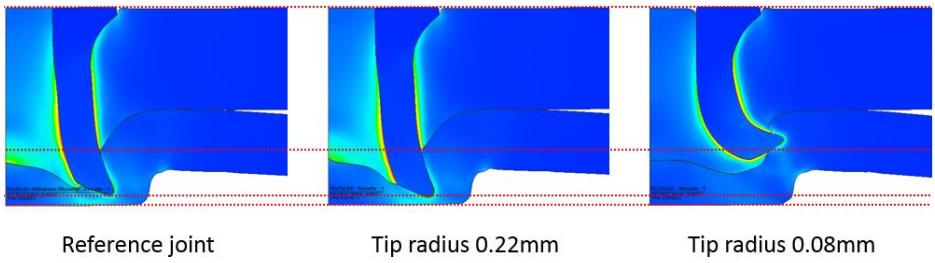

Figure 251, Differences caused by small changes in rivet tip geometry (reference/ standard rivet tip = 0.15mm, blunt tip = 0.22, sharp tip = 0.08mm)

For purposes of the simulation, this is a fantastic result as it clearly demonstrates the potential of simulation in terms of creating a robustness process window for manufacturing. The geometry of sheet has a small effect on each dimensions. X and Y dimensions (size of the coupon) can cause dishing of the material, the smaller the coupon, the more pronounced dishing effect. The Z dimension (thickness of the sheet) can also lead to small changes within the joint, however, this can be controlled relatively easily during sample preparation e.g. by setting the correct dimensions when cutting the coupons and checking the coupon thickness. As long as the simulation is modelling the same size coupons this should not cause an issue.

Equipped with the improved base simulation model incorporating all above findings and established settings, it is now possible to apply this to more practical examples of some novel concepts which will be the subject of the next chapter.

7 PRACTICAL APPLICATIONS

The previous chapter focused on developing a base simulation model (objective 1 and 2). A number of practical tests were completed to validate and feedback on the effectiveness and this led to creation of an improved and optimized base model capable of providing a good agreement across a wide range of joints providing sufficient external data is available such as materials and geometries.

This base model can now be applied to scenarios of practical applications to address issues coming to forefront of the SPR industry's priorities (this includes objectives 3A to 3F as per the introduction chapter).

7.1 Simulation of process window for sheet and rivet properties for BG rivet joining UHSS.

INTRODUCTION

In recent years, a new type of steel production has been developed to address the need to reduce the weight of a vehicle and improve safety by adding strength to the car. Instead of joining several small parts together, an entire part is press hardened all at once by use of a hot stamp press. The part is heated in the press to above its re-crystalizing temperature which allows the grains to grow large and create ductility in the part so as to aid forming. Once the part is formed into its required shape, it is quenched very rapidly in order to strengthen it. This process creates particularly hard steels e.g. 1500 MPa, and whilst it is beneficial approach in terms of the car safety and weight, it presents a challenge for joining due to its hardness. To address this development, Atlas Copco had recently adapted its range of rivets to include a BG rivet (also explained in chapter 2.1).

As mentioned previously, this rivet has been designed for stacks with the press hardened steel as top sheet which required higher column strength in order to pierce through the UHSS top sheet without excessive compression. There are some limitations but the rivet is suited to work with up to 1.4mm thick UHSS material with hardness of up to 1500 MPa if the bottom sheet is not too thin (below 2.0mm). The rivet was to be used by Jaguar Landrover on their new vehicle which used a large number of press hardened parts and due to early stages of the project there was no material available in the required gauge.

However, even with materials available testing of this material in context of SPR is challenging. This is due to the fact that the sheet material is hardened by quenching but this is not a uniform process which means different sections of the pressed part cool down at different rates causing the part to be

of non-uniform in hardness. In an ideal scenario, the hardness of different parts are indicated by the supplier but this does not happen as the suppliers provide the material spec as a range rather than a single value so whilst the part should be of hardness 1500 MPa, in reality, in some section this may reach hardness of 1800 MPa. This may present a scenario whereby the materials are too hard for the rivet and the joint that has been initially tested on small coupons not representative of the actual material may fall over in production.

An added complication are the tolerances of rivet which can slightly vary in hardness too (previously explained in section 4.1.3.7.2).

Therefore, as part of adapting to these new conditions, a way of testing the potential scenarios involving combinations of various hardness rivets with various hardness materials to estimate the worst case scenario had to be devised.

METHOD

A joint required for testing by JLR was as per below. This involves a BG rivet which has been already simulated as part of the development of the base model and requires a simulation set up with lower friction coating.

Joint:	1.2mm 1500 MPa Usibor + 2.5mm 6111 T4
Rivet:	BG0544A (5mm long, level hardness 6)
Die:	DG10-180 (flat-bottomed, Width=10.0mm, Height=1.8mm)

Due to shortage of coupons in this thickness, however, a different joint was completed with usibor thickness (1.5mm) that was available in order to validate the available flow curves for usibor which were supplied by Arcilor Mittal for Usibor 1500 MPs. The material arrived in laboratory conditions i.e. coupons rather than cut up parts of variable hardness. The joint was as follows:

Joint:	1.5mm 1500 MPa Usibor + 1.5mm 6016 T4
Rivet:	BG0446A (4mm long, level hardness 6)
Die:	DG09-140 (flat-bottomed, Width=09.0mm, Height=1.4mm)

Testing matrix was devised based on potential combinations of hardness of substrate materials and rivet materials exploring combinations of for example the softest rivet and hardest material etc. In order to establish whether this rivet is a feasible selection.

Rivet hardness selection was made on basis of overlap of tolerances between different hardness level around the nominal hardness 6 requested by the customer. The values were created by converting the values from Vickers hardness values to ultimate tensile strength with assistance of conversion tables (as explained in paragraph on hardness in section 4.1.3.6).

Heat treatment level	Hardness range (Hv 10kgf)
0	As forged
1	255-305
G	290-350
H	330-390
2	380-440
3	420-480
4	450-510
5	480-540
6	530-580
7	550-600

Table 60, Hardness levels of AC rivets

Sheet hardness levels to be tested were determined following a consultation with material supplier Arcilor Mittal, Atlas Copco R&D department coupled with review of available literature on upper and lower variables of Usibor (Eller et al, 2016) and boron (TuWien, 2015). A subsequent and informed adjustment was made to flow curves to reflect the possible manufacturing variables. This was done using the flow curve scaling factor which is a ratio by which the values of yield stress ($R_{p0.2}$) and/ or ultimate strength (R_m) can be adjusted to reflect a higher yield stress (value at the beginning of the flow curve) and / or UTS (value at the end of the flowcurve). Adjusting these $R_{p0.2\ and}$ R_m will lead or decrease/increase of the materials hardness. The scaling factor process is explained in greater detail in chapters 4.1.3.8.1 and 4.1.3.8.2. A testing matrix reflecting the adjustments has been created as per below:

Stack No	Variable	Rivet hardness [MPa]	Sheet hardness [MPa]	Scaling factor for Rp0.2 and Rm
Nominal joint	Benchmark from phase 1 test (simulate rivet and sheet material used via rivet batch and material certs)	c1800 (H6)	1500	n/a

Stack No	Variable	Rivet hardness [MPa]	Sheet hardness [MPa]	Scaling factor for Rp0.2 and Rm
1	Lower end of the rivet hardness with upper end of the material hardness	1600 (H5)	1600	1.135
2	Lower end of the rivet hardness with upper end of the material hardness	1600 (H5)	1700	1.27
3	Upper end of the rivet hardness with the lower end of the material hardness	1900 (H7)	1400	0.864
4	Upper end of the rivet hardness with the upper end of the material hardness	1900 (H7)	1600	1.135
5	Upper end of the rivet hardness with the upper end of the material hardness	1900 (H7)	1700	1.27
6	Lower end of the rivet hardness with the lower end of the material hardness	1600 (H5)	1400	0.864

Table 61, Testing matrix – Substrate material adjusted to reflect manufacturing variables

TESTING PROCEDURE

AC procedure for sample preparation, rivet insertion and joint examination, as outlined in sections 5.1 and 5.2 has been followed.

RESULTS AND DISCUSSION

The verification joint and simulation showed agreement within the tolerances of measurements as well as appearance so adjustment of this material proceeded as planned.

Joint:	1.5mm 1500 MPa Usibor + 1.5mm 6016 T4	
Rivet:	BG0446A (4mm long, level hardness 6)	
Die:	DG09-140 (flat-bottomed, Width=09.0mm, Height=1.4mm)	
	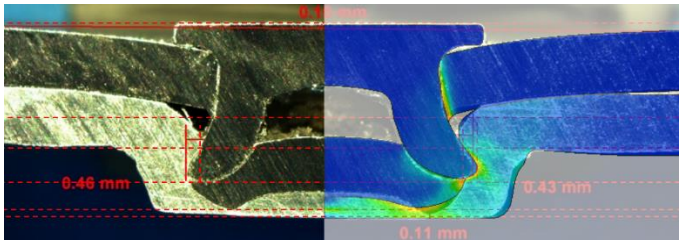	
Parameter	Physical test result [mm]	Simulation result [mm]
Interlock:	0.45 (Avg)	0.52
Tmin:	0.11mm	0.19
HH:	0.10mm	0.15mm

Table 62, Results – Verification joint

RESULTS AND DISCUSSION

Comparison of measurements:

Stack No	Variable	Rivet hardness [MPa]	Sheet hardness [MPa]	Scaling factor for Rp0.2 and	Interlock [mm]	Tmin [mm]	HH [mm]
Nominal joint	Benchmark from phase 1 test (simulate rivet and sheet material used via rivet batch and material certs)	1800 (H6)	1500	n/a	0.521	0.558	0.08

Stack No	Variable	Rivet hardness [MPa]	Sheet hardness [MPa]	Scaling factor for Rp0.2 and	Interlock [mm]	Tmin [mm]	HH [mm]
1	Lower end of the rivet hardness with upper end of the material hardness	1600 (H5)	1600	1.135	0.50	0.50	0.07
2	Lower end of the rivet hardness with upper end of the material hardness	1600 (H5)	1700	1.270	0.47	0.45	0.02
3	Upper end of the rivet hardness with the lower end of the material hardness	1900 (H7)	1400	0.864	0.55	0.56	0.07
4	Upper end of the rivet hardness with the upper end of the material hardness	1900 (H7)	1600	1.135	0.49	0.45	0.06
5	Upper end of the rivet hardness with the upper end of the material hardness	1900 (H7)	1700	1.270	0.48	0.43	0.05
6	Lower end of the rivet hardness with the lower end of the material hardness	1600 (H5)	1400	0.864	0.61	0.69	0.06

Table 63, Results – Substrate material adjusted to reflect manufacturing variables

Comparison of appearance:

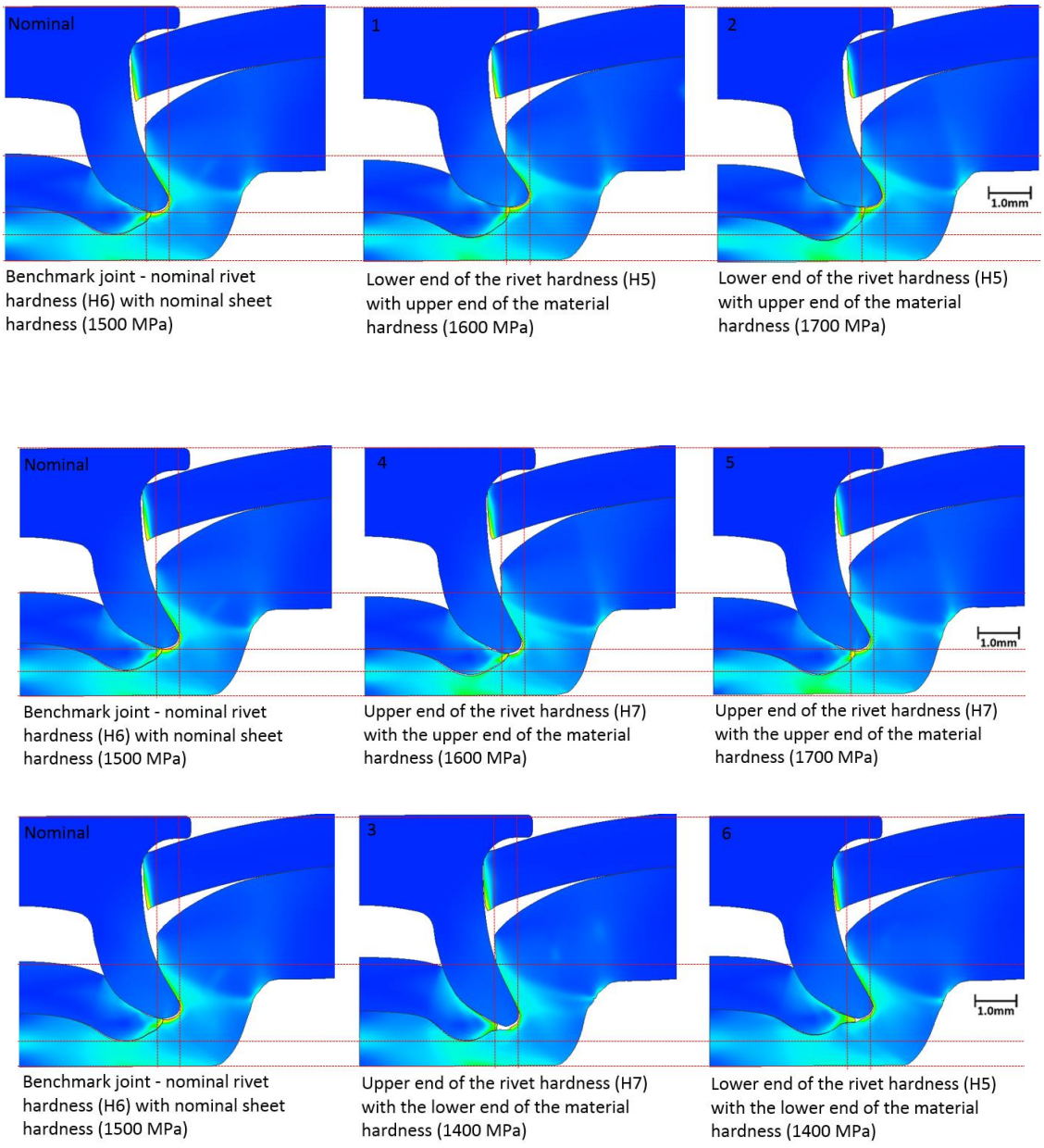

Figure 252, Axisymmetric view of all tested joints

Upon inspection of result, rivets and sheets behaviour are as expected. When comparing the softer-than-nominal rivet with increased hardness material, both increases (test 1 – by 100 MPa and test 2 - by 200 MPa) see the softer rivet compress increasingly. Had the material remained the same, this might have led to improved Tmin and Interlock which however, is not present due to the fact that the material is also harder so does not flow up the bore so easily and instead is pushed down by the rivet and thins out the soft aluminium on the bottom.

When comparing the harder than standard rivet, with increased material, no radical changes are seen except slightly lowered Tmin due to the rivet being harder than nominal and at the same still harder than the materials with increased hardness.

Lastly, upon comparison of both, harder and softer rivet with the softer material, a clear pattern can be seen where the softer material demonstrates more plasticity by flowing around the rivet leg more than in the other two comparisons. This has been seen to occur in the past in joints completed with softer UHSS material grades such as fortiform with UTS of 1050 MPa.

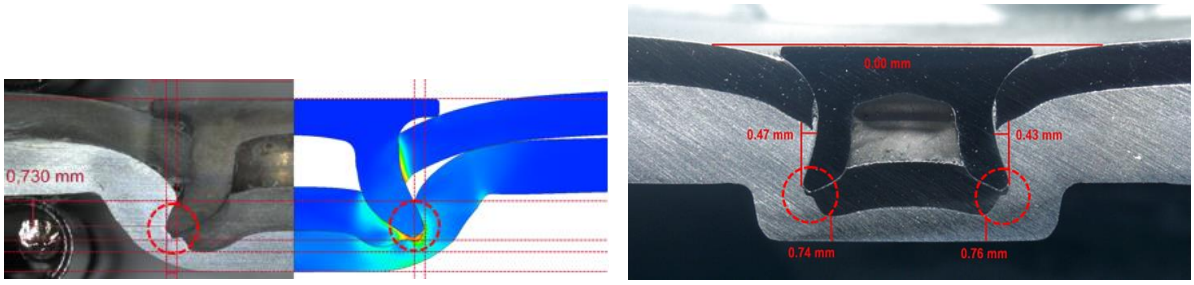

Figure 253, Example joint on the left – 1.5mm Fortiform (1050 MPa) + 1.5mm 5182. Example joint 2 on the right – 1.4mm Fortiform (hardness 1050MPa) + 3.0mm RC5754.

Rivet has also flared marginally more in the softer version which, in constellation with softer sheet material has not caused rivet compression and hence led also improved Tmin.

The measurements do not show drastic differences and are all in specification. The softest rivet and hardest material are possibly the only concerning results where rivet is considerably compressed which might be due to high residual stresses and is not recommended.

In summary, this exercise of simulating upper and lower values for both rivet and die has shown a great potential for envisaging the worst case scenario in production which is specifically beneficial n instances where automotive company is using a highly variable material such as press hardened steel.

The general guidance that can be observed based on this exercise is that since material suppliers provide materials at its lowest specification, it is likely to not to change to anything lower than supplied however, the materials' hardness is likely to vary upwards to the extent of 200 MPa (TechSpec, 2019).

To establish a process window it is therefore recommended to use flow curves at the value given by suppliers as well as at a value higher by 100 MPa and 200 MPa. In addition, the rivet hardness might change by 20 HV (TechSpec, 2019) which can translate into 65 MPa (BBS Stall Metaller, 2019). To fully estimate the potential of changes to the rivet due to manufacturing variables it is further recommended that rivet hardness is taken into consideration when testing for process window.

Therefore, in general, the following tests are recommended

- Usibor 1500 MPa with rivet hardness 6 and 7
- Usibor 1600 MPs with rivet hardness 5 and 6

The two above variations should cover the worst case scenario of combination or the softest rivet and the hardest material as well as hardest rivet and softest material.

The long term plan is to create a database of joints and include this information in there to create a concept of ‘fuzziness’. This is further elaborated in section on future work 9.2, xii.

7.2 Simulation to aid design of fully tubular rivet for narrow flange joining

INTRODUCTION

The trends in the automotive industry are continuously changing in order to improve current designs. One of these new concepts is an implementation of narrow flange by both JLR and Renault in order to increase visibility from the car by narrowing A pillars and thus improving safety aspect of the car. Using narrow flange has additional benefits in terms of weight reduction savings which are as per below:

- 2.3kg less of aluminium material used
- 0.25 litres less of dispensed adhesive
- 0.34kg less of adhesive weight

A narrow flange solution would save circa 2.64kg on a Jaguar F-Pace body.

In practical terms, this means that the riveted flanges would be reduced from the original 22mm to 15mm.

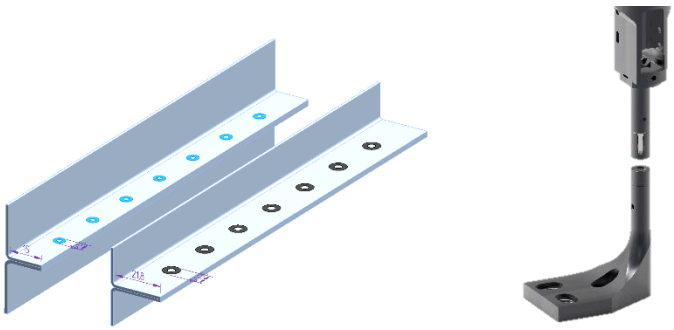

Figure 254, Illustartion of differences between standard and narrow flange, left, and new smaller nose, on the right.

In order to accommodate this, changes in equipment are needed. These will include a 25% reduction in nose diameter which will change from 16mm to 12mm and a design of a new narrower die. There are currently rivets that are compatible with the narrow flange which are standard semi-tubular 3.0mm and 4.0mm standard rivets, however, since the intended material for this area are specifically thin to thick Aluminium stacks, a new smaller tubular rivet is also being designed as a more suitable option.

Figure 255, Comparison of the proposed new smaller tubular rivets with a standard size tubular rivet.

The evaluation of influence of rivet geometry completed in chapter 6.6.3 has highlighted the benefit of using the simulation for optimisation of rivets and dies design before they are physically machined or manufactured. The results from this chapter also highlighted that the tip geometry at the lowest end of the tolerance band of +/-0.07mm (so tip radius 0.08mm) can severely reduce quality of the joint. This knowledge has been put to a practical use in a follow-on design of experiment aimed to resolve this issue. Since the current set of tolerances lead to a poor quality, the tolerance band was narrowed down from +/-0.07 to +/-0.05mm and a sensitivity study has been conducted in collaboration with R&D department to assess if reduction in tolerance can see this improve.

7.2.1 Test 1 – Narrowing down tolerance band

METHOD

A new testing matrix has been drawn up with slightly amended geometries based on the previous results and tightened tolerances.

Test No.	Shank [mm]	Bore [mm]	Tip [mm]	UHR [mm]	Length [mm]
B1	4	2.25	0.15	1.5	5.5
B2					5.58
B3					5.42
B4				1.65	5.5
B5				1.35	
B6			0.2	1.5	
B7			0.1		
B8	4.04	2.29	0.15		
B9		2.21			
B10	3.96	2.29			
B11		2.21			

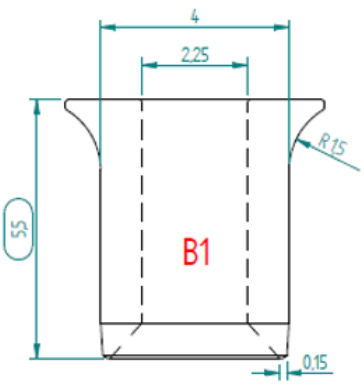

Table 64, Testing matrix – Narrow flange T rivets

TESTING PROCEDURE

AC procedure for sample preparation, rivet insertion and joint examination, as outlined in sections 5.1 and 5.2 has been followed.

RESULTS AND DISCUSSION

Results of testing are as follows:

Joint ref no.	Variable	+/- tolerances [mm]	H - Int [mm]	Tmin [mm]	HH [mm]	Force [kN]
B1	Length	5.5	0.375	0.293	0.021	35.2187
B2		5.58	0.374	0.282	0.018	34.7973
B3		5.42	0.345	0.318	-0.079	36.139
B1 (REF)	UHR	1.5	0.375	0.293	0.021	35.2187
B4		1.65	0.354	0.292	0.006	35.7813
B5		1.35	0.348	0.295	0.006	35.6928
B1 (REF)	Rivet tip radius	0.15	0.375	0.293	0.021	35.2187
B6		0.2	0.32	0.235	0.01	35.7273
B7		0.1	0.384	0.377	0.014	35.7003
B1 (REF)	Shank	4.0 - 2.25	0.375	0.293	0.021	35.2187
B8		4.04 - 2.29	0.349	0.303	0.001	35.972
B9		4.04 - 2.21	0.351	0.312	-0.003	36.5261
B1 (REF)	Bore	4.0 - 2.25	0.375	0.293	0.021	35.2187
B10		3.96 - 2.29	0.376	0.26	0.016	34.7701
B11		3.96 - 2.21	0.371	0.297	0.009	35.2239

Table 65, Test results – Narrowing of the tolerance bands

Upon comparison with the result with +/-0.07mm tolerance band, the results with reduced tolerance show improved results with significant decrease in flaring in the tip radius parameter where the tolerance range has been narrowed down from 0.08-0.22mm to 0.10-0.20mm, as shown below figures.

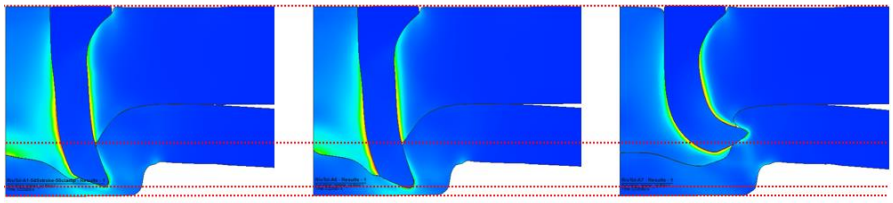

Reference joint Tip radius 0.22mm Tip radius 0.08mm

Figure 256, Axisymmetric view of results of initial geometry study with +/= 0.07mm tolerance band

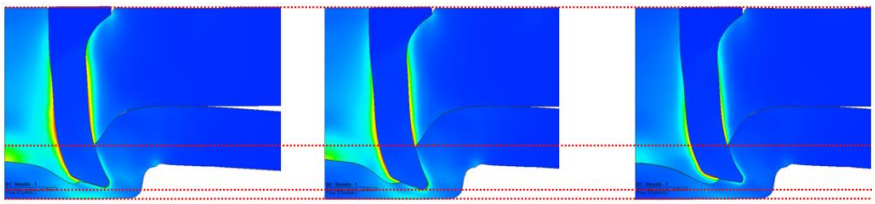

Figure 257, Axisymmetric view of results of initial geometry study with +/= 0.07mm tolerance band

In addition to improving the tip geometry, the reduced tolerance band works well with other parameters as shown by the measurements. Therefore, this new tolerance has been proposed to be actioned by the rivet forging department. However, on further investigations, it is clear that that the tip geometry tolerance of +/-0.05mm is not achievable within the current set-up in the forging area and reduced tolerances cannot be guaranteed so a new approach needs to be taken.

In addition, two new parameters were identified by R&D laboratory as potential subjects to manufacturing variation, flare angle and head width, both of which could have an impact on the resulting joints.

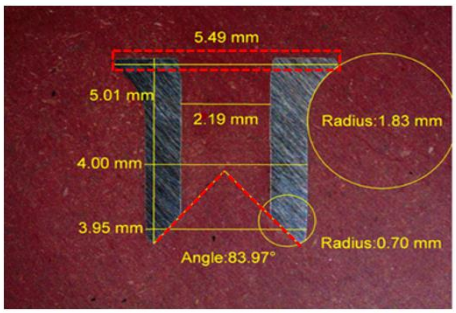

Figure 258, Head width and flare angle parameters highlighted in dashed red line.

Furthermore, as mentioned in chapter 7.2, the rivet materials hardness variation has an impact on the rivet performance and in is unclear whether this, coupled with geometry parameters will improve or make the current condition worse. Based on this, a new approach has been taken which aims to establish process capability of the new rivet by exploring the coupled effect of all parameters rather than examining them in isolation.

7.2.2 Test 2 – Coupled effect of rivet hardness and tip geometry

METHOD

First step is to understand the effect of hardness level of rivet on the tip geometry. To that end, all three different hardness levels (450 Hv-H3, 480 Hv – H4 and 510 Hv – H5) were tested against five different tip sharpness levels, starting from 0.11 and increasing to the current nominal size of 0.15mm

in 0.1mm increments. The three levels of material hardness were simulated using one hardness level above (H5) and one below (H3) the nominal hardness (H4). New CAD models were drawn up with small increments of tip sharpness.

Testing matrix:

Test C Number	Head	Shank (mm)	Bore (mm)	Tip (mm)	UHR (mm)	Length (mm)	Flare Angle	Hardness (Hv)	Hardness (AC rivet)
C01	5.35	3.96	2.29	0.11	1.35	5.58	84.5	450	H3
C02	5.35	3.96	2.29	0.12	1.35	5.58	84.5	450	H3
C03	5.35	3.96	2.29	0.13	1.35	5.58	84.5	450	H3
C04	5.35	3.96	2.29	0.14	1.35	5.58	84.5	450	H3
C05	5.35	3.96	2.29	0.15	1.35	5.58	84.5	450	H3

Test D Number	Head	Shank (mm)	Bore (mm)	Tip (mm)	UHR (mm)	Length (mm)	Flare Angle	Hardness (Hv)	Hardness (AC rivet)
D01	5.35	3.96	2.29	0.11	1.35	5.58	84.5	480	H4
D02	5.35	3.96	2.29	0.12	1.35	5.58	84.5	480	H4
D03	5.35	3.96	2.29	0.13	1.35	5.58	84.5	480	H4
D04	5.35	3.96	2.29	0.14	1.35	5.58	84.5	480	H4
D05	5.35	3.96	2.29	0.15	1.35	5.58	84.5	480	H4

Test E Number	Head	Shank (mm)	Bore (mm)	Tip (mm)	UHR (mm)	Length (mm)	Flare Angle	Hardness (Hv)	Hardness (AC rivet)
E01	5.35	3.96	2.29	0.11	1.35	5.58	84.5	510	H5
E02	5.35	3.96	2.29	0.12	1.35	5.58	84.5	510	H5
E03	5.35	3.96	2.29	0.13	1.35	5.58	84.5	510	H5
E04	5.35	3.96	2.29	0.14	1.35	5.58	84.5	510	H5
E05	5.35	3.96	2.29	0.15	1.35	5.58	84.5	510	H5

Table 66, Testing matrix - Coupled effect of rivet hardness and tip geometry

TESTING PROCEDURE

AC procedure for sample preparation, rivet insertion and joint examination, as outlined in sections 5.1 and 5.2 has been followed.

RESULTS AND DISCUSSION

Measurements:

Test C Number	Head	Shank (mm)	Bore (mm)	Tip (mm)	UHR (mm)	Length (mm)	Flare Angle	Hardness (Hv)	Hardness (AC rivet)	X Interlock [mm]	Y Interlock [mm]	Tmin [mm]	HH [mm]
C01	5.35	3.96	2.29	0.11	1.35	5.58	84.5	450	H3	0.156	0.309	0.8	0.1
C02	5.35	3.96	2.29	0.12	1.35	5.58	84.5	450	H3	0.389	0.485	0.72	0.061
C03	5.35	3.96	2.29	0.13	1.35	5.58	84.5	450	H3	0.364	0.546	0.66	0.069
C04	5.35	3.96	2.29	0.14	1.35	5.58	84.5	450	H3	0.393	0.597	0.52	0.011
C05	5.35	3.96	2.29	0.15	1.35	5.58	84.5	450	H3	0.404	0.781	0.329	0.018

Test D Number	Head	Shank (mm)	Bore (mm)	Tip (mm)	UHR (mm)	Length (mm)	Flare Angle	Hardness (Hv)	Hardness (AC rivet)	X Interlock [mm]	Y Interlock [mm]	Tmin [mm]	HH [mm]
D01	5.35	3.96	2.29	0.11	1.35	5.58	84.5	480	H4	0.447	0.712	0.598	0.008
D02	5.35	3.96	2.29	0.12	1.35	5.58	84.5	480	H4	0.446	0.804	0.425	0.013
D03	5.35	3.96	2.29	0.13	1.35	5.58	84.5	480	H4	0.45	0.61	0.498	0.011
D04	5.35	3.96	2.29	0.14	1.35	5.58	84.5	480	H4	0.395	0.858	0.298	0.04
D05	5.35	3.96	2.29	0.15	1.35	5.58	84.5	480	H4	0.364	0.847	0.293	0.007

Test E Number	Head	Shank (mm)	Bore (mm)	Tip (mm)	UHR (mm)	Length (mm)	Flare Angle	Hardness (Hv)	Hardness (AC rivet)	X Interlock [mm]	Y Interlock [mm]	Tmin [mm]	HH [mm]
E01	5.35	3.96	2.29	0.11	1.35	5.58	84.5	510	H5	0.463	0.591	0.584	0.013
E02	5.35	3.96	2.29	0.12	1.35	5.58	84.5	510	H5	0.46	0.801	0.355	0.018
E03	5.35	3.96	2.29	0.13	1.35	5.58	84.5	510	H5	0.435	0.876	0.286	0.015
E04	5.35	3.96	2.29	0.14	1.35	5.58	84.5	510	H5	0.437	0.963	0.316	0.019
E05	5.35	3.96	2.29	0.15	1.35	5.58	84.5	510	H5	0.386	0.91	0.266	0.016

Table 67, Test results - Coupled effect of rivet hardness and tip geometry

Visual attributes:

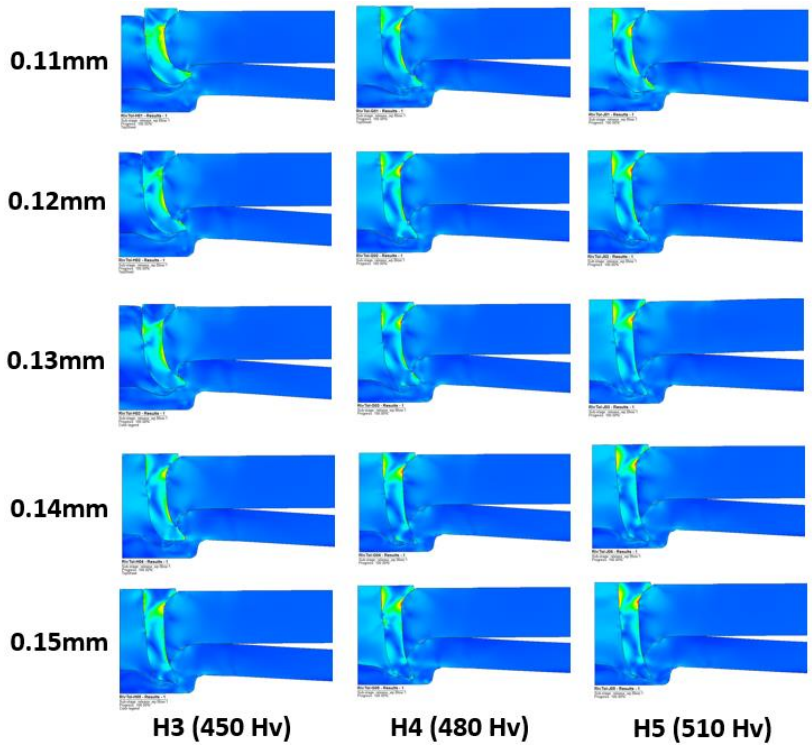

Figure 259, Axisymmetric view of joints completed in order to evaluate the coupled effect of hardness of tip sharpness.

The results are as anticipated, with the rivet with the lowest hardness (H3) and sharpest tip (0.11mm) out of the compared ones flaring out the most (top left corner on the image) and the rivet with nominal tip geometry (0.15mm) and increased hardness (H5) flaring out the least. Hardness seems to have a negligible effect across the rivets at tip sharpness 0.15mm however, as can be seen from the

graphs but when the softest rivet is coupled with low values of tip sharpness such as 0.11-0.13mm (up to 0.14mm with the softest variable H3), it seems to provide very unstable results. This can be seen in graphs below where all three measurements display instability in comparison to harder H4 and H5 until tip sharpness values of 0.14mm and 0.15mm are used.

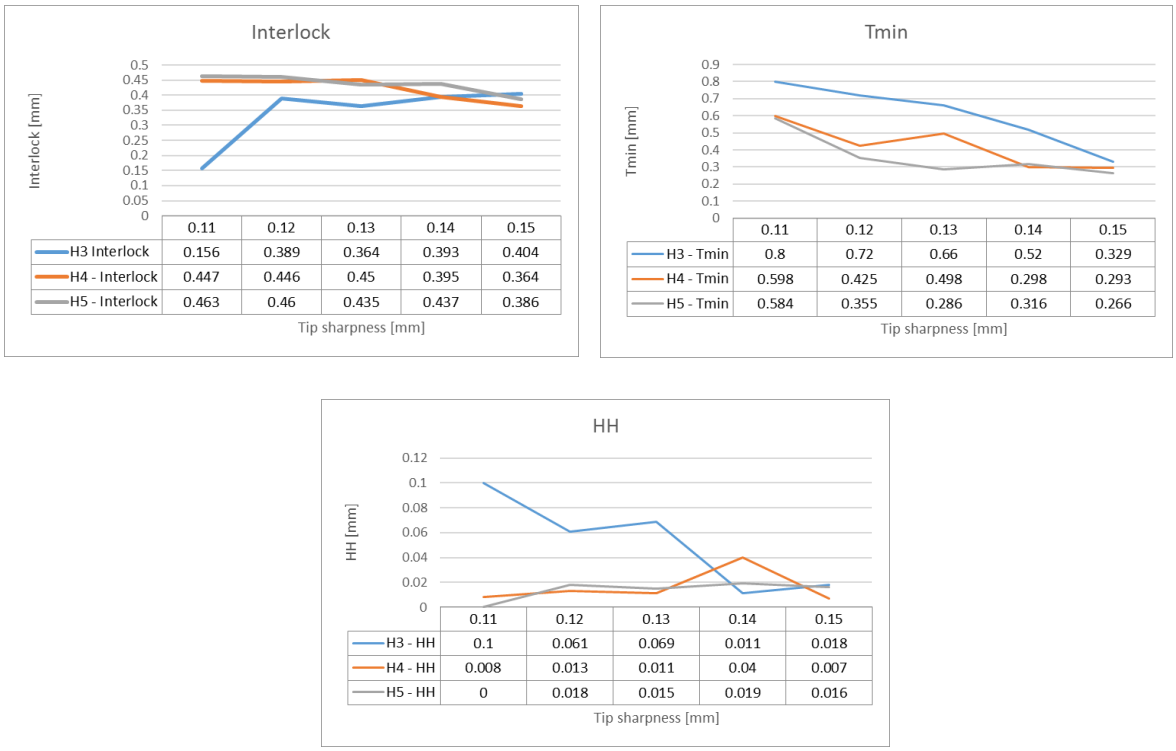

	0.11	0.12	0.13	0.14	0.15
H3 Interlock	0.156	0.389	0.364	0.393	0.404
H4 - Interlock	0.447	0.446	0.45	0.395	0.364
H5 - Interlock	0.463	0.46	0.435	0.437	0.386

	0.11	0.12	0.13	0.14	0.15
H3 - Tmin	0.8	0.72	0.66	0.52	0.329
H4 - Tmin	0.598	0.425	0.498	0.298	0.293
H5 - Tmin	0.584	0.355	0.286	0.316	0.266

	0.11	0.12	0.13	0.14	0.15
H3 - HH	0.1	0.061	0.069	0.011	0.018
H4 - HH	0.008	0.013	0.011	0.04	0.007
H5 - HH	0	0.018	0.015	0.019	0.016

Figure 260, Graph capturing instability in measurements of interlock (top left), Tmin (top right) and HH (bottom) with changing rivet hardness and tip geometry

Due to the fact that apart from the initial validation of the nominal joint with physical testing, no other validation took place up to this point, a decision has been made to physically validate the worst case scenario rivet, C1 (with lowest hardness level (H3) and sharpest rivet tip (0.11mm) from this study. To that end, a precise replication of a model of the C1 rivet has been machined on the CNC machine, inserted into the specified materials and cross sectioned. The below result has provided a very interesting result which is, according to the scorecard in 96% agreement with the simulation. Whilst the rivet leg seems to be more compressed in simulation, the overall result seems to reflect the behaviour of both sheets and rivet material relatively accurately.

SCORECARD		Value	Input	Total Agreement
Measurements	Interlock	20%	20%	
	Tmin	20%	20%	
	HH	20%	20%	
Visual attributes	Rivet leg compre	8%	8%	**96%**
	Top / Mid sheet s	8%	8%	
	Bottom sheet sha	8%	8%	
	Bore fill	8%	4%	
	Under leg materi	8%	8%	

Table 68, Comparison of physical and simulation results using scorecard.

Joint:	2.5mm 5182 + 1.5mm 5182	
Rivet:	TX0G44A (5mm long, level hardness 1)	
Die:	DG07-08 (flat-bottomed, Width=7.0mm, Height=0.8mm)	
	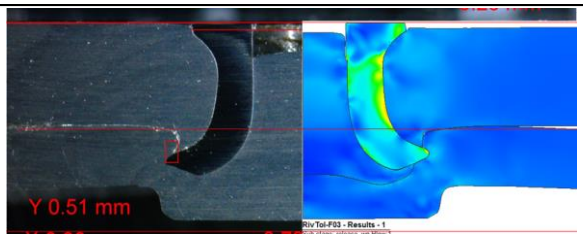	
Parameter	Physical test result [mm]	Simulation result [mm]
Interlock:	0.22	0.195
Tmin:	0.78	0.828
HH:	0.00	0.016

Table 69, Results – Verification joint

Having an insight into the coupled effect of material hardness and rivet tip radius size, the next step is to add further variables into the testing matrix, which leads to a further process capability study.

7.2.3 Test 3 – Process capability

METHOD

As before, the rivet material variation will be accounted by using one rivet hardness level below (H3) and one above (H5) the nominal (H4) whilst the additional geometrical parameters have been incorporated into the study as additional CAD models.

In light of the large number of parameters combinations, it has been decided to use an educated assumption that the extreme ends of the scale of several combined parameters were the worst case scenarios from the perspective of manufacturing variation. This included two scenarios:

- The shortest, bluntest and hardest rivet – tests F4, F5 and F6 in testing matrix
- The longest, sharpest and softest rivet – tests F8 and F9 in testing matrix

Both were compared to the nominal rivet with three levels of flare angle – tests F1, F2 and F3 in testing matrix. The ultimate aim to be achieved via this study is to, in light of lack of guarantee of suitable rivet tip tolerance band, establish the minimum suitable tip size with which the manufacturing tolerance of =/-0.07mm would be plausible.

Testing matrix:

Test F Number	Head [mm]	Shank [mm]	Bore [mm]	Tip [mm]	UHR [mm]	Length [mm]	Flare Angle	Hardness (Hv)	Hardness (AC rivet)
F1	5.5	4	2.25	0.15	1.5	5.5	82.5	480	H4
F2	5.5	4	2.25	0.15	1.5	5.5	84.5	480	H4
F3	5.5	4	2.25	0.15	1.5	5.5	80.5	480	H4
F4	5.65	4.04	2.21	0.22	1.65	5.42	82.5	510	H5
F5	5.65	4.04	2.21	0.22	1.65	5.42	84.5	510	H5
F6	5.65	4.04	2.21	0.22	1.65	5.42	80.5	510	H5
F7	5.35	3.96	2.29	0.08	1.35	5.58	82.5	450	H3
F8	5.35	3.96	2.29	0.08	1.35	5.58	84.5	450	H3
F9	5.35	3.96	2.29	0.08	1.35	5.58	80.5	450	H3

Table 70, Testing matrix - Process capability

TESTING PROCEDURE

AC procedure for sample preparation, rivet insertion and joint examination, as outlined in sections 5.1 and 5.2 has been followed.

RESULTS AND DISCUSSION

The simulations have provided the following results:

Test F Number	Head [mm]	Shank [mm]	Bore [mm]	Tip [mm]	UHR [mm]	Length [mm]	Flare Angle	Hardness (Hv)	Hardness (AC rivet)	X Interlock [mm]	Y Interlock [mm]	Tmin [mm]	HH [mm]
F1	5.5	4	2.25	0.15	1.5	5.5	82.5	480	H4	0.356	0.869	0.326	0.006
F2	5.5	4	2.25	0.15	1.5	5.5	84.5	480	H4	0.352	0.89	0.341	0.004
F3	5.5	4	2.25	0.15	1.5	5.5	80.5	480	H4	0.327	0.951	0.214	0.015
F4	5.65	4.04	2.21	0.22	1.65	5.42	82.5	510	H5	0.26	0.909	0.187	-0.078
F5	5.65	4.04	2.21	0.22	1.65	5.42	84.5	510	H5	0.247	0.849	0.189	-0.074
F6	5.65	4.04	2.21	0.22	1.65	5.42	80.5	510	H5	0.231	0.909	0.147	-0.08
F7	5.35	3.96	2.29	0.08	1.35	5.58	82.5	450	H3	0	0	0.954	0.083
F8	5.35	3.96	2.29	0.08	1.35	5.58	84.5	450	H3	0	0	1.041	0.055
F9	5.35	3.96	2.29	0.08	1.35	5.58	80.5	450	H3	0	0	1.022	0.051

Table 71, Test results - Process capability

Based on the results of testing of the rivet with 0.15mm tip geometry and its upper and lower specifications with tolerances of +/-0.07mm were tested, along with a number of different parameters, it has been confirmed that the combination of the longest, sharpest and softest rivet is

currently the worst case scenario. This is caused by all three rivets severely failing by inability to create interlock in the too soft material.

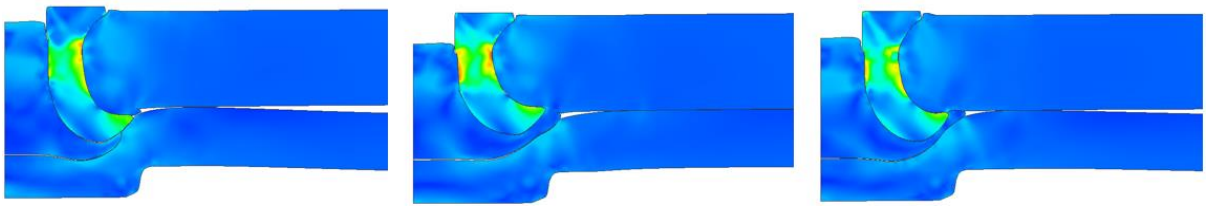

Figure 261, Axisymmetric view of joints with longest, sharpest and softest rivets and three different levels of flare angle – 82.5°, 84.5° and 80.5°. Results left to right – F 7, F8 and F9.

The scenario on the other end of the spectrum, the shortest, bluntest and hardest rivet has also had a notable effect on the measurements, especially where Tmin is concerned which is noticably reduced. However, since it currently does lead to a breakthrough of the bottom sheet, the focus will remain on the tip on the shaper end of the scale.

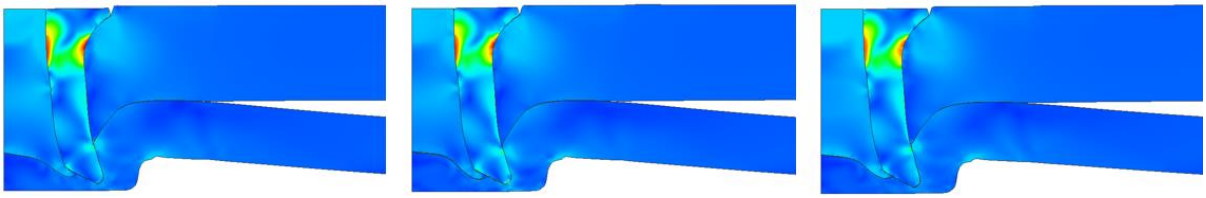

Figure 262, Axisymmetric view of joints with shortest, bluntest and hardest rivets and three different levels of flare angle – 82.5°, 84.5° and 80.5° Results left to right – F4, F5 and F6.

In light of the severe fail of the joints with 0.15mm nominal tip and lowest tolerance of +/-0.07mm and inability to reduce this tolerance to +/-0.05mm, a decision has been made to amend the initial tip geometry design from 0.15mm to 0.17mm. Without the option to reduce the tolerances band, this might present an alternative solution to maintaining the tip rivet geometry at 0.1mm even at the lowest end of the tolerance band. With the new specifications, the rivet is expected to be less sensitive to other changing parameters such as heat treatment levels i.e. hardness of the rivets etc. To confirm this hypothesis, further tests have been undertaken.

7.2.4 Test 4 – Coupled effect of improved tip geometry and flare angle

METHOD

Testing matrix:

Test G Number	Head [mm]	Shank [mm]	Bore [mm]	Tip [mm]	UHR [mm]	Length [mm]	Flare Angle	Hardness (Hv)	Hardness (AC rivet)
G1	5.35	3.96	2.29	0.1	1.35	5.58	82.5	450	H3
G2	5.35	3.96	2.29	0.1	1.35	5.58	84.5	450	H3
G3	5.35	3.96	2.29	0.1	1.35	5.58	80.5	450	H3

Table 72, Testing matrix - Coupled effect of improved tip geometry and flare angle

The same type of joint, the longest, sharpest and softest has been tested, however, on this occasion, the test was completed with 0.1mm tip geometry and three different levels of flare angle.

TESTING PROCEDURE

AC procedure for sample preparation, rivet insertion and joint examination, as outlined in sections 5.1 and 5.2 has been followed.

RESULTS AND DISCUSSION

Measurements:

Test G Number	Head [mm]	Shank [mm]	Bore [mm]	Tip [mm]	UHR [mm]	Length [mm]	Flare Angle	Hardness (Hv)	Hardness (AC rivet)	X Interlock [mm]	Y Interlock [mm]	Tmin [mm]	HH [mm]
G1	5.35	3.96	2.29	0.1	1.35	5.58	82.5	450	H3	0	0	0.927	0.103
G2	5.35	3.96	2.29	0.1	1.35	5.58	84.5	450	H3	0.001	0.036	0.936	0.067
G3	5.35	3.96	2.29	0.1	1.35	5.58	80.5	450	H3	0.188	0.286	0.828	0.02

Table 73, Test results - Coupled effect of improved tip geometry and flare angle

Visual attributes:

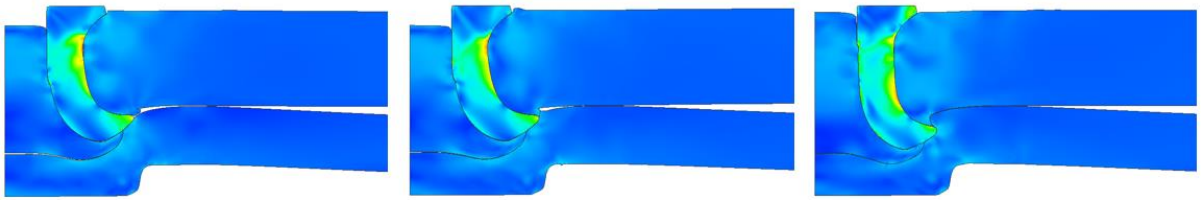

Figure 263, Axisymmetric view of joints with shortest, bluntest and hardest rivets and three different levels of flare angle – 82.5°, 84.5° and 80.5°. Results left to right - G1, G2 and G3.

Some improvements can be seen in the joints in comparison with the previous investigation of 0.08m tip geometry rivets where all rivets failed to create any interlock. Joint G2 (upper end of the flare angle parameter) has created some vertical interlock and joint G3 (lower end of the tolerance band) has created both vertical and horizontal interlock. In addition to demonstrating the improvements of the

joint by using 0.10mm tip geometry, an influence of the flare angle can be noted. It appears that the rivet with the narrowest flare angle (80.5°) gives the most improved values.

There is some irregularity that can be noted across all joint in terms of the influence of the flare angle, whereby it seems that in this particular test, the nominal value, joint G1 i.e. the middle of the tolerance value is worse than the both of the upper and lower values. Other than some level of imbalance between the tip and the flare angle where geometries work against each other during the forming process, this is currently unexplained. Despite manufacturing rivets for a number of years, the company does not have precise knowledge on the impact of this feature as its potential effect has been noted only during the recent geometry sensitivity study. This parameter will firmly remain on the list of future research avenues.

Based on the results above and the trends shown by simulation, the rivet design team has decided to amend the initial rivet design with 0.15mm radius on tip geometry to 0.17mm in order to accommodate the non-changeable tolerance band of +/-0.07mm. Whilst further work is needed on the design of the rivets, the above studies also demonstrated the benefits of using simulation which has played an instrumental part in the re-design of this particular rivet. Machining the worst case scenario rivet in Test 2 has provided validation for the simulation and ensured that a certain level of confidence can be put into simulations of new rivet designs.

This study has also proven its innovative potential by expanding on the previous testing involving press hardened steel (chapter 7.2) by including both geometry and hardness of materials as with the previous has also shown additional benefits of a not only estimating process window of a joint but in doing so guiding a design of a new rivet. Based on the simulation pointing out the trends, only the worst case scenario rivet was manufactured for testing, saving a lot of time and work in process.

7.3 Simulation of Solid SPR riveting joining process (Swage riveting)

INTRODUCTION

The automotive industry is experiencing an increasing need to reduce the weight of the vehicle and thin sheets of aluminium and steel are becoming the focus of joining processes. Whilst SPR has become the leading joining technique for joining dissimilar materials such as aluminium and steel up to 1000 MPa, joints using UHSS steel over 1000 MPa remain a challenge for SPR using standard semi or fully tubular rivet. The recently launched more robust BG rivet (as explained in section 7.1) has resolved some of the issues and works well in joining of UHSS steel up to 1500 MPa and up to 1.4mm in thickness. However, the condition for this is that the bottom sheet has to be a ductile aluminium

alloy such as 5xxx series to accommodate the slug (the disc cut out by the rivet legs) that is not ductile enough to displace into the bore of the rivet. This alloy also needs to be at least 2.0mm in thickness due to potential thinning out of Tmin when adhesives are added into the joint.

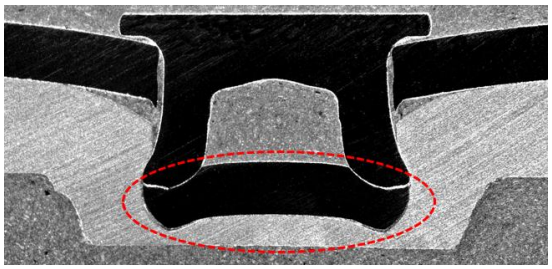

Figure 264, Example of a slug not being displaced int othe bore of the rivet

If the bottom sheet's hardness is to increase or thickness to reduce below 2.0mm or both, the BG rivet will not be able to create a sufficiently robust joint able to perform reliably in production. An example of this is below where a solution using SPR is not available. As shown in the image below of a rivet being used to join 1.4mm thick 1470 MPa strong steel to 2.0mm thick aluminium of 7xxx series which is considerably harder than common aluminium from series 5 and 6xxx. When shallow die is used to accommodate lack of ductility the rivet collapses (the effects of shallow dies are illustrated in section 7.1). When a deeper die is used to counter the rivet collapse by supporting it from below, severe cracking on the bottom sheet occurs with a risk that it will eventually propagate to the rivet leg.

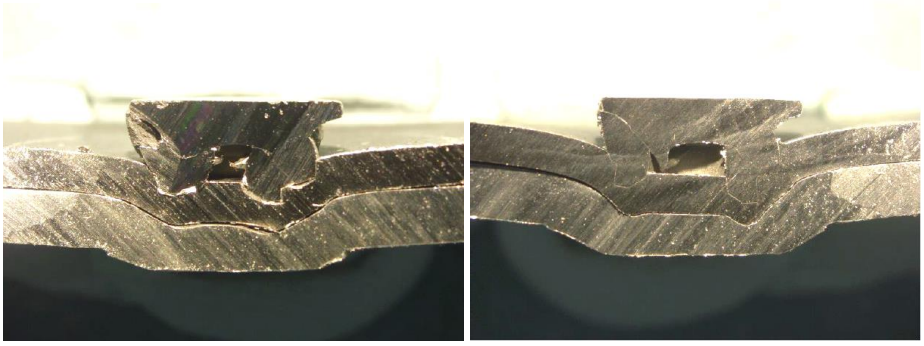

Figure 265, Shallow die to causes the rivet to collapse

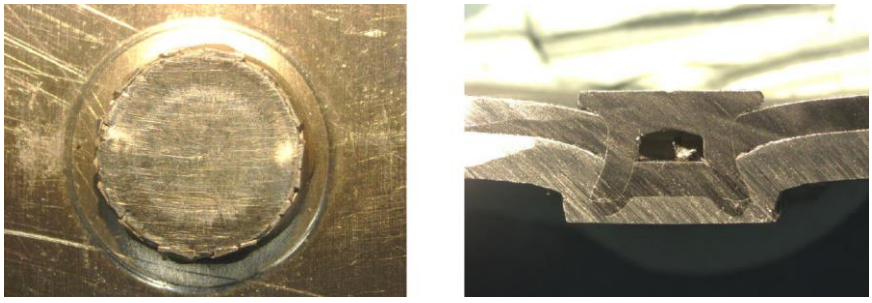

Figure 266, Deeper die creates a better joint but causes cracking on the button

Another issue with the conventional SPR method when joining UHSS is if the stack is reversed and UHSS steel is on the bottom sheet. This is a scenario that currently cannot be joined using any SPR rivet as this process relies on the ductility of material being joined to allow flaring of the rivet legs.

To address the shortage of ductility in both above mentioned cases, a new solid self piercing process has been designed, termed swage riveting. This is a completely new technique of joining and the only similar methodology currently available is work completed by Jäckel et al (2014) on kerb konus (explained in chapter 2.10.5). Following the success with conventional SPR methods, simulation has been employed to aid the design process of this process.

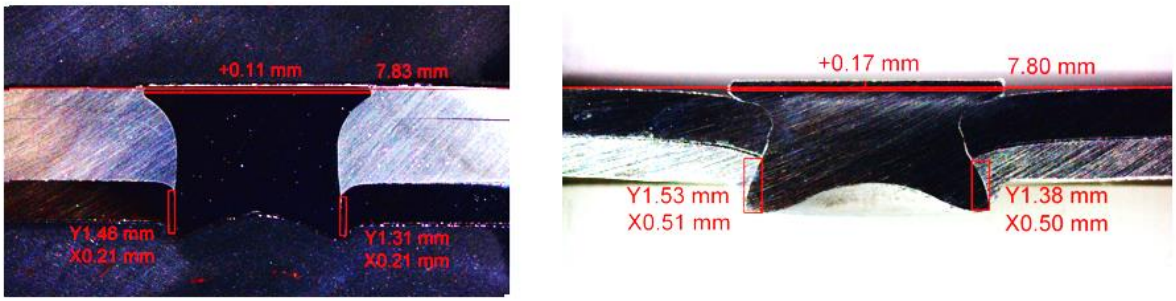

Figure 267, Example of swaged rivets

The first phase of this experiment consisted of setting up a swage model in simulations. This has drawn on the accumulated knowledge of simulation gained via modelling of SPR. The second phase was to validate the model on physical tests of swage joints.

TESTING PROCEDURE

AC procedure for sample preparation, rivet insertion and joint examination, as outlined in sections 5.1 and 5.2 has been followed.

7.3.1 Development of the swage simulation model

The Swage process consists of two stages. In the first stage, the stack is positioned between the punch and a hollow die as shown in image below.

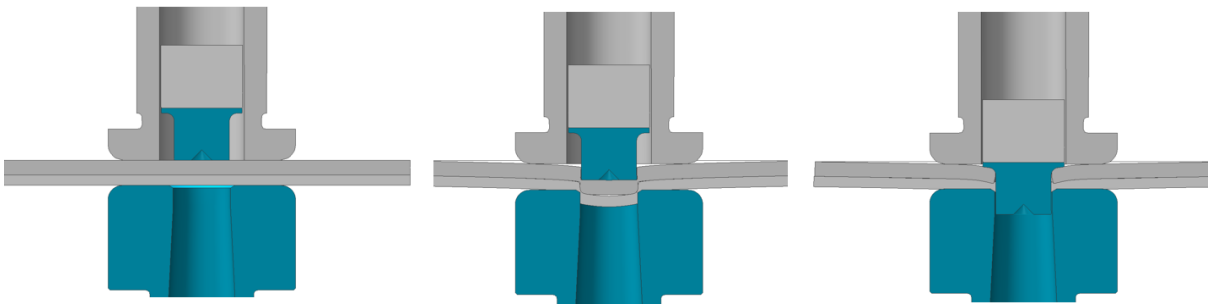

Figure 268, Solid SPR – schematic of stage 1 rivet insertion process

The punch then presses the solid rivet into the sheets, cutting a hole into the sheets in process. The punched out discs of material (slugs) are removed through a hollow die and the punch keeps pushing the rivet until the rivet head is either flush with the top sheet or in case of a countersunk head, the head sits firmly on top of the top sheet.

Next, the hollow die is replaced by a raised die and the riveted joint in pushed down by the press until the bottom parts of the rivet split and flare outwards and upwards, creating an interlock.

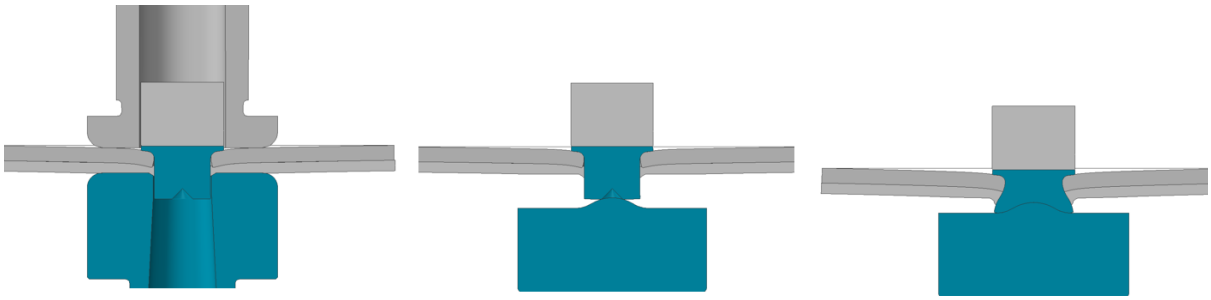

Figure 269, Solid SPR – schematic of stage 2 rivet insertion process

In order to set up the model demonstrated above, an SPR model has been used, with some parts and settings retained and some were replaced by settings more suited to the process of swage insertion.

Parameters remaining the same:

- Press – same press was used as for SPR as current equipment is currently being used for testing stage of swage. Gross energy input was determined based on sensitivity study whilst the selection of velocity was made based on physical test.
- Friction – same friction values were used as those for SPR. The swage is currently under development and for any testing to date, standard Atlas Copco coating (HLO) has been used. A new coating and more suitable coating might be developed, however, all the recent swage testing has been completed using standard rivet coating which means that the existing friction settings can be used.

Parameters adjusted to new process:

- Geometries
- Clamp
- Material removal criteria (cut distance)

Changes to all of the above aspects will be discussed in the next section.

7.3.1.1 Geometries

Dies

As mentioned above the standard die used in SPR processes has been replaced by the hollow and raised dies for stages 1 and 2 respectively.

Figure 270, Stage 1 – hollow die (left), stage 2 – raised die (right)

Additional fixtures

A separate set of cylindrical clamping jigs were added into the process later.

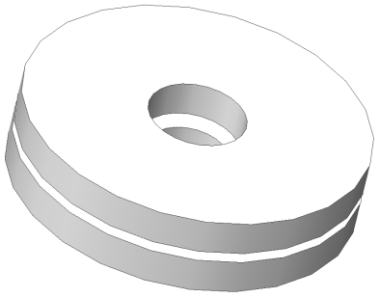

Figure 271, Illustration of jigs used for swage

Geometries retaining history of stresses and strains

Due to the process of swage joining happening over two separate stages, the geometries from the first stage had to be imported into the second one with the previous deformation. This is a relatively easy process, however, it has to be kept in mind that along with the deformation of the shape all stress and strain historical data should be transferred to the next stage as well.

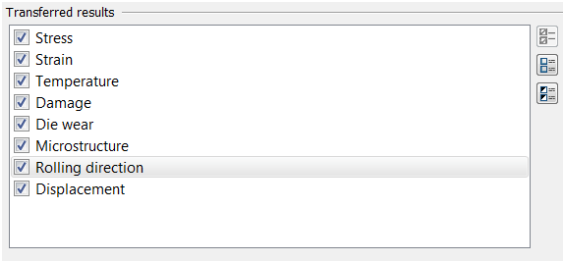

Figure 272, Properties transferred from 1st stage of solid riveting (swage)

7.3.1.2 Clamp

With SPR process, the R&D engineers consider the flush HH indication of a full rivet insertion. This concept was applied to the swage. However, during the process of the model set up, a UHSS top sheet was used which caused higher than usual dishing, which was then subsequently transferred into the second stage, causing the head height to be too high in comparison with the physical cross section of the joint – as shown demonstrated in the images below.

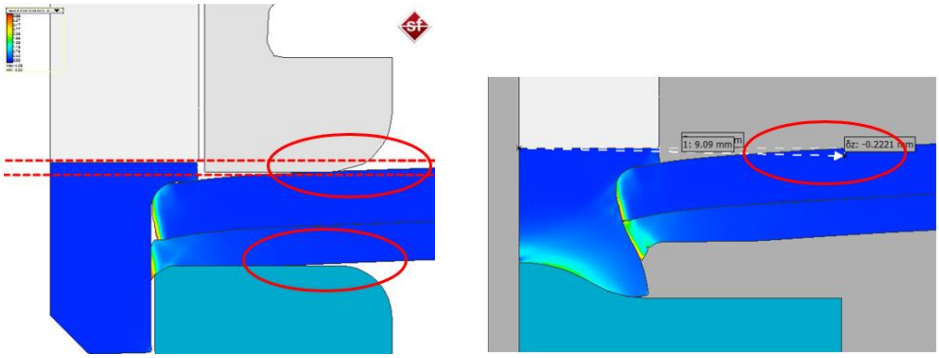

Figure 273, Dishing of the stop sheet in absence of fixtures and support of a die

At this point it was clarified that the physical process also used fixtures to prevent this dishing of the top sheet from happening. As a result of this, a set of cylindrical fixture have been provided for simulation to replicate the joint very closely. It should be highlighted that the fact that the numerical modelling has accounted for the dishing in absence of the fixtures and generated a result that was different from the physical cross section added a certain level of confidence to the process of simulation.

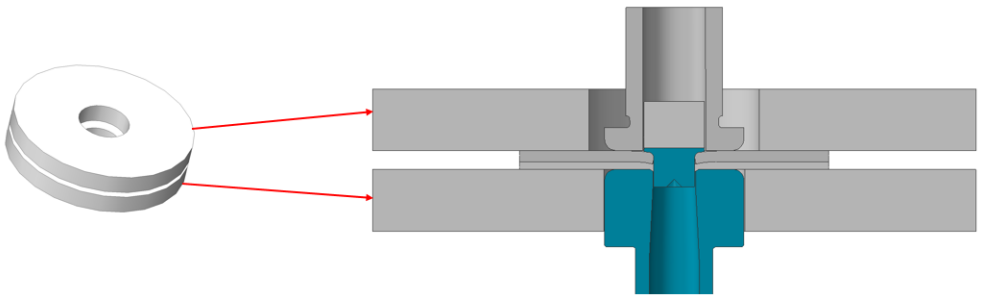

Figure 274, Demonstration of the fixtures added to the process

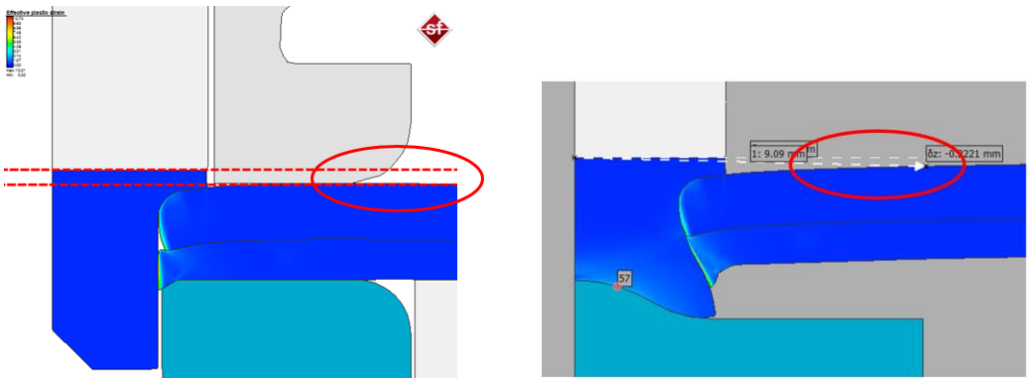

Figure 275, Correct examples of HH in swage riveting

7.3.1.3 Cut distance

The main difference is that in the stage 1, the sheets are not being pierced and formed but rather punched out so removing these needs to be accounted for in the model. This was resolved by increasing the percentage of parts to be removed from the process (further explained in section 4.1.1.2.5.1). For SPR, this setting is very low (0.005%) due to the need to reflect the reality of the process which does not lose any material and any element removal is only used to prevent any potential meshing issues with too small elements. A sensitivity study was conducted which revealed that a value of 30% is sufficient to remove the discs from the model once punched out.

7.3.2 Validation of the swage model

Upon completion of the swage model set-up several joints were tested in order to validate the model.

METHOD

The newly set up model was used to simulate the below joints:

Joint 1:	1.4mm Usibor 1500 + 1.0mm RC5754
Rivet:	K50E44E
Die:	Hollow die Ø5.5, pip die DP1.0

Joint 2:	1.0mm RC5754 + 1.4mm Usibor 1500
Rivet:	K50G44A
Die:	Hollow die Ø5.9, pip die DP1.0

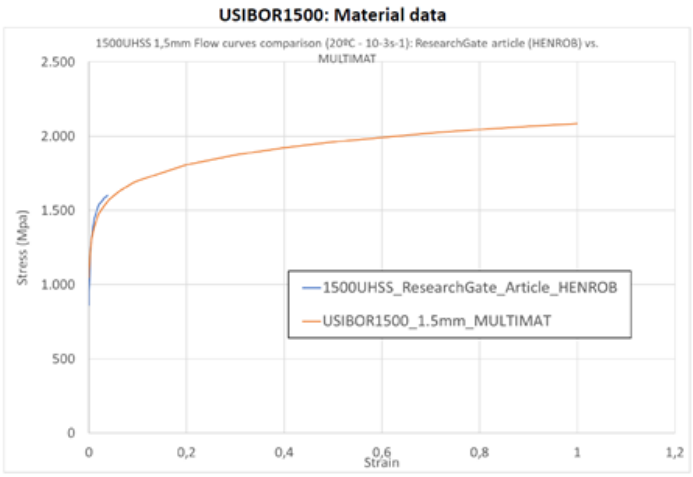

Figure 276, Flow curve used for this test is Usibor 1500

Velocity used for the joints were 220mm/s for stage 1 and 280 mm/s for stage 2 of joint 1 insertion. Joint 2 used velocity of 160mm/s for stage 1 and 280 mm/s for stage 2.

TESTING PROCEDURE

AC procedure for sample preparation, rivet insertion and joint examination, as outlined in sections 5.1 and 5.2 has been followed

RESULTS AND DISCUSSION

7.3.2.1 Joint 1 results

The results were captured after both stages.

Joint 1:	1.4mm Usibor 1500 + 1.0mm RC5754	
Rivet:	K50E44E	
Die:	Hollow die Ø5.5, pip die DP1.0	
	Stage 1 Stage 2 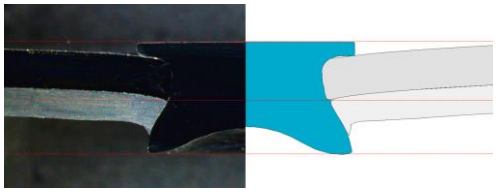	
Parameter	Physical test result [mm]	Simulation [mm]
Interlock:	0.67	0.69
Tmin:	N/A	N/A
HH:	0.17	0.14

Table 74, Results – Joint 1

Force-displacement curves

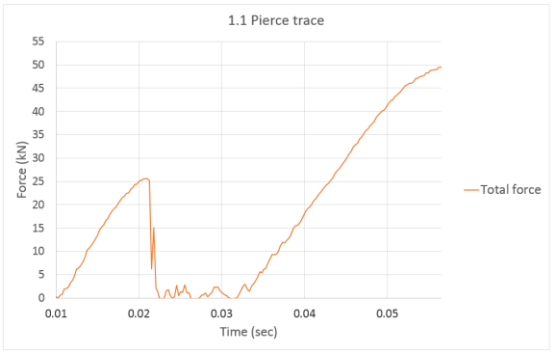

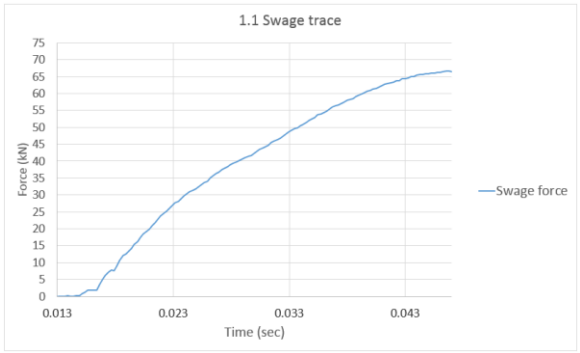

Figure 277, Force-displacement curves for swage joint 1 – physical testing

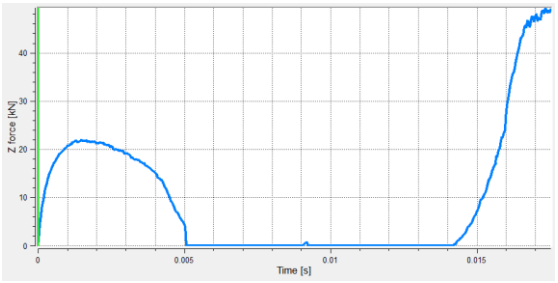

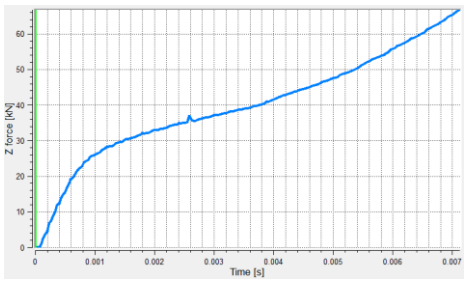

Figure 278, Force-displacement curves for swage joint 1 – simulation

7.3.2.2 Joint 2 results

Joint 2:	1.0mm RC5754 + 1.4mm Usibor 1500	
Rivet:	K50G44A	
Die:	Hollow die Ø5.9, pip die DP1.0	
	Stage 1 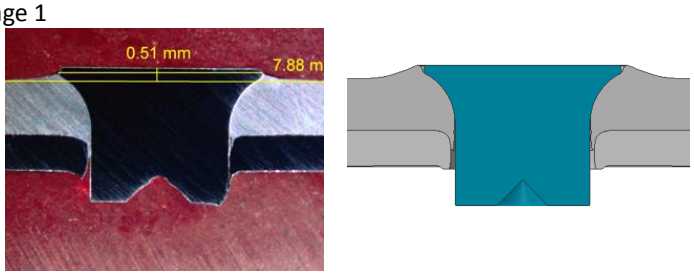 Stage 2 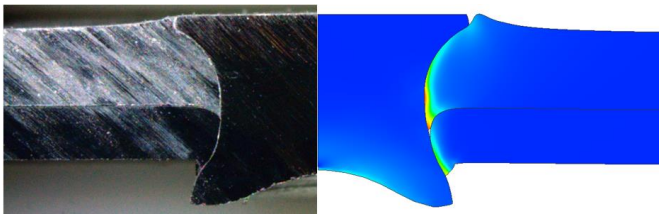	
Parameter	Physical test result [mm]	Simulation [mm]
Interlock:	0.68	0.65
Tmin:	N/A	N/A
HH:	0.27	0.38

Table 75, Results – Joint 2

Force-displacement curves

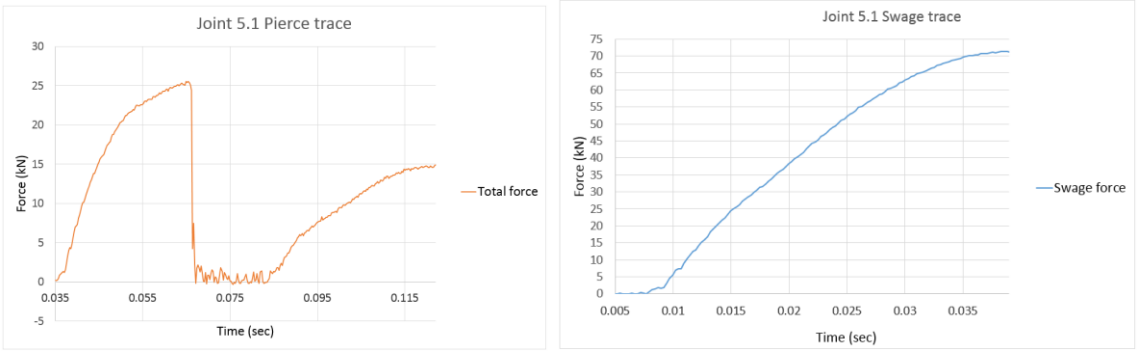

Figure 279, Force-displacement curves for swage joint 2 – simulation

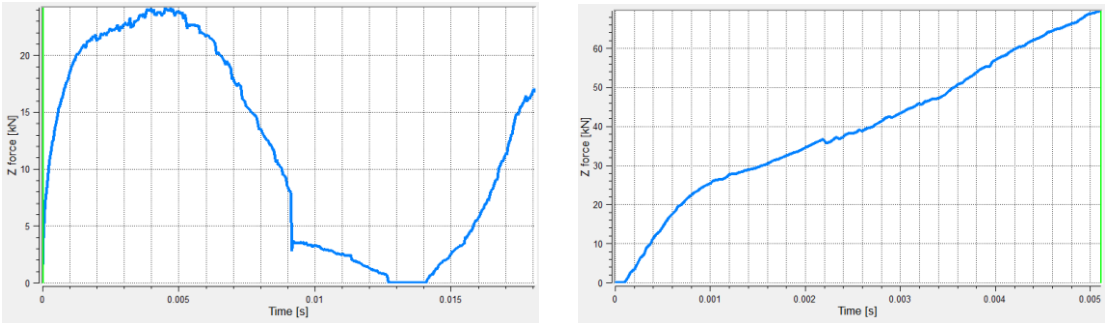

Figure 280, Force-displacement curves for swage joint 2 – simulation

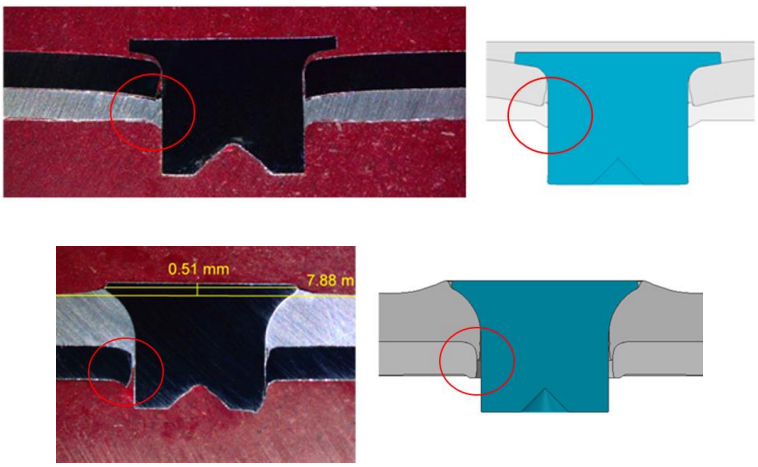

Figure 281, Example of good agreement between mid stage of swage

The swage model can be considered successful as good correlation between physical and simulation outcomes can be seen in both joints and both of their individual stages. This includes specific features of the way the ductile aluminium is shaped around the usibor sheet, moving upwards in the gap between the usibor sheet and the rivet in joint 1 and behaving the same in the opposite direction in the joint 2 as shown the two images above.

The interesting fact about the features displayed in the mid stage cross sections that during the testing of swage process, the results of the first were on no occasion cross sectioned as they were simply moved onto the next stage immediately. However, after seeing the above mid stage results via simulation, the accuracy of the simulation was called into question as doubts were raised about whether the material does form in this way. Cross sections of the first stage joints were therefore completed to validate the results of the simulation which confirmed that numerical modelling was correct. This additional test has specifically highlighted the benefits of the simulation in supporting a R&D processes and has confirmed its potential for predictive capability.

Whilst the force-displacement curves do not match exactly throughout the insertion due to the servo press not being available in the software (as explained in section 6.3.3) both are representative of a typical shape of the force displacement curve for both stages for both joints.

Furthermore, same level of forces have been achieved in both joints.

Joint no.	Test type	Pierce force		Swage force [kN]
		Sheet 1 [kN]	Sheet 2 [kN]	
Joint 1	Physical test	20	50	64
	Simulation	25	50	66
Joint 2	Physical test	25	15	70
	Simulation	25	17	71

Table 76, Results – comparison of forces from physical and simulation tests

7.4 Summary

Following a large amount of testing carried out for purposes of this chapter, the next few paragraphs will aim to summarize the findings.

The FE modelling software and the base model developed in chapter 6 has been initially applied to a task of predicting a robustness of the joining process window for joints with newly launched BG rivets designed for UHSS material, Usibor1500 (section 7.1). This particular material has a high variability in hardness due to its production process of quenching and cooling non-uniformly throughout a pressed part. When supplied by material suppliers, this material is usually described as its bottom end of the hardness spectrum but in reality the hardness can climb up to 200 MPa higher. Using material with this extent of variability can potentially lead to some unfavourable results once in production and can eventually cause the joint to fall over and might required a change in process design such as changing a rivet for example. This can be prevented by using simulation in order to establish limitations of the selected rivet (as shown in Table 63 and Figure 252) and pre-empt any possible falling over in production by selecting a stronger rivet accordingly.

Following the success of establishing the material process window as per above, this concept has been expanded on in section 7.2 using newly designed 4mm tubular rivet for narrow flange. The included idea of combining material process window from the previous application with ideas based on the interesting results from study on influence of rivet geometry in section 6.3.8.1. This meant that the process window will include variations in materials as well as geometry to establish a process window. This would also allow to test the hypothesis that the rivet manufactured at the bottom of its hardness

tolerance band, highest at its length tolerance band and lowest at its tip geometry tolerance band was the worst case scenario in SPR production.

The study has yielded a particularly good result as the simulation was validated by a joint with a rivet purposefully machined as softest, longest and sharpest version of the standard rivet and the results were in a very good agreement (as shown in figure below) suggesting that FE modelling can be particularly beneficial to the industry when used in this way.

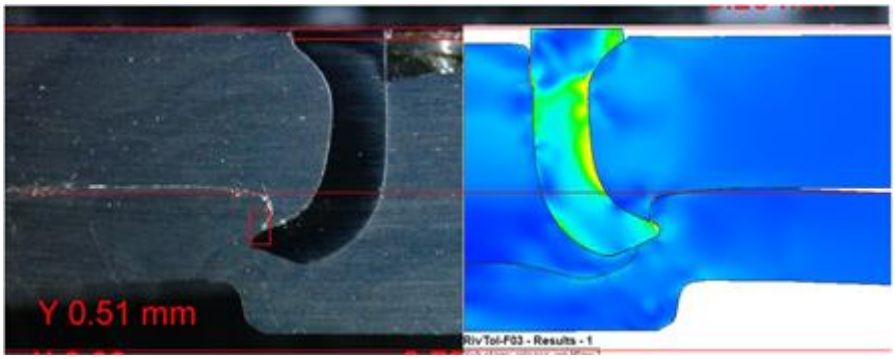

Figure 282, Sharpest, longest and softest rivet resulting from production variability

The last practical application was simulation of a newly designed concept for joinining, i.e. Solid riveting or Swage riveting. As explained in the chapter 7.3, this concept has been developed due to pressures from automotive to use UHSS steels as bottom sheets, which is impossible for standard SPR rivet to flare in and create interlock. Unlike with the previous project, this task required a new set up of the simulation model first before moving on to the practical application. Once the model was set up, two examples of swage riveting were completed and the initial results show a lot of potential for future of R&D support using FE modelling.

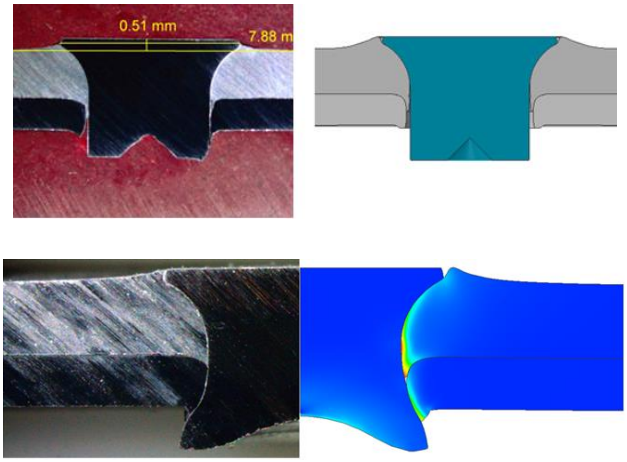

Figure 283, Swage riveting example

Based on all three types of practical applications of FE modelling in this chapter, it is possible to say that this a great potential to be a useful tool for both process window testing and supporting R&D. Both concepts would be particularly useful in an industry which is currently relying heavily on physical testing which is both time consuming and costly.

Other than reducing the amount testing that can be done with available materials, FE modelling can be also applied proactively in instances where material is not available and a certain condition cannot be tested. This could see a creation of a master database using the fuzziness concept where joints are tested for a number of other conditions in addition to the parameters of materials and geometries mentioned above. Due to the long term nature of this idea, this will be further discussed in the section on Future work section.

8 DISCUSSION

8.1 Introduction

Each of the tasks tested and described in the experimental stage in chapter 6 include a brief discussion about the findings for that particular topic. This chapter discusses the findings of the literature review and brings them together with the simulation studies whilst relating them to the objectives set for this research project.

8.2 Selection and evaluation of out of the box version of the selected software (Objective 1A and 1B)

In order to create a base model for numerical modelling of SPR, a suitable software type had to be selected. A number of researchers have attempted to simulate the SPR process and a number of software packages are available to do so with. Software types such as MSC.Marc, LS-Dyna (used by Casalino and Rotondo, 2008, Moraes, 2015) MSC.AutoForge (used by Bouchard et al, 2008, Hahn and Dolle, 2009, Varela et al, 2018), Abaqus (used by Westgate, 2001, 2002, Westerberg, 2002), Ansys (used by Casalino and Rotondo, 2008) and Deform (used by Khezri, 2000, Melander, 2003) were most frequently employed for simulation of SPR. Simufact software has gained prominence in recent years when work has been conducted using this software by Carandente (2016), Honsch (2018) and Kraus (2018) The software has been used also by automotive manufacturers such as Audi, Renault and Jaguar Landrover (TechSpec, 2019). As outlined in section 6.2, the selected software was Simufact which is a specifically good position for simulation SPR as it uses a powerful MSC.Marc solver and uses the latest advancement in contact definitions such as segment-to-segment contact which is particularly useful for SPR where a very complex contact between multiple segments is modelled. It furthermore uses a combined friction model which is particularly beneficial in SPR where stresses can exceed the materials UTS multiple times. The two variable parameters (outside the materials which are set according to engineering tables) that were shown to have the most significant effect are friction and clamping method. The latter has not been particularly well researched in literature to date and whilst friction has been research extensively, a good set of parameters applicable across different coatings are not available at this moment.

8.3 Development of the base simulation model (Objective 2)

8.3.1 Development of friction parameters (Objective 2A)

As discussed in chapters 4.1.5 and specifically 6.3.1, friction is an important factor in simulations of SPR and has a significant effect in some joints.

As such this field has been previously researched by a number of researchers throughout the years (Melander, 2003, Khezri et al, 2000, Atzeni et al, 2005, 2009, Xu, 2006, Kato, 2007, Krishnappa, 2008, Abe, 2009, Mucha, 2011, Caradente et al, 2016, Honsch et al, 2018, Kraus, 2018, Varela et al, 2018).

With exception of Honsch (2018), most of the researchers have used a Coulomb friction model to simulate SPR. It is the belief of the author that the Combined model of friction, which as explained in chapter 4.1.5.6, is a more suitable option for simulation of friction used in this work. This is due to the fact that it covers friction of materials in their elastic deformation stage (covered by coefficient of friction) as well as when the materials start plastically deforming (covered by interface friction factor). This is in contrast to a sole use of Coulomb's friction model which only covers friction in elastic stage after which the coefficient of friction becomes irrelevant.

The research by the above authors mainly includes friction tightly configured to a small number of stacks (up to three) with very little variation in terms of different rivets using any specific coatings or sheet materials. For the first time, this work has included a friction study that validates friction settings on a larger number (12) of joints and covers a wide range of different types of rivets with two different coatings and mixture of materials (aluminium and steel).

The design of experiment completed on these joints has suggested using two different sets of friction values, depending on the coating used on the rivet (i.e. H00 or HL0, also explained in chapter 4.1.5.6).

Using these settings (shown in chapter 6.3.1.4) has proven to deliver realistic outputs in terms of comparison of physical and simulated joint. One could consider these settings quite high with friction coefficient reaching value of 0.3 and interface friction factor reaching value of 0.6 in comparison to previous researchers. However, simulation of same joint using a number of values generated by other researchers has shown reduced agreement in measurements as well as typical features of SPR joints (section 6.3.1.3.2) in comparison with this newly established friction model (referred to in Figure 171 and Figure 172). Simulations were also conducted with higher than necessary friction to find limiting parameters Figure 177.

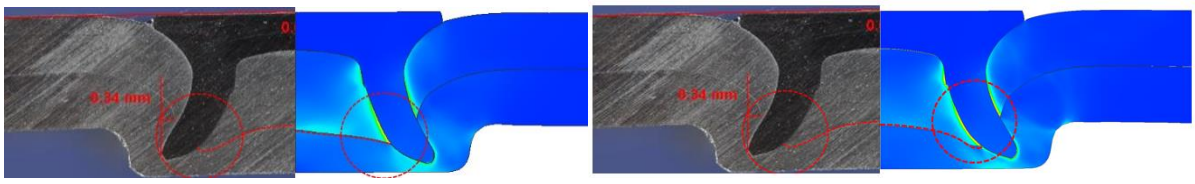

Figure 284, Comparison of physical cross section with simulation using with friction levels from literature (left) and newly established friction settings (right).

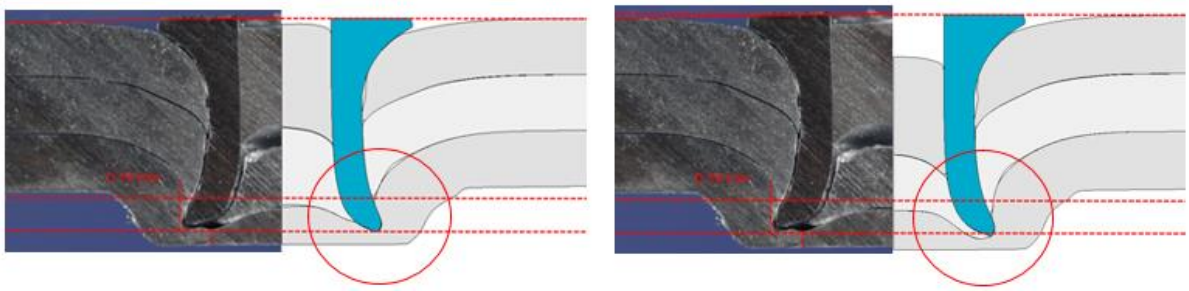

Figure 285, Example of excessive friction set to find limiting parameters.

To validate these levels of friction, joints have been physically tested using both, excessively added lubricant to decrease friction as well as no added coating to excessively reduce friction. All instances of physical tests have shown similar characteristics to those displayed in simulations. This included the lack of drag down of the material under the rivet leg and straight line between the rivet legs in the joints with lower friction (as suggested by other authors). This contrast with the bell like shape and dip of sheet material below the rivet leg as shown in Figure 284 with the new friction model. The physical joints have also displayed decreased bore fill, reduced interlock and reduced Tmin due to the excessive drag down of the material below the rivet leg as shown in Figure 285) when excessively high friction was used.

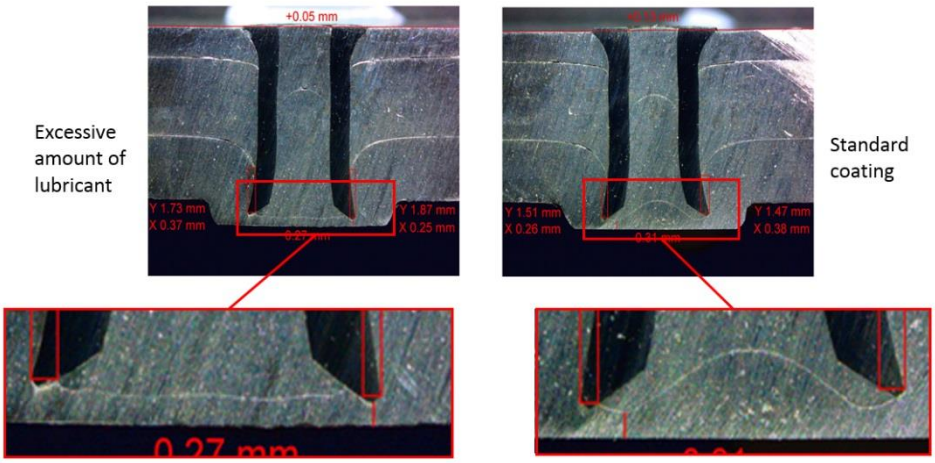

Figure 286, Joint completed with excessive amount of coating vs standard coating

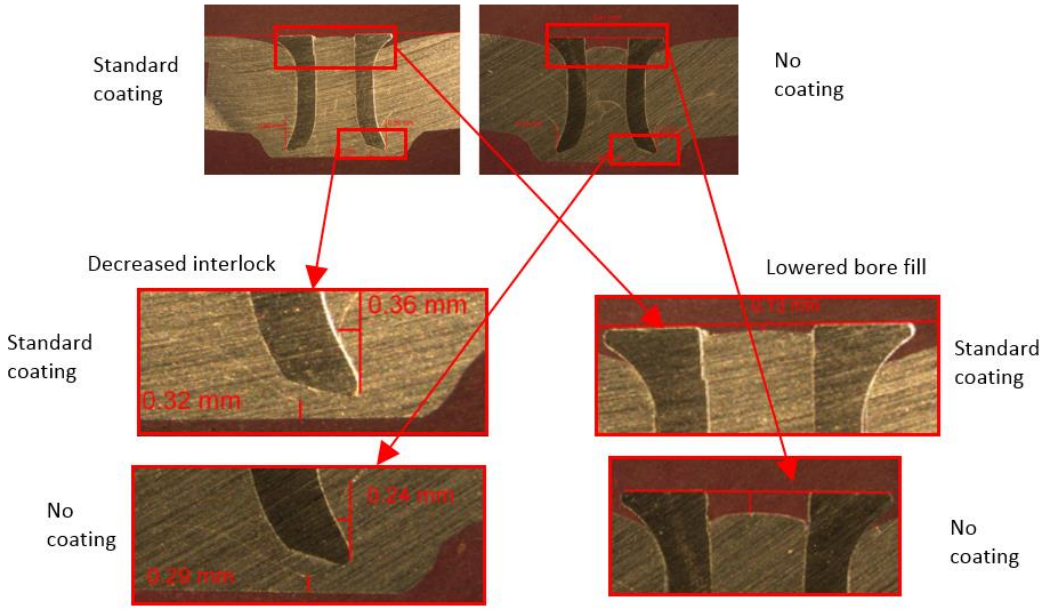

Figure 287, Joint completed with standard coating vs no coating

Despite the same trends and good agreement of measurements being exhibited in both physical and simulations results, there is further scope for improvement of friction by investigating influence of more coatings as well as other variables potentially exerting some level of influence. However, the author is satisfied that the current model captures the behaviour of the friction reasonably sufficiently.

8.3.2 Effect of different joint clamping methods (Objective 2B)

To author's knowledge, clamping is mentioned only in few research papers – those of Khezri (2000), Porcaro et al (2006) and Carandente (2016). Porcaro used a pre-clamp mechanism by using a displacement for the nose first, followed by the punch and both Khezri and Carandente used a spring with force of 5 kN to model the clamp mechanisms.

As explained in the literature review, Simufact also uses spring to direct the clamping mechanism. However, to imitate the process clamping method employed in the sponsoring company, a new additional model referred to as intermediate clamp was designed. This clamp engages only a short time (0.525mm on average) before the end of the insertion process as shown in image below.

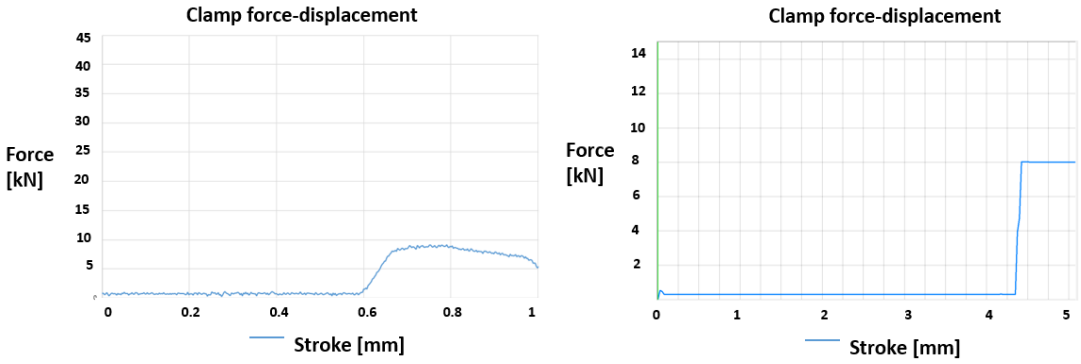

Figure 288, Force-displacement curves extracted from servo setter (left) and new simulation intermediate clamp method (right).

The choice of clamping method in Atlas Copco SPR production is known to influence the riveting result for some types of joint stacks, however, little work has been published on this topic. Therefore, the difference between using a pre-clamp and an intermediate clamp was investigated for range of aluminium and mixed material joint stacks in section 6.3.2. The materials included stacks for aluminium/ aluminium, HSS steel to aluminium and UHSS steel to aluminium. The aluminium to aluminium (1.5mm AA5182 + 1.5mm AA5182) stack has shown no effect of clamping. The effect on stack with HSS (1.5mm DP600 material + 1.5mm AA5182) was negligible. However, the effect of the clamp with high strength steel stack (1.5mm Fortiform + 1.5mm AA5182 with newly designed BG rivet) has shown a significant effect on the quality of the joint. An illustration of this is shown in the image below, where stack the has been captured below at roughly the same time into the insertion. The stack with intermediate clamp exhibiting a considerably lower interlock despite appearing to be closer to full insertion than the joint with preclamp.

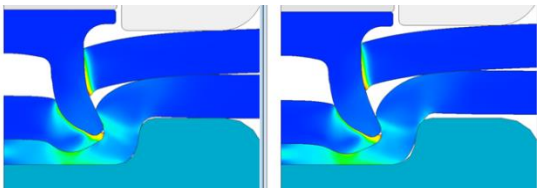

Figure 289, A joint with preclamp (left) and intermediate clamp (right) captured cc4.4nm into the stroke.

Tmin can also be seen as reduced and there is a large internal gap which will be present even after full insertion as shown in image below.

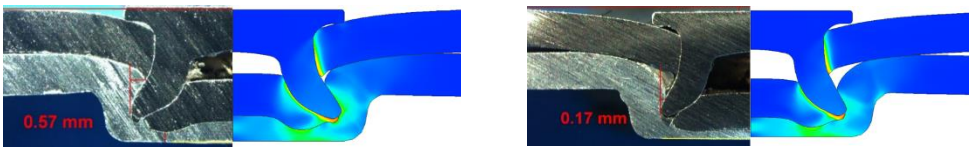

Figure 290, A joint with preclamp (left) and intermediate clamp (right)

Although use of intermediate clamp prevents hardening of the materials (as explained in chapter 4.1.2.3.1), with the advance of UHSS materials the effect of intermediate clamp on the joint is not desirable due to the lowered interlock. This has been noted and the equipment department is working towards an adjustable clamp mechanism that can be set for individual stacks.

8.4 Simulation of fully tubular rivets (Objective 3A)

Fully tubular rivet (T rivet) is one of the recently launched new products by Atlas Copco, and as such it has not been simulated previously. It is the author's belief that the T rivet simulations have therefore been conducted for the first time as part of this work. The initial simulations of this rivet were specifically conducted as part of chapter 6.3.1.3.1, where friction was determined by sensitivity studies. This was a priority due to the fact that this rivet used a new, low friction coating to prevent early flaring and compression due to shallow dies used this these rivets. Good agreement was achieved in simulations using a specific set of friction values accounting for a lower friction coating added to the T rivet.

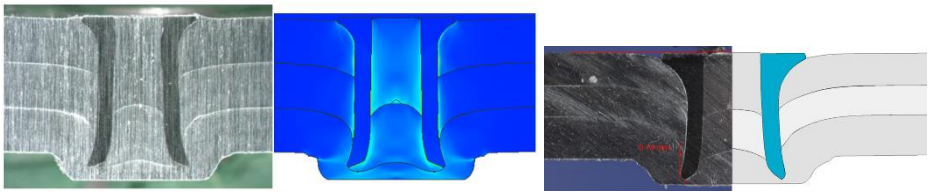

Figure 291, Example of Trivet simulations

Apart from the friction levels and adding a third joining partner i.e. third sheet (the main advantage of the T rivet is that they are better at riveting 3 stack joints due to sufficient space in the bore to accommodate the material displacement) no significant changes needed to be made to the base model.

During the testing of friction for T rivet slightly inconsistent results were being output for some of the joints which led to examination of all other parameters. This investigation has revealed that some of the dimensions of models for simulations such as flare angle and tip geometry have been drawn up inconsistently with the drawings used for production, which led to a variation in tip geometry. This has now been addressed and rivet models for simulations have been re-drawn to correct specifications reflecting the geometries of manufactured rivets.

The presumed effect of a wider angle is that the added material on the foot of the rivet (example below – rivet T511-2) creates more of an obstacle for the sheet material to flow around which means that the piercing of the sheet is reduced due to increased resistance of the material flowing less.

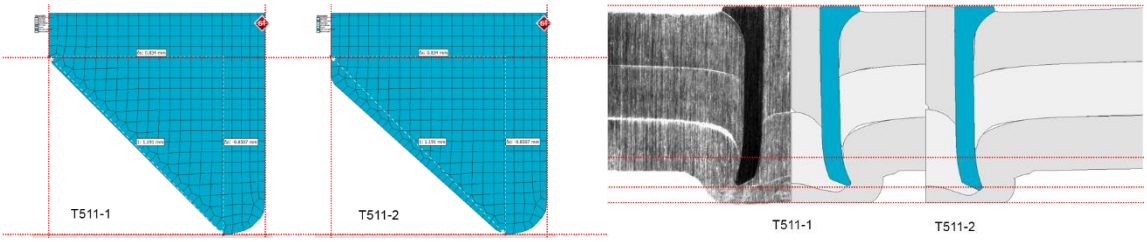

Figure 292, An example of difference in drawing

A new fully tubular rivet has also been further simulated as part of the rivet optimisation which will be discussed in the section 8.9.

8.5 Mixed material riveting of UHSS to aluminium and Process window for sheet and rivet properties (Objective 3B & 4A)

SPR is best suited to joining softer and more ductile aluminium to aluminium however, mixed materials joining, especially joining of harder steels UHSSs and press hardened steels is on the rise due to increasing safety of the vehicles as well as weight reduction. A number of researchers have successfully attempted to join and simulate dissimilar materials such as Magnesium AZ31 (Moraes, 2015), DP600 (Khezri et al, 2000, Westerberg, 2002) TRIP800 (Khezri, Melander 2000). These materials are common in joining as the standard SPR rivets are sufficient. Abe et al (2008) was one of the few researchers to have simulated joining UHSS material boron to aluminium using a standard rivet. However, to succeed with such high strength steel and conventional rivet, a die had to be optimized. In viewpoint of Atlas Copco it is not advisable to rivet UHSS materials with standard C rivet as this puts too much stress on rivet which can lead to crack propagation (Briskham, 2016).

Atlas Copco have designed a new higher column strength rivet with larger shank diameter as a specific response to increased use of hot stamp steel to aluminium by JLR.

An additional problem with hot stamp steel is that the materials hardness has proven to vary across the part which presents a challenge for joining. Combined with manufacturing variation of rivet, this might affect the robustness of the rivet once in production. Since physical lab testing can only test the material and rivets supplied, this led to a request from the JLR to try using the simulation to test a combination of upper and lower sheet material property with upper and lower tolerance band for rivet hardness to estimate the process window for using the new rivets in production. The innovative

part of this exercise is the ability to adjust flow curves using the scaling factor option to reflect upper and lower values of the sheet material. The scaling was carried out on the basis of advice from steel supplier.

The simulation pointed out that the worst case scenario was with lowest rivet hardness and highest material hardness where particularly high compression was seen in the rivet as shown in image below. However, despite the compression, the measurements were not impacted by this variation.

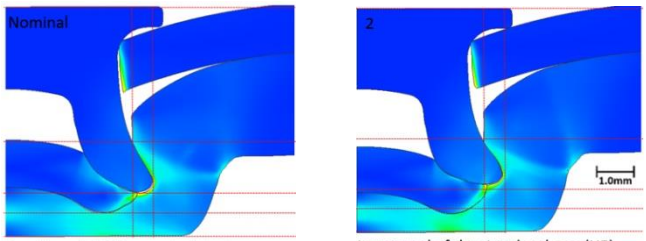

Benchmark joint - nominal rivet hardness (H6) with nominal sheet hardness (1500 MPa)

Lower end of the rivet hardness (H5) with upper end of the material hardness (1700 MPa)

Figure 293, Nominal and worts case scenario UHSS steel joint

Some level of physical validation might be needed as with the study on optimisation of rivet where the nominal joint and worst scenario joint were selected for physical testing. However, in absence of material to test this presents at least some reassurance that the rivet will be robust enough in production. This study shows great potential for simulation to be used for creating a process window for individual combinations of materials and rivet and estimating robustness of these joints in production.

8.6 Simulation to aid design optimisation of new 4mm shank diameter T-rivets in combination with new narrow flange equipment (Objective 3C & 4B)

A good opportunity for a simulation of a particularly innovative project has been created when a narrow flange was requested by a customer in order to reduce weight of the vehicle and at the same time increase visibility from the vehicle by reducing the width of the B Pillars, thus increasing its safety. The estimated weight saving is cc2.64kg per car (Williams, 2019). In order to be able to rivet a narrow flange, a new, smaller and narrower type of rivet and die need to be developed. Since an interim small die initially designed for 3mm rivets can be used for these purposes, the focus is on the development of the rivet geometry which has also been requested to be a fully tubular rivets.

Since making small changes to a rivet geometry and validating it physically is time and resource consuming, numerical modelling has been employed to support optimisation of the geometry of this

new rivet. To author's knowledge no data has been published so far in optimisation of a rivet. Whilst there has been some research by Mucha (2011 and 2016) and Abe et al (2009) in using simulation for a successful optimisation of dies, the rivets and their more complex geometries have not yet been designed with aid of simulation.

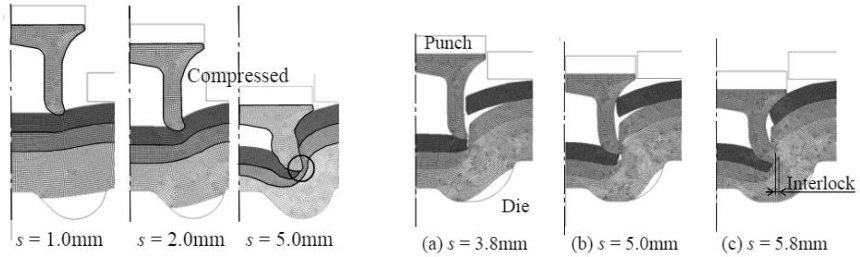

Figure 294, Optimisation of dies by Abe et al (2009)

The chapter 7.2 therefore documents a series of tests where small adjustments geometry of a number of rivet parameters and rivet hardness were made to estimate the worst case scenario from the perspective of manufacturing variations. The preliminary results pointed out that the softest, longest and sharpest rivet is the worst case scenario due to the increased residual stress in an excessively flared out rivet. The simulation has been used to carry out most of the testing and a physical sample of the new rivet was only machined at nominal geometry and hardness. Following simulation tests, another physical sample was machined with the worst case scenario of a narrowest tip, highest rivet lengths and lowest hardness. There was a good agreement of the sample:

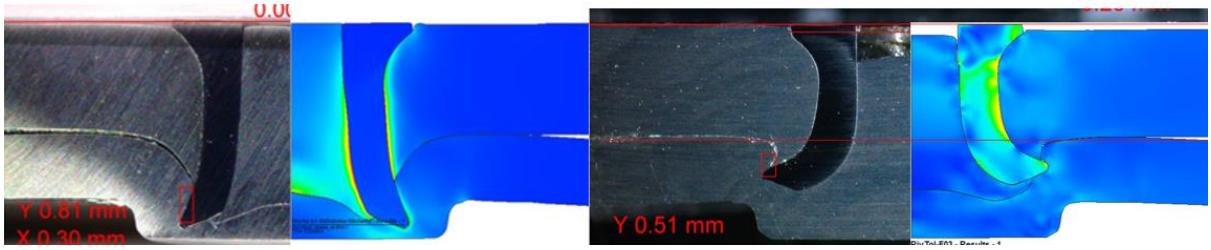

Same rivet at nominal geometry and hardness (left) and worst case scenario of longest, sharpest and softest rivet

Figure 295, Results of rivet optimisation study on narrow flange T rivet

The good agreement of the joints with physical samples has successfully confirmed through a direct example that simulation can be particularly beneficial in optimising rivet geometry. This involves testing a large number of small incremental geometry changes in combination with other production variables and in process reducing a number of physical time consuming testing. The intention is to publish this work to fill in the gap in the currently available research.

8.7 Swage solid SPR riveting joining process (Objective 3D)

Swage method, introduced in chapter 7.3, is a new two stage SPR method specifically aimed at joining stacks that are too difficult to be joined by conventional SPR method. As explained before, this includes joints with UHSS steel as to sheet and harder bottom sheet or UHSS as bottom sheets. This is a completely new technique of joining and the only similar methodology currently available is work completed by Jäckel et al (2014) on kerb konus (explained in chapter 2.10.5). This method also involves two stages where a slug is punched out from sheets by insertion of a grooved rivet in the first stage. In the second stage the bottom sheet forms interlock around the rivet by being pressed into the grooves of the rivet by a die. The disadvantage of this method is that the joint strength is dictated by the strength of the aluminium on the bottom of the joint. As such it would not be suited to joining sheets of steel with low ductility or steel as bottom sheet which is required increasingly.

In order to simulate the swage joining, a new simulation model has been developed which, to the best of author's knowledge has not done previously. Development of this model involved creating an additional step in the insertion process using geometries from the previous step so that they retain the history of stresses and strains.

The validation of this model by physical testing has shown an excellent agreement with simulation.

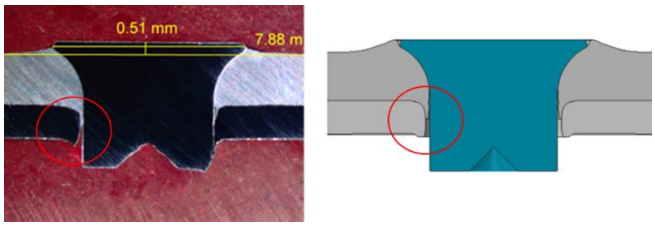

Figure 296, Example of agreemenet of simulation and physical test of first stag of swage joining

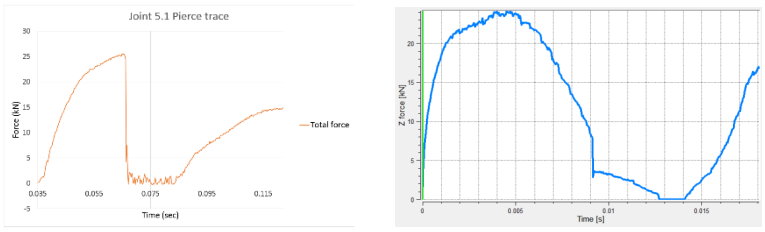

Figure 297, Example of agreement of force-displacement curves corresponding to the image above.

This highlights the significant benefit of using simulation to support product development studies such as this. If combined with process window testing completed in the previous studies, this is likely to provide a comprehensive approach to research and development and reduce the amount of physical testing.

9 CONCLUSIONS

9.1 Conclusions

This aim of this chapter is to bring together all the key findings based on the work carried out within this thesis and highlight the novel work that this thesis has achieved in view of the objectives set out in chapter 1.

Objective 1: Selection and evaluation of the software

Following the research conducted as part of the literature review and in line with Objective 1, the Simufact software was selected on the basis of its advantages over its competitors (Objective 1A - 1.2.1.1). Preliminary testing with the out of the box software in order to establish its capability in its current status followed (Objective 1B part 1 - 1.2.1.2). This highlighted that whilst selection of this software was a correct decision, to be effective and reliable, there were areas of the FE modelling that currently needed calibration and more research in order to reflect the SPR procedure of the supplier equipment the physical testing was carried out with. Follow on sensitivity testing (Objective 1B part 2 - 1.2.1.2), identified Clamping and Friction as two most significant areas for improvement followed by a number of other topics that required further knowledge such as effective meshing method, influence of geometry and material definitions, damage modelling etc.

Following on from this, work aimed at developing a base model commenced on the areas identified above.

Objective 2 – Development of the base model

This objective's focus in on the development and validation of a suitable clamping method and friction model.

2A: Develop friction parameters for different rivet coatings 1.2.1.1

An extensive testing of friction examined the effect of each friction pairing within the joint and identified the effects on sheet and rivet behaviour when friction levels change in isolation (e.g. Interlock is decreased when friction level is between rivet and sheets is increased). Combined knowledge of these behaviours was then applied to a joint and all friction pairings were individually calibrated to achieve agreement between simulation and physical test. To address the two different

coatings used on AC rivets (standard rivet coating H00 and tubular rivet coating HL0), this exercise was conducted on two different stacks, one using semi tubular rivet, the other a fully tubular rivet. The exercise revealed that the suitable friction levels were considerably higher than expected (with majority of the pairings using $\mu = 0.3$ and $m = 0.6$, whilst default model used values $\mu = 0.1$ and $m = 0.2$) so the model was validated on a number of other joints which resulted in a good agreement between the simulation and physical test. Established values were since applied to and validated by a number of further joints with positive results and hence this accomplishment has proven to be a valuable contribution to the field of SPR simulation. The friction model values can be found in section 6.3.1.4 - Figure 171 and Figure 172.

2B: Investigate the effect of different joint stack clamping methods using simulation (1.2.2.2)

The second parameter identified as needing improvement was clamping method. Consequently, a new set up was developed reflecting the fact that the clamping in AC setters engages during the process of the insertion rather than before it starts as it is in the default clamping model. The new model was then validated on three different joints using different hardness of materials and provided and the simulation results were in good agreement with the physical test. This exercise has given insight into how the resulting joint is formed via a video of the simulated insertion process which is unavailable to view during physical test due to its speed. Viewing this process of insertion in slower motion has confirmed the hypothesis proposed by AC recently, suggesting that whilst the AC's current clamping set up works well for Aluminium stacks with high ductility, it is less suitable for joints with UHSS materials. The AC are already working on a new setter with a new clamping method and simulation will be part of this process.

As part of the development of the base model stage, more parameters such as meshing method, influence of geometry and material definitions, damage modelling etc. were tested in order to understand how they work and to be able to apply these in a manner that reflects the insertion process of AC SPR.

Objective 3: Application of base model

Once validated, the newly developed base model has been applied to scenarios of practical applications for further validation and to address issues coming to forefront of the SPR industry's priorities. This includes a number of topics which will be discussed below.

3A: Apply SPR simulation to fully tubular rivets (1.2.3.1)

The new fully tubular rivets use in the recently launched Jaguar F-pace and Ford F150 require a very low friction coating to assist the flow of aluminium up to the top of the rivet bore; the development of simulation for tubular rivets first required the development of friction parameters for the new low friction coating to limit early flaring. A correct simulation of this rivet has been made possible by the previous friction research which allowed identification of the low friction coating settings for the simulation model. A close match to the physical test results was achieved for a range of validated joints which is proving beneficial for future of testing and application of fully tubular rivets. It should be highlighted that no previous work was found on this topic in the published literature and the author believes this work was the first research study conducted on the simulation of T-rivets.

3B: Apply SPR simulation to mixed material riveting of UHSS to aluminium (1.2.3.2)

New rivet higher column strength designs with larger rivet shank diameters are being developed in the test lab to enable SPR to join high strength hot stamp steel to aluminium. This development work provided an opportunity to explore the use of simulation for this new challenging type of joint stack. Little or no previous SPR simulation work has been conducted on riveting UHSS to aluminium, especially not with the new development rivet designs.

As with the new tubular rivet, the correct simulation of this rivet was made possible through the work completed on friction as the new rivet with higher column strength, BG type, also uses the low friction coating. As a result, application of the base model saw simulations in good agreement with the real physical joint tests and the correctly converged solution is ready to be applied in a follow on testing which is part of another objective, 3E, and is elaborated on later on in this section.

3C: Apply SPR simulation to the new development of joining narrow flanges (1.2.3.3)

This study has investigated simulating a new, smaller 12mm diameter nose on the new narrow flange riveting equipment combined with the new 4mm rivet shank diameter and new 12mm die diameter. Design of this rivet is in response to a automotive industry demand for greater visibility in a vehicle.

This objective is closely tied to objectives 2A and 3A where a correct simulation of a standard size tubular rivet with a correctly specified low friction setting has been applied to a new set up of a narrow flange and involved creating a narrower punch and nose models. Simulation of this model has further confirmed that the model for tubular rivets is correct, as the completed simulation has shown an agreement with a particularly typical sign of a narrow flange joining which is the downwards dishing

of the bottom sheet as shown below which is not seen in the standard sized tubular rivets. This is a sign that simulation model is correctly set up and is transferrable to new products.

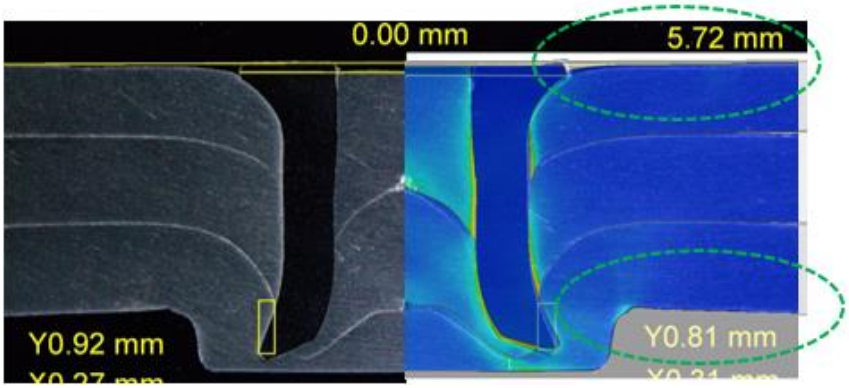

Figure 298, Example of a correct narrow flange joint simulation.

3D: Apply SPR simulation to the new swage solid SPR riveting joining process (1.2.3.4)

In line with the conclusions from the above objective suggesting that the base model is correctly set and transferrable to new and novel products, the intention was to push this further and also test this out on a completely new process.

The development lab were working on developing new two stage equipment and new solid rivets to create a new solid riveting product solution for joints with UHSS on the bottom sheet, which are not possible with conventional SPR but are needed in the industry in order to address the carbon emission reduction aim.

This process is called Solid self-piercing rivet or Swage riveting and the base model was applied to this process. As with narrow flange riveting a set of new CAD models were required to address the differences in the models as well as adding another phase to the simulation.

The results of these modifications was a new model that was successfully validated by physical tests of two different swage joints (section 7.3) and has shown a great potential for future research of new products and created a platform to support an ongoing development.

There is a significant potential for a publication and the author planning to submit a paper on this in near future.

Objective 4: Utilisation of validated simulation models

Following the successful application of the base simulation model developed in objective 2 and its further modifications in objective 3, the question what other benefits can a simulation bring to the industry apart from just simply replicating a joint and validating it with its physical counterpart completed in laboratory conditions. The two models, standard SPR and narrow flange SPR model were therefore applied to studies determining process windows for manufacturing variables that can potentially occur once the joint is outside the laboratory conditions and in a manufacturing environment.

4A: Process window simulation for tolerance range of sheet material and rivet properties (1.2.4.1)

This task is a follow on from objective 3B where the requirement was to use the simulation base model for a newly developed rivet designed specifically for UHSS materials (Usibor1500) which is highly in demand by automotive industry currently due to its increased strength. However, hardness of this material can be particularly variable due to its manufacturing process, causing decreasing ductility. With this issue, as well as the potential manufacturing variable of the rivet hardness in mind, a simulation study was launched (section 7.1) for a joint used by an automotive company JLR to assess a combination of upper and lower sheet material property with upper and lower tolerance band for rivet hardness to estimate the process window for using the new rivets in production.

The results from this tolerance band study indicated the joints would work at the upper and lower material properties conditions with the upper and lower hardness of the rivet, even in the scenario which has the lowest sheet material hardness with the highest rivet material hardness and its reverse version of the hardest sheet materials hardness with the lowest rivet material hardness.

4B: Using SPR Simulation to aid the design and optimisation of new rivets (1.2.4.2)

This task is a follow on from objective 3C where the requirement was to apply the base model for tubular rivets to a new smaller shank size T-rivet for narrow flange and provided a good opportunity to apply simulation in order to not just replicate the joint but also to the design optimisation of this new rivet. The simulation study that was conducted built on the successful example of the hardness process window in objective 4A and in addition to material hardness parameter, added a parameter of changing rivet geometry that could occur within the allowed manufacturing variation to predict the effect of upper and lower values on joint quality. Two of these, geometry and hardness variations, were physically tested to validate the simulation results (section 7.2). The results from this simulation study resulted in a change being made to the rivet production tolerances, and the nominal size selected for the rivet geometry with very little physical testing. This is considered to be a significant

achievement as it is the first time the sponsoring company used SPR simulation to choose the geometry and tolerance range to apply to a new rivet product.

9.2 Recommendations for Future Work

i. Expand the simulation work to use simulation for designing and optimising new dies.

ii. Develop an adjustable press type i.e. a package that allows individual input in the Simufact software to enable different models of setter to be programmed into the software so that users can select and test different setter models according to the customer requirements. To include the ability to start with an insertia fly press to bring the punch up to a fast start speed, and then add extra energy during the rivet insertion. This development request has been presented to Simufact in France by webex and they have set up a project to work on this request.

iii. Conduct further work on friction to validate a wider range of rivet coatings with develop the Simufact software to have an option to select different rivet coatings with different coating friction levels.

iv. Conduct further work to expand the currently available research on use of various damage models and Gurson-Tvergaard damage model in particular in order to accurately describe ductile fracture in SPR simulation.

v. Improve the material property flow curve data sets available to cover a wider range of materials by conducting compression and in plane torsion testing on material samples using a Gleeble machine.

vi. Expand the work started in this study on the optimisation of rivet designs to explore a wide range of rivet designs and different joint stacks to aid the development of new rivets and increase the understanding of how SPR rivets behave during insertion.

vii. Combining both the rivet design and the die design together by simulating the effect of changing both to optimise how they work together could lead to some improvements in rivet and die designs.

viii. Expand the work started in this study to investigate different clamping arrangements.

ix. Re-evaluate Agreeability scorecard to reflect emerging importance of flow pattern deformation features in a joint. Whilst the measurements of HH, Interlock and Tmin are important indicators of quality of a joint, the fact that simulation captures very specific features of changes geometries is in itself an equally good indicator of simulation accuracy (as for example shown in chapter 6.3.1.3.3 on friction). Based on this, a re-consideration of

weightings of the scoring should be carried out. It has also been further suggested that adding an option within the software to convert the visual qualitative deformation features into a quantitative measurement by adding an option in the software to measure radii of specific geometry shapes after deformation. This suggestion will be relayed to the software engineers.

x. Investigate the simulation of joints containing adhesive to develop a method for including the lubricative effect of adhesive in the rivet insertion simulation. Combine this with the effect of different clamping arrangements on adhesive flow.

xi. Employ the solid SPR (swage) simulation model developed in this study to continue the development and optimisation of rivets and dies for the new swage riveting process.

xii. Investigate the option of developing a master database which would serve as a tool for rivet and die rationalisations (i.e. selection of rivets and dies for multiple joints of one setter in order to reduce costs). The database will aim to bring together physical results where available and their simulated counterparts. Gaps in physical testing e.g. if some rivet sizes are missing from range can then be covered by simulation using the existing data for calibration of materials. Further benefit of this database also is applying the idea of process window to create a 'fuzziness' concept to SPR simulation. This involves simulating a number of parameters that may be subject to variability predominantly such as material hardness, rivet and sheets geometries but also clamping engagement point and coating and others with a view to establish a process window for each particular stack. Due to the size of this project, this remains a long term plan which will be built on over time.

10 REFERENCES

Abe,Y. et al (2009) Self-piercing riveting of high tensile strength steel and aluminum alloy sheets using conventional rivet and die. J Mater Process Technol 209:3914–392.

Abe, Y., Kato, T., Mori, K. (2008) Self-pierce riveting of three high strength steel and aluminium alloy sheets. April 2008International Journal of Material Forming 1:1271-1274 DOI: 10.1007/s12289-008-0134-9.

Abe. Y. et al (2008) Joinability of aluminium alloy and mild steel sheets by self piercing rivet. J of Mat Process Tech 177:417-421.

Abe, Y., Kato, T., Mori, K. (2009) Self-piercing riveting of high tensile strength steel and aluminium alloy sheets using conventional rivet and die. J Mater Process Technol 209(8):3914–3922.

Altan, T. et al (2011) Determining the flow stress curve with yield and ultimate tensile strengths, Part I. Stamping Journal. [Online] Available: https://www.thefabricator.com/article/metalsmaterials/determining-the-flow-stress-curve-with-yield-and-ultimate-tensile-strengths-part-i [Accessed Jan 2017].

Alves, L.M. at al (2011) Revisiting the Fundamentals and Capabilities of the Stack Compression. Experimental mechanics. DOI: 10.1007/s11340-011-9480-5.

Anon. Plastic deformation and stress-strain curves. University of Babylon, Baghdad. Publication 12_24290_1049 [online] Available: http://www.uobabylon.edu.iq/eprints/publication_12_24290_1049.pdf [Accessed Jan 2017].

Armstromg, P.E., Hockett,J.E.., Sherby, O.D. (1982) Large strain multidirectional deformation of 1100 aluminum at 300 K. Journal of Mechanics and physics of solids. 30 (1-2): 37-58.

ASTM Standard A370. Mechanical Testing of steel products.

ASTM E8 (2013) Standard Test Methods for Tension Testing of Metallic Materials.

Atzeni, E, et al (2003) Analysis pf the self piercing riveting process. In: Proceedings of the sixth AITEM Conference, Gaeta, Italy 281-292.

Atzeni E, et al (2009) Experimental and numerical appraisal of self-piercing riveting. CIRP Annals Manuf Technol 58(1):17–20.

Atzeni, E., Ippolito, R., Settineri, L. (2007) FEM modeling of selfpiercing riveted joint. Key Eng Mater 344:655–662.

Altan, T. et al (2012) Sheet Metal forming – Fundamentals. ASM International. [Online] Available: http://www.asminternational.org/documents/10192/3477814/05340G_Sample.pdf/274eeee5-af5e-4920-8607-ecad5682a521 [Accessed Oct 2016].

Ashby, M.F. et al (1996) Engineering Materials 1: An Introduction to their Properties and Applications. Butterworth-Heinemann, Oxford.

Atzeni, E. et al (2005) Experimental and numerical investigation on self-piercing riveting. SME Technical Paper TP05PUB94.

Atzeni, E. et al (2004) Numerical and laboratory experiments on self-piercing riveting. In proceedings of the fourth CIRP International seminar on Intelligent Computation in Manufacturing Engineering, 305-309. Sorrento, Italy.

Audi (2017) Presentation on joining of the A7 car body. In proceedings of JoiningInCarBodyEngineering 2017.

Banabic, D. (2012) Influence of material models on the accuracy of the sheet forming simulation. Mater. Manuf. Proc. 27:304–308.

Barkanov , E. (2001) Introduction to the Finite element method. Institute of materials and structures, Faculty of Civil engineering, University of Riga, Riga.

Barnes, T.A., Pashby, I.R. (2000) Joining techniques for aluminium spaceframes used in automobiles. Part II. Adhesive bonding and mechanical fasteners. Journal of Material Processing and Technology 99:72–79.

Bailyn, M. (1994) A Survey of Thermodynamics. New York, NY: American Institute of Physics Press.

BBS Stal Metaller (2019) Hardness conversion table - Tensile strength, Vickers, Brinell and Rockwell. BBS Stal Metaller [Online] Available: https://www.bbshalmstad.se/en/infocenter/hardness-conversion-table/ [Accessed Jan 2017].

Belytschko, T, Liu, W.K., Moran, B., Elkhodary, K.I. (2000) Nonlinear Finite Elements of Continua and Structures. John Wiley and sons, London

Benham, P.P. et al (1996) Mechanics of Engineering materials. Addison Wesley Longman Limited, Essex.

Bonora, N., Testa, G., Iannitti, G., Ruggiero, A. and Gentile, D. (2018) "Numerical simulation of self-piercing riveting process (SRP) using continuum damage mechanics modelling", Frattura ed Integrità Strutturale, 12(44):161-172.

Bouchard, P.O. (2005) 3D numerical modelling of damage and fracture. Towards an integrated approach between forming process and structural analysis. In proceedings of the 8th EASFPRM conference, Cluj-Napoca.

Bouchard, P.O., et al (2008) Numerical modelling of self-pierce riveting—from riveting process modelling down to structural analysis. J Mater Process Technol 202(1-3):290–300.

Bowden, F.P., Freitag E.H. (1958) The Friction of Solids at Very High Speeds. I. Metal on Metal; II. Metal on Diamond. Proceedings of the Royal Society of London. Series A.

Briskham, P. (2016) Self piercing riveting. In proceedings of ALFED seminar, Detroit, Michigan.

Briskham, P. (2019) Internal discussions. Atlas Copco, Deeside, UK.

Bruschi, S. et al (2014) Testing and modelling material behaviour and formability in metal sheet forming. CIRP Annals - Manufacturing Technology CIRP Annals - Manufacturing Technology 63: 727–749

Budynas, R. G. (2015). Shigley's Mechanical Engineering Design—10th ed. McGraw Hill. p. 233. ISBN 978-0-07-339820-4.

Cacko, R. et al (2004) Initial optimisation of self piercing riveting process by means of FEM. Steel grips 2 307-310.

Caltech (2018) Cool cosmos. Section 'How does heat travel' [Online] Available: http://coolcosmos.ipac.caltech.edu/cosmic_classroom/light_lessons/thermal/transfer.html [Accessed June 2018].

Campos, H. (2014) Hydraulic bulge test for stress-strain curve determination and damage calibration for Ito-Goya model. In proceedings from 11th World Congress on Computational Mechanics (WCCM XI).

Chandramouli, R. (2015) Material behaviour in metal forming. SASTRA University, Thanjavur.

Changqing, D. (2013) Nonlinear Strain Path Forming Limit of a Reverse draw. AIP Conference Proceedings 1567.

Chen , Y. et al (2009) Stress-strain behaviour of aluminium alloys at a wide range of strain rates . International journal of solids and Structures 46: 3825-3835.

Casalino, G., Rotondo, A., Ludovico, A. (2008) On the numerical modeling of the multiphysics self piercing riveting process based on the finite element technique. Adv Eng Software 39(9):787–795.

Carandente, M. et al (2016) Improvements in numerical simulation of the SPR process using a thermos-mechanical finite element analysis. Journal of Mat Processing Technol 236:148-161.

Clarke, C. (2007) Influence of manufacturing on self-pierce rivets. Internal document at Atlas Copco, Deeside.

Clough, R. W. (1960) The finite element method in plane stress analysis. Proc. American Society of Civil Engineers 23:345-378. In proceedings of 2nd Conference on Electronic Computation, Pitsburg, Pennsylvania.

Courant, R. (1943) Variational methods for the solution of problems of equilibrium and vibrations. Bulletin of the American Mathematical Society 49:1-23.

Crisfield, M. A. (1991). Non-linear Finite Element Analysis of Solids and Structures 1. Chichester, England: John Wiley & Sons Ltd.

Chu, Y. et al (2012) Determination of the Flow Curve at High Strain Rates Using Electromagnetic Punch Stretching. Journal of Materials Processing Technology 212:1314–1323.

Davies, G. (2012) Chapter 2— Design and material utilization. Materials for Automobile Bodies. Butterworth-Heinemann, Oxford, 17–91.

Dieter, G.E. (1988) Mechanical Metallurgy. McGraw-Hill International, Oxford.

Dix, E.H. (1950) Trans ASM, 42, 1057, 1950

Dixit, U.S., Narayanan, R.G. Ganesh, R. (2013) Metal Forming: Technology and Process Modelling Paperback. Tata McGraw Hill Education Private Limited, New Delhi.

Dezhi, L. et al (2017) Self-piercing riveting-a review. Internation journal of Advanced Manufacturing Technology 92:1777–1824.

Donev J.M.K.C. et al. (2018) Energy Education - Braking [Online]. Available: https://energyeducation.ca/encyclopedia/Braking. [Accessed: October 8, 2019].

Drossel, W.G., Jäckel, M. (2014) New die concept for self-pierce riveting materials with limited ductility, Key Engineering Materials 611–612 1452–1459.

Durandet, Y., Deam, R., Beer, A., Song, W., Blacket, S. (2010) Laser assisted self-pierce riveting of AZ31 magnesium alloy strips. Mater Design 31(1):S13–S16.

Durandet, Y. et al (2010) Laser assisted self-pierce riveting of AZ31 magnesium alloy strips, Materials and Design 31S13–S16. Archives of civil and mechanical engineering 83 – 93.

Easton, M. et al (2008) Magnesium alloy applications in automotive structures. JOM Journal of the Minerals. Metals and Materials Society 60:57.

Eckstein, J. (2009) Numerische und experimentelle Erweiterung der Verfahrensgrenzen beim Halbhohlstanznieten hochfester Bleche. Dissertation for the University of Stuttgart, Stuttgart.

Eller, K. et al (2013) Constitutive modelling of quench hardenable boron steel with tailored properties. Forming Technology Forum 19 – 20.

Eller T.K et al (2016) Determination of strain hardening parameters of tailor hardened boron steel up to high strains using inverse FEM optimization and strain field matching.Journal of Materials Processing Technology 228:43–58.

Elmelin (2019) Which Metals Dissipate Heat the Best. [Online] Available: https://elmelin.com/which-metals-dissipate-heat-the-best/ [Accessed June 2018].

Engineering ToolBox (2004) Friction and Friction Coefficients for various Materials. [online] Available at: https://www.engineeringtoolbox.com/friction-coefficients-d_778.html [Accessed Oct 2017].

Eckstein, J. (2004) Potential der Finite-Elemente-Methode zum Stanznieten höherfester Stähle Diplomarbeit, Institut für Flugzeugbau, University of Stuttgart, Stuttgart.

Euro Car Body Conf (2018) Benchmark Data Jaguar I-PACE.

Fallahiarezoodar, A. et al (2015) R&D update: Determining flow stress data by combining uniaxial tensile test and biaxial bulge test. Stamping journal. [online] Available https://www.thefabricator.com/stampingjournal/article/stamping/r-d-update-determining-flow-stress-data-by-combining-uniaxial-tensile-and-biaxial-bulge-tests [Accessed Nov 2017].

Fan, D. et al (2007) Critical review of hot stamping technology for automotive steels. In proceedings of the Materials and Science Technology conference, Detroit, Michigan.

Field, J.E. et al (2004) Review of Experimental Techniques for High Rate Deformation and Shock Studies. International Journal of Impact Engineering 30:725–775.

Fratini, L., Ruisi, V.F. (2009) Self-piercing riveting for aluminum alloys-composites hybrid joints. Int J Advanced Manufacturing Technology 43:61– 66.

Fu, M., Mallik, P.K. (2001) Effect of process variables on the static and fatique properties of self piercing riveted joints in aluminium alloy 5754. Society of automotive engineers 2001-010825.

Gardstram, J. (2006) Simulation of mechanical joining for automotive applications. Licentiate thesis for Royal Institute of Technol, Sweden.

Gerritsen, C. (2016) Self piercing riveting – a guide to best practice Section 1 Introduction and contents. TWI. [online] Available: http://www.twi-global.com/technical-knowledge/best-practice-guides/self-piercing-riveting-section-1-introduction-and-contents/. [Accessed August 2016].

Gese, H., Dell H. (2004) Modelle für die Plastizität und das Versagen vom Aluminiumblech AC300(3,0 mm) in den FEM-Programmen LS-Dyna und AUTOFORM Technischer Bericht, München.

Grote, K.-H., Feldhusen, J. (2011) Dubbel: Taschenbuch für den Maschinenbau. Springer Verlag, Berlin/ Heidelberg.

Grujicic, M., Snipes, J.S., Ramaswami, S., Abu-Farha, F. (2014) Self-piercing riveting process and joint modelling and simulations. Solids and structures (SAS) 3.

Hamidon, M.H. et al (2019) Investigation of mechanical testing on hybrid composite materials. Chapter in: Failure Analysis in Biocomposites, Fibre-Reinforced Composites and Hybrid Composites. Woodhead Publishing Series in Composites Science and Engineering 133-156.

Han, L. et al (2006) Effect of sheet materials coatings on quality and strength of self-piercing riveted joints. In proceedings of SAE World Congress paper no. 2006-01-0775

Han, L., Chrysanthou, A. (2008) Evaluation of quality and behaviour of self-piercing riveted aluminium to high strength low alloy sheets with different surface coatings. Mat. and Design 29 (2): 457-468

Han, L., Thornton, M,, Shergold, M. (2010) A comparison of the mechanical behavior of self-piercing riveted and resistance spot welded aluminum sheets for the automotive industry. Mater Des 31(3):1457–146.

Hahn, O., Dolle, N. (2001) Numerische simulation des ¨f¨ugeprozesses beim stanznieten mit halbhohlniet vonduktilen blechwerkstoffen. Universit¨at Paderborn. LWF journal of materials processing technology 199 (2008) 27–36 Schriftreihe 48, Shaker Verlag, Aachen, ISBN3-8265 -9427-4.

Harish, A. (2019) Implicit vs Explicit Finite Element Method (FEM): What is the Difference? [online] Available: https://www.simscale.com/blog/2019/01/implicit-vs-explicit-fem/ [Accessed June 2017].

Haque, R. (2017) Quality of self-piercing riveting (SPR) joints from cross-sectional perspective: A review. Archives of Civil and Mechanical engineering 18: 83-93.

He, X., Pearson, I., Young, K. (2008) Self-pierce riveting for sheet materials: state ofthe art. J. Mater. Process. Technology 199:27–36.

He, X., et al (2013) Numerical and experimental investigations of self piercing riveting. Int J Adv Manuf Technol 69:715-712.

He, X., Gu, F., Ball, A.(2011) Recent developments in finite element analysis of self piercing riveted joints. Int J Adv Manuf Technol 58:643-649.

He, X., Pearson, I., Young, K. (2008) Self-pierce riveting for sheet materials: state of the art. J Mater Process Technol 199(1–3):27– 36.

Henrob (2005) Henrob Self-Pierce Fastening – Overview of the Process. Internal presentation at Henrob.

Henrob (2015) Products catalogue. Henrob intranet, Deeside, UK.

Henrob 1 (2016) Applications. Henrob [online] Available: http://www.henrob.com/applications/automotive/ [Accessed July 2016]

Henrob 2 (2016) Applications. Henrob [online] Available: http://www.henrob.com/applications/air-conditioning-industry/ [Accessed July 2016]

Henrob 3, (2016) Applications. Henrob. [online] Available: http://www.henrob.com/applications/road-sign-manufacturing/. [Accessed July 2016]

Henrob 4, (2016) Applications. Henrob. [online] Available: http://www.henrob.com/applications/other-self-pierce-riveting-industries/ [Accessed July 2016]

Hill R. (1948) A theory of yielding and plastic flow of anisotropic metals. Proc R Soc A 193:281–97.

He X.C. et al. (2007) Finite Element Analysis of Self-Pierce Riveted Joints. Key Engineering Materials, 344: 663-668.

Helmenstine, A. M. (2019) Specific Heat Capacity in Chemistry.[Online] Available: ThoughtCothoughtco.com/definition-of-specific-heat-capacity-605672 [Accessed June 2018].

Henrob, (2015) Henrob Self-Pierce Fastening – Overview of the Process. Internal presentation at Henrob.

Hoang, N.H., Porcaro,R., Langseth,. M, Hanssen, A.G. (2010) Selfpiercing riveting connections using aluminum rivets. Int J Solids Struct 47(3–4):427–439.

Hochholdinger, B. at el (2009) Determination of flow curves by stack compression tests and inverse analysis for simulation of hot forming. In proceedings of the 7th European LS-Dyna conference. Salzburg, Austria.

Hoffmann, H., et al.: Handbuch Umformen, Carl Hanser Verlag, Munich, 2012.

Hönsch, F. et al (2018) Numerical simulation and experimental validation of self-piercing riveting (SPR) of 6xxx aluminium alloys for automotive applications. Journal of Physics: Conf. Series 1063 (2018) 012081.

Hönsch, F. et al (2019) Deformation Behavior of High-Strength Steel Rivets for Self-Piercing Riveting Applications. In proceeding of AIP Conference Proceedings 2113, 050002.

Hrennikov, A. (1941) Solution of problems in elasticity by the frame work method. Journal of Applied Mechanics, 8:169-175.

Hu, X.H et al. (2014) Edge fracture prediction of traditional and advanced trimming processes for AA6111-T4 sheets. J of Manuf Science and Eng. Transactions of ASME 136(2).

Hua, L.et al (2014) A Constitutive Model of 6111-T4 Aluminum Alloy Sheet Based on the Warm Tensile Test. Journal of Materials Engineering and Performance 23(3): 1107–1113.

Huang, L. et al (2018) Simulation of self-pierce rivet insertion using smootherd particle Galerkin method. 15th LS-Dyna coference, US.

Hutton, D.V. (2004) Fundamentals of Finite Element Analysis. McGraw-Hill. New York.

Hutton, D.V. (2004) Fundamentals of Finite Element Analysis. McGraw-Hill. New York.

Instron (2017) Vickers Test. [online] Available at https://www.instron.us/our-company/library/test-types/hardnesstest/vickers-test [Accessed March 28th 2017]

Jäckel, M., Kraus C., Kropp, T. (2014) Effects of increased tool velocity on mechanical joining of steel and aluminum sheet metals. Conference on Assembly Technologies and systems. In proceedings of CIRP 23: 24 – 28.

Jäckel, M., Grim, T., Landgrebe, D. (2016) Approaches for Mechanical Joining of 7xxx Series Aluminum Alloys," AIP Conf. Proc., 1769, 100010.

Jäckel, M. et al (2018) Overview of Current Challenges in Self-Pierce Riveting of Lightweight Materials. In proceedings of The Eighteenth International Conference of Experimental Mechanics, Brussels.

Jäckel, M. et al (2018) Standardization of Flow Curve Determination for Joining by Forming. Presentation for Cornet Project – Flow Curve JbyF. Fraunhofer Research Institute, Dresden.

Jäckel, M. et al (2018) Numerical simulation of thermal supported self pierce riveting of an ultra high strength aluminium alloy. Journal of Physics. Conference series 1063 012074.

Johnson, P., Cullen, J..D, Sharples, L., Shaw, A., Al-Shamma, A.I. (2009) Online visual measurement of self pierce riveting systems to help determine the quality of mechanical interlock. Measurement 42 (5):661-667

Junhe, L. et al (2013) A hybrid approach for modelling of plasticity and failure behaviour of advanced high-strength steel sheets. International Journal of Damage Mechanics 22(2):188-218.

Kaars, J. et al (2018) Determining material data for welding simulation of press hardened steel. Metals 89100: 740

Kahrimanidis, A. (2015) Process Design of Aluminum Tailor Heat Treated Blanks Materials. Materials 8(12),: 8524-8538.

Kato, T., Abe, Y., Mori, K. (2007) Finite element simulation of selfpiercing riveting of three aluminium alloy sheets. Key Eng Mater 340-341:1461–1466.

Kelly, P.A. (2012) Solid mechanics Part II – Lecture notes. The University of Auckland. Auckland.

Khezri, R., E. Sjöström, and A. Melander (2000) , Self-piercing riveting of high strength steel, Swedish Institute.

Khezri, R., Sjostrom, E., Melander, A. (2000) Self piercing riveting of high strength steel. Swedish Institute for metal research, Stockholm IM-2000-554.

Khezri, R., A. Melander, A. (2006) New technology for self piercing riveting of TRIP800 in 1+1 and 1+2 mm sheet thickness. 2006, Swedish Institute for Metal Research: Stockholm, Sweden.

Kim, M.G., Kim, J.H., Lee, K.C., Yi, W. (2005) Assessment for structure stiffness and fatigue life in self piercing rivet of car bodies. Key Eng Mat 297-300.

Kim, H., Kardes, N. (2012) Friction and Lubrication. In: Altan, T., Tekkaya, A.E. (2012) Sheet Metal forming – Fundamentals. ASM International. [online] Available: http://www.asminternational.org/documents/10192/3477814/05340G_Sample.pdf/274eeee5-af5e-4920-8607-ecad5682a521 [Accessed Oct 2016].

King,. RP., O'Sullivan, J.M., Spurgeon, D., Bentley, P. (1995) Setting load requirements and fastening strength in the self pierce riveting process, In proceedings of the 11th National Conference of Manufacturing research, Leicester, UK. 57-61

Kraus, C. et al (2018) Measuring device and values to determine friction parameters in mechanical joining. Fraunhofer IWU, Dresden.

Krishnappa, U.S. (2008) Numerical investigation of self-piercing riveted dual layer joint, in Department of Mechanical Engineering, Master thesis, Wichita State University, India.

Kunogi, M. (1954) A review of ring-compression testing and applicability of the calibration curves. J. Sci. Res. Inst. 2 63.

Lai, M., Brun, R. (2007) Latest developmenst in sheet metal forming technology and materials for automttive application: the use of ultra high strength steels at Fiat to reach weight reduction at sustainable costs. Key Eng Materials 341:1-8.

Li, N. et al (2016) Experimental investigation of boron steel at hot stamping conditions. Journal of materials processing technology 228:2-10

Litherland, H. (2016) Self-piercing riveting case study of Volvo FH12 truck cab. TWI. [online] Available: http://www.twi-global.com/news-events/case-studies/self-piercing-riveting-case-study-of-volvo-fh12-truck-cab-154/. [Accessed September 2016].

Lou, M., et al (2014), Influence of resistance heating on self-piercing riveted dissimilar joints of AA6061- T6 and galvanized DP590. Journal of Materials Processing Technology 214:2119–2126.

Ma, Y., Lou, M., Yang, Z., and Li, Y., (2015) Effect of Rivet Hardness and Geometrical Features on Friction Self-Piercing Riveted Joint Quality. J. Manuf. Sci. Eng., 137(5), 054501.

Ma, Y.W. et al (2019) Effects of Process Parameters on Crack Inhibition and Mechanical Interlocking in Friction Self-Piercing Riveting of Aluminum Alloy and Magnesium AlloyJ. Manuf. Sci. Eng. 141(4):041005

Marciniak, Z. (1961) Influence of the Sign Change of the Load on the Strain Hardening Curve of a Copper Test Subject to Torsion. Archiwum Mechaniki Stosowanj 13:743–751.

Marr, T. et al (2014) The Strengthening Effect of Phase Boundaries in a Severely Plastically Deformed Ti-Al Composite Wire Metals 4(3): 37-54.

Mashayekhi, M (2016) Lecture: Comparison of implicit and explicit procedures. [online] Available: https://mashayekhi.iut.ac.ir/sites/mashayekhi.iut.ac.ir/files/u32/presentation4.pdf . [Accessed Oct 2017].

Markou,G. (2014) Why some numerical problems are not converging with very fine mesh? [online] Researchgate forum, University of Pretoria, Pretoria.Available: https://www.researchgate.net /post/Why_some_numerical_problems_are_not_converging_with_very_fine_mesh. [Accessed Jun 2017].

Matsumura, Y., Ogawa, S., Misaki, T. (2007) Dissimilar metal joint technology for aluminum roof. Auto Technol 61(4):78–82.

Matweb (2017) ArcelorMittal Usibor® 1500 Ultra high strength steel, Cold Rolled. [online] Available:http://www.matweb.com/search/datasheet.aspx?MatGUID=91e2b6fce3824a5db29 16553f23a4760&ckck=1 [Accessed May 2017].

Miller, J., Walters, J. (2016) Design of experiments in Cold forming. Fastener Technology International 35-37.

Mis, M. (2019) Flow curve generation. AtlasCopco, Deeside.

Moraes, J.F.C., Jordon, J.B., Bammann, D.J. (2015) Finite element analysis of self pierce riveting in Magnesium Alloy sheets. Journal of Eng Mat and Technol 137/0210002-1

Moraes, J., Jordon, J., and Ilieva, E., (2018) Influence of the Friction Coefficient in Self-Pierce Riveting Simulations: A Statistical Analysis, SAE Int. J. Mater. Manf. 11(2):123-130.

Mori, K., Kato, T., Abe, Y., Ravshanbek, Y. (2006) Plastic joining of ultra high strength steel and aluminum alloy sheets by self piercing rivet. CIRP Annals - Manuf Technol 55(1):283–286

MSC.Marc 2013.1, Volume A: Theory and User Information, USA, 2013.

Mucha, J. (2011) A Study of Quality Parameters and Behaviour of Self-Piercing Riveted Aluminium Sheets with Different Joining Conditions. Strojniški vestnik - Journal of Mechanical Engineering 57(4): 323-333.

Mucha, J., Witkowski W. (2018) Mechanical behavior and failure of riveting joints in tensile and shear test. Strength of Materials 47:5.

Murakami, Y. (1998) Proc. 6th Int. Conf. on Aluminium Alloys, ed. T. Sato et al, Japan Inst. Of Light Metals, 1:3.

Netoa, D.M. et al (2017) Thermo-mechanical finite element analysis of the AA5086 alloy under warm forming conditions. University of Coimbra, Portugal.

Neugebauer, R. Mauermann, R. Grützner (2005) Combination of hydroforming and joining, Steel Research International 76 (2005) 939–944.

Nikishkov, G.P. (2004) Introduction to Finite Element Method. University of Aizu, Japan.

NPTEL (2016) Stress strain curves. [online] Available: https://nptel.ac.in/courses/112107146/12. Accessed Jul 2016

Novelis (2017) Flowcurves for metals frequently used in automotive industry. Novelis, Detroit.

Nutor, R.K. et al (2017) Using the Hollomon Model to Predict Strain-Hardening in Metals. American Jpurnal of materials synthesis and processing, 2 (1):1-4

Packo, P., Uhl, T. (2011) Multiscale approach to structure damage modelling, University of Science and Technology Krakow, Warsaw.

Palaniswamy, H., Billur, E. (2012) Plastic Deformation – flow stress, anisotropy and formability. In: Altan, T., Tekkaya, A.E. (2012) Sheet Metal forming – Fundamentals. ASM International. [online] Available: http://www.asminternational.org/documents/10192/3477814/05340G_Sample.pdf/274eeee5-af5e-4920-8607-ecad5682a521 [Accessed Oct 2016].

Pawelski, O. (1967) Über das stauchen von holzylindern und seine eignung zur bestimmung der formänderungsfestigkeit dünner bleche. Archiv für Eisenhüttenwesen, 38:437-442.

Peetz A, Hahn O. (2001) Untersuchungen zur Fertigung sowie zum Festigkeitsund Alterungsverhalten hybrid gefügter Aluminiumfeinbleche am Beispiel Stanznieten-Kleben. Berichte aus dem Laboratorium für Werkstoff- und Fügetechnik 47Aachen: Shaker.

Pellegrini, D. et al (2011) Effect of Warm Forming Conditions on AZ31B Flow Behaviour and Microstructural Characteristics. International Journal of Material Forming 4:155–161.

Pickin, C.G., Young, K., Tuersley, I. (2007) Joining of lightweight sandwich sheets to aluminium using self pierce riveting. Mater Des 28(8): 2361-2365.

Polmear, I.J. (2004) Aluminium Alloys – A Century of Age Hardening. MATERIALS FORUM 28. Institute of Materials Engineering Australasia Ltd.

Popov, V. (2010) Contact mechanics and friction. Springer, Berlin.

Porcaro, R., Langseth, M., Hanssen, A.G., Zhao,. H, Weyer, S., Hooputra, H. (2008) Crashworthiness of self-piercing riveted connections. Int J Impact Eng 35:1251–1266.

Porcaro, R., Hanssen, A.G., Langseth, M., Aalberg, A. (2006a) The behaviour of a self piercing riveted connection under quasi static loading conditions. Int J Solids structure 43:5110-5131.

Porcaro, R. et al (2006) Self piercing riveting process: an experimental and numerical investigation. J Mat Process Tech. 171 (1):10-20.

Qi, H. (2006) Finite Element Analysis (MCEN 4173/5173) [online] Available: http://www.colorado.edu/MCEN/MCEN4173/chap_01.pdf. [Accessed 3rd August 2016].

Raabe, M. (2016) Material Theory. Simufact, Kassel.

Rajesh, E, Prakash, M.S., (2013) Analysis of friction factor by employing the ring compression test under different lubricants. International Journal of Scientific & toolbox 4, Issue 5, 1163 – 1171.

Ramberg, W., Osgood, W.R. (1943) Description of stress–strain curves by three parameters. Technical Note No. 902, National Advisory Committee For Aeronautics, Washington DC.

Ramezani, M. et al (2010) Combined Experimental and Numerical Analysis of Bulge Test at High Strain Rates Using Split Hopkinson Pressure Bar Apparatus. Journal of Materials Processing Technology 210:1061–1069.

Rauch, E.F. (1992) The Flow Law of Mild Steel Under Monotonic or Complex Strain Path. Solid State Phenomena 23(24):317–334.

Ritz, W. (1909) Über eine Neue Metode zur Lösung gewisser Variationsprobleme der Matematischen Physik . J. Reine Angew. Math., 1909(35):1-61.

Roth, C.C., Mohr, D., (2014) Effect of strain rate on ductile fracture initiation in advanced high strength steel sheets: experiments and modeling. Int. J. Plast. 56:19–44.

Ruprechter, F., Kepplinger, G., Dolle, N., Martin, M., Ageorges, C. (2006) Fatigue life estimation of self piercing rivets in car body development based on local stresses using node independent meshing. VDI Berichte (1967 II):777–795

Schey, J.A. (1987) Introduction to Manufacturing processes. McGraw-Hill International, Oxford.

Simões, V. et al (2018) The influence of warm forming in natural aging and springback of Al-Mg-Si alloys. International Journal of Material Forming 12: 57.

Simufact (2013) Applications. MSC Software company, Kassel.

Singh, H.(2003) Fundamentals of Hydroforming, Society of Manufacturing Engineers, Dearborn, Michigan.

Smith, R.L., Sandland, G.E. (1922) An Accurate Method of Determining the Hardness of Metals, with Particular Reference to Those of a High Degree of Hardness, Proceedings of the Institution of Mechanical Engineers 1: 623–641.

Schmitz, G.J., Prahl, U. et al (2016) Handbook of software solutions for ICME. Willey-VCH, Weinhem

PR ES (2018) Atlas Copco SPR specification, Sept 2018 version.

Stromstedt, E. (2002) Finite element simulation of crash testing of self-piercing rivet lap shear joint specimens, Swedish Institute for Metal Research Report No. IM-2002-022.

Stuhmeyer, A. (2005) Self piercing riveting. Paper presented at the 5th LS-Dyna European conference Birmingham, UK.

Sui, B., Du, D., Chang, B., Huang, H., Wang, L. (2007) Simulation and analysis of self-piercing riveting process in aluminum sheets. Material Science and Technology 15(5):713–717.

Sun, X., and Khaleel, M. A. (2007) Dynamic strength evaluations for self-piercing rivets and resistance spot welds joining similar and dissimilar metals. International Journal of Impact Engineering 34:1668–1682.

Sun, X., Stephens, E. V., and Khaleel, M.A. (2007) Fatigue behaviors of self-piercing rivets joining similar)and dissimilar sheet metals. International Journal of Fatigue 29:370–386.

Sung, J.H. et al (2010). A plastic constitutive equation incorporating strain, strain-rate, and temperature. Int. J. Plast. 26:1746–1771.

Swift, H. (1952) Plastic instability under plane stress. J. Mech. Phys. Solids 1:–18.

Tang, D., Barthelemy, B., Yuan, H. (2002) Self-pierced rivet (SPR) modelling in aluminium structure crash analysis. In proceedings of the ASME International Mechanical Engineering Congress and Exposition IMECE 2002, November 17–22, New Orleans, LA, 207–222.

TechSpec (2019) Communications with Technical Specialists at Atlas Copco.

TechSpec1 (2019) Communications with Technical Specialists at MSC software company.

TechSpec2 (2018) Communications with Technical Specialists at JLR.

Tekkaya, A.E. (1982) Determining stress-strain curves of sheet metal in the plane torsion test. CIRP Ann Manuf Technol 31:171–4.

Testa, G. et al 1 (2018) Numerical simulation of self-piercing riveting process (SRP) using continuum damage mechanics modelling. Frattura ed Integrità Strutturale, 44:161-172.

Testresources (2019) What is a Compression Test? [online] Available: https://www.testresources.net/applications/test-types/compression-test/ [Accessed May 2019].

Traphöner H. et al (2018) Material characterization for plane and curved sheets using the in-plane torsion test – An overview. Journal of Materials Processing Technology 257:278-287.

Traphöner, H. (2018) Influence of manufacturing processes on material characterization with the grooved in-plane torsion test. International Journal of Mechanical Sciences 146–147:544–555.

TU Wien (2015) Testing and fitting of Henrob rivets. Wienna University of technology, Wienna.

Tura, A. Introduction to Finite Element Analysis (FEA) or Finite Element Method (FEM). University of Victoria. [online] Available: http://www.engr.uvic.ca/~mech410/lectures/FEA_Theory.pdf [Accessed August 2016].

Turetta, A. et al (2006) Investigation of 22MnB5 Formability in Hot Stamping Operations. Journal of Materials Processing Technology 177:396–400.

Turner, M. J. et al (1956) Stiffness and deflection analysis of complex structures. Journal of Aeronautical Science, 23(9):805-824.

TWI (20016) Technical knowledge – summaries. [online] Available: https://www.twi-global.com/login/?returnurl=%2ftechnical-knowledge%2fknowledge-summaries%2fself-piercing-riveting%2f. [Accessed March 2016]

Uthaisangsuk, V. (2009) Microstructure Based Formability Modelling of Multiphase Steels. PhD dissertation. RWTH-Aachen University.

University of Babylon (2017) Plastic deformation and stress-strain curves. [online] Available: http://www.uobabylon.edu.iq/eprints/publication_12_24290_1049.pdf.[Accessed on July 2017].

Varela, S. et al (2018) MULTIMAT: Simulation of SPR joints. Presentation, Tecnalia, Bilbao.

Verleysen, P. et al (2011) Effect of Strain Rate on the Forming Behaviour of Sheet Metals. Journal of Materials Processing Technology 211:1457–1464.

Visnic, B. (2019) Stuck on structural adhesives, SAE Automotive Engineering.

Vivio, F., Ferracci, M. (2009) Modelling of riveted joints with a new rivet element. SAE International 2009-01-0025.

Vorobyov, A. et al (2013) Single-Impact Self-Pierce Riveting. National Aerospace University KhAI. [online] Available: http://khai-era.khai.edu/uploads/editor/40/4708/sitepage_29/files/Single-Impact%20self-pierce%20riveting.pdf [Accessed May 2016].

Wang, J.W. et al (2011) Self-piercing riveting of wrought magnesium AZ31 sheets, Journal of Manufacturing Science & Engineering 133 031009-031001-031009-031009.

Whitacre, D. (2019) Unlocking Structural Efficiency through Aluminum Innovation, Automotive Engineering Expo, Nuremburg Messe.

Wi, M. (2018) Prediction of plastic flow localisation with shell element in thick AHSS sheets. In proceedings of 17th International conference on Metal forming, Japan.

Williams, S. (2018) Presentation on benefits of narrow flange. Atlas Copco, UK.

Wei, L, Y., Wang, Z., and Li, Y. (2013) Friction Self-Piercing Riveting of Aluminum Alloy AA6061-T6 to Magnesium Alloy AZ31B. J. Manuf. Sci. Eng., 135(6):061007.

Westerberg, C. (2002) Finite element simulation of crash testing of selfpiercing rivet joints, peel specimen, in Structural Mechanics, LUND University: LTH.

Westgate, S.A. et al. (2001) The development of lightweight selfpiercing riveting equipment, in SAE World Congress, Paper No. 2001–01-0979.

World Auto Steel (2017) Advanced High Strength Steels application guidelines v6. Presentation for WorldAuto Steel 2017

Xu, Y. (2006) A close look at self-piercing riveting—computer simulation is a noteworthy alternative to physical testing of joints, in The fabricator.

Yaw, L.L .(2009) Nonlinear Static - Explicit and Implicit Analysis Example. E. F. Cross School of Engineering, Walla Walla University.

Yin,, Q. et al (2014) An experimental and numerical investigation of different shear test configurations for sheet metal characterization. International journal of solids and structures 451: 1066-1074.

Yin, Q. et al (2015) A grooved in-plane torsion test for the investigation of shear fracture in sheet materials. International Journal of Solids and Structures 66:121–132.

Zienkiewic, O.C., Taylor RL (1967) Finite element method: The basics. Butterworth-Heinemann. Oxford.

Zhu, X. et al (2018) New features for metal forming in LS-Dyna. LSTC. In proceedings of 15th LS-Dyna conference, Detroit.